NASA Technical Memorandum 73285

Final Report of GEOS-3 Radar Altimeter Study for the South Atlantic Bight

C. D. Leitao
N. E. Huang
C. L. Parsons
C. G. Parra
J. D. McMillan
and
G. S. Hayne

May 1980

National Aeronautics and Space Administration

Wallops Flight Center
Wallops Island, Virginia 23337
AC 804 824-3411

NASA Technical Memorandum 73286

Final Report of GEOS-3 Radar Altimeter Study for the South Atlantic Bight

C. D. Leitao
N. E. Huang
C. L. Parsons
C. G. Parra
J. D. McMillan
and
G. S. Hayne

May 1980

National Aeronautics and Space Administration

Wallops Flight Center
Wallops Island, Virginia 23337
AC 804 824-3411

NASA Technical Memorandum 73286

Final Report of GEOS-3 Radar Altimeter Study for the South Atlantic Bight

C. D. Leitao, N. E. Huang, and C. L. Parsons

NASA Wallops Flight Center
Wallops Island, Virginia 23337

C. G. Parra and J. D. McMillan

EG&G, Washington Analytical Services Center, Inc.
Pocomoke City, Maryland 21851

and

G. S. Hayne

Applied Science Associates, Inc.
Apex, North Carolina 27502

This study was funded through Interagency Agreement AA551-IA8-39
between the Bureau of Land Management
and the National Aeronautics and Space Administration.

NASA

Wallops Flight Center

TABLE OF CONTENTS

INTRODUCTION

The ability to measure ocean currents and certain ocean wave and wind speed characteristics over large ocean areas and long periods of time could have significant impact upon open ocean and coastal activities. Ship routing, search and rescue operations, oil spill modelling, meteorological and oceanographic research, and recreational activities are just a few of the areas where quick and reliable information is desired. With the advent of satellite altimetry, it is now possible to estimate many of these ocean characteristics with surprising accuracy.

Three products which can be estimated from satellite altimetry have particular importance. They are geostrophic ocean current position and velocity, significant wave height (SWH), a statistical parameter which relates the height of the ocean waves to mean sea level, and surface wind speed. All of these products can be computed on a global basis and in near real-time.

The National Aeronautics and Space Administration (NASA) Geodetic Experimental Ocean Satellite (GEOS-3) spacecraft (figure 1) was launched from the Air Force Western Test Range on April 9, 1975. The satellite orbits the earth every 101.8 minutes in a near-circular, 65-degree retrograde orbit. The primary instrument on board the 340 Kg satellite is the radar altimeter, developed for NASA by the General Electric Corporation. The altimeter operates at a frequency of 13.9 GHz, transmitting 100 pulses per second. The pulses transmitted by the altimeter reflect from the earth's surface and are received by the spacecraft yielding an altitude measurement with an RMS accuracy of 70 cm. This configuration gives a footprint size of 3.6 km wide and 11 km along the track from an orbit of 840 km with zero eccentricity. A detailed technical discussion of the GEOS-3 radar altimeter is given by Hofmeister et al., (ref. 1).

The altimeter is instrumented with 16 sample and hold gates which provide information about the shape and amplitude of the return waveform. This information can be used to determine a number of interesting and useful parameters including water-land and water-ice boundaries, ocean surface wind speed, and significant wave height. At the insistence of the GEOS-3 Project Scientist, H. R. Stanley, an experimental version of a SWH estimating algorithm was built into the altimeter processing software (ref. 2). Several refinements to the original SWH algorithm were produced as a result of the analysis of early GEOS-3 on-orbit data. The analysis also led to the development of algorithms to provide ocean sea surface wind estimates and the water-ice and water-land boundary estimates.

These estimates proved to be so useful that, in 1978, NASA established the GEOS-3 Near-Real-Time Data System for disseminating Gulf Stream boundary positions and world-wide significant wave height and wind speed estimates. In the near-real-time system, the

GEOS-3 data were acquired from the 13 NASA Space Tracking and Data Network locations or the ATS-6 satellite and transmitted to the NASA Goddard Space Flight Center (GSFC) in Greenbelt, Maryland, where they were buffered to magnetic tape in real-time. The buffered data were then transmitted to the Computer Sciences Corporation INFONET center in Beltsville, Maryland, where significant wave height and wind speed were computed and made available to user-supplied terminals on a call-up basis. At the same time, the buffered magnetic tapes were sent to NASA Wallops Flight Center (WFC), where, using predicted orbits, an estimation of the position of the Gulf Stream was calculated. This information was then also sent to the INFONET center.

Due to the efforts and the early recognition of the potential of the GEOS-3 radar altimeter data by the Bureau of Land Management (BLM) Outer Continental Shelf Office and in particular by Dr. E. D. Wood, an interagency agreement was reached between BLM and NASA. This report represents the first application of GEOS-3 data for a large, comprehensive environmental study such as BLM's South Atlantic Bight Study.

DATA PROCESSING FOR SEA SURFACE TOPOGRAPHY

The study of the general ocean circulation has long occupied the central stage of physical oceanography and the most important phenomena in the ocean circulation investigations are the major boundary current systems such as the Gulf Stream and Kuroshio. For the Gulf Stream, most of the results from past studies have been summarized by Stommel (ref. 3) in a classic work. Although the results are voluminous, our knowledge of the global ocean circulation in general and the Gulf Stream in particular is still quite limited. Recently, the development of an accurate radar altimeter operational under all weather conditions has reached a new level of success. Direct measurement of the sea surface topography with an accuracy of ± 20 cm for one second averaging from a stable moving reference platform provided by a satellite is now possible. This offers a direct way to measure the dynamic topography which until now could only be inferred from hydrographic data. The measurements made by a satellite altimeter are illustrated by figure 2. An ideal altimeter will yield measurements on satellite altitude which may be expressed as:

$$h_a = h_s - h_g - \Delta h \tag{1}$$

where h_a is the satellite altitude measured by the altimeter, h_s is the satellite height above a reference spheroid determined from the satellite tracking data, h_g is the geoidal deviation from the spheroid due to gravitational anomalies and Δh is the height deviation from the geoid due to the dynamic processes in the ocean such as the currents and the tides. From the altimeter data, the surface current can be calculated directly from the surface slope using the geostrophic equation (ref. 4).

The overall data processing is summarized in figure 3 in the form of a flowchart. An attempt to more fully explain each step is presented here. The initial task consists of obtaining a search of the data files for passes within the study area. Many of the passes are eliminated due to a variety of reasons, among them: lack of orbital data, poor data, data obtained over land only, and data of only a few seconds duration. Once a set of data is initially obtained, each GEOS-3 pass within that set is identified by orbit number, time, latitude and longitude. This information goes into the Dynamic Ocean Surface (DOS) computer program which is designed for the purpose of obtaining a sea surface profile from the altimeter height data.

Sea Surface Height Profiles

Averaged altimeter measurements are preprocessed and converted to sea surface heights as defined by Leitao et al., (ref. 5) and treated here as raw sea surface heights. The preliminary data processing procedure used for this study by the DOS computer program is summarized in figure 4. The raw sea surface heights shown in A are first edited to eliminate anomalies due to internal instrument noise. The edit criterion is based on a predicted sea surface height calculated from fitting a straight line through the last eight seconds of data (80 data points representing 60 km in physical distance). Any point differing from the predicted height by more than two meters (approximately three standard deviations of the noise level of 70 cm) is replaced by the predicted height value. Results point out that less than 1% of the calculated predicted data are used. The edited sea surface height data shown in B are then filtered using an 81-point, equal weight, mid-point filter. This filter is chosen since it reduces the noise without seriously compromising the sea surface signature. The eight seconds are selected so that the accuracy could be maintained below the 10 cm level; and the noise level is sufficiently reduced prior to differentiation. After the filtering process, the smoothed sea surface height is referenced to the Mader (ref. 6) 5' x 5' geoid (See C). Subtracting the geoid from the smoothed sea surface height results in a residual which is nearly flat in the open ocean as shown in D. Next, to minimize the error between the geoid and the smooth sea surface height south or east of the mean position of the Gulf Stream, a linear fit is made to the residuals over the section representing the open ocean. The straight line is then subtracted from all residuals thus removing any potential orbital bias or slope errors and producing an estimate of the sea surface profile as shown in E. Once all the sea surface profiles are obtained for each calendar month, they are compiled onto monthly tapes. Thus, thirty-six monthly tapes are available.

The determination of where to fit the data to the geoid is first done blindly. A second fit is then performed once the first attempt is analyzed. Since temporal changes in the sea surface could have affected this second or a-posteriori fit, it is decided to further analyze this problem. At this point all passes within the study area are grouped

geographically by bands running parallel to the GEOS-3 subsatellite tracks, each band having a width of 2.5° of latitude at the equator (figure 5). Each band is subsequently analyzed independently of the others and each individual pass within each band inspected to ascertain the maximum southern excursion of the Gulf Stream within each band. Once this analysis is performed, it is found that by dividing each band into five sub-bands the extreme excursions are better modelled. The difference in time and position between a determined parallel and the location of the maximum southern excursion of the Gulf Stream is calculated for each pass within a sub-band. The time for the termination of the fit to the geoid is then calculated geometrically (figure 6).

About 25% of the GEOS-3 passes are corrected by this method and the new, corrected, monthly compiled data tapes are evaluated. To facilitate the data handling, all data are stored on disk at a rate of every tenth measurement. A short study was conducted to analyze the differences between the point to point sea surface profiles and the every tenth profile (figure 7). The results point out that there is no significant difference between the tenth second and the one second data. Hence, one second data are used.

Sea Surface Topographic Maps

With all the data stored on disk, each month's data are processed by first using the MODSEAHT computer program, a modification of SEAHT (ref. 7). MODSEAHT combines all the monthly profiles using a minimum variance technique to minimize the differences in height at the intersecting points. The adjusted values of the topographic height which minimize the errors at the intersecting points are treated as the directly measured dynamic heights for the month. These adjusted data are then reticulated for automatic contouring. This technique divides the scanned area into 1/2 degree cells. All adjusted measurements occurring within a cell are averaged and cells with no observations are filled by averaging two-way linear interpolations, one along a constant band of latitude and the other along a constant band of longitude. Once all the cells are filled, blank cells are filled with a coded -9999, and an automatic contouring technique is applied. This produces sea surface topographic maps with contour lines from +200 cm to -200 cm with a contour interval of 20 cm.

Using the 1/2° x 1/2° contour maps, a 1° x 1° averaging of the sea surface flow is performed. The geostrophic component of velocity is calculated and positioned according to the contours as observed in the topographic maps. The calculations are based on the simplified geostrophic equation:

$$V = \frac{g}{\rho \; 2\Omega \; \sin\phi} \cdot \frac{\Delta h}{\Delta L} \qquad (2)$$

where V is the geostrophic surface velocity; g is the gravity acceleration of 980 cm/sec^2; ρ, the density of sea water taken as 1 g/cm^3; Ω the angular speed of the earth; ϕ, the latitude; Δh, the total height difference; and ΔL, the horizontal distance between contours. Graduated arrows are then placed on the map indicating the magnitude and the direction of the sea surface flow.

DATA PROCESSING FOR SIGNIFICANT WAVE HEIGHT AND WIND SPEED

Various experiments performed at WFC (refs. 8, 9, 10) and at other sites by other principal investigators (refs. 11, 12, 13) indicate that the GEOS-3 data compare favorably with other estimates and measurements of sea state and surface winds. The first large scale comparison of GEOS-3 data with independently derived sea state information presented several variations of the original significant wave height algorithm and estimated the accuracy of the altimeter-derived significant wave height to be 55 cm (ref. 14). Present studies at WFC estimate the accuracy of the altimeter-derived wind speed to be 1 m/sec. The algorithms derived in this section have been in use at WFC in preprocessing the GEOS-3 altimeter data since July of 1975. The same algorithms were used at GSFC in the near-real-time data network established in March of 1978.

Significant Wave Height Estimation Algorithm

The model used to obtain the waveform geometry for negligible significant wave heights is based on the geometry of a square pulse impinging upon a flat sea surface as illustrated in figure 8. A pulse of duration T leaves the spacecraft (observer) at time $t = 0$, and traverses a distance H to the sea surface, arriving at time $t = t_1$, where it is reflected back to the satellite at time $t = t_2 = 2t_1$. Therefore

$$t_2 = \frac{2H}{c} \tag{3}$$

where c is the speed of light. At $t = t_3 = t_2 + \tau$ where $\tau < T$, the square pulse is observed impinging upon the sea surface, where an expanding circular area is illuminated. The radius r of the area is related to H by

$$r^2 = (H+h)^2 - H^2 = 2Hh + h^2 \simeq 2Hh \tag{4}$$

since $h^2 << 2Hh$. The time $t = t_3$ is given by

$$t_3 = t_2 + \tau = \frac{2H}{c} + \tau \tag{5}$$

and corresponds to the two-way travel time between the satellite and point P on the surface. Therefore,

$$\tfrac{1}{2}\left(\frac{2H}{c} + \tau\right) = \frac{H + h}{c} \tag{6}$$

or

$$\frac{H}{c} + \frac{\tau}{2} = \frac{H}{c} + \frac{h}{c} \tag{7}$$

which yields

$$h = \frac{c\tau}{2} \tag{8}$$

Combining equations (4) and (8) yields

$$r^2 = Hc\tau \tag{9}$$

and the area of the illuminated region is given by

$$a = \pi r^2 = \pi Hc\tau \tag{10}$$

Note that the observed area of the illuminated region, or equivalently the power received by the satellite, increases linearly with time. When t becomes greater than t_4, the trailing edge of the pulse has reached the sea surface and the area illuminated becomes an annulus with inner radius $_5$ and outer radius $_6$ given by

$$r_5^2 = Hct_5 \tag{11}$$

$$r_6^2 = Hct_6 \tag{12}$$

and width W and area A given by

$$W = r_6 - r_5 = Hct_6 - Hct_5 \tag{13}$$

$$A = \pi r_6^2 - \pi r_5^2 = \pi Hc(t_6 - t_5) = \pi HcT \tag{14}$$

Since the area of the annulus remains constant, the power received at the satellite remains constant until the antenna-beamwidth effects cause the power received to decay.

The characteristics of a square pulse impinging upon a sea surface with negligible SWH as seen from the satellite can be summarized in four stages: (1) no power is received until the leading edge of the pulse is observed striking the sea surface, (2) after the leading edge of the pulse reaches the surface and before the trailing edge does, the power received increases linearly with time, (3) after the trailing edge of the pulse reaches the surface, the power received remains at a constant plateau value, and(4) after the antenna-beamwidth effects become non-negligible, the power received begins to decay. These four stages are depicted in figure 9, which represents the idealized mean return pulse shape. Due to the nature of the altimeter, the instantaneous power received fluctuates, making it necessary to average a number of pulses in order to determine the mean pulse shape. The GEOS-3 satellite receives the return pulses in 16 waveform sampling gates. These 16 values, called Instantaneous Return Samples (IRS), are collected 100 times per second by the satellite and averaged on-board in an attempt to construct an accurate representation of the mean pulse shape. The 16 values of average IRS's are called Average Return Samples (ARS) and are computed using an exponentially decaying averaging technique over a period of approximately 2 seconds. It is the slope of the ARS's which is examined to determine significant wave height.

When a square pulse impinges upon an ocean surface with non-negligible significant wave height, the shape of the mean return pulse is altered. The geometry of a sea surface with non-negligible significant wave heights is illustrated in figure 10. Note that the crests of the waves are illuminated prior to the time at which the calm sea would have been illuminated. Similarly, the troughs of the waves are not illuminated until after the time at which the calm sea would have been illuminated. The net result of these effects is that the mean power received for non-negligible sea state does not reach its full plateau value until after the time at which the mean power received from a calm sea reaches its plateau values. The leading edge of the mean pulse shape for several non-negligible sea states is characterized in figure 11. From this figure it can be seen that the slope of the mean return pulse is related to significant wave height. If the mean pulse shape for negligible sea state was known precisely, then the significant wave height could be determined by analyzing the departure of the mean return pulse for the non-negligible sea state from the mean return pulse shape for calm sea.

It has been shown (refs. 15, 16, 17) that the mean return waveform can be treated as a convolution of the composite of the transmitted pulse and transmitter and receiver bandwidth effects, the non-coherent surface (calm sea) impulse response, the ocean surface height probability density function, and the tracking loop jitter. The bandwidth effects and the probability density function can be modeled as Gaussian distributions, the calm sea impulse can be modeled as a step function, and the tracking loop jitter is assumed to be unaffected by sea state.

Assuming that pointing angle errors have negligible effect upon the leading edge of the waveform, Brown and Miller (ref. 18) have shown that a good approximation of the return power can be represented as a Gaussian function

$$y(t) = a\ P\ (\frac{t-b}{c}) + d \tag{15}$$

where a is the return waveform amplitude; b is the time origin; c is the return waveform risetime; d is the return waveform baseline amplitude. The evaluation of the function P in equation 15 is performed by:

$$P\ (z) = \int_{-\infty}^{z} \frac{1}{2} \exp\ (-q^2/2)\ dq \tag{16}$$

Therefore, it is necessary to estimate the four parameters a, b, c, and d from which the slope of the return waveform, and in turn the significant wave height, can be determined. The technique used to estimate the four-parameter function y(t) is the method of least squares (ref. 19).

The convolution model for the mean return waveform assumes that the risetime parameter c is a composite of two Gaussian distributions: the calm sea pulsewidth σ_c and the rough sea rms σ_s, both expressed in nanoseconds. Since the convolution of two Gaussian distributions is itself a Gaussian distribution,

$$c^2 = \sigma_s^2 + \sigma_c^2 \tag{17}$$

The significant wave height is defined as four times the rms sea height relative to mean sea level. Conversion to units of meters by multiplying by the two-way speed of light yields

$$SWH = 4\sigma_s = 0.6\ \sqrt{c^2 - \sigma_c^2} \tag{18}$$

Significant wave heights have been computed on thousands of passes of GEOS-3 data and it has been found that the algorithm typically converges within 2 or 3 iterations. In addition, it has been determined that the final converged estimate of significant wave height is not particularly sensitive to the initial guesses of a_o, b_o, c_o, and d_o. In practice, the same initial guesses are used for all passes. For each significant wave height estimate after the first frame of data, the converged values of a, b, c, and d for the previous frame of data are used as the initial guesses for a_o, b_o, c_o, and d_o. Therefore, it is necessary to have an accurate estimate of the calm sea pulse width (σ_c) in order to calculate significant wave height using equation (18). Early in the GEOS-3 mission, many passes of the satellite over areas where ship measurements indicated calm

seas were analyzed in order to determine that value of σ_c which would yield an estimate of SWH = 0 for those passes. The value arrived at was 7.49 nanoseconds. This value has been examined (refs. 9, 10) and found to be accurate.

Due to the electronic characteristics of the altimeter, the mean return waveform represented by the ARS's contains noise. Waveforms from two adjacent data frames can differ substantially, even though the altimeter is receiving data from ocean areas only a few kilometers apart. This fact, combined with the inherent errors introduced in the estimation process, can produce an estimate of c which causes the term under the radical in equation (18) to become negative. This is especially true when the sea state is very calm. It should be noted that for moderate values of significant wave height, small errors in the estimate of c do not cause large errors in the calculated value of significant wave height. However, the estimate of significant wave height is very sensitive to even small errors in c for calm seas.

When the noise characteristics of the altimeter, the estimation errors, and the algebraic sensitivity of the estimate to c are combined, it is obvious that smoothing the estimate should provide more confidence in its accuracy, especially when the sea state is calm. Empirical studies indicate that the longest segment over which the return pulse can be assumed to be correlated is approximately 140 kilometers (or 21 seconds). A sliding 21-second rectangular filter has been employed by the significant wave height estimation software to smooth the estimate. Either the estimate of c or the calculated value of significant wave height can be smoothed and the results have been shown (ref. 14) to be nearly identical. For computational ease, the estimate of c is smoothed in this investigation. Even when the estimate is smoothed, the term under the radical in equation (18) can still become negative. Such cases have no physical meaning and a value of SWH = 0 is assumed.

Wind Speed Estimation Algorithm

A widely used parameter in the analysis of radar returns is σ_o, which is the radar backscattering per unit scattering area and is a measure of the surface as a radar reflector. It has been shown (ref. 20) that $\sigma_o(0°)$, which is the value of σ_o for no off-nadir pointing angle, may be written as

$$\sigma_o(0°) = \alpha \frac{R\,(0°)^2}{\overline{\zeta}^2_{1r}} \tag{19}$$

where α is a constant of proportionality which depends upon the density of the slopes of the filtered surface, $R(0°)^2$ is the Fresnel power reflection coefficient for the sea at normal incidence and 13.9 GHz, and $\overline{\zeta}^2_{1r}$ is the mean square slope of the filtered surface, which can be logarithmically related to the wind speed W by

$$\overline{\tau}_{1r}^{2} = A \ln(W) + B \tag{20}$$

Assuming that α remains essentially unchanged with variations in wind speed,

$$\sigma_o\,(0^\circ) = \frac{R_o(0°)^2}{A \ln(W) + B} \tag{21}$$

Rearranging terms and using -2.1 dB for $R_o\,(0°)^2$ gives

$$W = \exp\left(\frac{10^{-x} - B}{A}\right) \tag{22}$$

where $x = \dfrac{\sigma_o(0°) + 2.1}{10}$ and $\sigma_o\,(0°)$ is given in dB. The linear coefficients A and B were determined by fitting a curve to the GEOS-3 $\sigma_o\,(0°)$ estimates where wind speed ground truth was available. These data, shown in figure 12, suggest the use of a cusped curve. The least squares determination of these constants (ref. 21) yields different values for wind speeds above and below 9.2 m/sec. For wind speeds below 9.2 m/sec, A is 0.02098 and B is 0.10075, whereas for wind speeds above 9.2 m/sec, A is 0.08289 and B is -0.012664.

Thus, using equation (22), wind speed can be determined solely as a function of $\sigma_o(0°)$. It should be noted, however, that the received power decreases in a predictable manner as the satellite pointing angle increases from nadir. Since the GEOS-3 pointing angle varies by as much as 0.8°, this effect must be accounted for in the calculation of σ_o. Brown and Curry (ref. 22) developed a scheme for correcting σ_o for pointing angle variations and that scheme has been implemented in the wind estimation algorithm.

RESULTS

The results of this investigation consist of a series of sea surface topographic maps and two sets of histograms, one depicting the Significant Wave Height and the other the ocean surface wind speed.

Altimeter Data Set

For the purpose of this investigation, it has been necessary to select GEOS-3 altimeter passes whose ground tracks enter the BLM coverage area, which comprises, for the SWH and wind speed study, an area from latitude 27° to 35° N and longitude from the U.S. coastline to 284° E; and 26° to 37° latitude and a longitude of 2° farther east for sea surface topographies.

After the altimeter passes which enter the BLM areas are identified, it is necessary to ascertain the altimeter status and the telemetry mode of the data. Any passes when the

altimeter status indicates that the altimeter is not locked in the tracking mode, usually during and shortly after the time when the satellite passes over land, cannot be included in the data set. The telemetry mode can be: global, intensive with no waveforms, intensive with 8 waveforms or intensive with 16 waveforms. If the altimeter is in the global mode an accurate sea surface height cannot be estimated for this area due to the noise of the measurements. Also no waveform information is reported so that the SWH cannot be estimated. If the altimeter is operating in the intensive mode, waveform information may be or may not be reported. Since all 16 ARS's are required in order to estimate SWH, only the intensive mode with 16 waveforms can be accepted for the computation of the SWH. All intensive modes can be used to obtain the sea surface heights and all modes can be used to calculate the wind speed. The data products described below have been reduced when the appropriate data rate and telemetry modes were in effect.

Sea Surface Topographic Maps

The end product of the sea surface height measurements obtained by the GEOS-3 radar altimeter and processed as described above is a series of sea surface topographic maps which include not only height contours but also graduated arrows indicating the magnitude and direction of the surface geostrophic flow. At the same time that the monthly sea surface maps are produced, a map showing the sub-satellite tracks for the passes included in each month is prepared and they are shown as figures 13, 14, 15. A three-year mean sea surface topographic map was also produced by averaging six half-year mean reticulated data tapes. The average was done in a way similar to the monthly maps. All measurements falling into a 1/2 degree cell were averaged and empty cells were interpolated. An indication of the total amount of passes in the three years of data collection is found in figure 16. Maps of mean sea surface topography created for each month in the three years of this study from July 1975 to June 1978 in addition to the above mentioned three year mean map appear as Appendix A.

Significant Wave Height and Wind Speed Histograms

The histograms for significant wave height and wind speed are presented in Appendices B and C. In each figure, the axis of abscissa is graduated in meters and the axis of ordinate is graduated in percent. In addition, each bin of the histogram is labeled with the actual number of samples included in the bin and each figure contains the number of points in the total distribution as well as the mean and standard deviation of the distribution.

The BLM study region was divided into five areas (see figure 17). Each area represents a different sector of the ocean, the areas contain the following environments: (1) coastal waters, northern sector; (2) coastal waters, southern sector; (3)

Gulf Stream waters, northern sector; (4) Gulf Stream waters, southern sector; and (5) Sargasso waters. Notice that the division between northern and southern sectors occurs at about the area of the Blake Escarpment where the Gulf Stream changes course from almost due north to more northeasterly. The histograms for each of the five BLM areas and a composite histogram of all the areas are given for each month, composite of all years; for each season, also a composite of all years; and for the entire study time. For seasonal histograms, winter is defined as December, January, and February; spring as March, April, and May; summer as June, July, and August; and fall as September, October, and November.

DISCUSSION

The results obtained in this investigation are discussed here. For a more convenient interpretation, they have been divided into two sub-sections: Sea Surface Topographic Maps and Significant Wave Height and Wind Speed Histograms.

Sea Surface Topographic Maps

Two conflicting problems immediately appear when attempting to understand the mean topographic sea surfaces obtained from the individual profiles in the GEOS-3 data base. The first is the number and distribution of passes in the geographic area and the second is the time scale resolution of the oceanographic phenomena of interest. Since the GEOS-3 radar altimeter did not acquire data continuously over the region of interest because of scheduling and power constraints, the number and distribution of passes in the Gulf Stream area are somewhat random during most time periods. This constraint forces the number of passes available per unit of time to be highly variable. Figure 18 shows that the distribution of crossing points ranges from 0 to 76 per month. With no crossing points, any analysis using the data from January, 1976, will be futile. The data from June 1977, on the other hand, shows much promise because with 28 crossings, a reasonable monthly topographic surface is computed. Using the data depicted for April 1977, with the densest coverage for any month, 76 crossing points, results in a reliable surface. Therefore, before estimating any surface over a specified time interval, the distribution statistics and the distribution and number of crossing points of the passes should be evaluated prior to making interpretations of the results.

The following is a series of short explanatory comments on the sea surface topographic maps produced for this study:

July 1975 There is a well-distributed coverage of north-to-south passes integrated with a dense coverage of south-to-north passes in the northern part of the study area and one pass in the southern reaches. A conspicuous Gulf Stream can be traced throughout the entire bight with a well defined Charleston Bump. A marked depression at 33° N, 284° E could be an eddy soon to be absorbed by the main current.

August 1975 There is a fairly dense coverage in the central parts of the bight with an untied pass in the southern reaches. The extreme northern parts are thinly covered by a north-to-south pass. The Gulf Stream can be traced in the entire bight. However, little emphasis should be placed on the southern part where the untied pass may have contributed to a very sharp slope. The area around the Charleston bump is well defined by a small hump.

September 1975 The coverage for this month is well distributed with almost no area better than another. The main body of the Gulf Stream can be traced throughout the bight, losing sharpness toward the extreme northern reaches. The Charleston Bump appears as a flattish lunate area. The most distinguishable feature is a 80 cm depression located at 30° N, 282° E which has been identified as a cold water eddy.

October 1975 Coverage for this month is adequate; there is a large gap between north-to-south passes yet this gap is well covered by south-to-north passes. The only open area where caution should be applied appears to be at about 30° N, 281° E where there is a large area with no coverage. The Gulf Stream is well defined except in the northern reaches where it appears to flow inland. This is probably due to the appearance of a body of cold water shoreward of the Gulf Stream. A cold water eddy can be identified at 29.5° N, 282° E.

November 1975 Passes during this month form a very well distributed grid with no distinguishable portions of poor coverage. The Gulf Stream is well defined with a surprising absence of the Charleston Bump. The cold body at Onslow Bay is still present.

December 1975 North-to-south coverage is good as is the south-to-north although they do not combine to produce a symmetrical grid. This month is marked by four zones of very cold water shoreward of the Gulf Stream and a pronounced shoreward shift of the Gulf Stream near Savannah.

January 1976 There is a fairly even distribution of north-to-south passes; unfortunately, there were no south-to-north passes to tie it down. Analysis from this month should be approached cautiously at best. Due to these problems, there is an evident northeast-southwest elongation and a pronounced depression at about 30° N, 282.5° E. This position is coincident with the path of an eddy, but it could also be coincidental.

February 1976 Although only six passes are obtained, the spacing of the north-to-south passes and the fact that these are tied by two south-to-north passes help to obtain a somewhat clearer topography. Nonetheless, caution is again exercised. The Gulf Stream is fairly evident but there are no eddies present.

March 1976 This is another poor month regarding the number and location of passes. Particularly poor in coverage and immediately evident in the topographic map is the extreme southern portion where there is a lack of data between passes.

April 1976 Here again, although the number of passes is not large, their spacing is good enough to produce a fairly accurate map. The southern sector again shows signs

of a systematic interpolation. The Gulf Stream shows fairly well with a pronounced Charleston Bump. Only one eddy is evident, located at about 30.5° N, 282° E.

May 1976 This month appears to be well covered by both north-to-south and south-to-north passes. Unfortunately, the most shoreward of the north-to-south passes is not tied to the south-to-north passes thus leaving a fairly large open space close to shore. No eddies are apparent and the Gulf Stream is observed throughout the bight.

June 1976 Although not too many passes cover the area, those present are fairly well distributed producing a good coverage. The topographic map shows many more features than the previous several months. The Gulf Stream is traceable up to about 33° N where it becomes diffused. A large cold water depression is evident at 33° N, 282.5° E and an eddy is observed at 30.5° N, 281.5° E.

July 1976 There is a good distribution of passes with only one south-to-north pass untied to the rest of the system. The topographic map shows a clearly defined Gulf Stream, two cold water areas close to shore, and two eddies. The Charleston Bump is well defined and a smaller bump is also evidenced at 29.5° N, 281° E.

August 1976 A very good spacing of passes is evidenced this month. Two south-to-north passes in the extreme southern reaches are not tied to the rest. The topographic map shows a well defined Gulf Stream running the entire length of the map with a strong showing of the Charleston Bump. There are no eddies visible.

September 1976 The passes within this month are well distributed, and only in the extreme southern reaches is there an untied pass. The Gulf Stream is well defined throughout the map and the Charleston Bump is well marked.

October 1976 Coverage for this month is more than adequate. The only less desirable feature is a large void in the north-to-south passes fairly close to land. Yet this deficiency is more than made up by a good number of crossing south-to-north passes. The topographic map shows a well marked Gulf Stream and a very cold depression shoreward at about Long Bay.

November 1976 Coverage for this month is only fair. Spacing between north-to-south passes is too wide except close to shore. South-to-north passes are absent in the northern reaches. The Gulf Stream is visible throughout and the depression off Long Bay is still shown.

December 1976 The passes in this month are almost identical to those in last month providing only a fair coverage. The Gulf Stream is observed fairly well. There is a conspicuous absence of the Charleston Bump and the depression off Long Bay is still present.

January 1977 Although the number of passes is not large, the spacing is fairly symmetrical providing a very good coverage. The Gulf Stream is very distinct throughout. The depression off Long Bay is still shown and no eddies are identified.

February 1977 Very good coverage is again provided for this month and only one south-to-north pass near the extreme end is untied. The Gulf Stream is again shown

throughout. The depression at Long Bay is shifted north and the Charleston Bump is very conspicuous.

March 1977 Again, coverage for this month is quite good with two untied passes in the southern reaches. The Gulf Stream is readily observed. The depression at Long Bay seen in the last few months has now moved northward into Onslow Bay. A noticeable Charleston Bump is shown immediately west of a cold water eddy located at 30.5° N, 281.5° E.

April 1977 Coverage for this month is excellent, due not only to a large number of passes but also to the spacing of these passes. The Gulf Stream is well defined with a very interesting loop at about 30° N, 279.5° E. The depression off Onslow Bay has moved farther north and has intensified. The Charleston Bump is shown much farther out at sea than ever observed. It is shown at about 30° N, 282° E rather than at a more customary 30.5° N, 281° E.

May 1977 Large spaces between south-to-north passes reduce the quality of this month's data. The Gulf Stream is not readily followed in its entirety due to a large Charleston Bump which could be due to the lack of passes in that area. The depression off Onslow Bay has again moved south to the proximity of Long Bay.

June 1977 The month of June is also of poor quality in coverage due to the poor spacing of the passes. The Charleston Bump appears as a large elongated feature extending well offshore. The depression off Long Bay has now intensified.

July 1977 Good coverage for this month is provided by an adequate supply of south-to-north passes crossing the north-to-south passes which lack a pass through the center of the area. The topographic map shows a well developed Gulf Stream, the Charleston Bump and the Long Bay depression. No eddies are visible.

August 1977 A good spacing of passes provides very good coverage for this month. The Gulf Stream is well described and so is the Charleston Bump. A noticeable feature is what appears to be a cold eddy just east of the Bump and located at about 30.5° N, 281° E. This depression is about 60 cm deep.

September 1977 Coverage for this month is only fair, mainly because there are only three south-to-north passes and these are somewhat north of center. The topographic map shows a well developed Gulf Stream but it is not well described south of about 30° since there is no coverage there; thus, the values are interpolated.

October 1977 Passes within this month are well spaced; unfortunately, some of the south-to-north passes stop short of the coastline. The Gulf Stream for this month presents an interesting anomaly at 30° N, 280.5° E. This anomaly, a bump of more than 40 cm in height, is well off the location of the Charleston Bump.

November 1977 Coverage for this month is adequate, but there is a large spacing between south-to-north passes. The topographic map reflects this void; the Gulf Stream is not continuous.

December 1977 The passes comprising this month are not only few, but their spacing yields only nine crossing points. The topographic map reflects this quality. In the southern reaches where there are six of the nine crossing points, the Gulf Stream is well defined. In the northern reaches, it is diffused.

January 1978 The lack of passes for this month, and the arrangement of these passes which yield only three crossings, result in a very poor topographic map. Only the very general circulation pattern can be identified.

February 1978 This is again, a poor month for coverage. Attention should be placed at the close contour at the extreme southern parts. These are the product of automatic interpolation due to a lack of data.

March 1978 The number of passes available for this month produces a slightly better coverage. Due to the lack of passes in the southern sections, the Gulf Stream is not modelled south of 32°. The most noticeable feature is the large depression off Long Bay.

April 1978 A good coverage is provided by a fairly dense spacing of north-to-south passes with only four north-to-south passes tying the system. The topographic map shows a Gulf Stream which is traceable throughout. A large depression off Long Bay is now accompanied by another depression off Onslow Bay.

May 1978 This is again a poorly covered month with poor quality due to the arrangement of passes. There is a very wide open space in the center of the region. The result of this coverage is readily apparent in the topographic map. The almost north-south contour lines in the center of the map should be interpreted with extreme caution as they may be the product of automatically interpolating values where there are no measurements.

June 1978 This month presents a good coverage as passes in both directions are well distributed. The topographic map shows a distinct Gulf Stream. A Charleston Bump is displaced south and the cold water depressions off Long and Onslow Bays are present.

The resulting three-year mean surface contains several interesting oceanographic and geodetic areas. First, the Gulf Stream is very well-defined from the Florida Straits to approximately 33° N including the effects due to the Charleston Bump just below 32° N. The lack of a streamline just east of Cape Hatteras is rather puzzling. Two explanations are possible. First, it is believed that the reference geoid is not able to resolve the steep gravity anomaly in that region where the Gulf Stream also tends to hug the shelf break. Second, just southeast of Cape Hatteras there seems to be a semi-permanent eddy field produced by the coalescing eddies (ref. 23). In a survey of the maps published by NOAA in GULFSTREAM covering the same period, eddies were found to exist in this area the majority of the time. This may be responsible for the depression southeast of Cape Hatteras and it may also cause the distortion of the contours that delineate the Gulf Stream. The relatively flat surface in the Sargasso Sea is as expected except for the dome centered at 27° N, 284° E. This large dome results from three different problems: the referenced geoid, the data processing, and a combination of pass distribution and

interpolation. First, the geoid has been found to read low by approximately 80 cm compared to an altimetric geoid derived by Marsh et al. (ref. 24). Second, sections of the northbound passes in the same area were edited when orienting the individual profiles. However, the edited sections were included in the creation of the surface map thus leading to the dome effect. And third, the east-west orientation of the southern streamline results from missing data in the Bahama Islands region. Those points were then interpolated using profiles on each side of the Islands to complete the gridded surface.

Significant Wave Height and Wind Speed Histograms

The monthly significant wave height and wind speed histograms produced during this study have been cursorily examined and found to be deficient in a statistical sense for characterizing the oceanic conditions on a month-to-month basis during the GEOS-3 data collection period. For the 36 months between July 1975, and June 1978, the number of measurements of wind speed per month in the South Atlantic Bight varied from 86 to 801. The average number of samples was 360 but there were 10 months when the number was less than 170. In each individual BLM sub-area the number would be of course much smaller. Additionally, the telemetry mode settings needed for the collection of SWH measurements were not programmed as often as were the settings needed for windspeed measurements. Hence, the number of samples available for the monthly histograms would be less for the SWH data set. For wind speed analysis, all BLM areas are combined into one which yields, for the worst month a total of 86 samples. The credibility of that month's histogram can be characterized as follows. Given the inclination of the satellite's orbit, the maximum length of a GEOS-3 groundtrack through the BLM composite area is about 800 km. For a sampling period of 3.2 seconds and an effective groundspeed of approximately 7 km/sec, it is possible that about 86 samples be taken during a single orbit. With only 86 samples in a histogram, it is possible that all data were collected from only a few orbits. If these occurred during atypical weather conditions then that month's data is not characteristic of the entire month's sea conditions.

Several of the monthly data sets are most likely undersampled. Others are undoubtedly truly representative of the environmental conditions. To remain conservative, it is apparent that averaging for more than one month is desirable. But, for maximum impact it is desirable that the GEOS-3 data be used to describe the sea state and wind speed in a continuous fashion for the entire GEOS-3 lifetime. To accomplish this, and to superficially characterize the effects of geographic location within the South Atlantic Bight the following three kinds of analysis have been performed in which spatial and temporal averaging were employed.

The average monthly histograms have been studied and they reveal the annual variations in significant wave height and wind speed for the composite BLM area. Figure 19 shows the variation of the mean and variance for these histograms. Both means are smallest in

the summer and largest in the winter as expected. The distribution mean for wind speed varies through a much larger range than does the SWH mean. This will be discussed in more detail below. The SWH and wind speed distribution variances seem to undergo similar cycles through the year but a physical explanation of their behavior will be discussed also in the description of the second analysis.

With only about three years of data available for analysis, it is reasonable to assume that the year-to-year variability of the environmental conditions is large enough to render the preceding average annual cycle less than optimum. Therefore, to keep the sample size of the SWH and wind speed histograms sufficiently large and yet still show the year-to-year fluctuations, a sliding three-month window was used in a second kind of analysis. The behavior of the means of the resulting SWH and wind speed distributions is shown in figure 20. The annual cycles are clearly seen. Although there is a double maximum in the SWH variability in the fall and winter of 1978, these cycles are generally single-peaked. The small irregularities seen from year to year are, of course, masked in the annual average cycle shown in figure 19. Figure 21 shows the corresponding variances for the sliding window distributions. The SWH histogram variance does not undergo well-defined yearly cycles, perhaps because the range of sea states common to the South Atlantic Bight is small. The distribution for mid-winter may be only 30-40 cm wider than is the distribution for mid-summer. This, in turn, is only a fraction of the width of the bins used in these analyses. For the wind speed data, however, the situation is much clearer. The variance is minimal in mid-summer, but there appears to be two maxima for each year's data record. These are centered around the maxima of the distribution means shown in figure 20. This can be interpreted in the following fashion: when the large-scale weather patterns change in the fall, there are periods of time in which the environmental conditions still resemble those of the summer. In between, however, storm systems begin to move through the area increasing the wind speed which, if substained for a sufficient period of time, also increases the SWH. Hence, the range of SWH and wind speed values occurring in this season is increased reflecting these two different weather regimes. In terms of the wind speed histogram, at least, this appears as an increase in the variance. By mid-winter, there are fewer and fewer mild periods so that although the mean wind speed continues to increase to its maximum, the variance drops. In springtime, the process is repeated in the reverse direction.

The final kind of analysis pertains to the spatial variability of SWH and wind speed. To avoid undersampling, it is decided that each BLM area can be studied if sufficient temporal averaging is done. Hence, the monthly histograms for each area are added to those from other years, and the means of the resulting average monthly histograms are plotted in figure 22 for the wind speed data. For SWH, no detectable difference in distribution means or variances are found between the BLM areas. For wind speed there is an apparent difference. The mean wind speed for area 3 consistently exceeded the means for

the other areas. No explanation will be tendered but the well-known prevalence of high winds near Cape Hatteras, North Carolina suggests that the meteorological conditions of the region are accurately reflected in these histogram analyses. The GEOS-3 data set used in this study can easily be analyzed in other ways and in various degrees of detail. The analyses above are merely examples of the kind of climatological studies that are possible.

CONCLUSIONS

The analysis of long-term altimeter data for sea surface topographies leads to the following conclusions. Due to the various uncertainties in geoid, orbit, and intrinsic noises, the mean surface topographic maps are to be evaluated with extreme caution. Among the uncertainties, the accuracy of the geoid is the most critical element because the geoid anomalies can have, not only the same wavelength as ocean dynamic phenomena, but the geoid signal magnitude can also be much higher. The difference between the long-term (three years) and any short-term mean (one month) reveals the changes of Gulf Stream path and some eddy movements. In principle, the uncertainty of the geoid should not be a problem here, but it still causes difficulty. In this case, difficulty comes from the data density from the altimeter. The long-term mean is produced by using the average of all the adjusted heights within a 1/2 degree square. There could be considerable geoid change within such an area. The averaging process reduces the true variations.

Furthermore, it is apparent that seasonal and annual variations in significant wave height and wind speed are readily detectable using waveform data from satellite radar altimetry. This is demonstrated with GEOS-3 measurements over the South Atlantic Bight for this study. Different degrees of spatial and temporal averaging are used to ensure that undersampling is avoided. On the smallest spatial scale tested, some differences in the resultant wind speed distributions are found to agree with the known climatology of the area. No wave height spatial difference is detected, an expected observation given the low wave heights found in the South Atlantic Bight.

ACKNOWLEDGEMENT

The study was funded by the Department of Interior, Bureau of Land Management, New Orleans Outer Continental Shelf Office, under interagency agreement AA551-IA8-39. The authors wish to thank Mrs. J. B. Merrill for typing the manuscript.

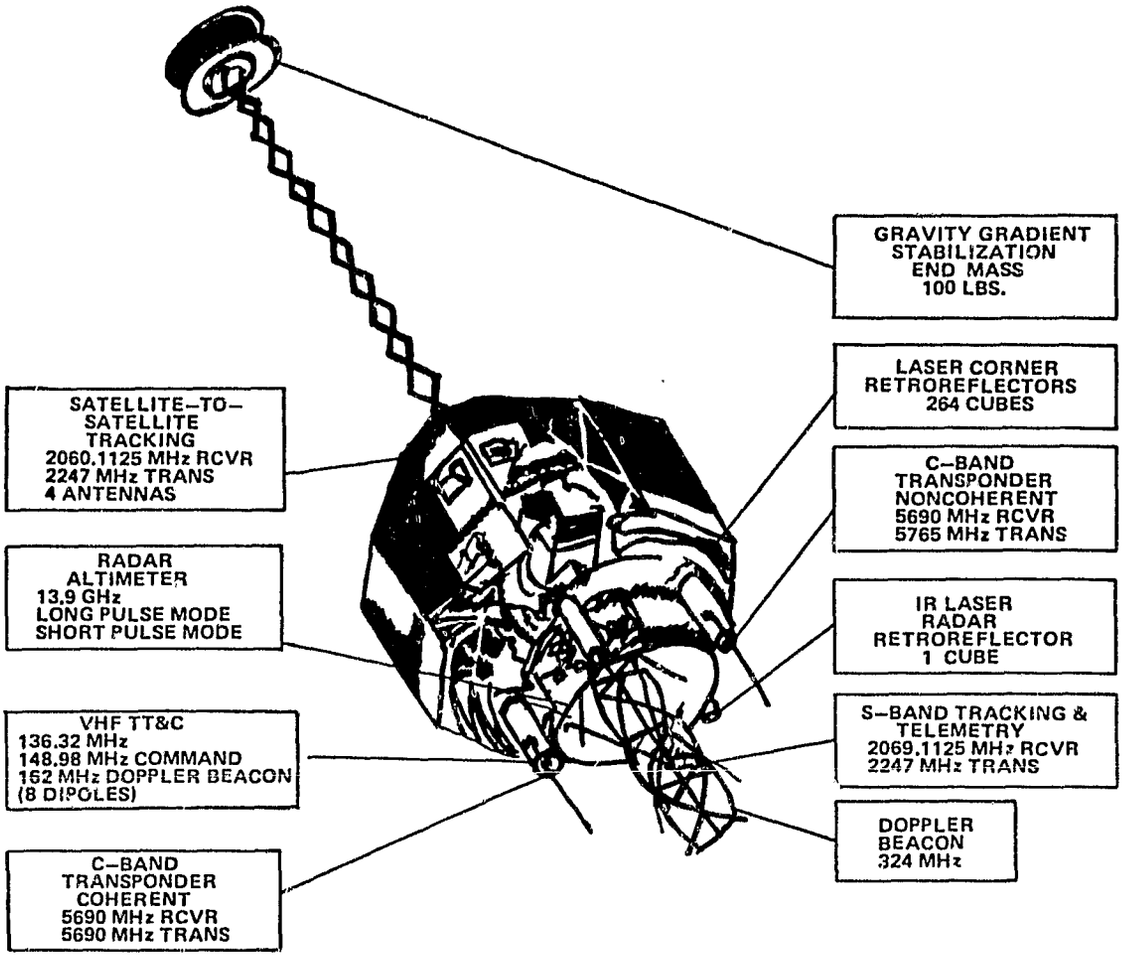

Figure 1. GEOS-3 Spacecraft

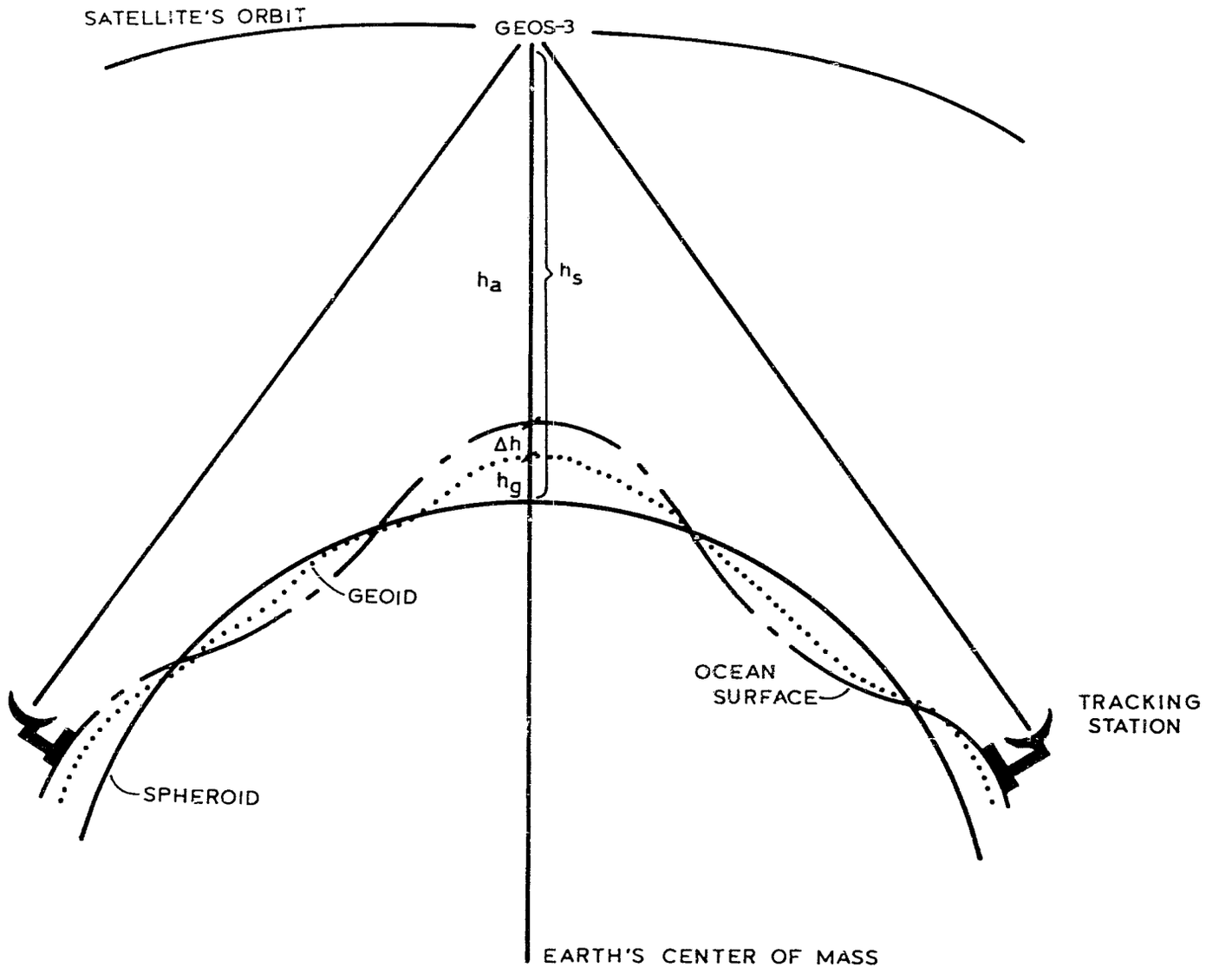

Figure 2. GEOS-3 Radar Altimeter Geometry

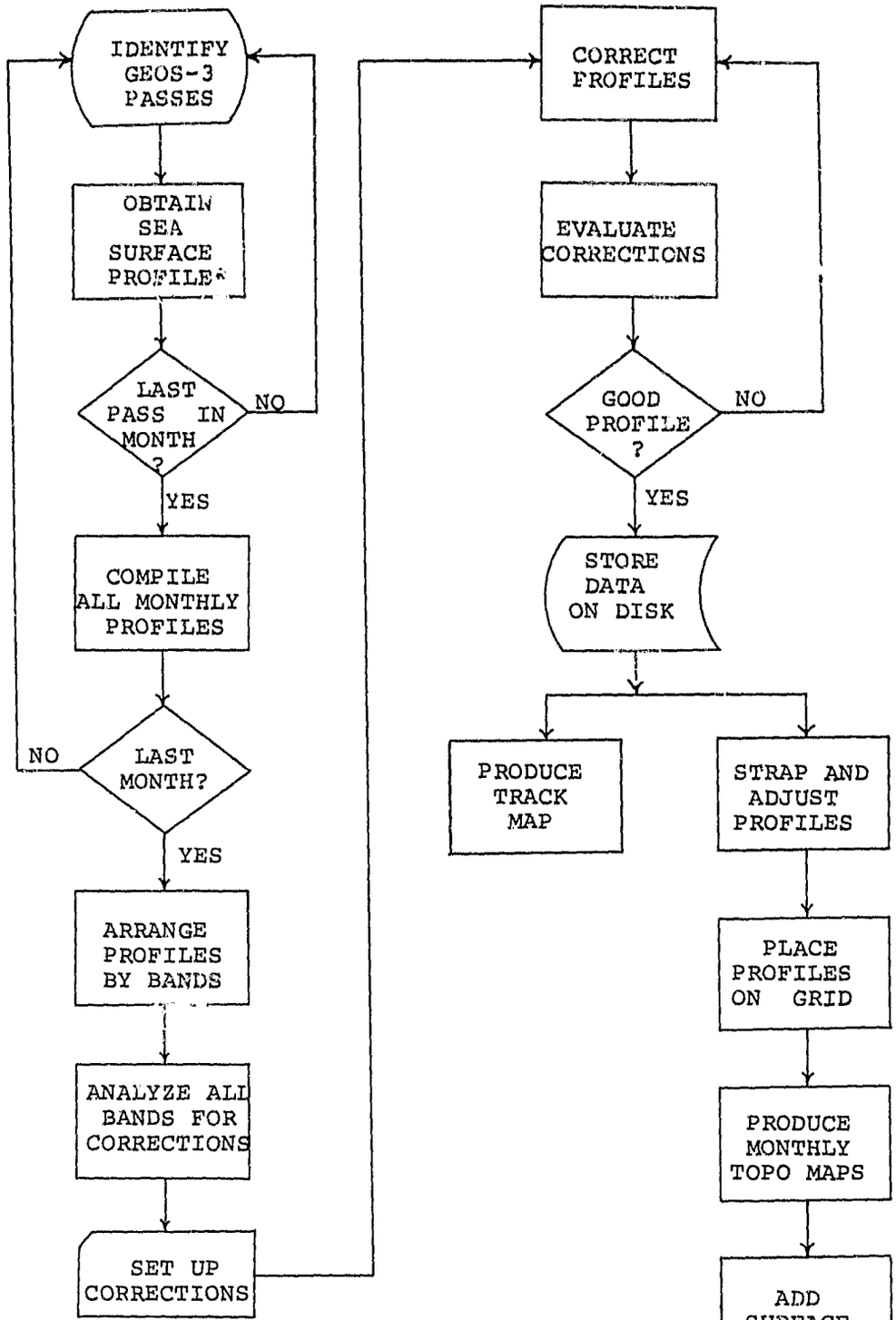

*See preliminary data processing.

Figure 3. Overall Sea Surface Height Data Processing

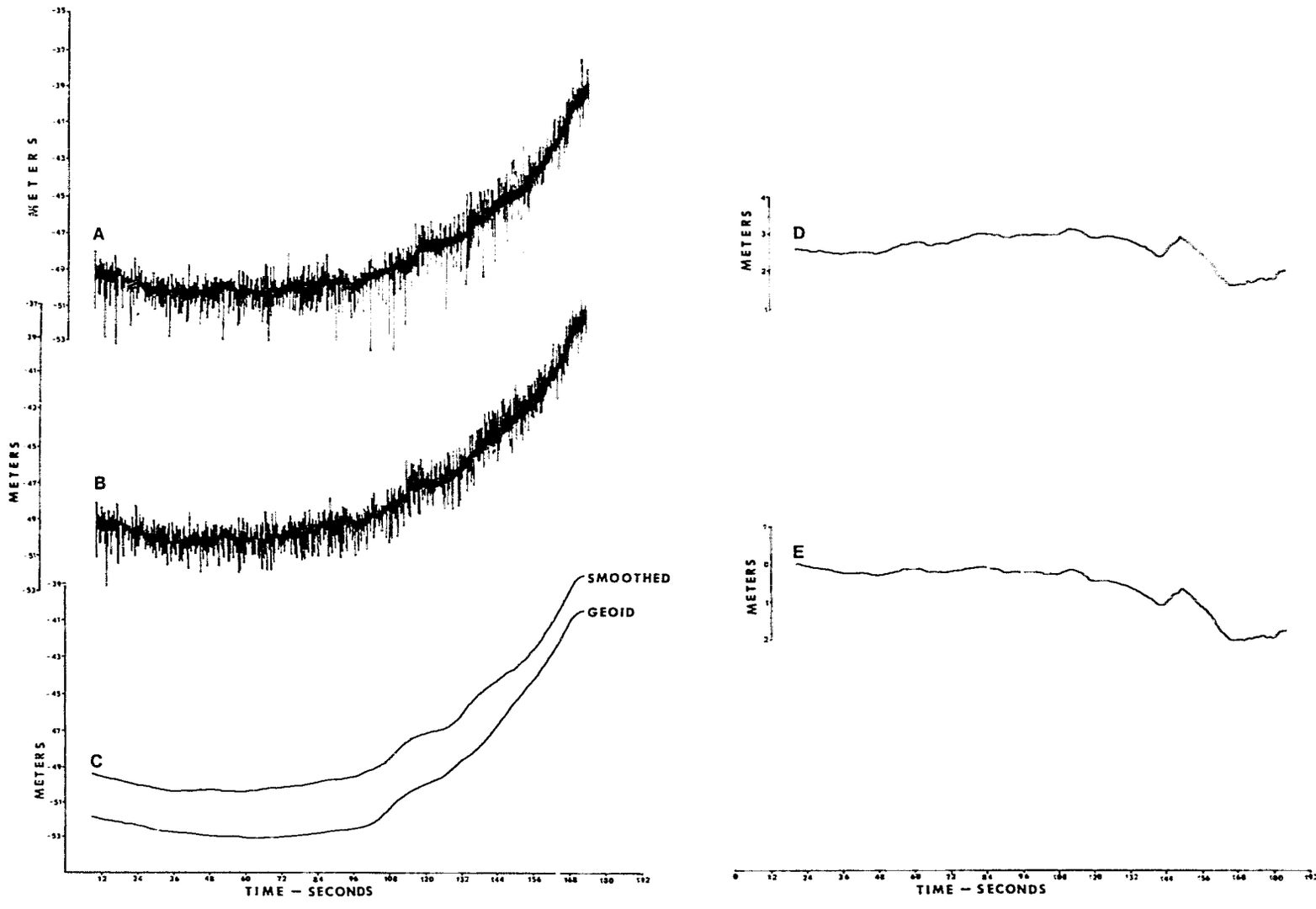

Figure 4. Preliminary Data Processing by DOS Computer Program

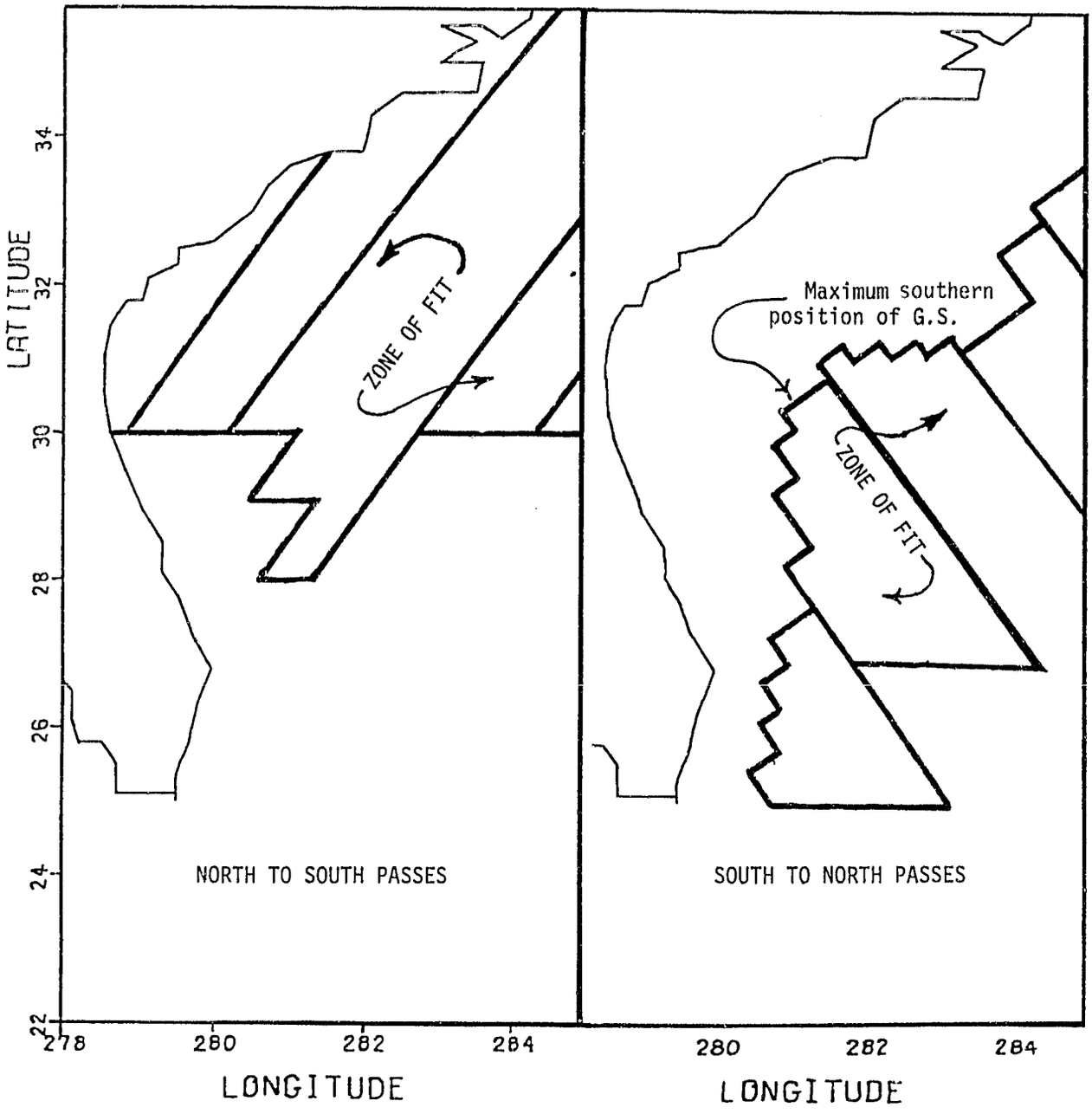

Figure 5. Bands of Sub-satellite Tracks Developed to Correct Sea Surface Profiles

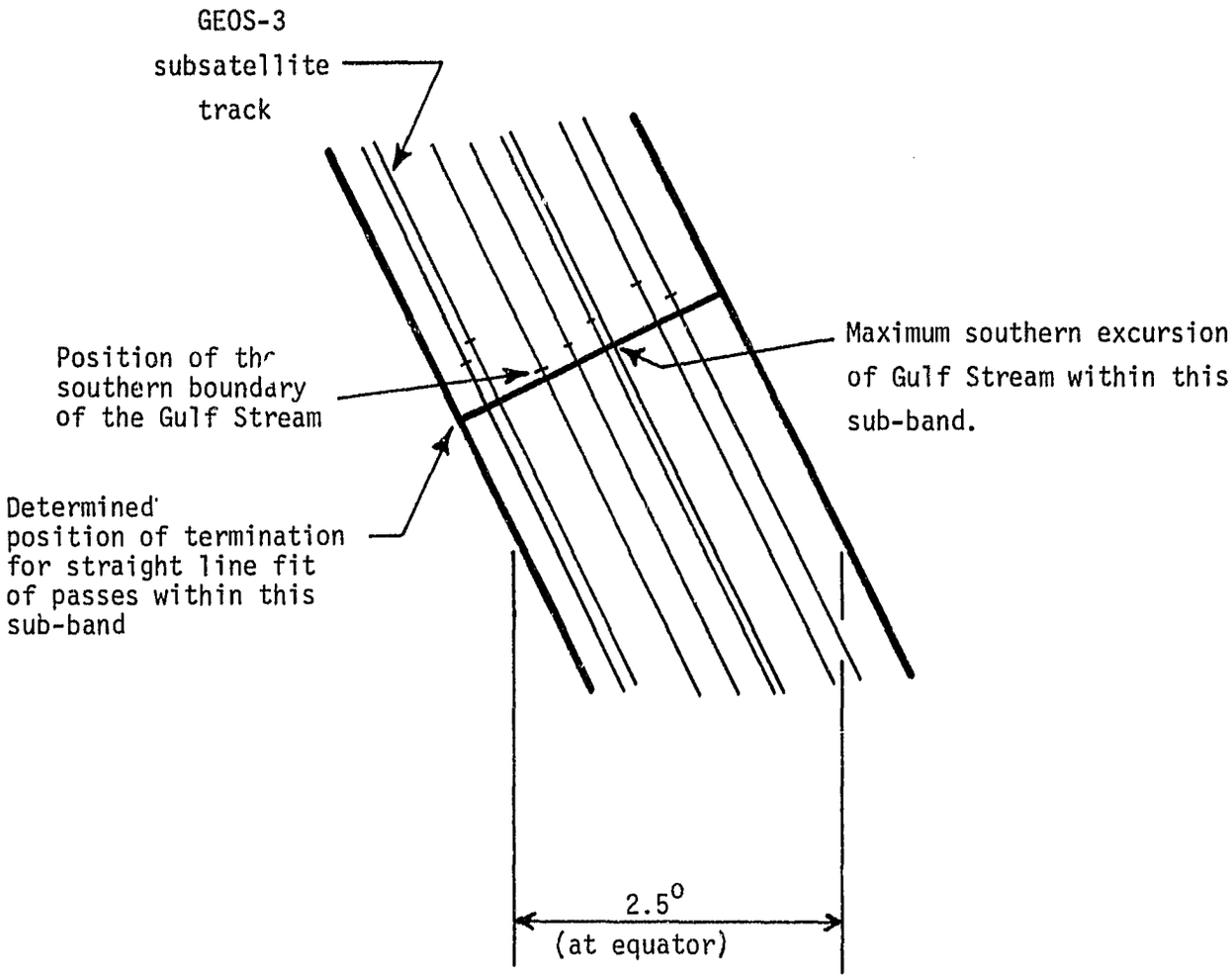

Figure 6. Sub-band Analysis for the Determination of the Position of the Termination of the Straight Line Fit

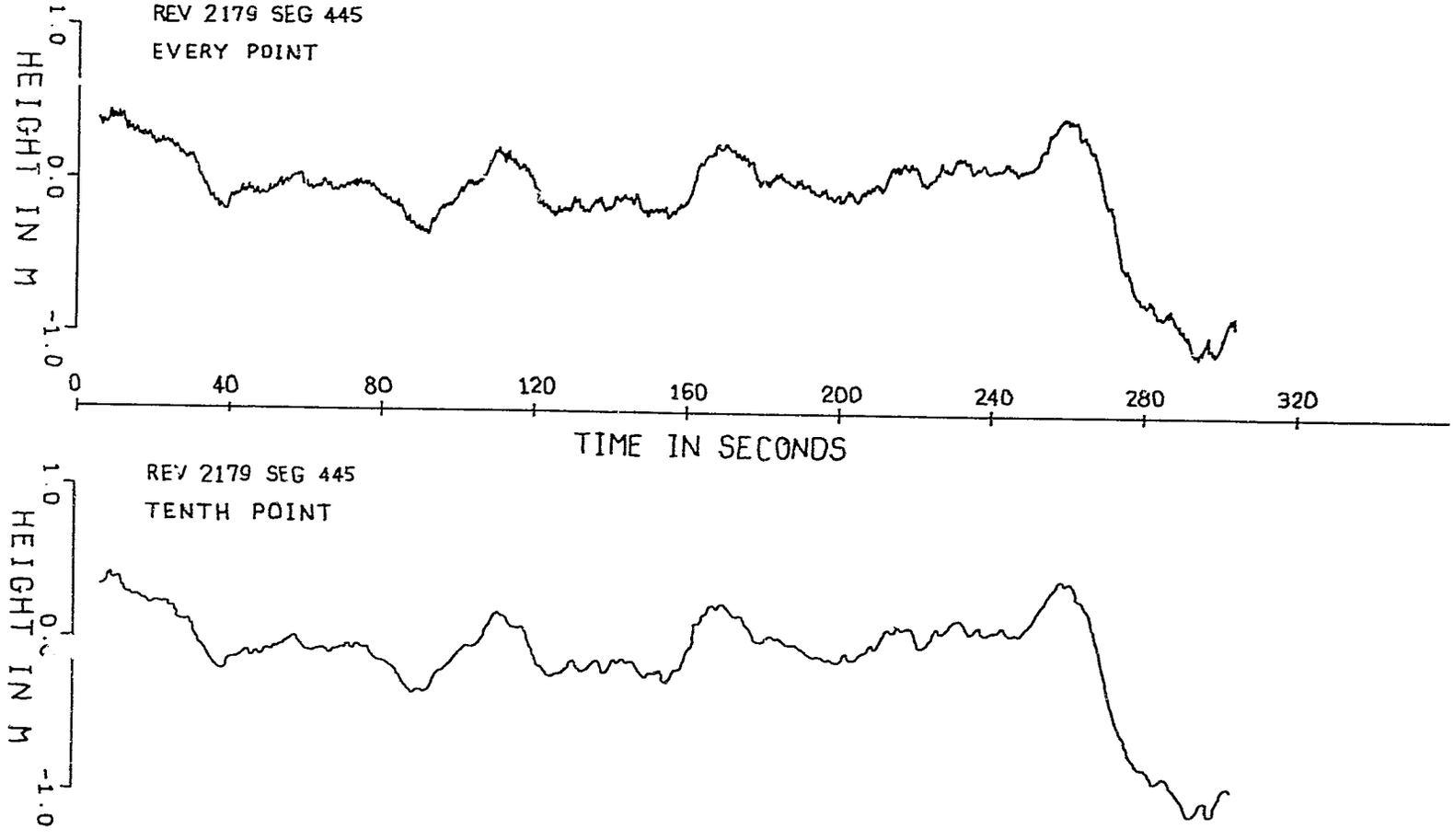

Figure 7. Comparison of Full and Thinned-out Sea Surface Profile

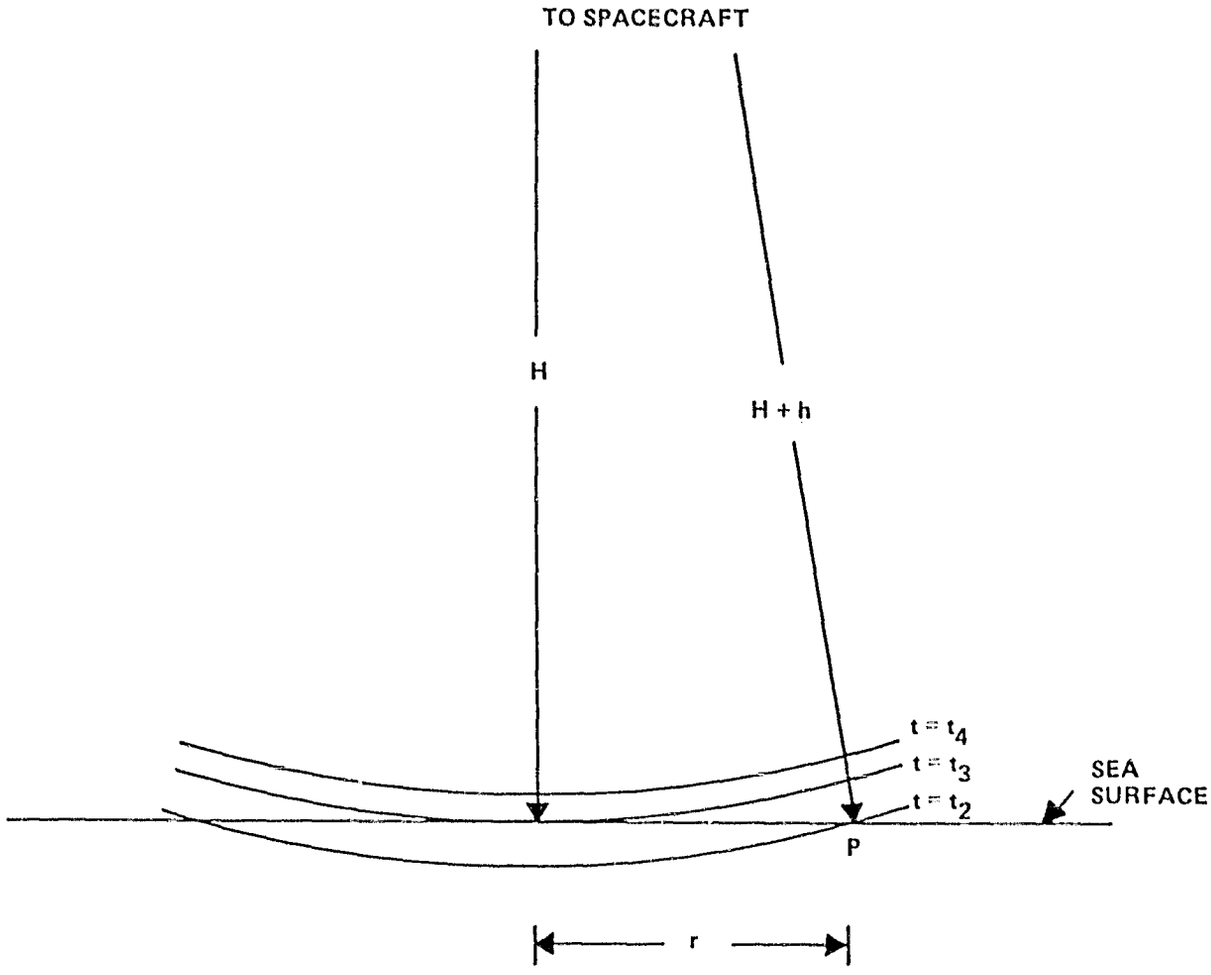

Figure 8. Square Pulse Impinging Upon a Flat Sea Surface

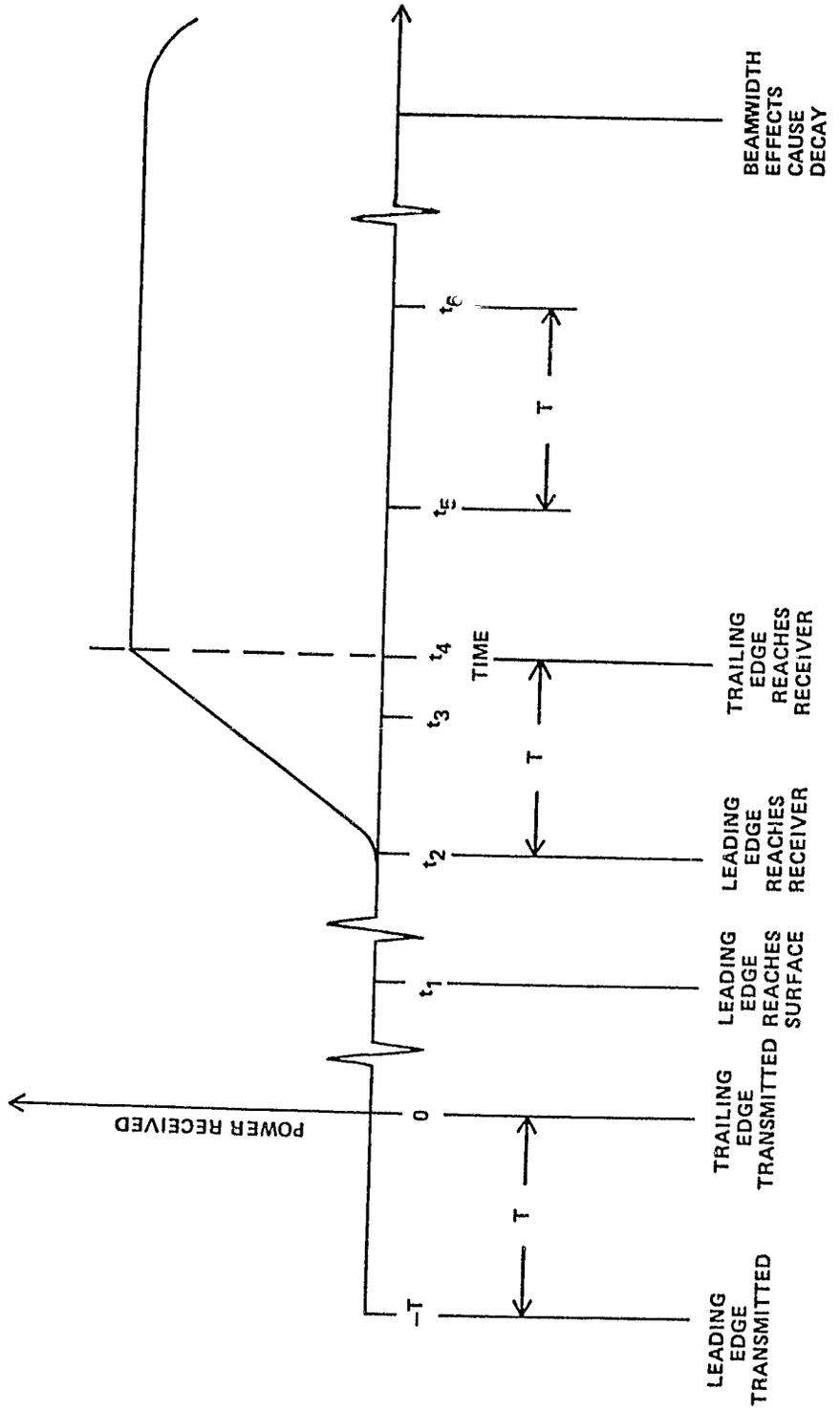

Figure 9. Idealized Mean Return Pulse Shape

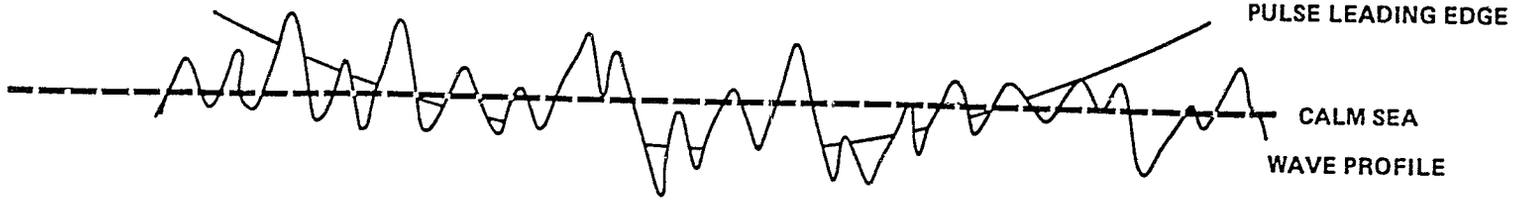

Figure 10. Square Pulse Impinging Upon Rough Sea Surface

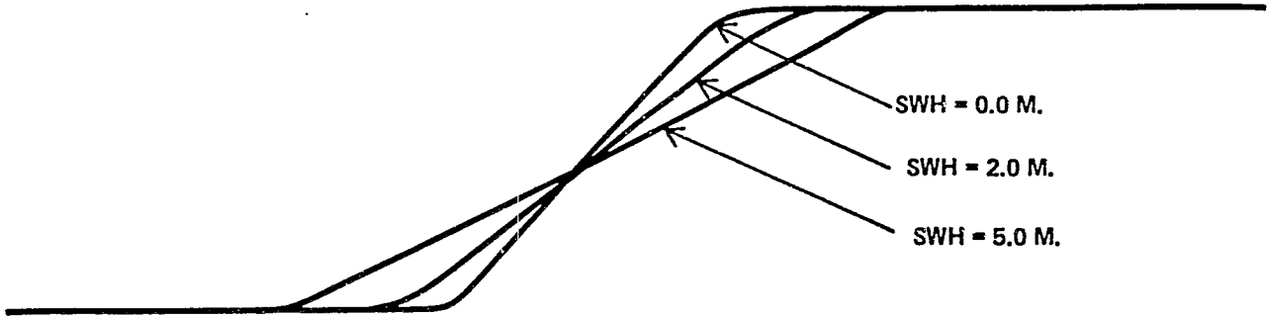

Figure 11. Idealized Mean Return Pulse Shape for Several Values of SWH

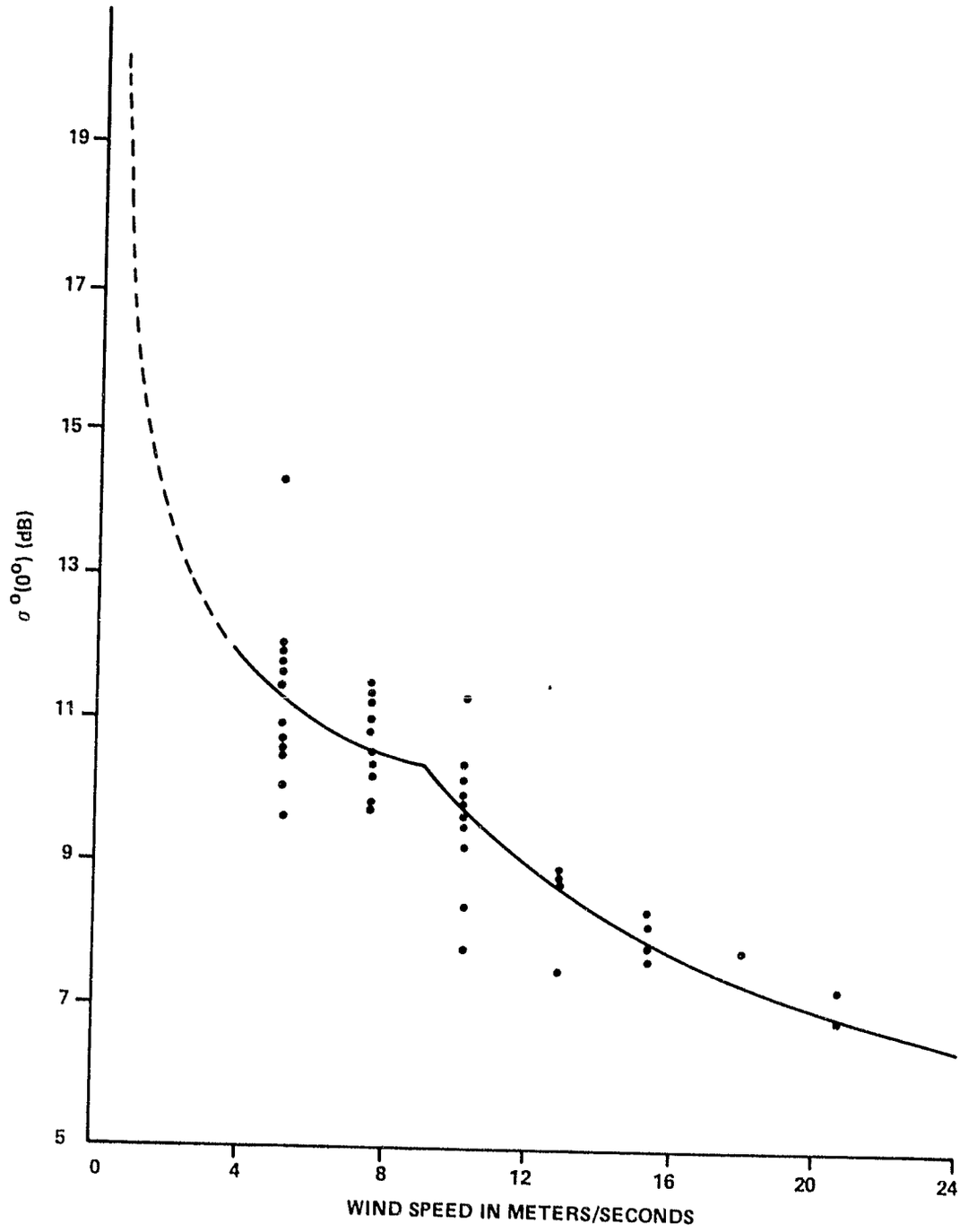

Figure 12. σ°(0°) Versus Wind Speed

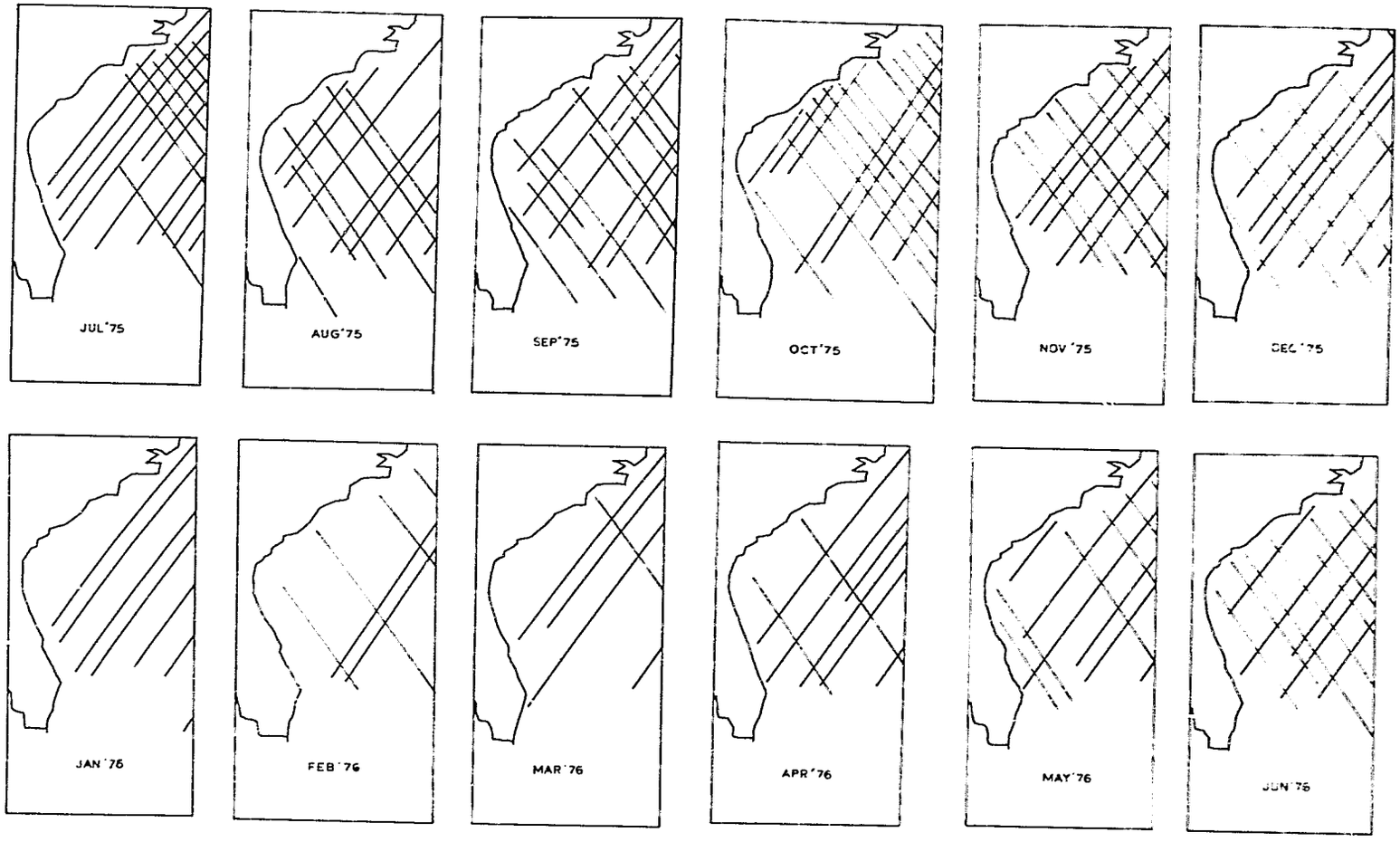

Figure 13. GEOS-3 Sub-satellite Tracks of Passes Used for the Monthly Sea Surface Topography July 1975 to June 1976

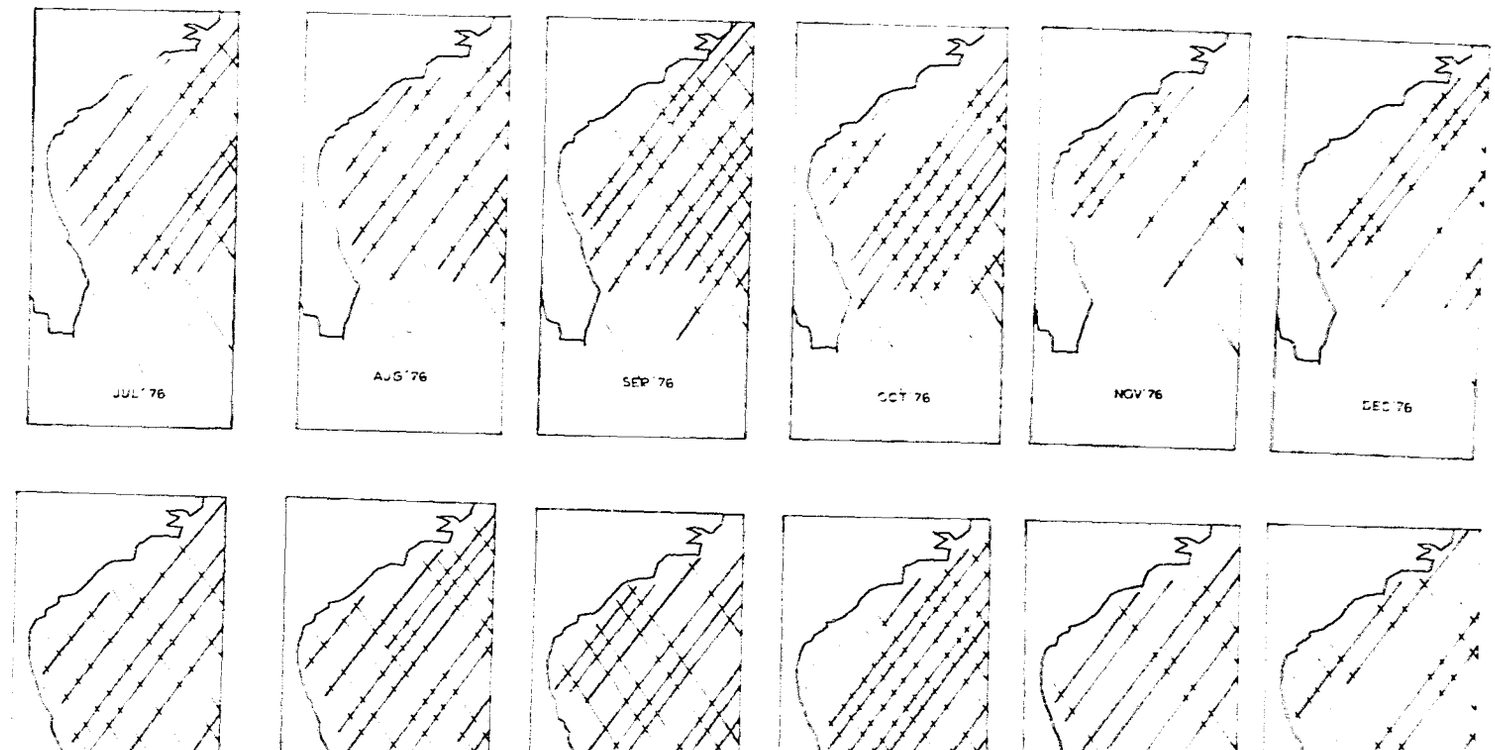

Figure 14. GEOS-3 Sub-satellite Tracks of Passes Used for the Monthly Sea Surface Topography July 1976 to June 1977

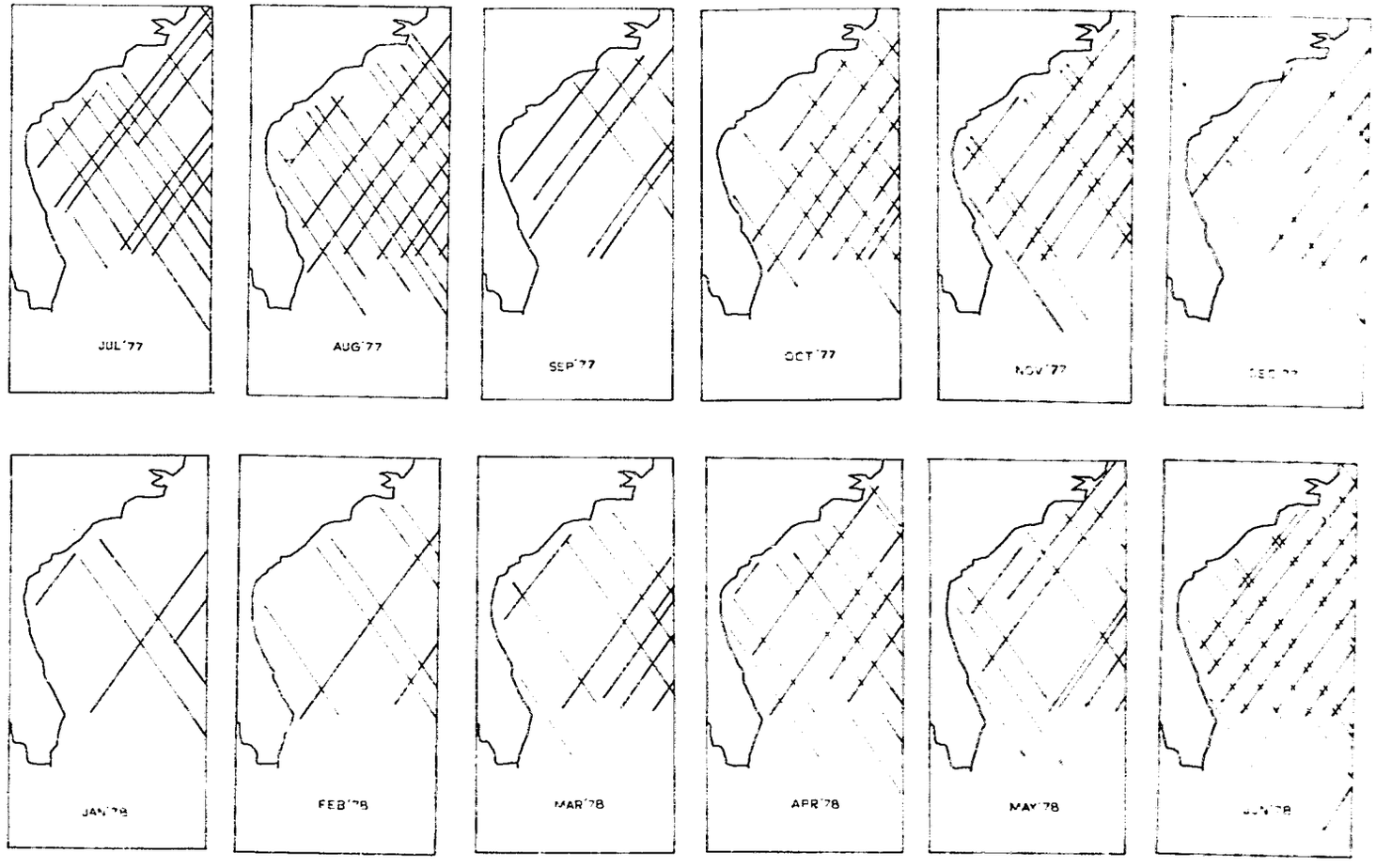

Figure 15. GEOS-3 Sub-satellite Tracks of Passes Used for the Monthly Sea Surface Topography July 1977 to June 1978

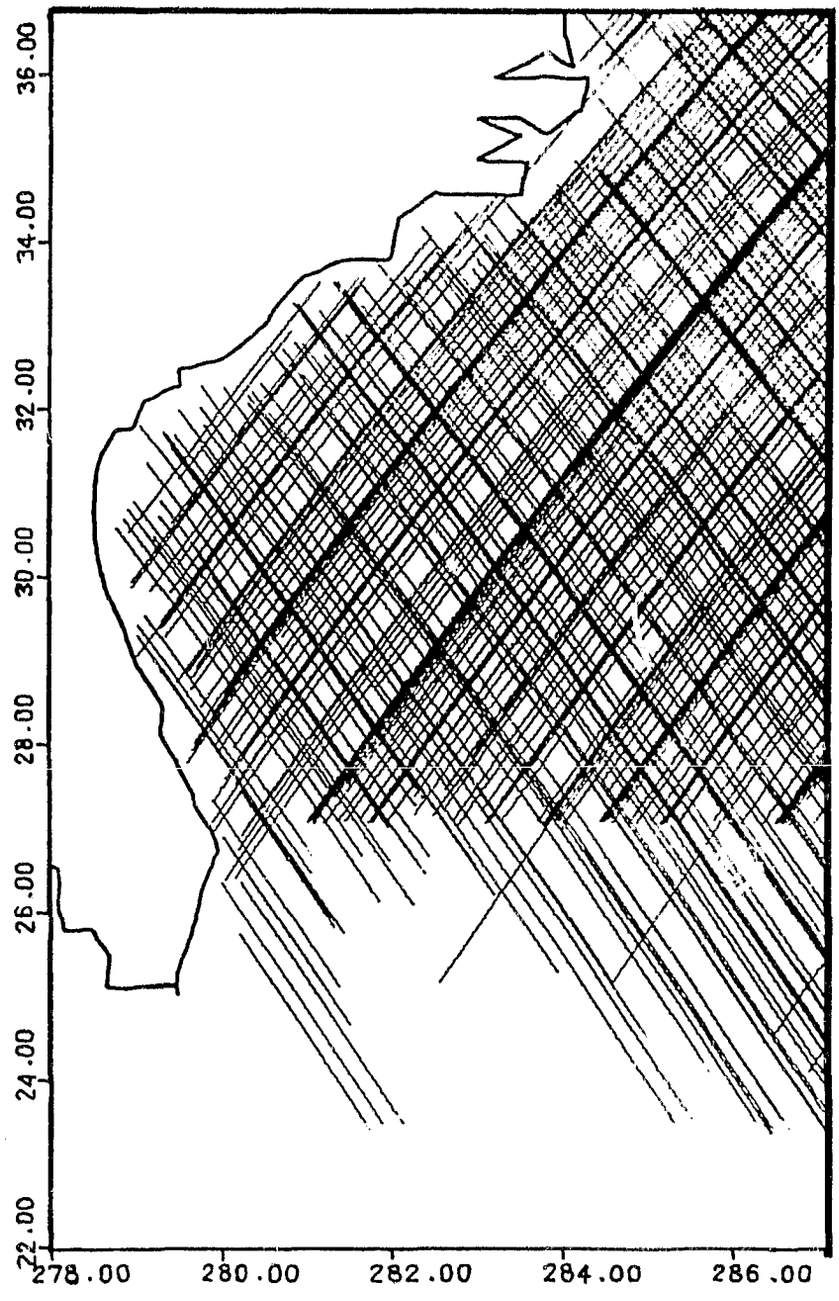

Figure 16. GEOS-3 Sub-satellite Tracks Used for Sea Surface Topography Three-Year Mean

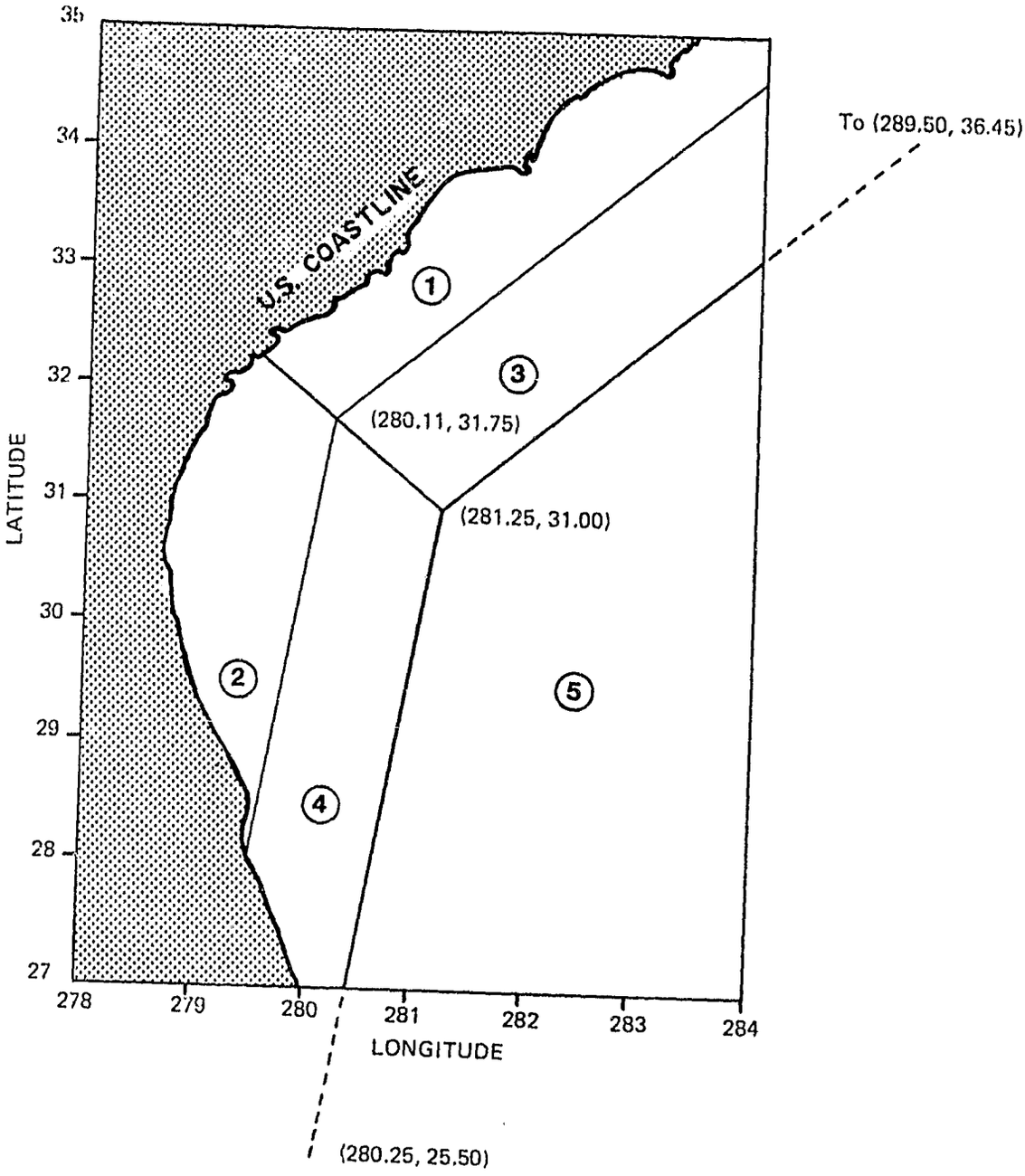

Figure 17. BLM SWH and Wind Speed Investigation Areas

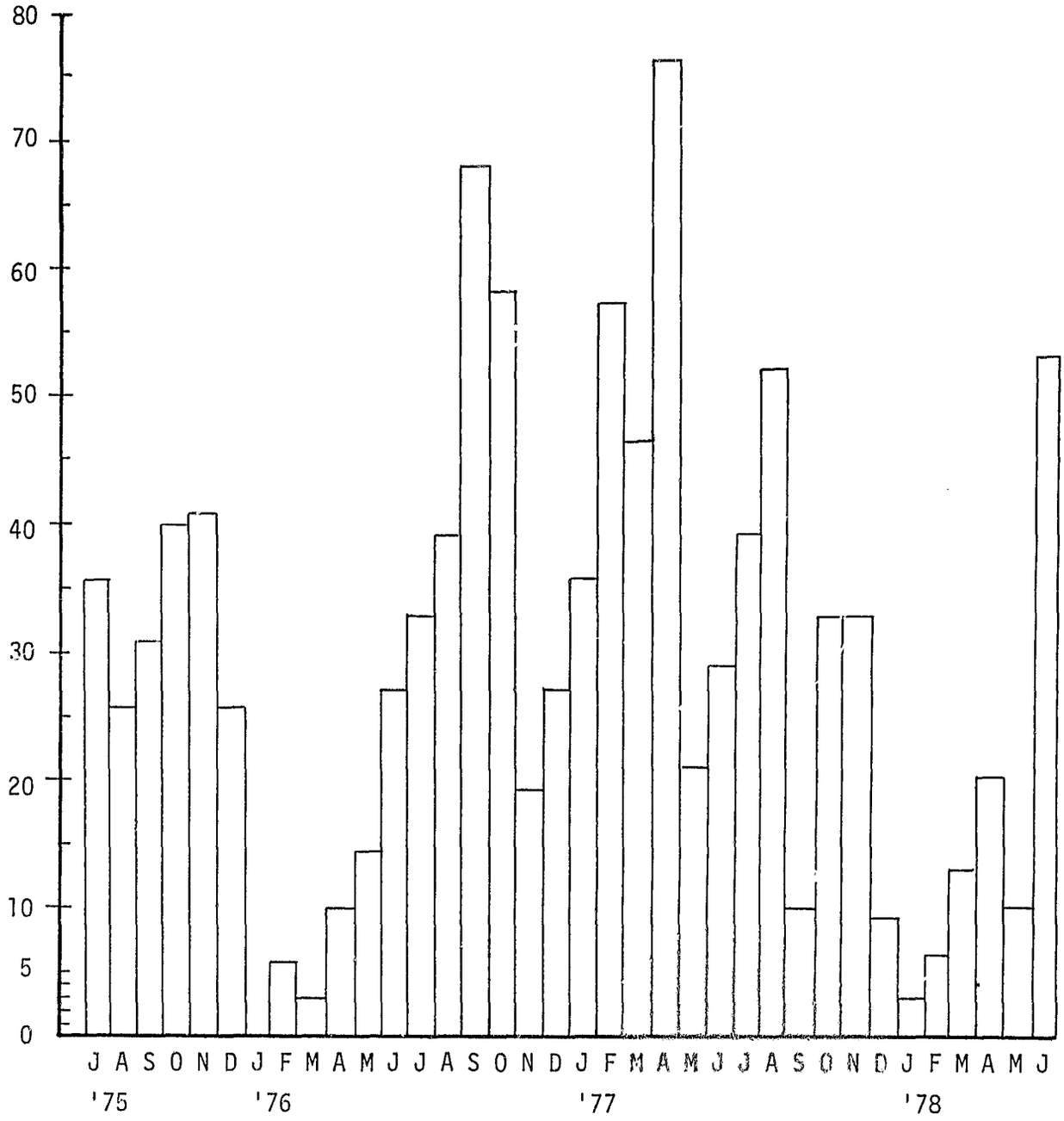

Figure 18. Monthly Frequency Distribution of the Number GEOS-3 Crossings Over the Study Area

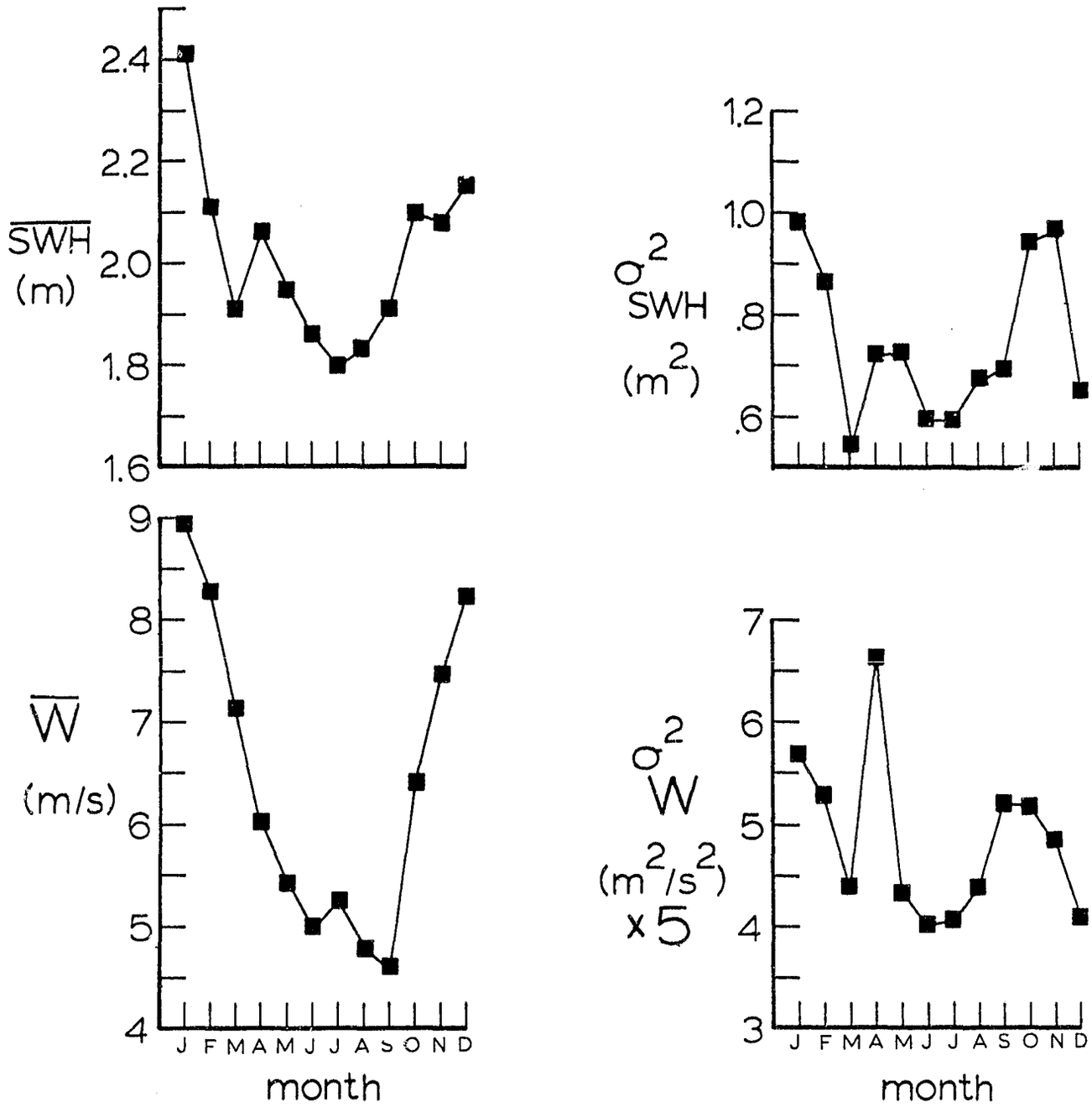

Figure 19. Means and Variances for the Average Monthly Significant Wave Height ($\overline{SWH}$) and Mean Wind Speed ($\overline{W}$) Distributions for the GEOS-3 Data Set

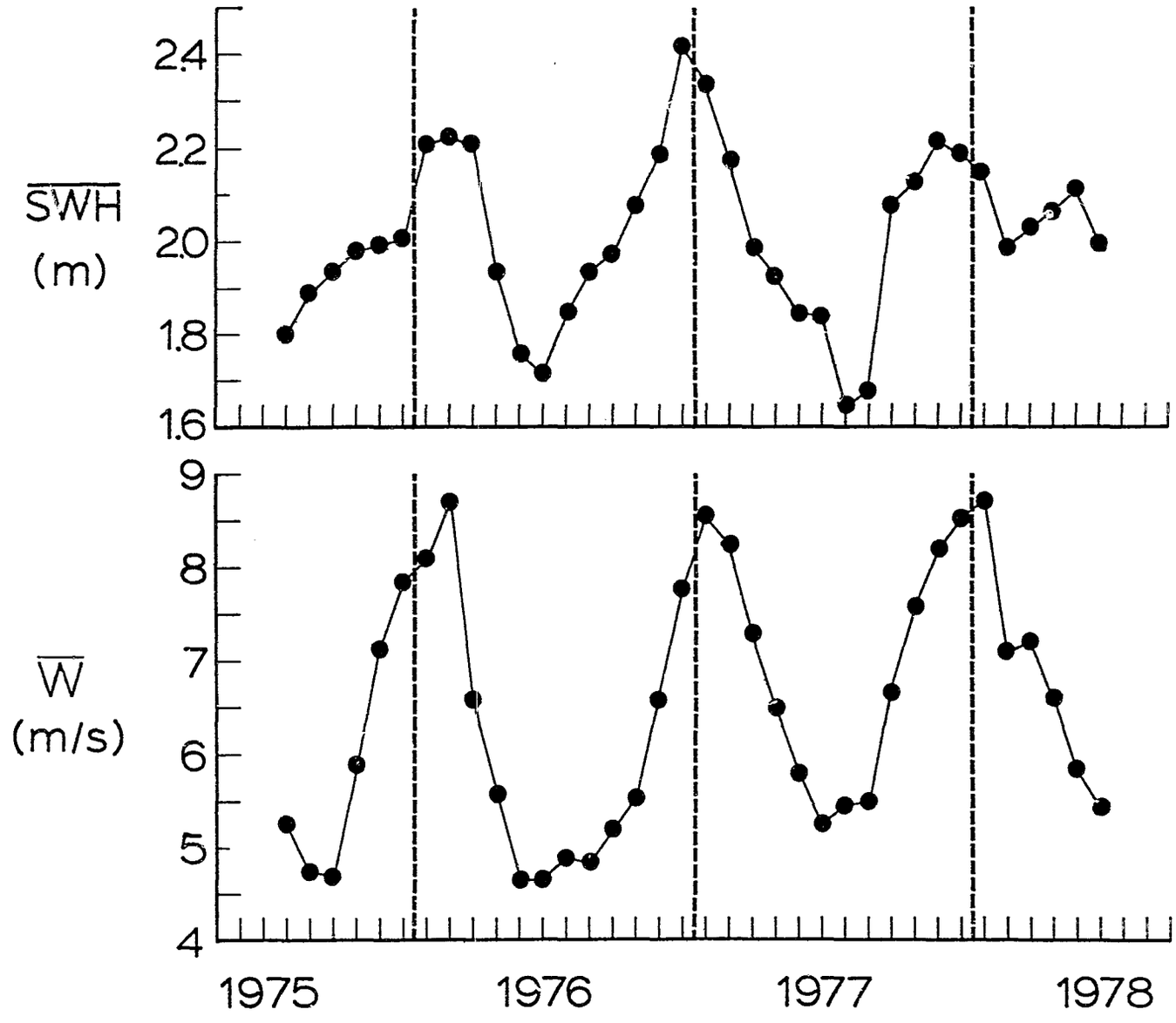

Figure 20. Monthly Variation of the Mean Significant Wave Height ($\overline{SWH}$) and Mean Wind Speed ($\overline{W}$) Distributions for the GEOS-3 Data Set

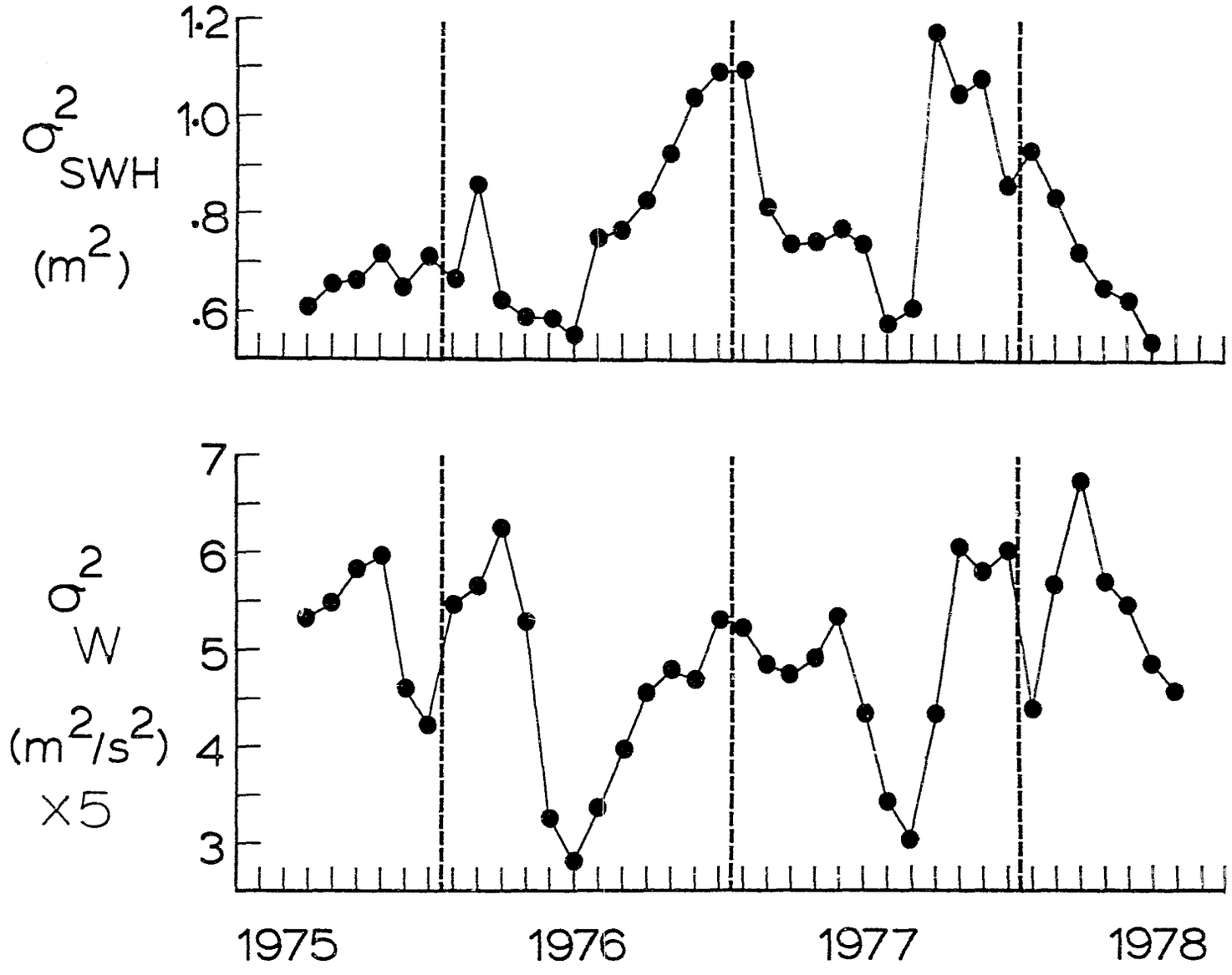

Figure 21. Monthly Variation of the Significant Wave Height Variance (σSWH) and Wind Speed Variance Distributions (σW) for the GEOS-3 Data Set

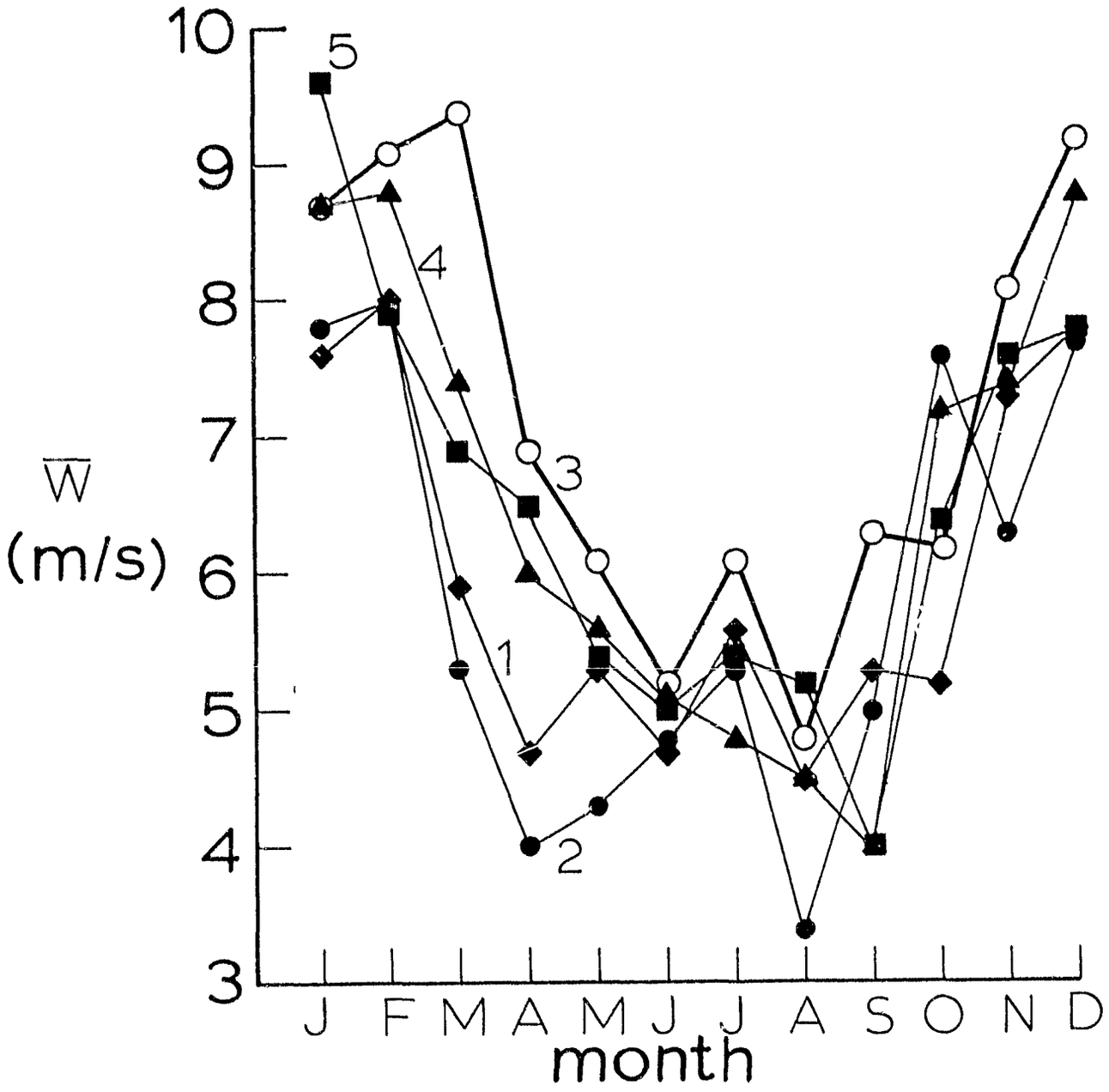

Figure 22. The Average Monthly Mean Wind Speed ($\overline{W}$) Distribution for each BLM Area

REFERENCES

1. Hofmeister, F. L., B. N. Keeney, T. W. Godbey and R. T. Berg: Design Error Analysis of the GEOS-C Radar Altimeter. Utica, New York, General Electric Co., Aerospace Electronics Systems Dept., 1975
2. Hayne, G. S., L. S. Miller and G. S. Brown: Altimeter Waveform Software Design. NASA CR-141419, 1977
3. Stommel, H.: The Gulf Stream: A Physical and Dynamical Description. 2nd ed., Berkeley, University of California Press, 1965
4. Fofonoff, N. P.: Dynamics of Ocean Currents. The Sea, 1, M. N. Hill, Ed., Interscience, 1962
5. Leitao, C. D., N. E. Huang and C. G. Parra: Remote Sensing of Gulf Stream Using GEOS-3 Radar Altimeter. NASA TP-1209, 1978
6. Mader, G. L.: A Revised 5' Gravimetric Geoid and Associated Errors for the North Atlantic Calibration Area. NASA CR-156851, 1979
7. Allen, C. P., and C. F. Martin: SEAHT, A Computer Program for the Use of Intersecting Arcs of Altimeter Data for Sea Surface Height Refinement. NASA CR-141432, 1977
8. Walsh, E. J., E. A. Uliana and B. S. Yaplee: Ocean Wave Heights Measured by a High Resolution Pulse - Limited Radar Altimeter. Boundary-Layer Meteorology, v. 13, pp. 263-276, 1978
9. Walsh, E. J.: Extraction of Ocean Wave Height and Dominant Wavelength from GEOS-3 Altimeter Data. J. Geophys Res, v. 84, no. B8, pp. 4003-4010, 1979
10. Parsons, C. L.: GEOS-3 Wave Height Measurements: An Assessment During High Sea State Conditions in the North Atlantic. J. Geophys Res, v. 84, no. B8, pp. 4011-4020, 1979
11. Fedor, L. S., T. W. Godbey, J. F. R. Gower, R. Guptill, G. S. Hayne, C. L. Rufenach, and E. J. Walsh: Satellite Altimeter Measurements of Sea State - An Algorithm Comparison. J. Geophys Res, v. 84, no. B8, pp. 3991-4001, 1979
12. Gower, J. F. R.: The Computation of Ocean Wave Heights from GEOS-3 Satellite Radar Altimeter Data. Remote Sensing of Env., v. 8, pp. 97-114, 1979
13. Pierson, W. J. and R. E. Salfi: A Brief Summary of Verification Results for the Spectral Ocean Wave Model by Means of Wave Height Measurements Obtained by GEOS-3. J. Geophys Res, v. 84, no. B8, 4029-4040, 1979
14. McMillan, J. D. and N. A. Roy: A Comparison of GEOS-3 H 1/3 Data with National Buoy Data. Paper presented at the Final GEOS-3 Investigators Meeting, New Orleans, La., 1977

15. Brown, G. S.: Backscattering from a Gaussian Distributed Perfectly Conducting, Rough Surface. NASA CR-141424, 1977

16. Brown, G. S.: The Average Impulse Response of a Rough Surface and Its Applications. IEEE Trans. on Antennas and Propagation, v. AP-25, no. 1, pp. 67-74, 1977 (Also appears in IEEE Trans. Oceanic Engineering, v. OE-2, no. 1, pp. 67-74, 1977)

17. Pierson, W. J. and E. Mehr: Average Return Pulse Form and Bias for the S193 Radar Altimeter on Skylab as a Function of Wave Conditions. In: The Use of Artificial Satellites for Geodesy, S. W. Henrickson et al., ed., Geophysical Monograph Series, v. 15, pp. 217-226, 1972

18. Brown, G. S. and L. S. Miller: Final Report for Task D Under Engineering Studies Related to the GEOS-C Radar Altimeter. NASA CR-137462, 1977

19. Hayne, G. S.: Initial Development of a Method of Significant Waveheight Estimation for GEOS-III. NASA CR-141425, 1977

20. Anonymous: Geodynamics Experimental Ocean Satellite (GEOS-3) Near-Real-Time Significant Waveheight and Wind Speed Data System. NASA, Wallops Flight Center Report, 1978

21. Brown, G. S.: Estimation of Surface Wind Speeds Using Satellite-Borne Radar Measurements at Normal Incidence. J. Geophys Res, v. 84, no. B8, pp. 3974-3978, 1979

22. Brown, G. S. and W. J. Curry: The Estimation of Pointing Angle and σ^0 from GEOS-3 Radar Altimeter Measurement. NASA CR-141426, 1977

23. Lai, D. Y. and P. L. Richardson: Distribution and Movement of Gulf Stream Rings. J. Phys. Oceanog., v. 7, pp. 670-683, 1977

24. Marsh, J. G., G. H. Wyatt, T. V. Martin, J. J. McCarthy and P. S. Chovitz: Sea Surface Estimation in the North Atlantic Using GEOS-3 Altimeter Data. J. Marine Geodesy, (in press)

APPENDIX A

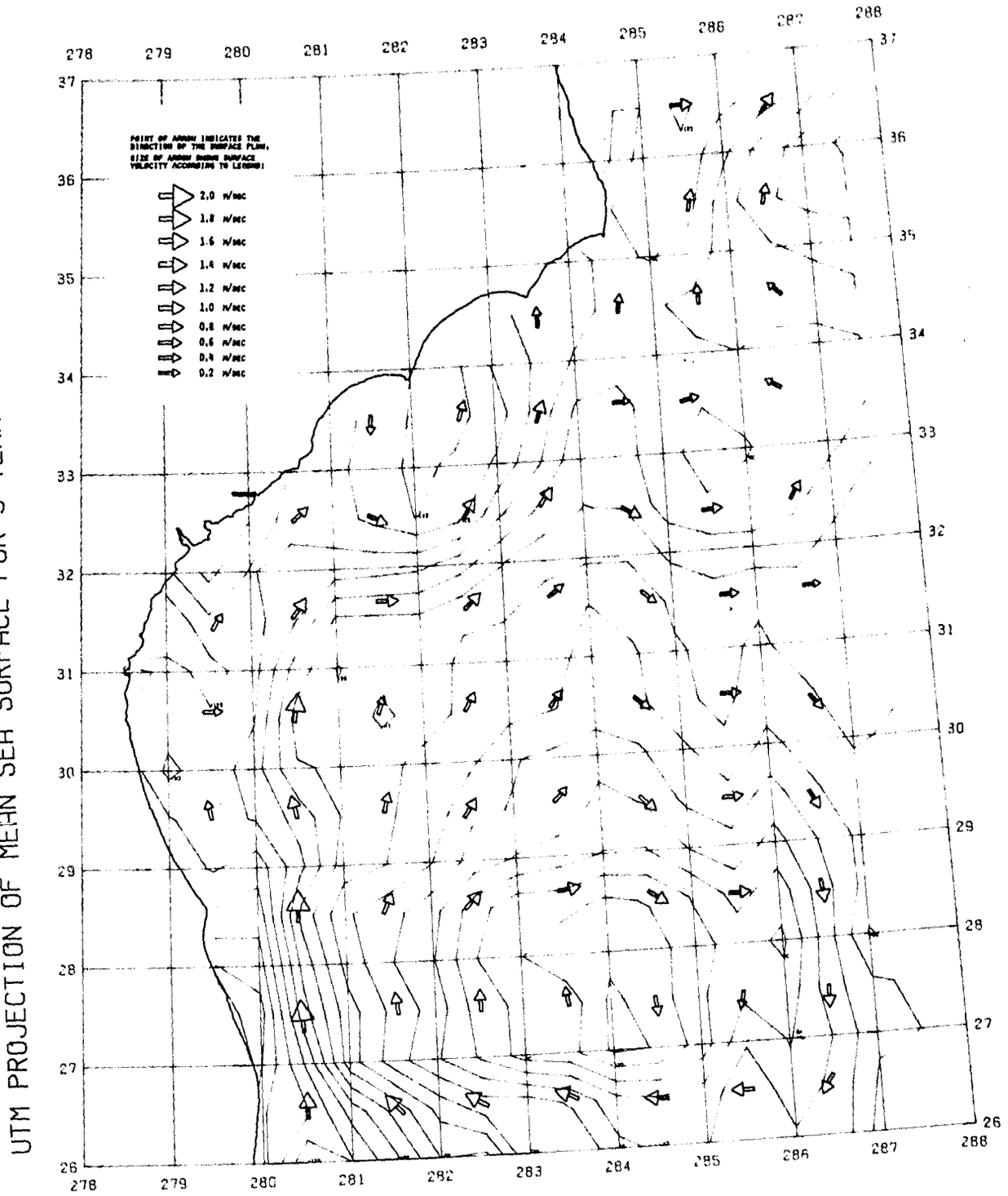
UTM PROJECTION OF MEAN SEA SURFACE FOR 3-YEAR MEAN
POINT OF ARROW INDICATES THE DIRECTION OF THE SURFACE FLOW.
SIZE OF ARROW SHOWN SURFACE VELOCITY ACCORDING TO LEGEND:
2.0 m/sec
1.8 m/sec
1.6 m/sec
1.4 m/sec
1.2 m/sec
1.0 m/sec
0.8 m/sec
0.6 m/sec
0.4 m/sec
0.2 m/sec
278 279 280 281 282 283 284 285 286 287 288
37 36 35 34 33 32 31 30 29 28 27 26

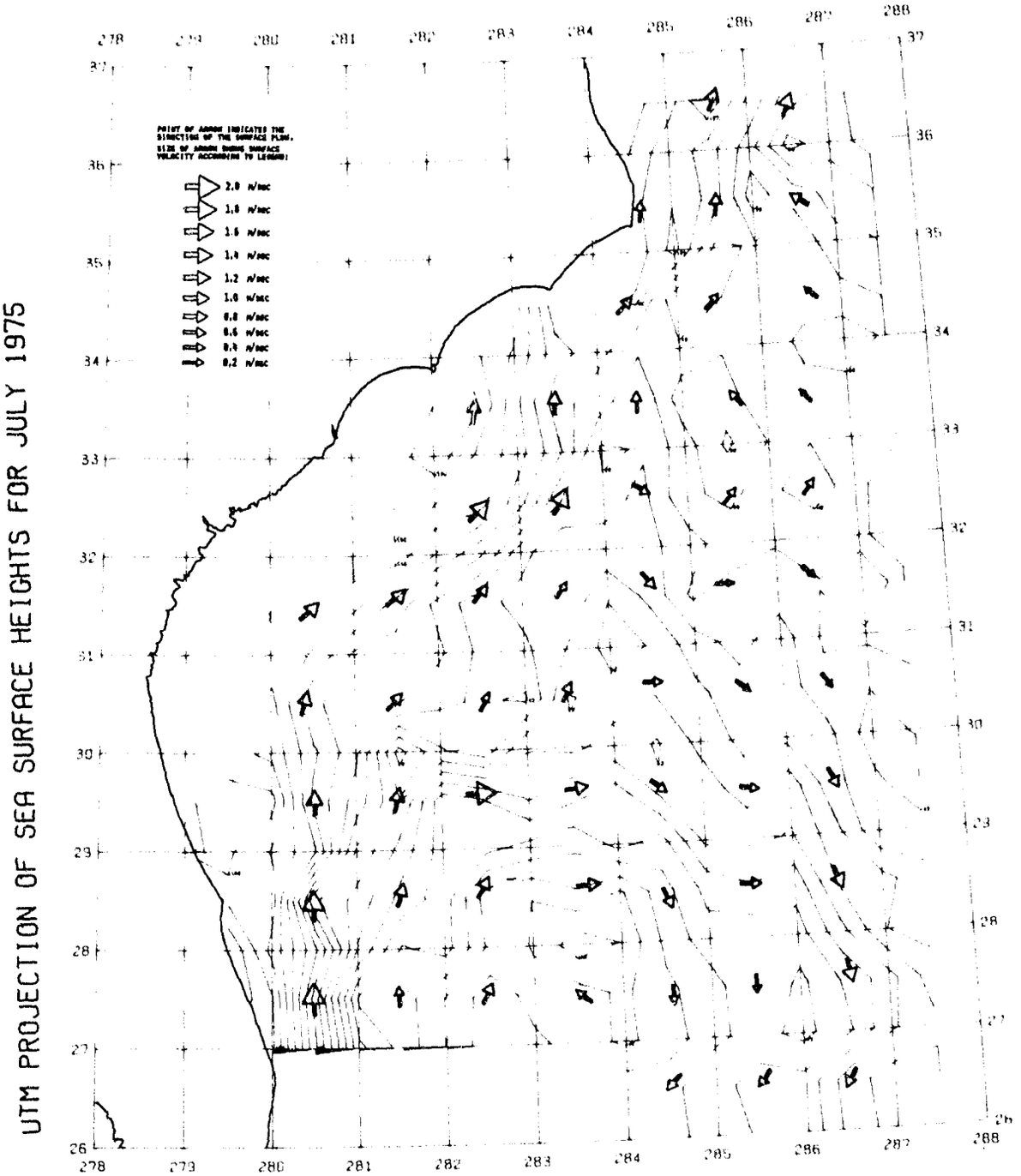
UTM PROJECTION OF SEA SURFACE HEIGHTS FOR JULY 1975
POINT OF ARROW INDICATES THE DIRECTION OF THE SURFACE FLOW.
SIZE OF ARROW SHOWS SURFACE VELOCITY ACCORDING TO LEGEND:
2.0 m/sec
1.8 m/sec
1.6 m/sec
1.4 m/sec
1.2 m/sec
1.0 m/sec
0.8 m/sec
0.6 m/sec
0.4 m/sec
0.2 m/sec
278
279
280
281
282
283
284
285
286
287
288
26
27
28
29
30
31
32
33
34
35
36
37

UTM PROJECTION OF MEAN SEA SURFACE FOR AUGUST 1975

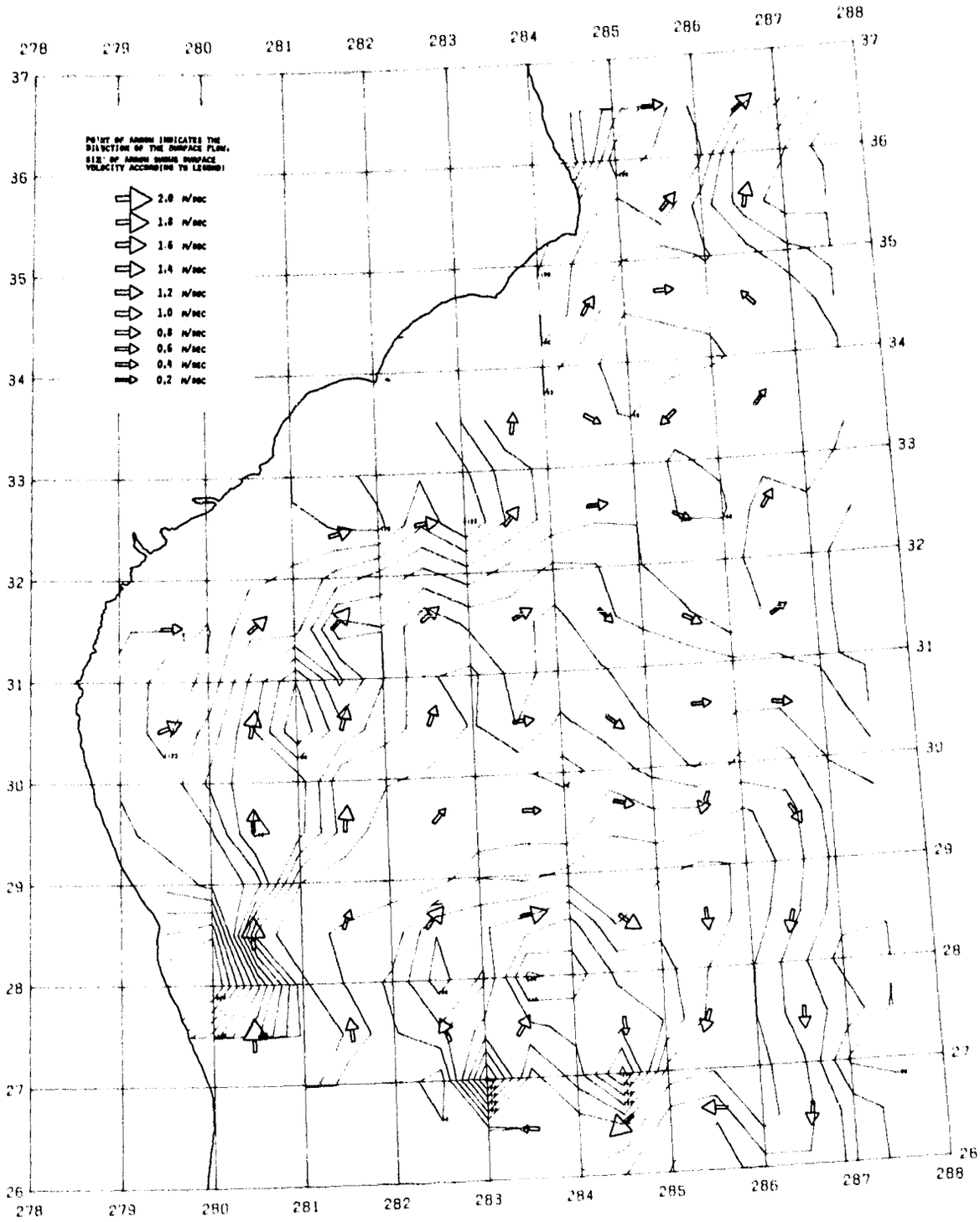

UTM PROJECTION OF MEAN SEA SURFACE FOR OCTOBER 1975

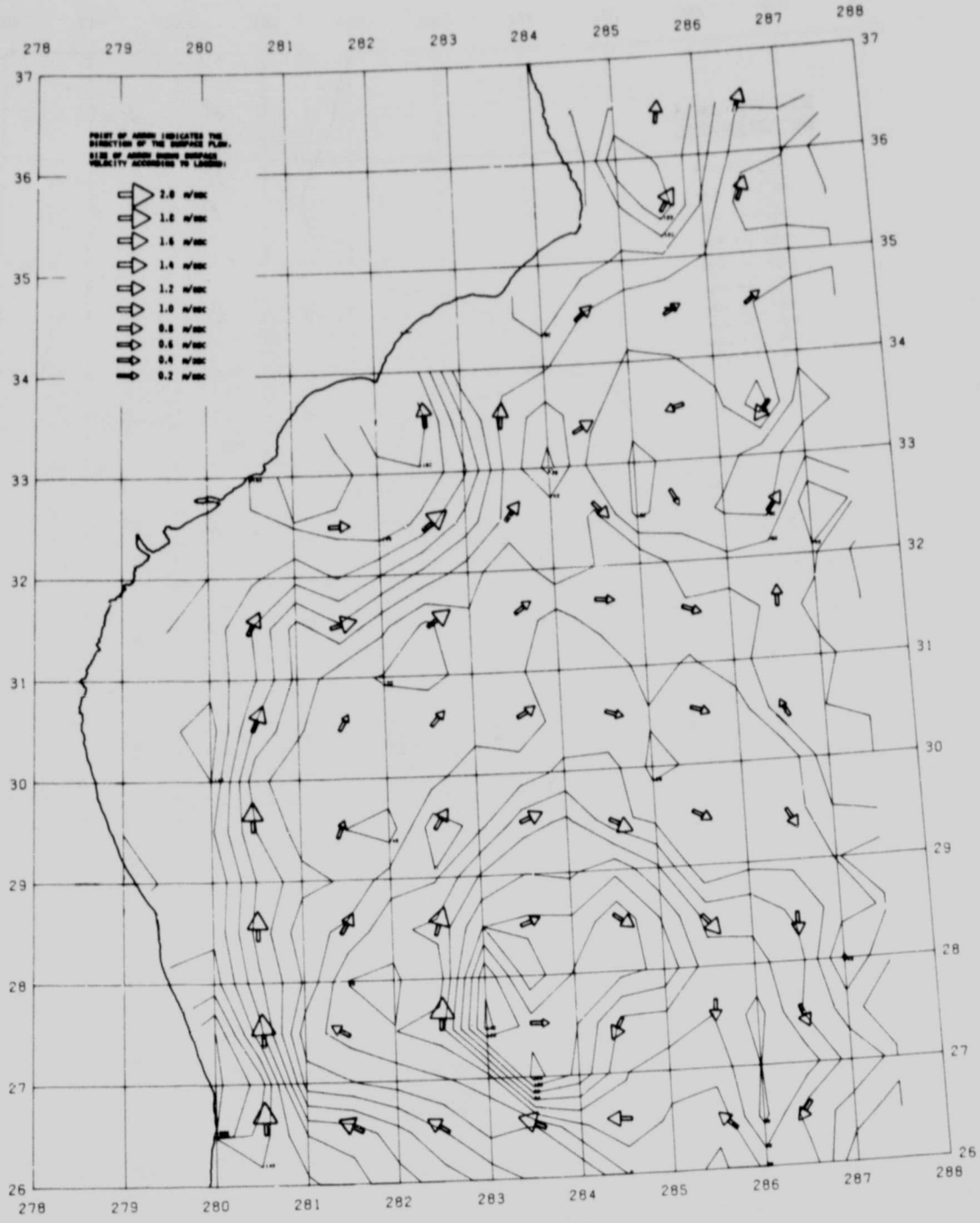

UTM PROJECTION OF MEAN SEA SURFACE FOR NOVEMBER 1975

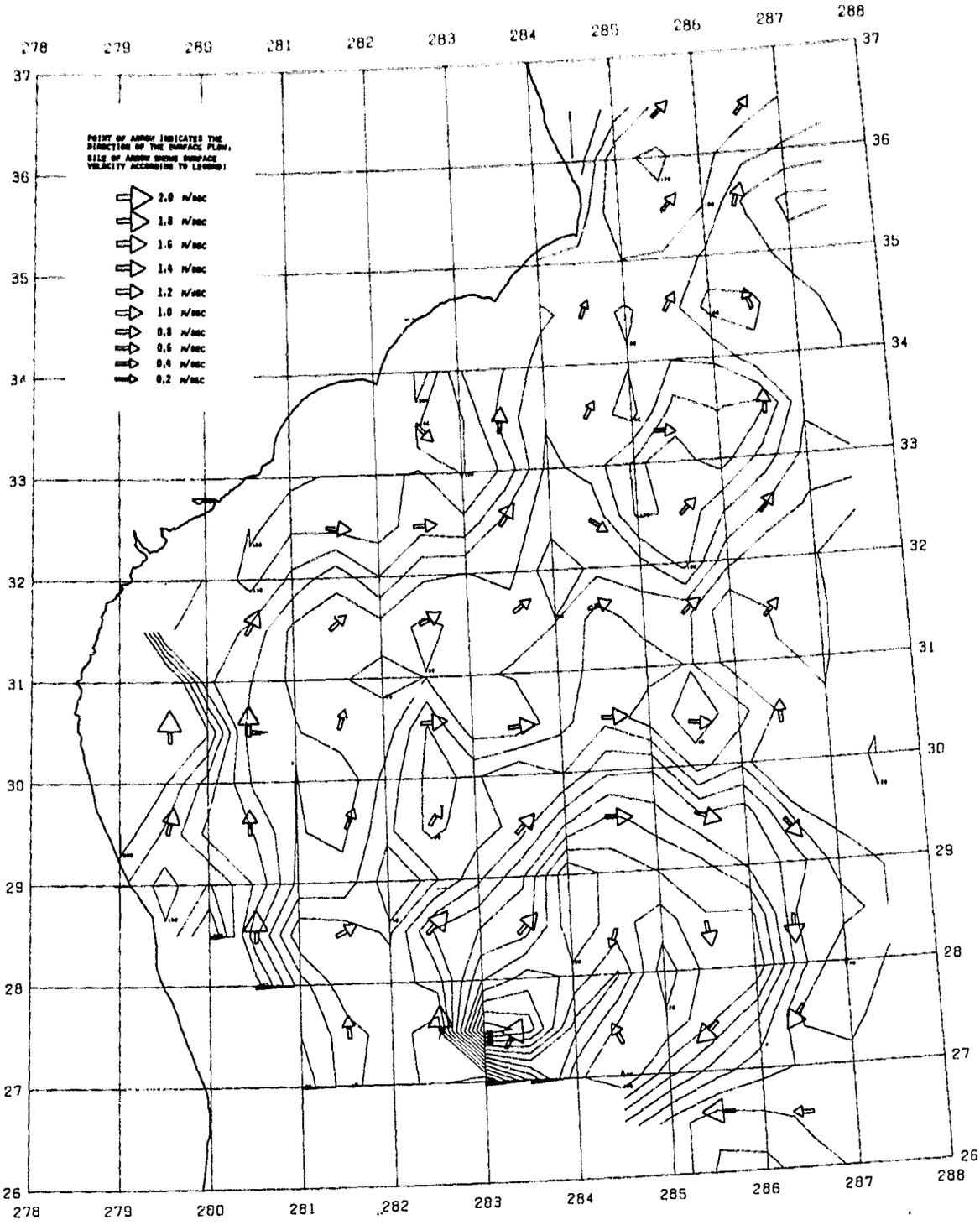

UTM PROJECTION OF MEAN SEA SURFACE FOR DECEMBER 1975

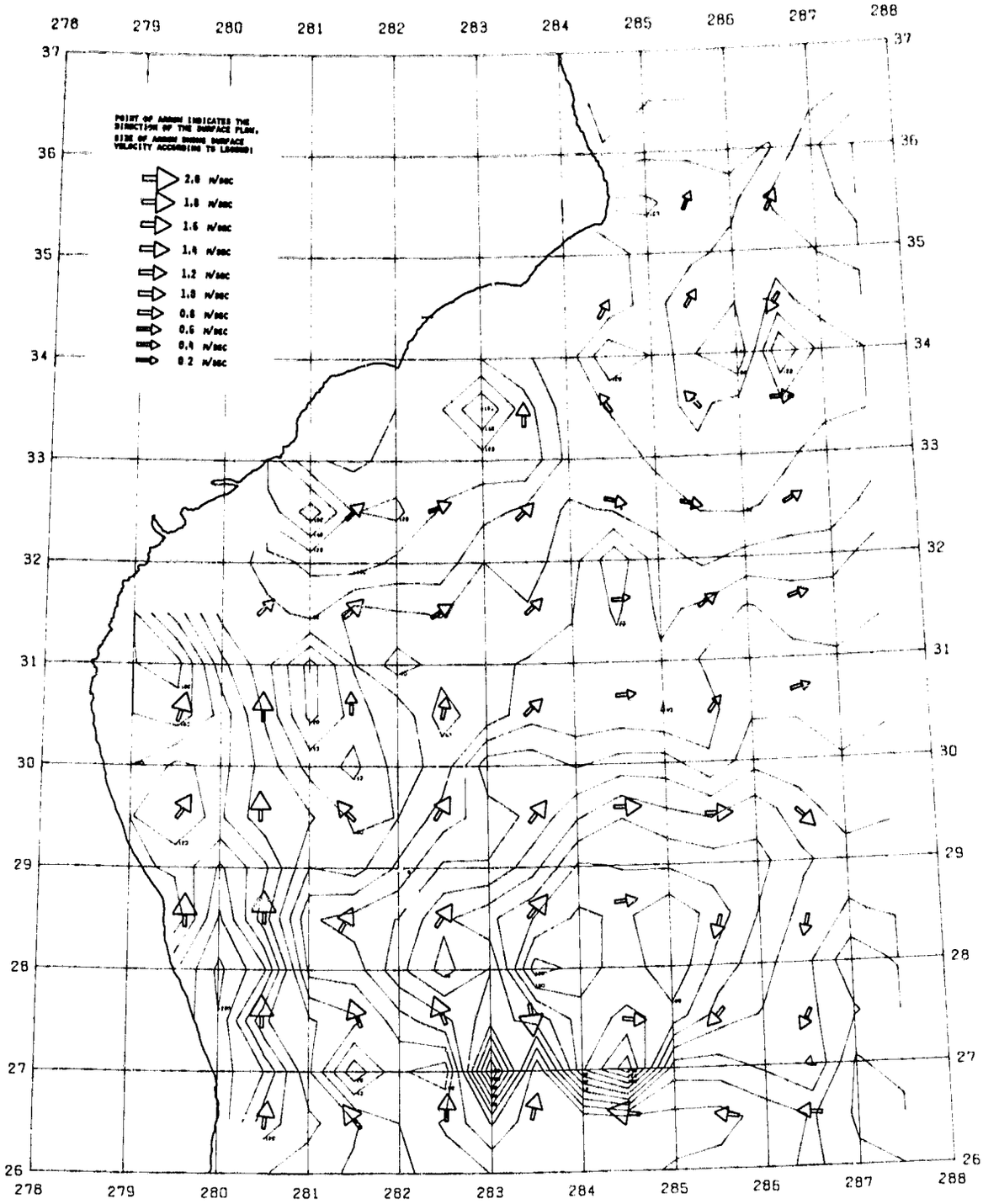

UTM PROJECTION OF MEAN SEA SURFACE FOR JANUARY 1976

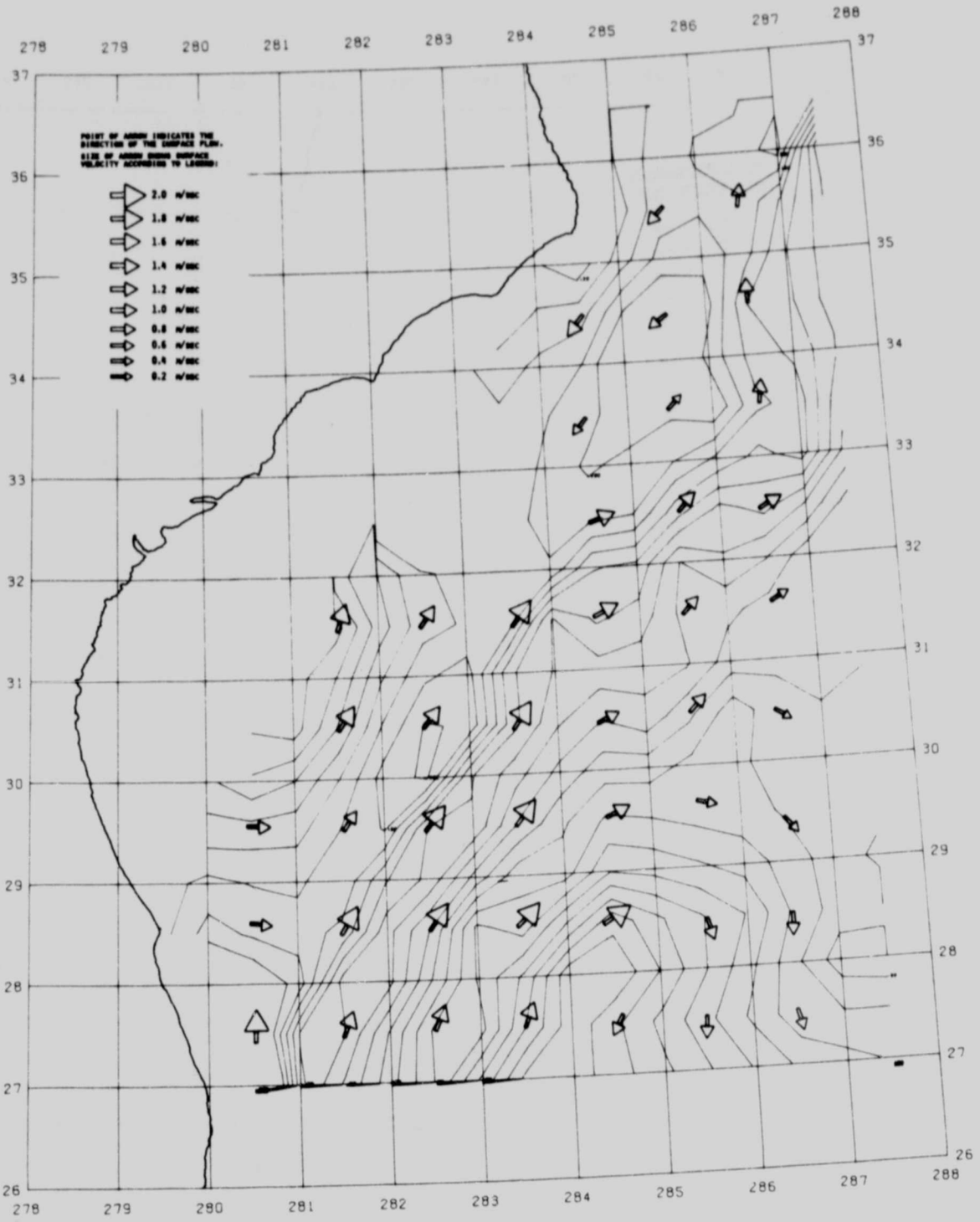

UTM PROJECTION OF MEAN SEA SURFACE FOR FEBRUARY 1976

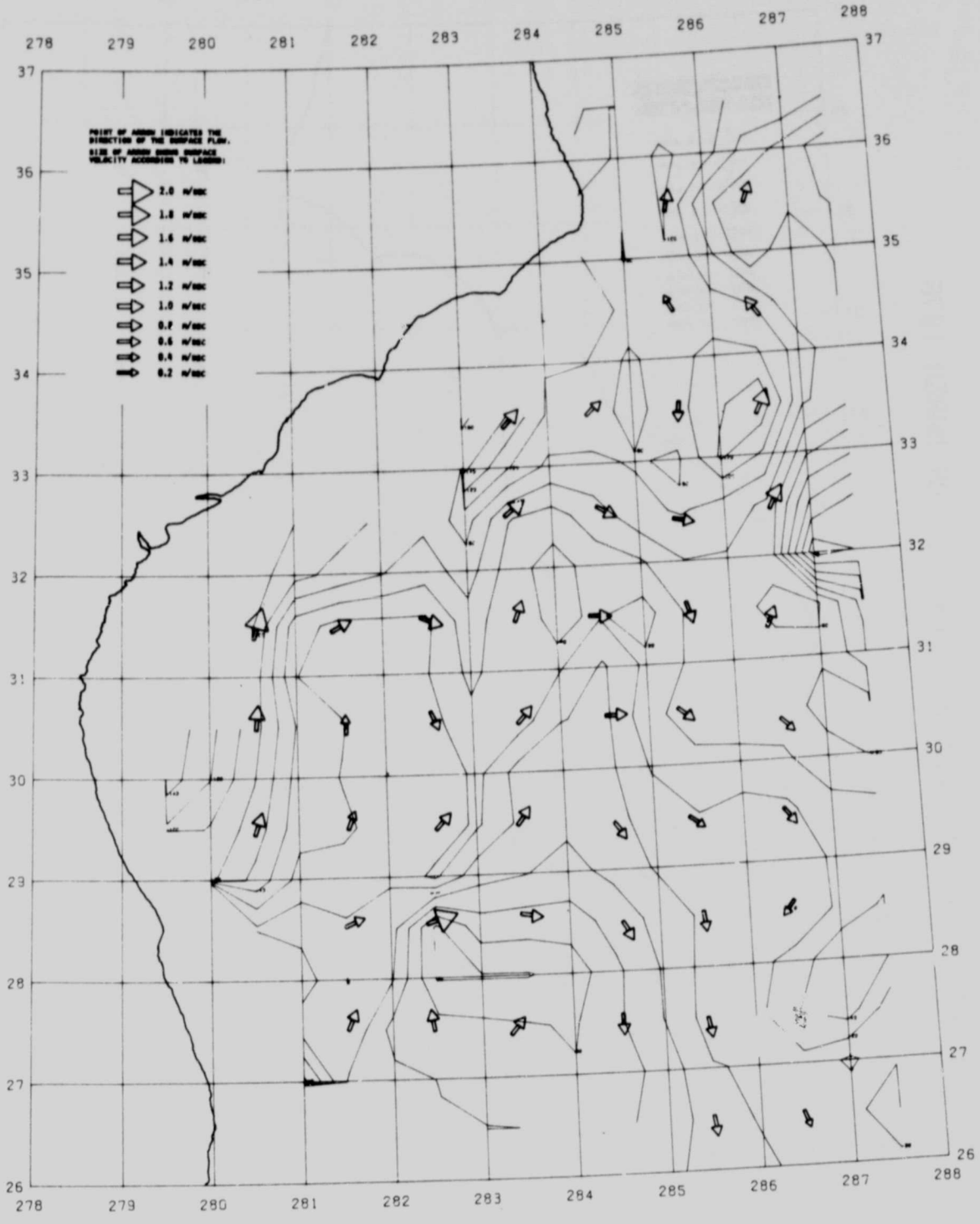

UTM PROJECTION OF MEAN SEA SURFACE FOR MARCH 1976

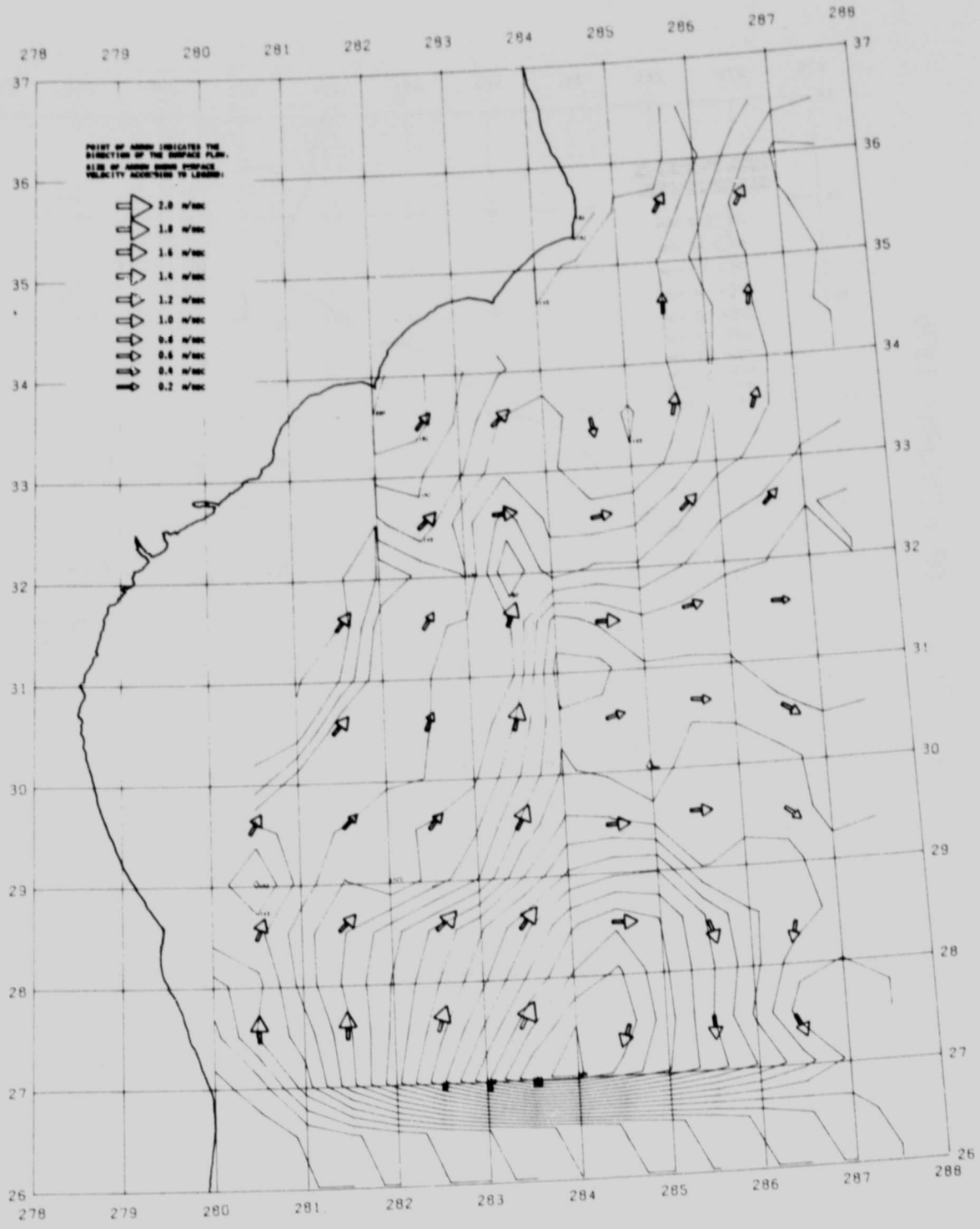

UTM PROJECTION OF MEAN SEA SURFACE FOR APRIL 1976

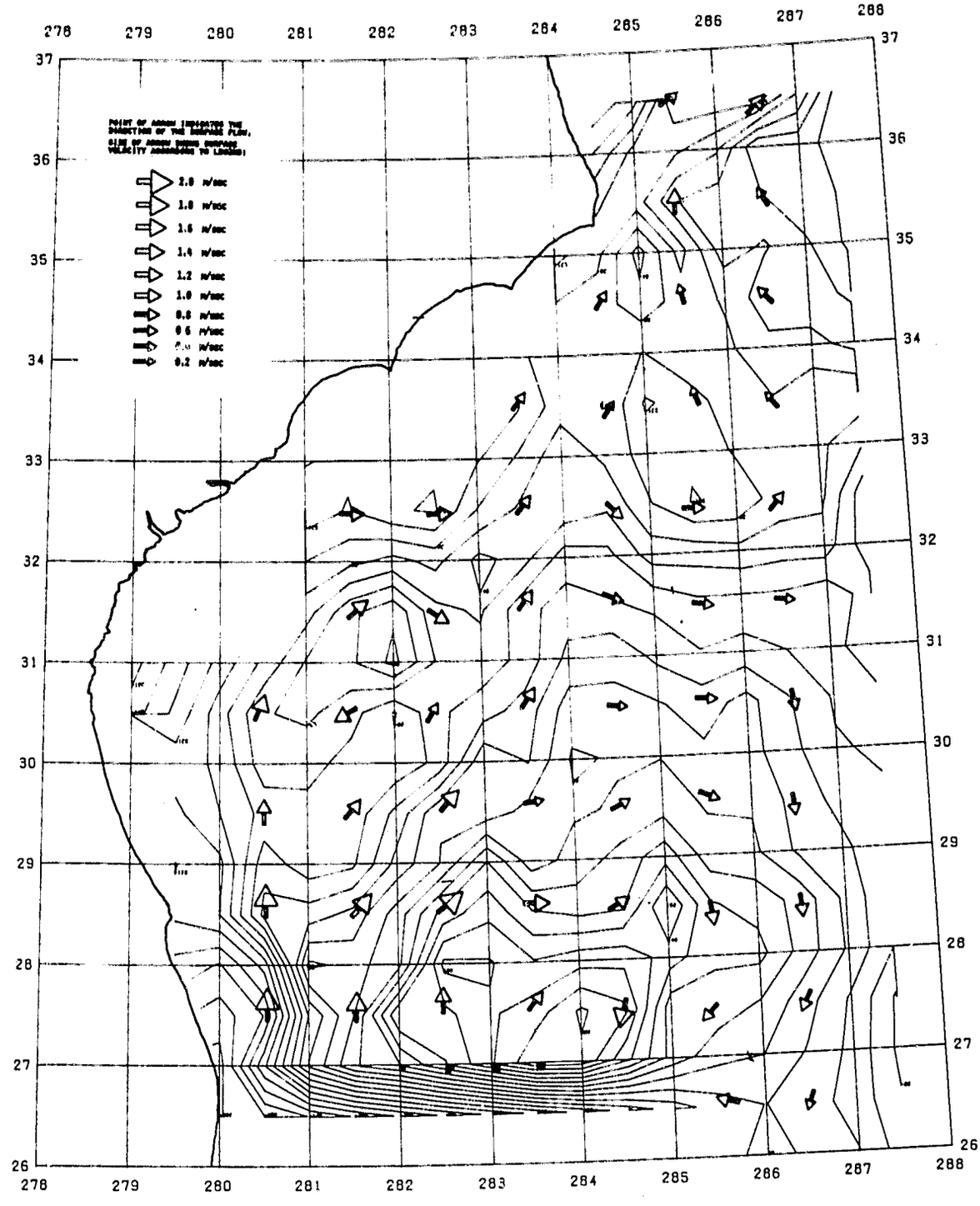

UTM PROJECTION OF MEAN SEA SURFACE FOR MAY 1976

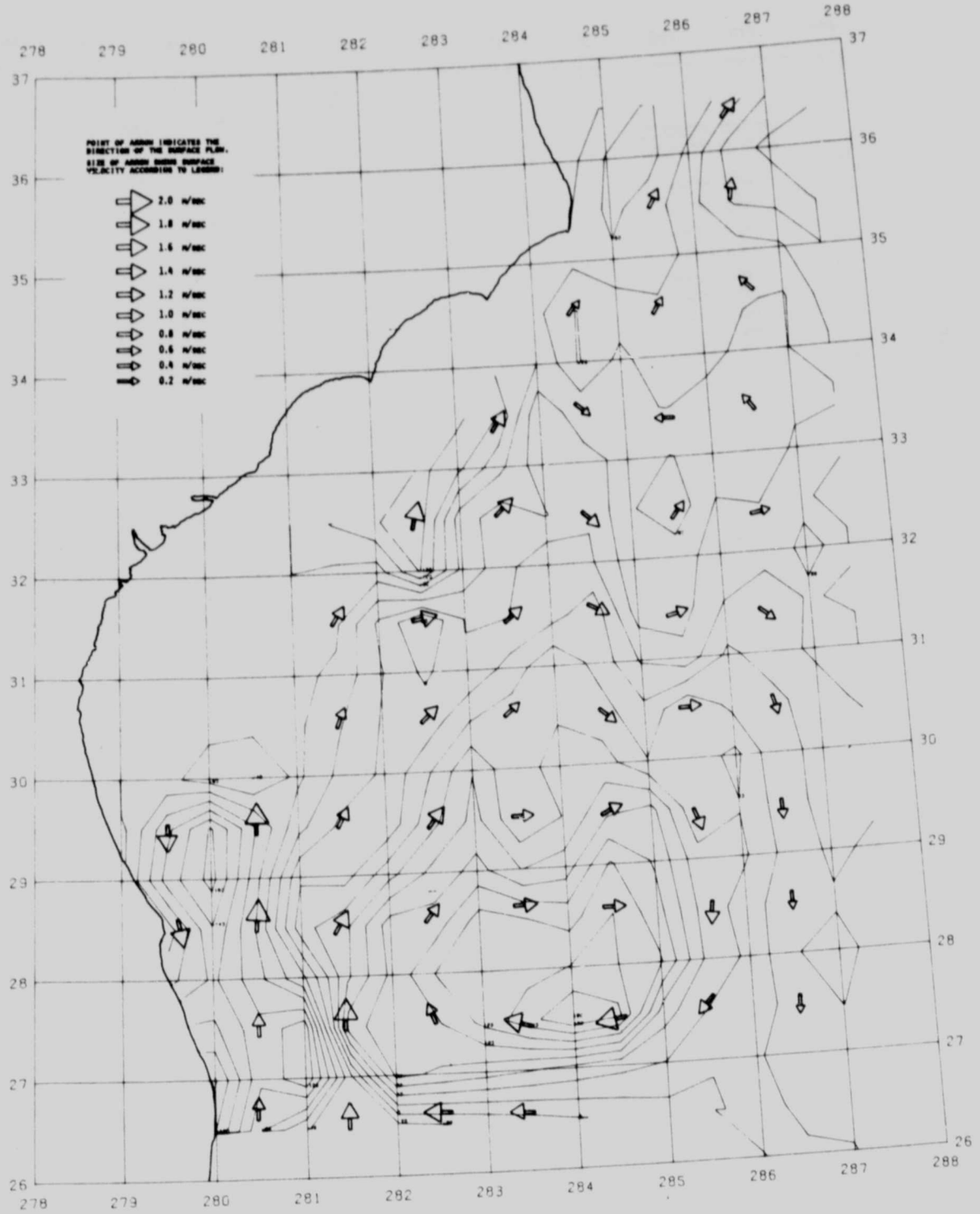

UTM PROJECTION OF MEAN SEA SURFACE FOR JUNE 1976

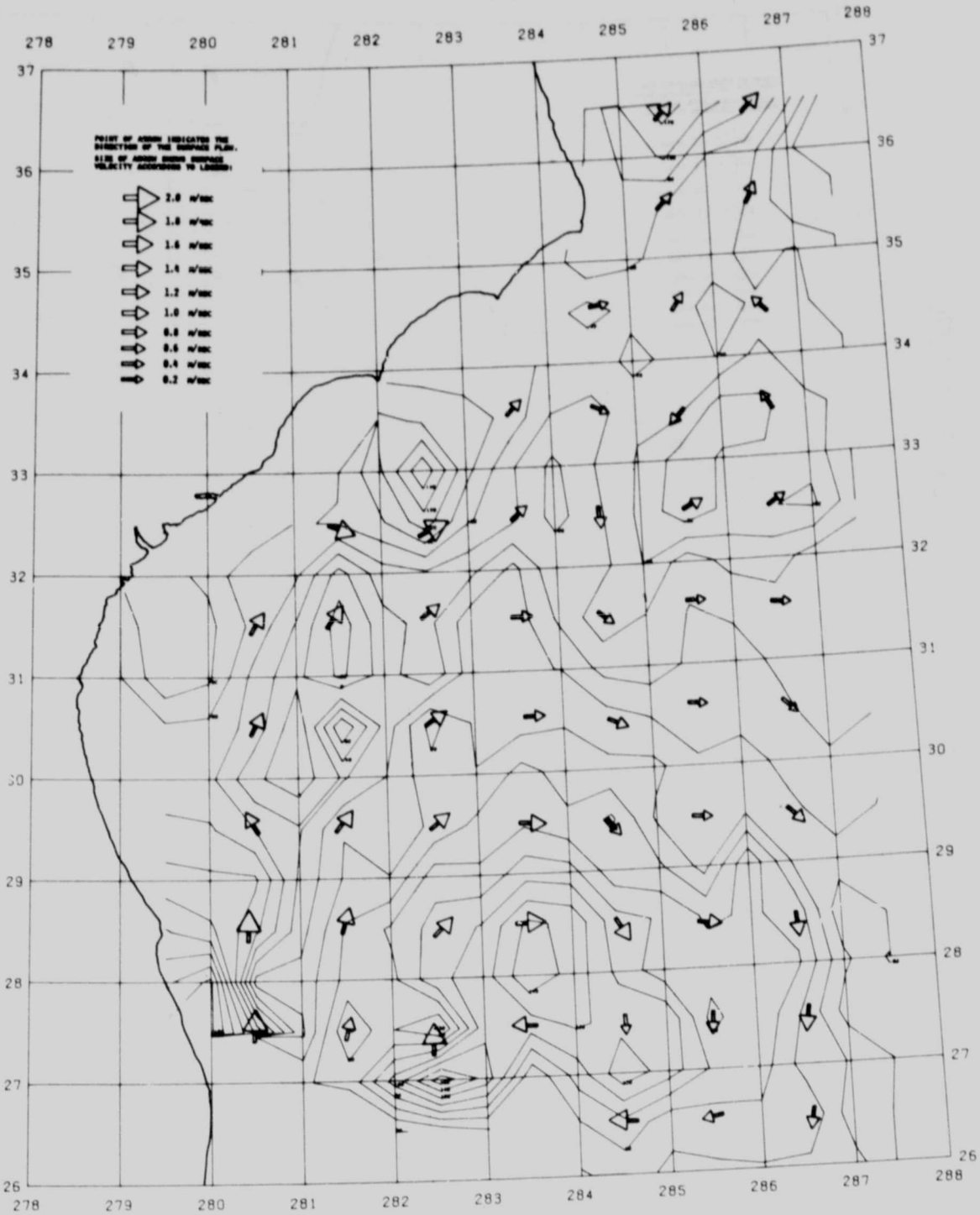

UTM PROJECTION OF MEAN SEA SURFACE FOR JULY 1976

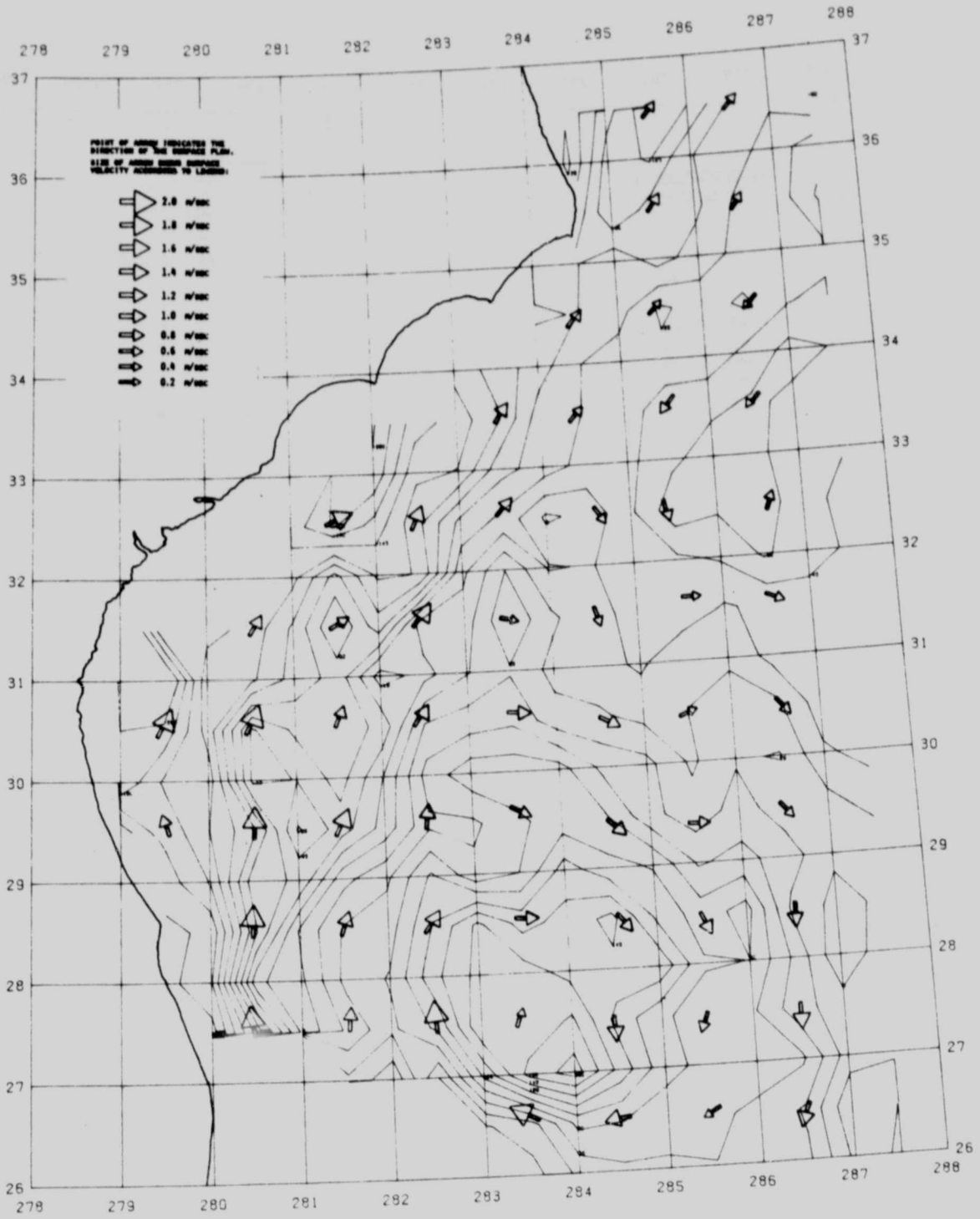

UTM PROJECTION OF MEAN SEA SURFACE FOR AUGUST 1976

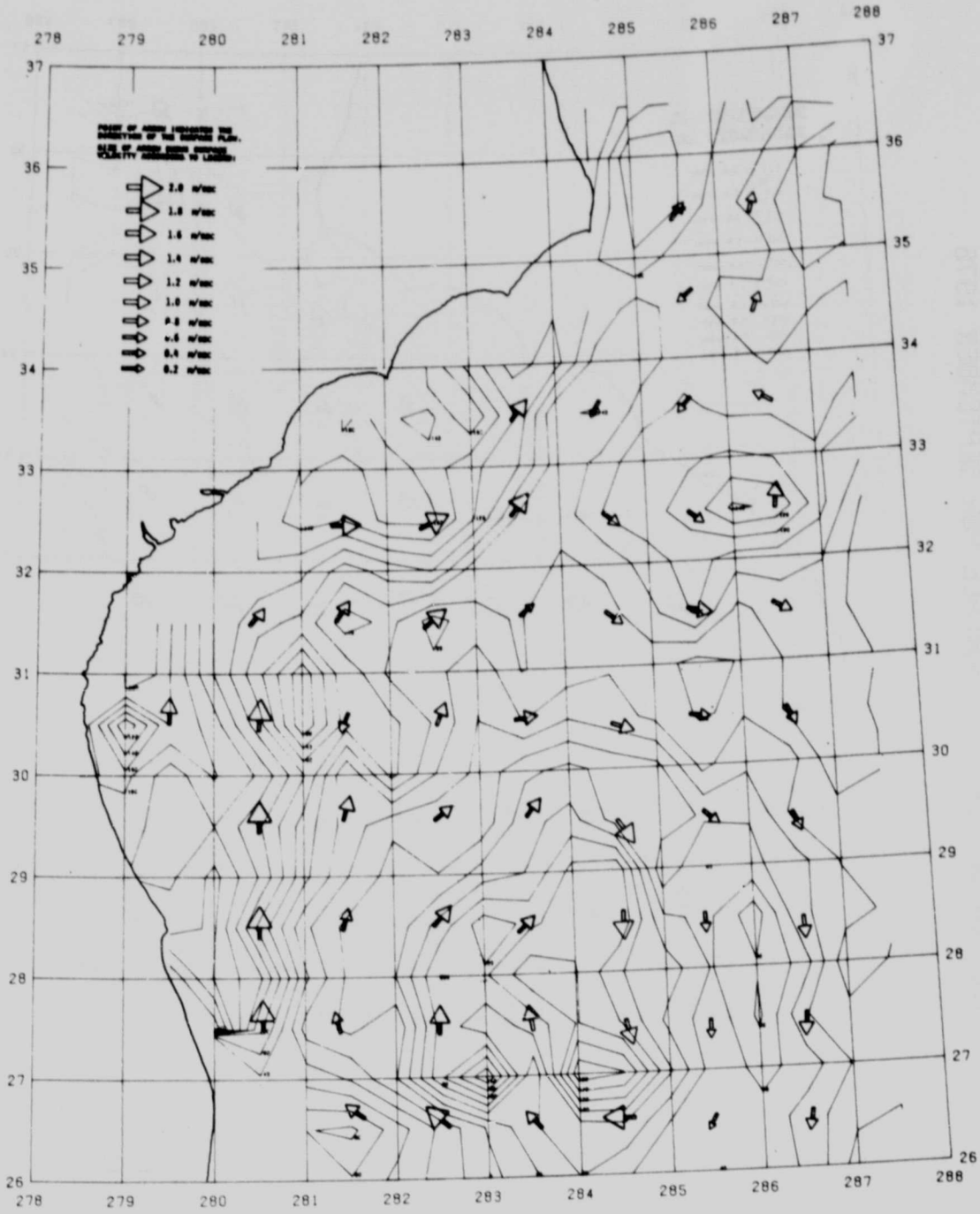

UTM PROJECTION OF MEAN SEA SURFACE FOR SEPTEMBER 1976

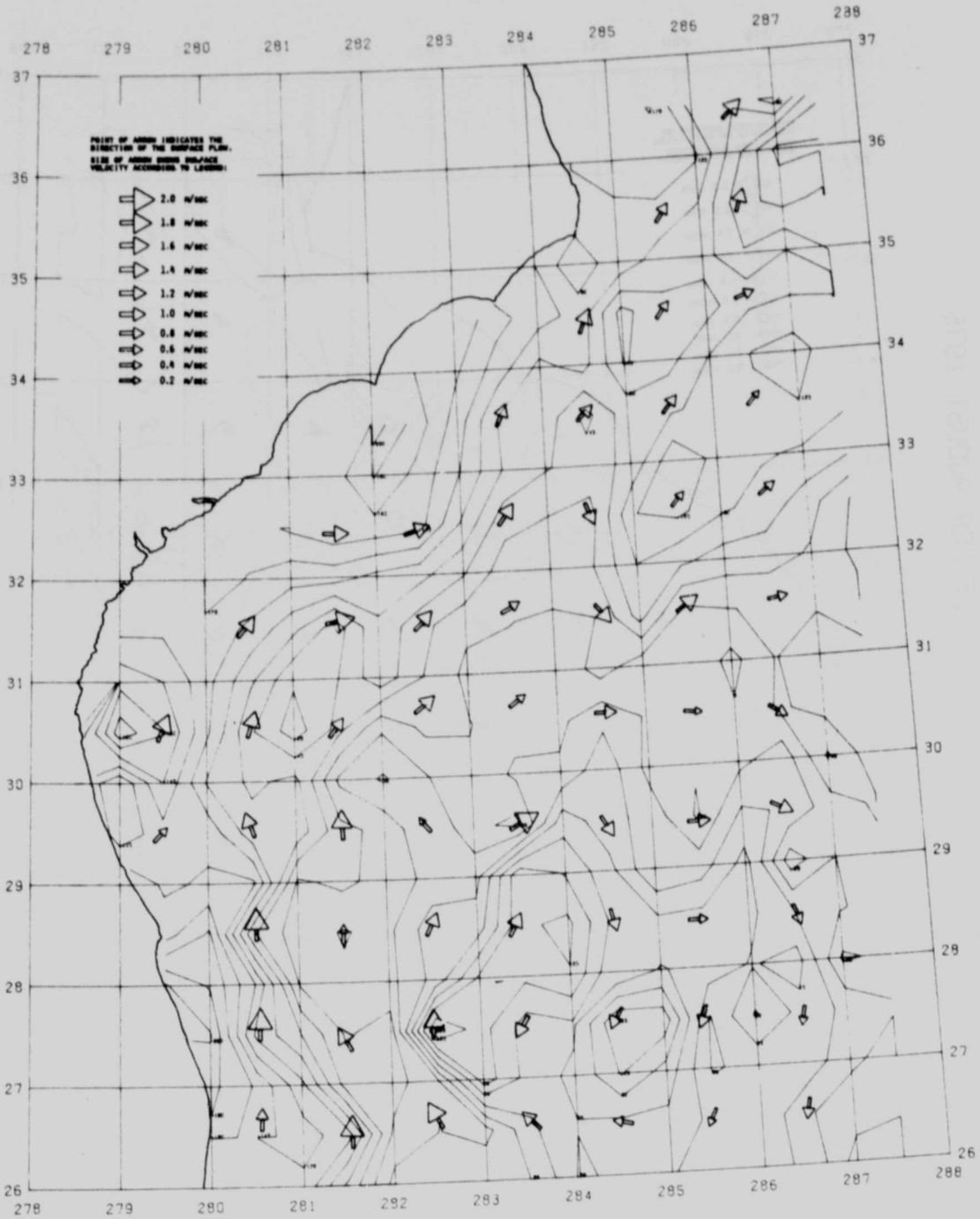

UTM PROJECTION OF MEAN SEA SURFACE FOR OCTOBER 1976

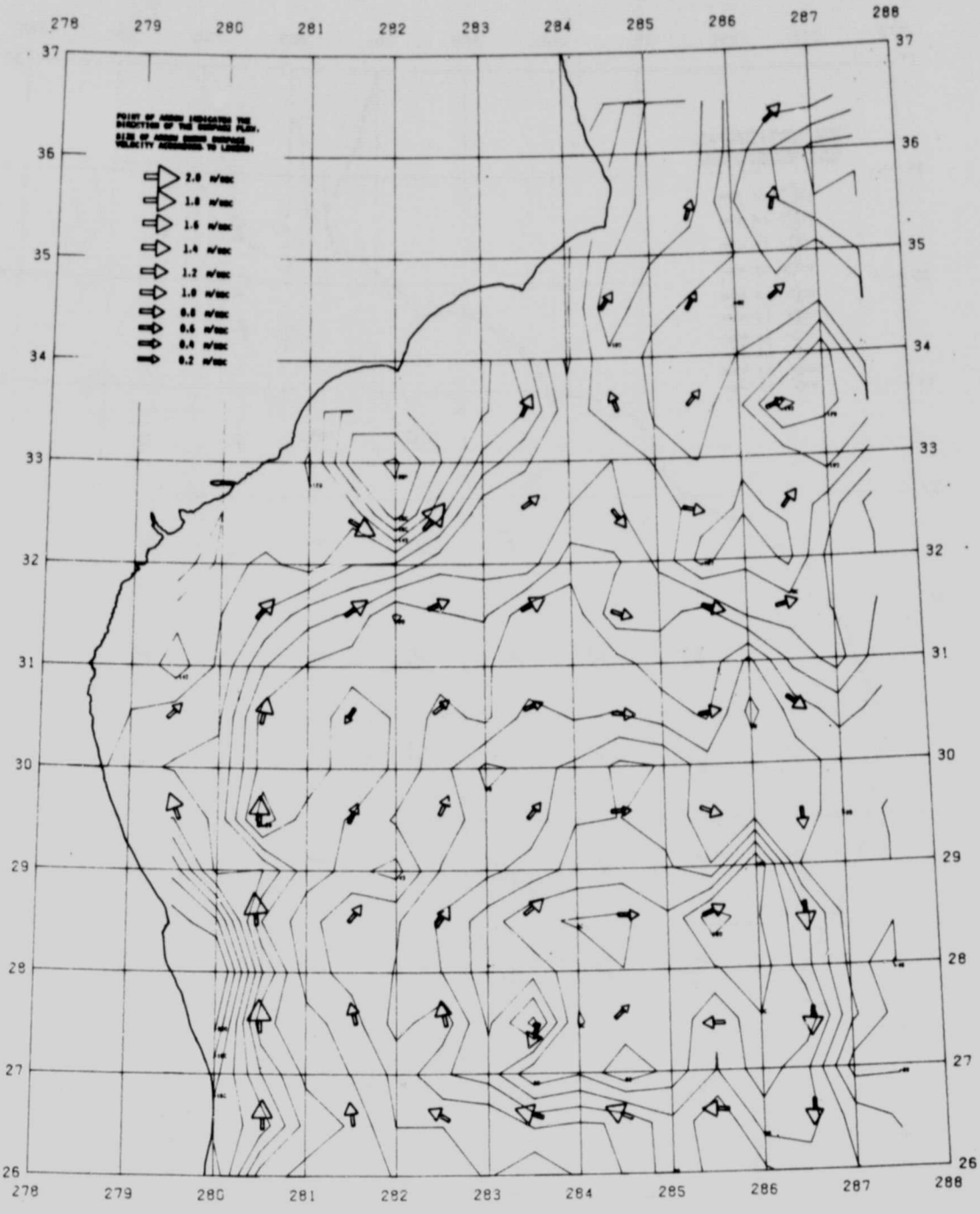

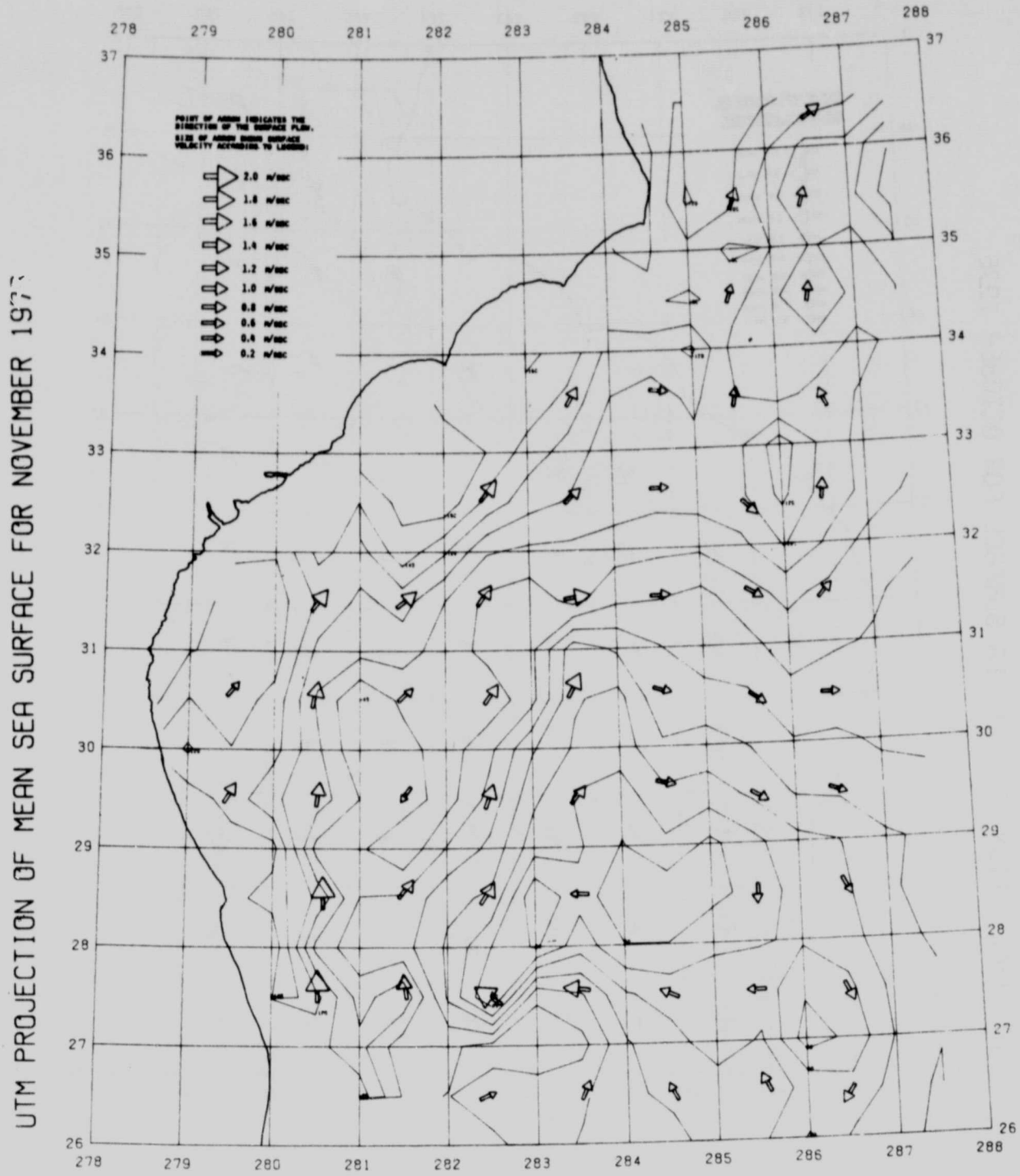
UTM PROJECTION OF MEAN SEA SURFACE FOR NOVEMBER 197
278
279
280
281
282
283
284
285
286
287
288
37
36
35
34
33
32
31
30
29
28
27
26
2.0 m/sec
1.8 m/sec
1.6 m/sec
1.4 m/sec
1.2 m/sec
1.0 m/sec
0.8 m/sec
0.6 m/sec
0.4 m/sec
0.2 m/sec

UTM PROJECTION OF MEAN SEA SURFACE FOR DECEMBER 1976

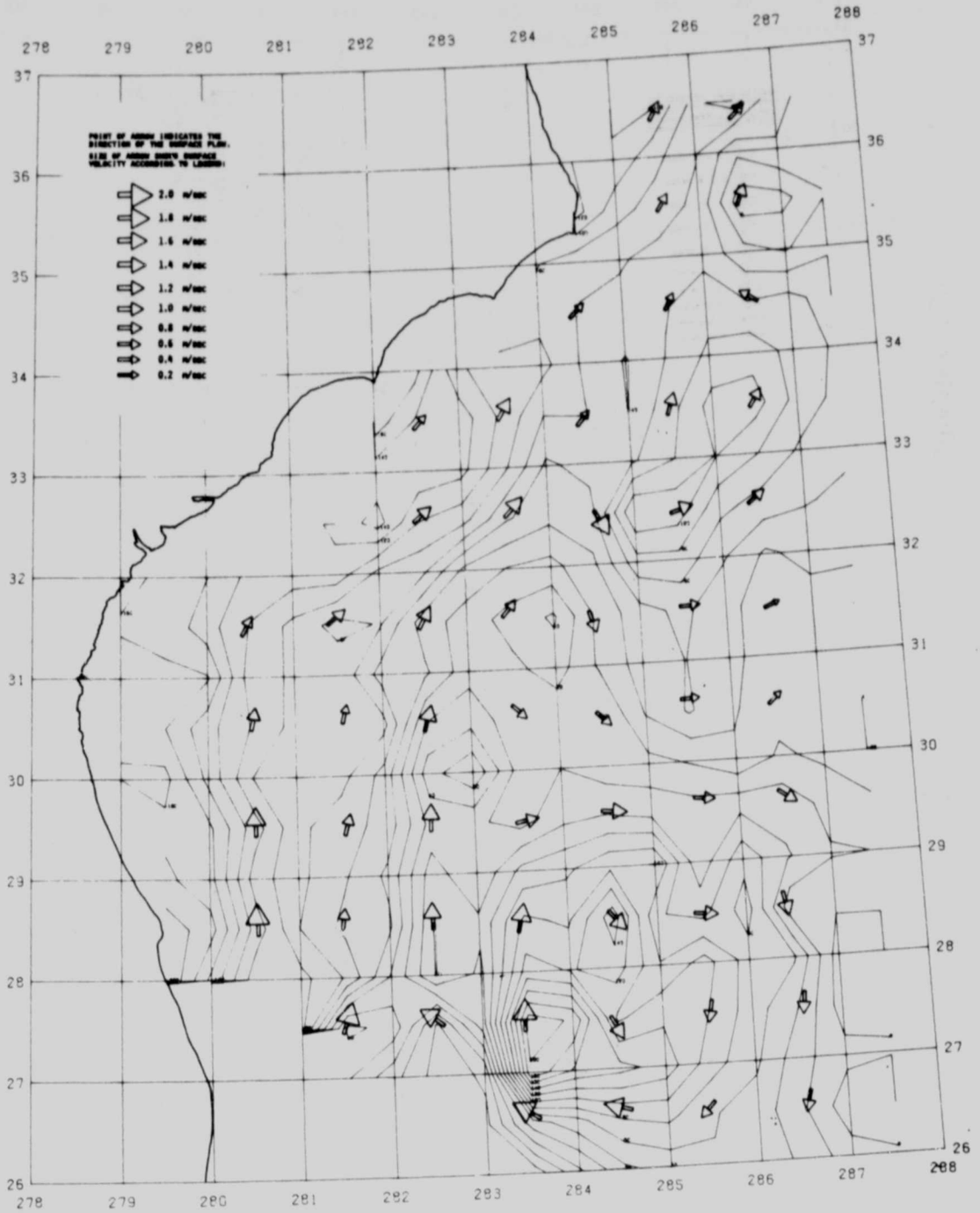

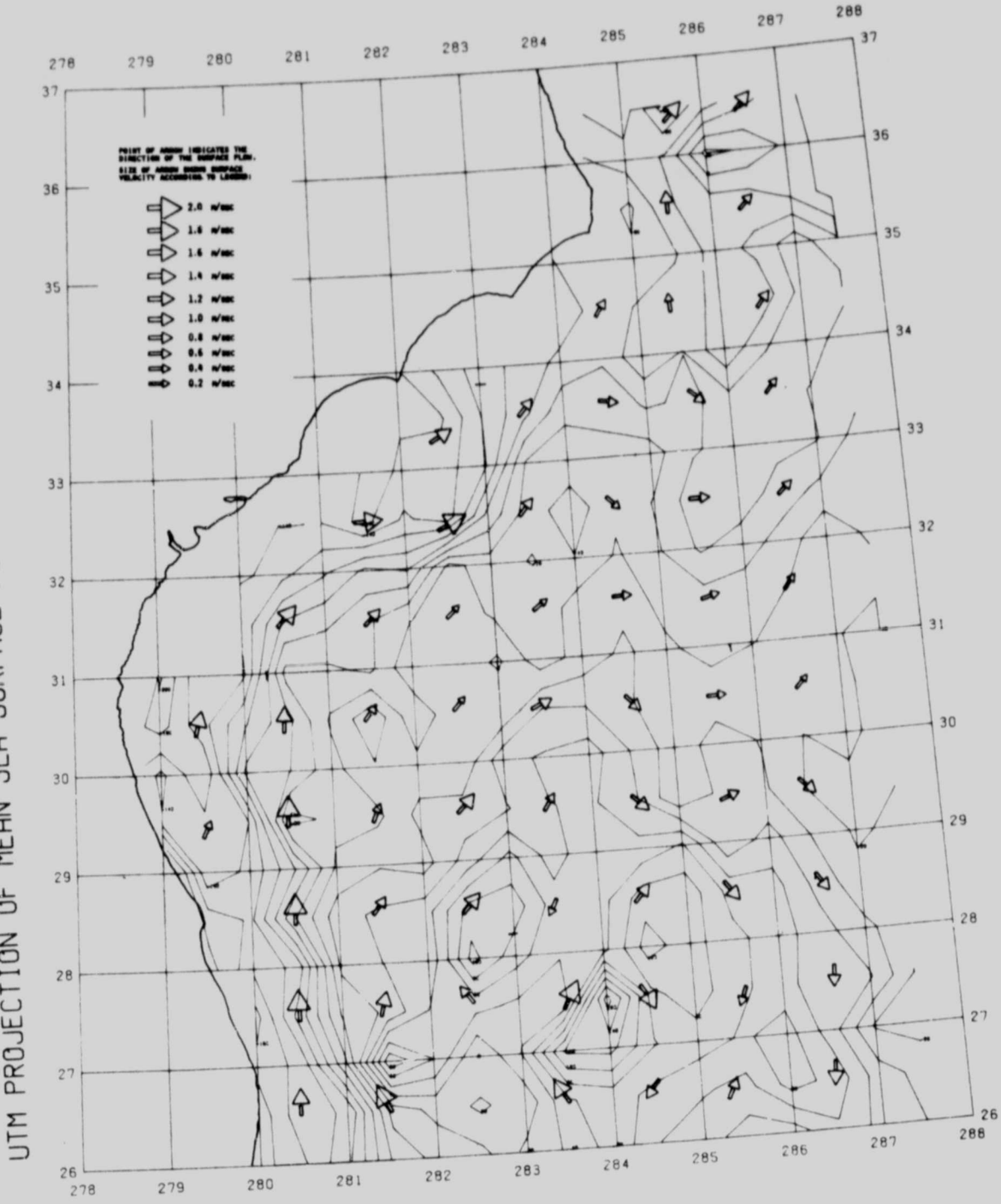
UTM PROJECTION OF MEAN SEA SURFACE FOR JANUARY 1977
278
279
280
281
282
283
284
285
286
287
288
37
36
35
34
33
32
31
30
29
28
27
26

UTM PROJECTION OF MEAN SEA SURFACE FOR FEBRUARY 1977

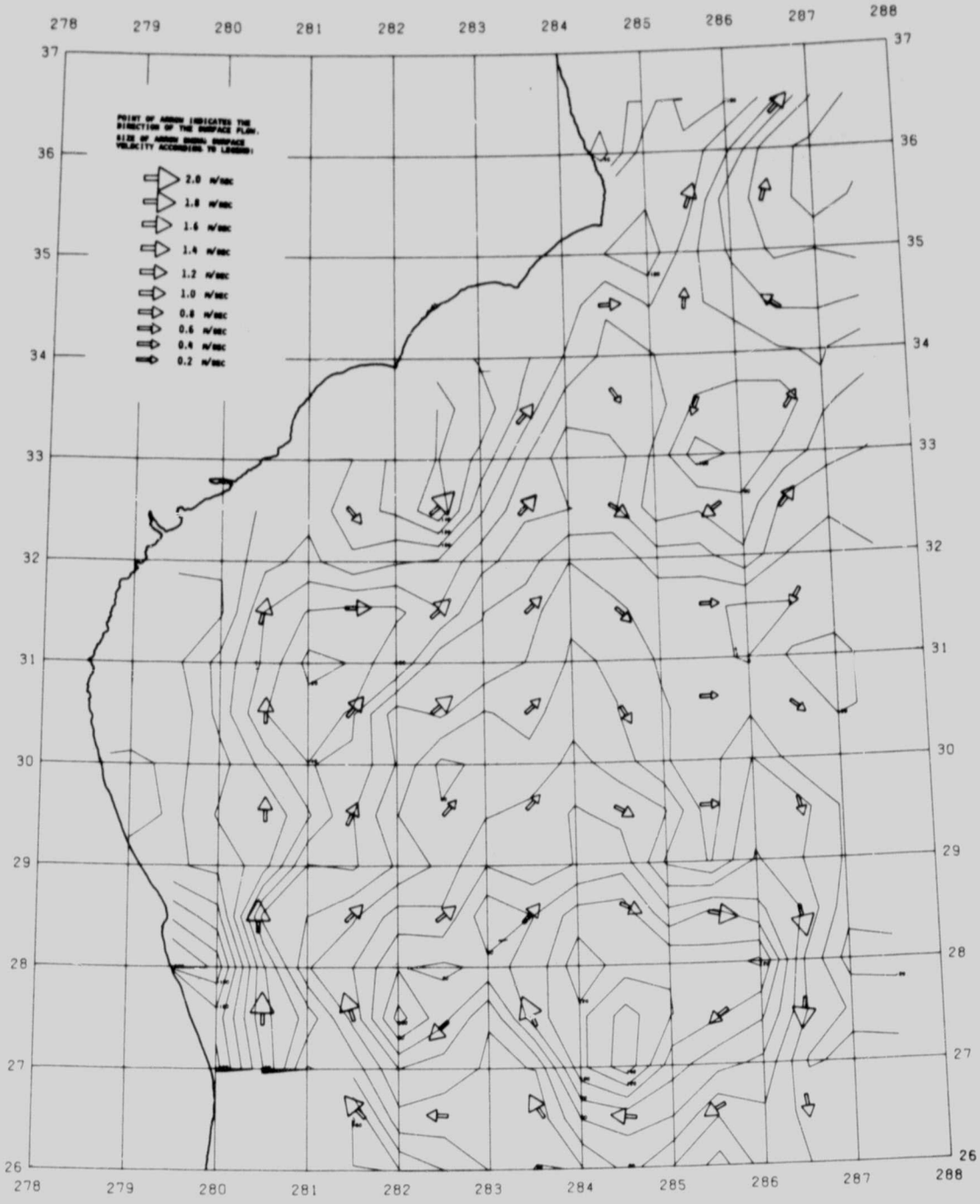

UTM PROJECTION OF MEAN SEA SURFACE FOR MARCH 1977

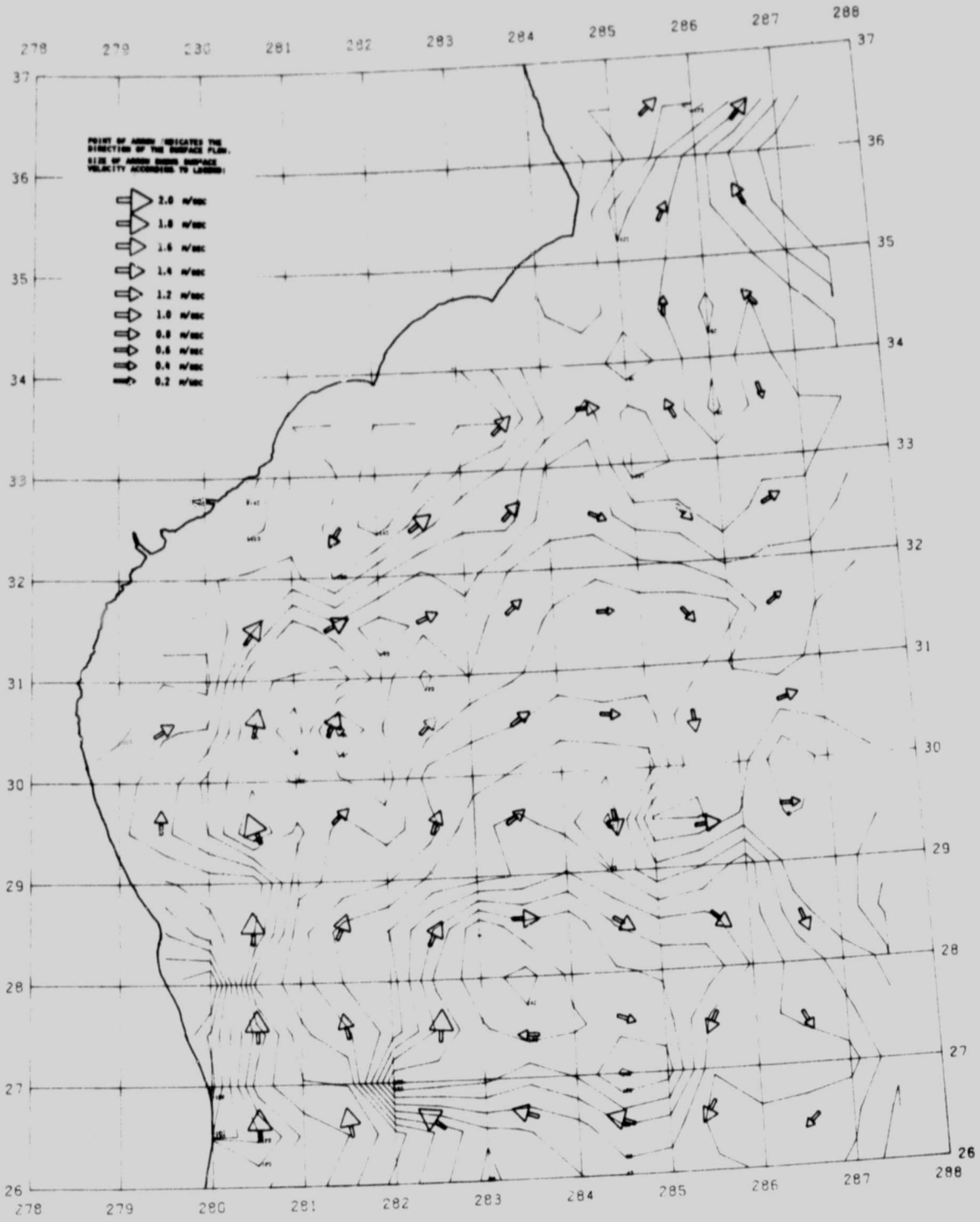

UTM PROJECTION OF MEAN SEA SURFACE FOR APRIL 1977

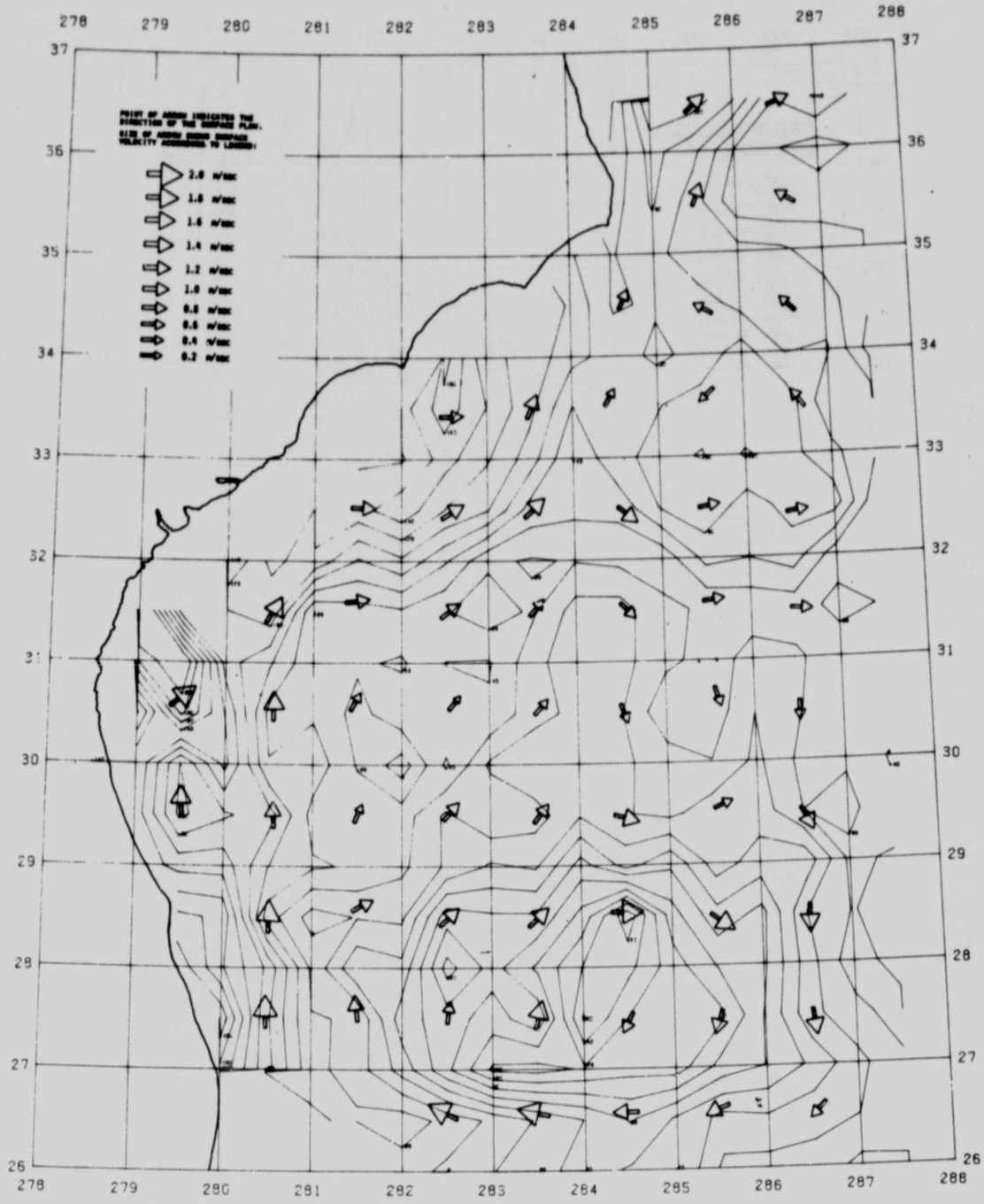

UTM PROJECTION OF MEAN SEA SURFACE FOR MAY 1977

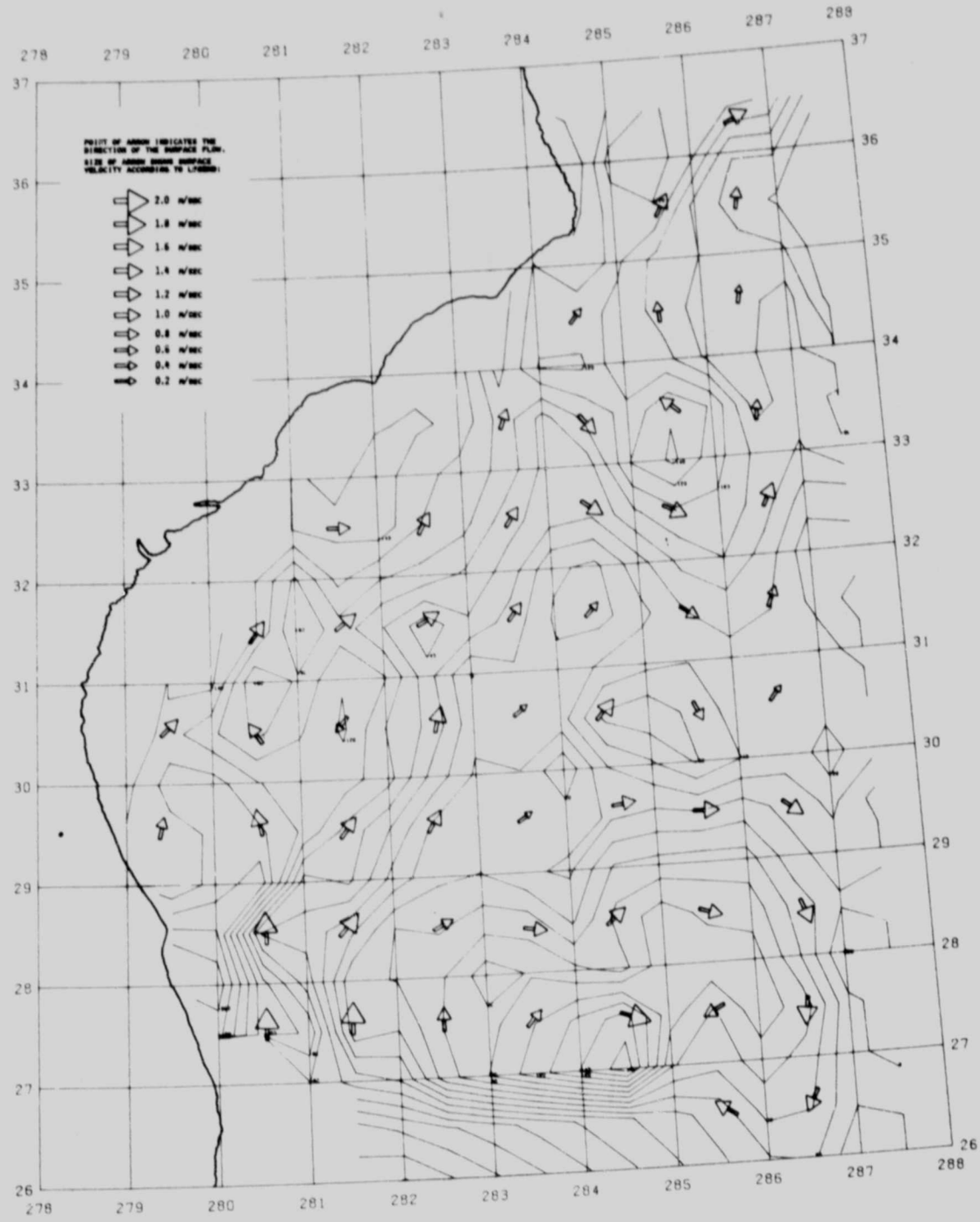

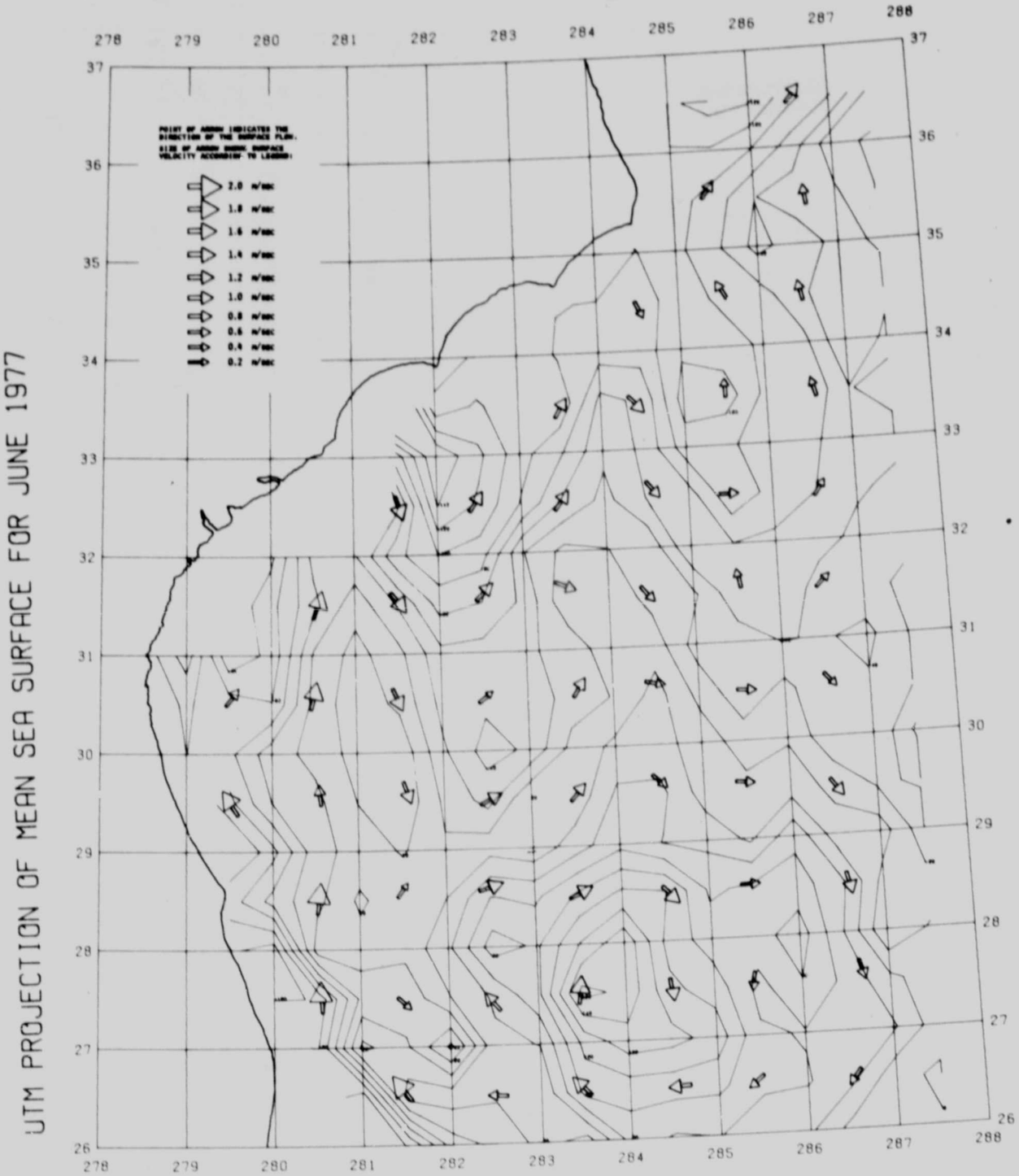
UTM PROJECTION OF MEAN SEA SURFACE FOR JUNE 1977
278
279
280
281
282
283
284
285
286
287
288
37
36
35
34
33
32
31
30
29
28
27
26

UTM PROJECTION OF MEAN SEA SURFACE FOR JULY 1977

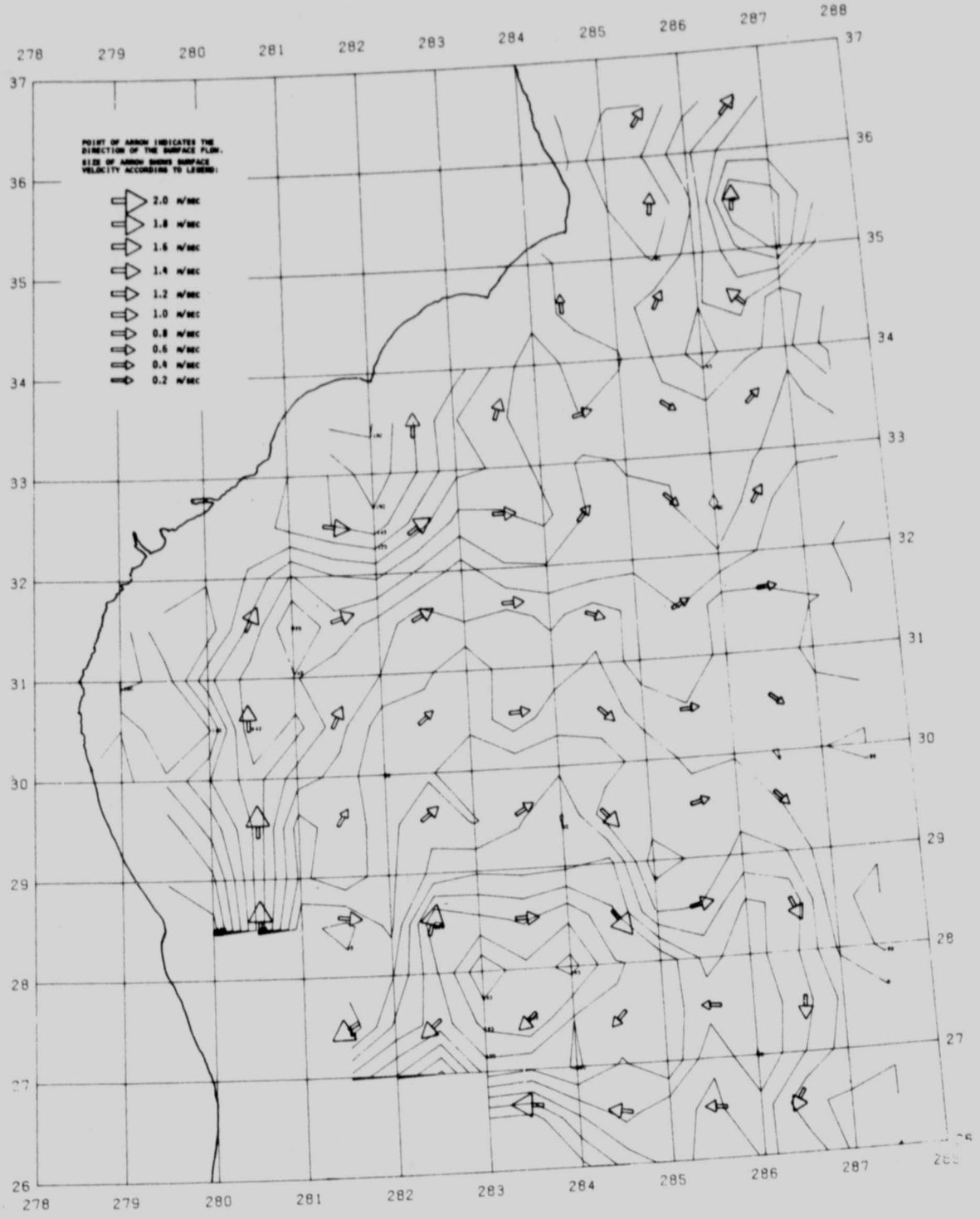

UTM PROJECTION OF MEAN SEA SURFACE FOR AUGUST 1977

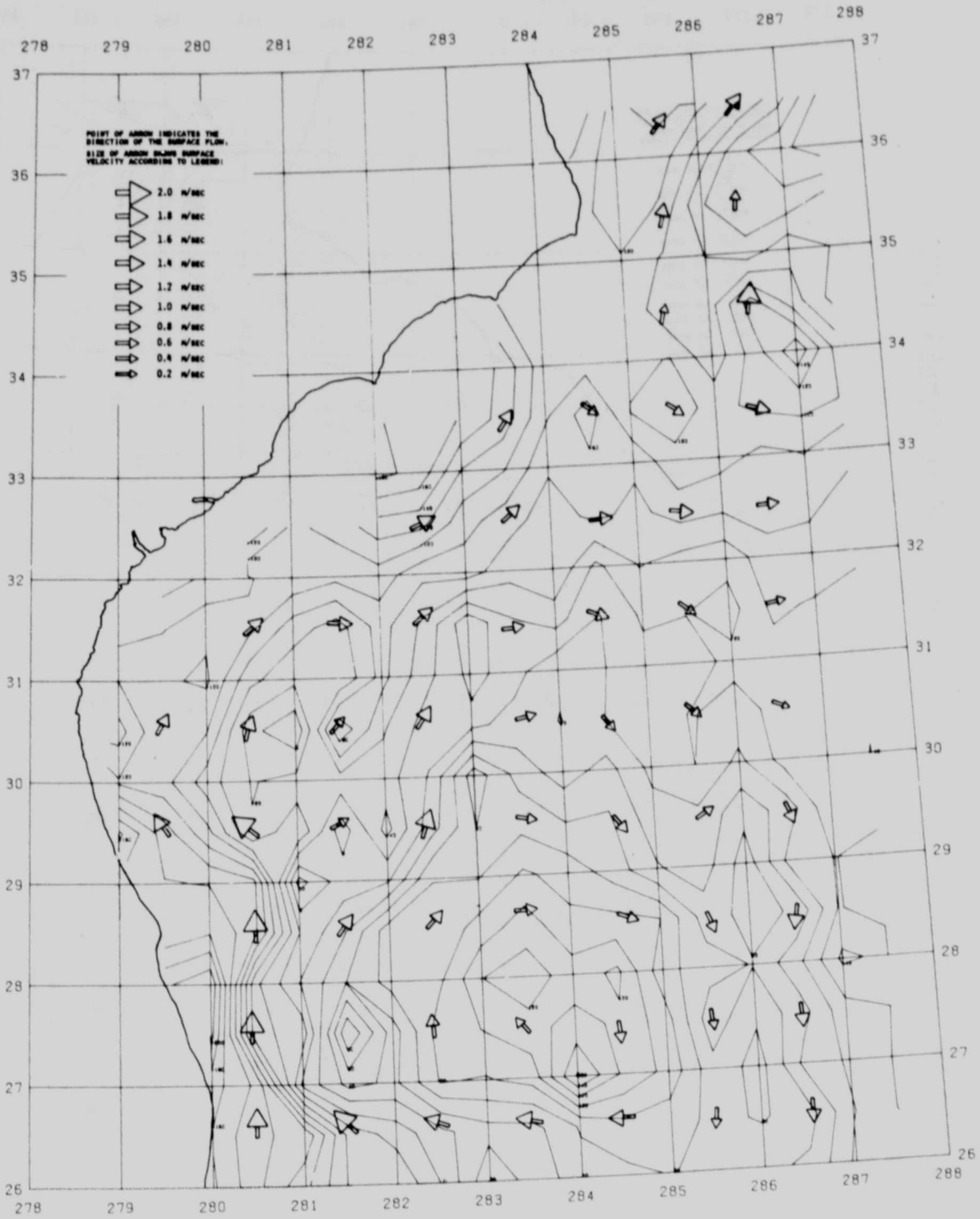

UTM PROJECTION OF MEAN SEA SURFACE FOR SEPTEMBER 1977

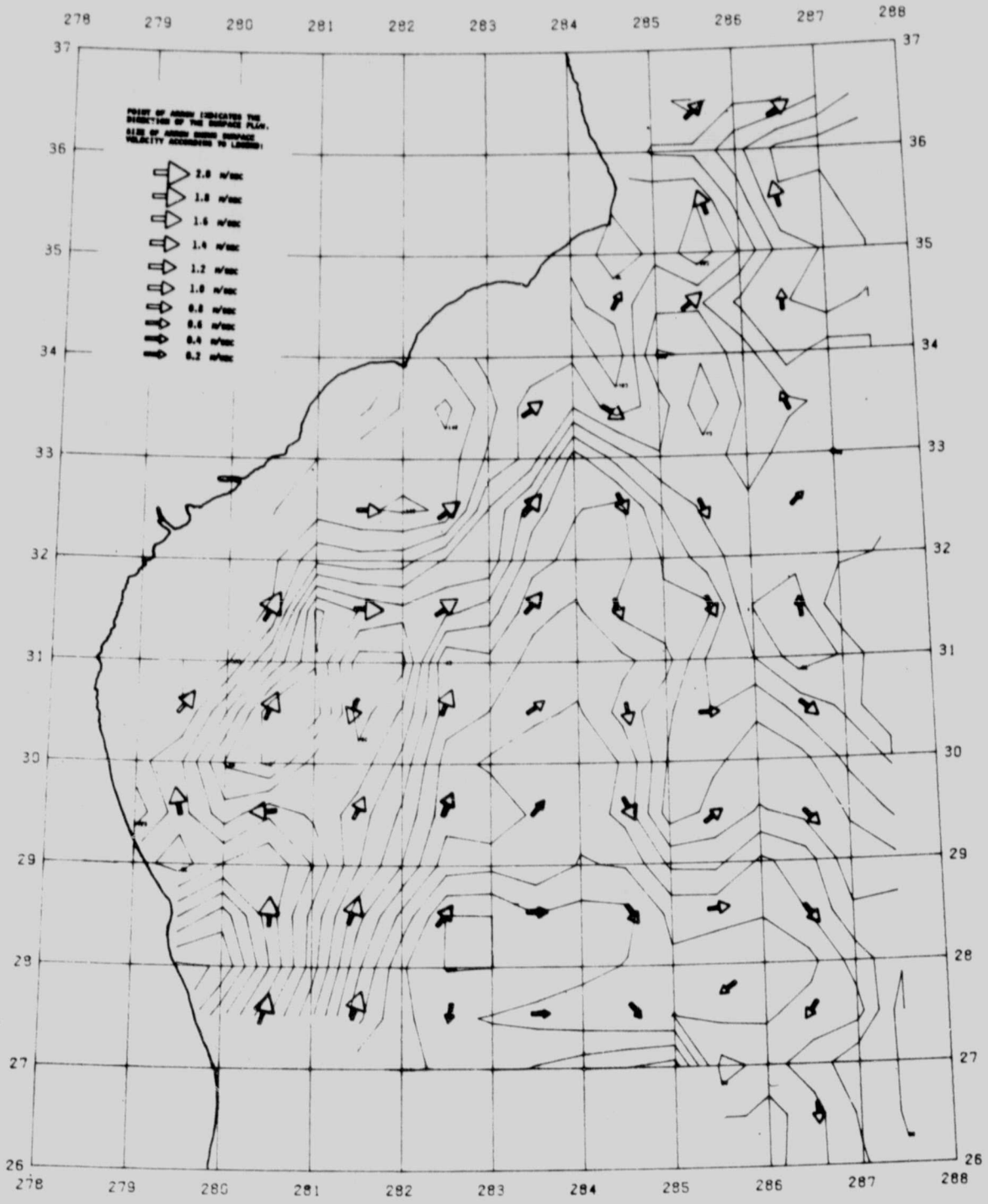

UTM PROJECTION OF MEAN SEA SURFACE FOR OCTOBER 1977

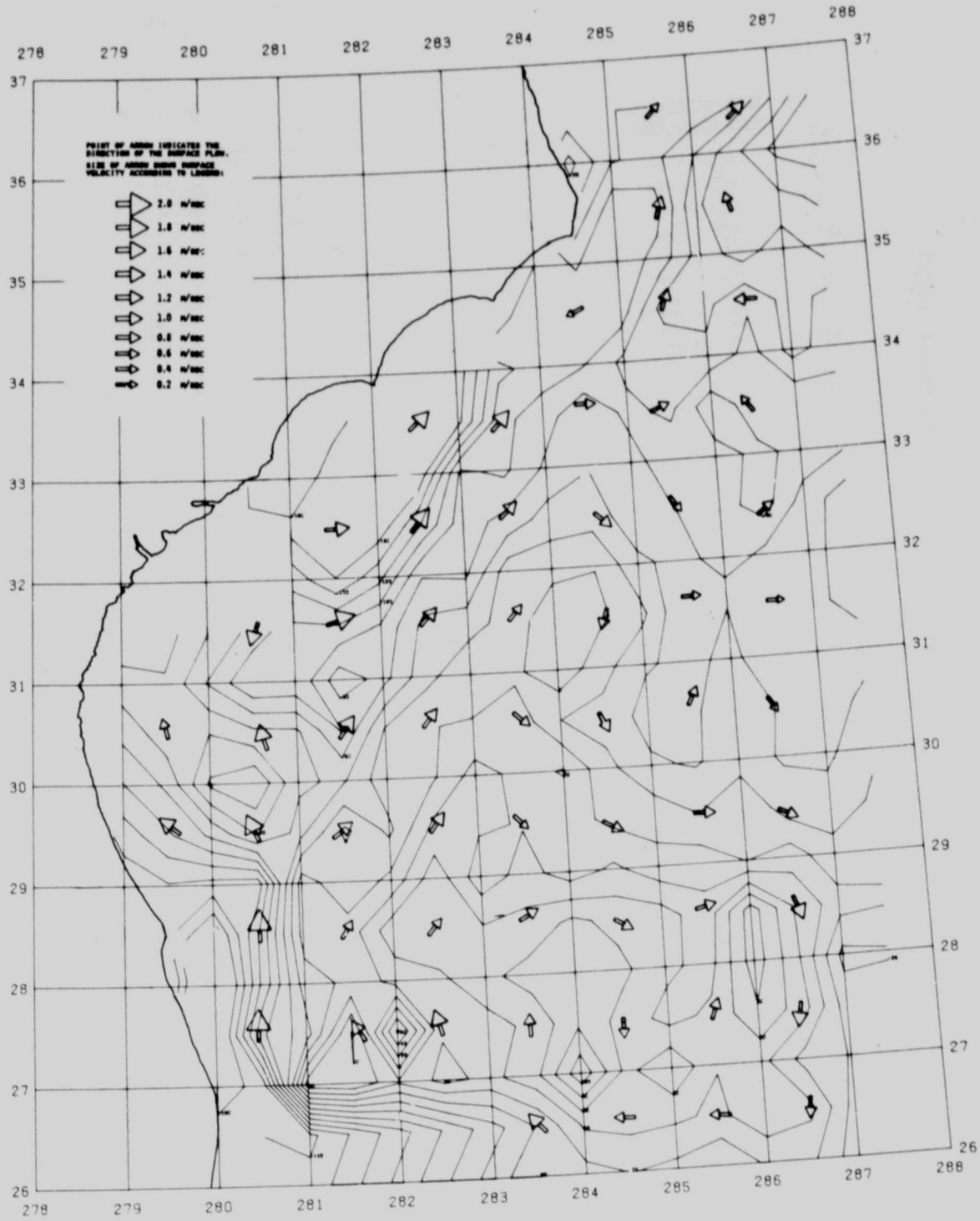

UTM PROJECTION OF MEAN SEA SURFACE FOR NOVEMBER 1977

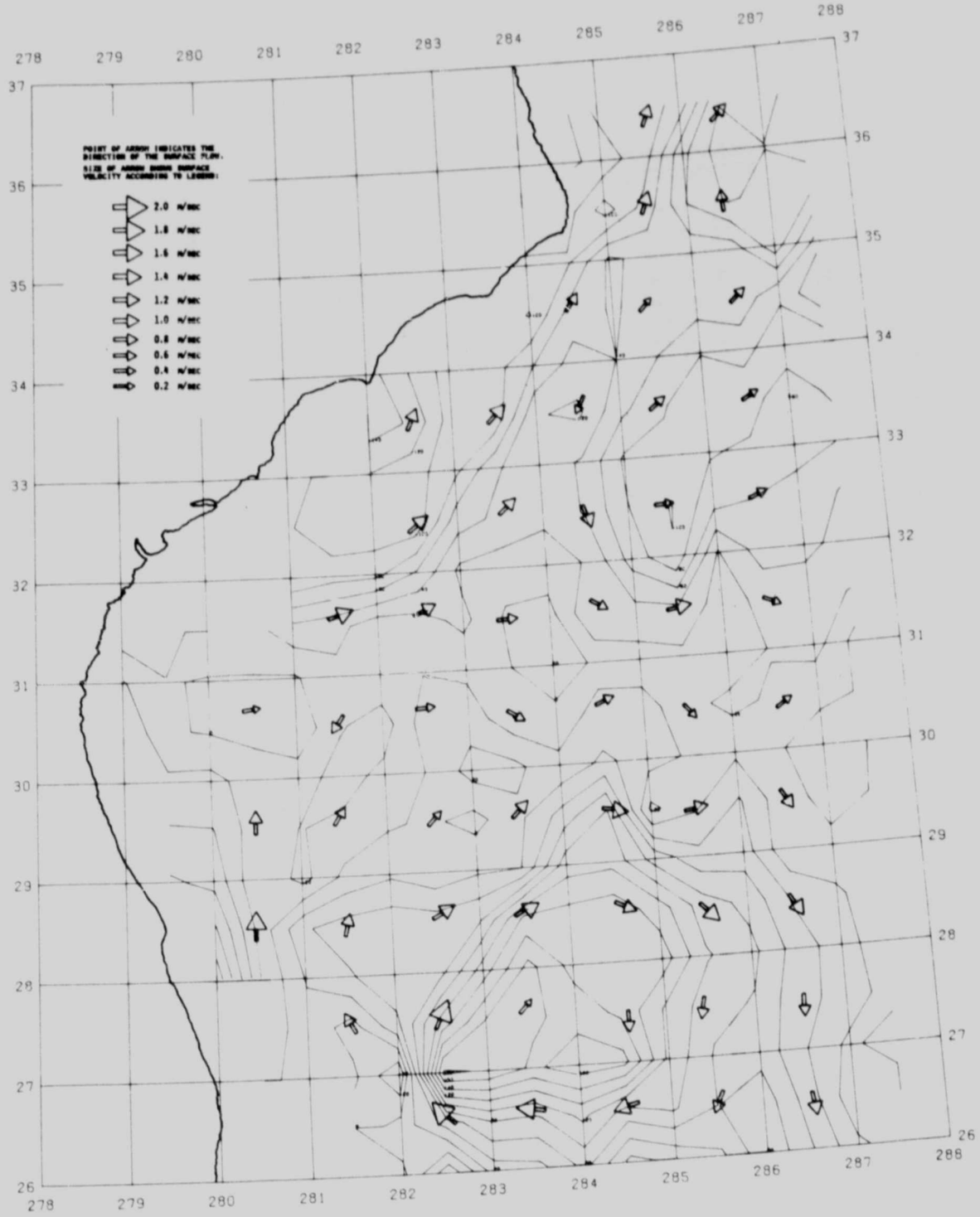

UTM PROJECTION OF MEAN SEA SURFACE FOR DECEMBER 1977

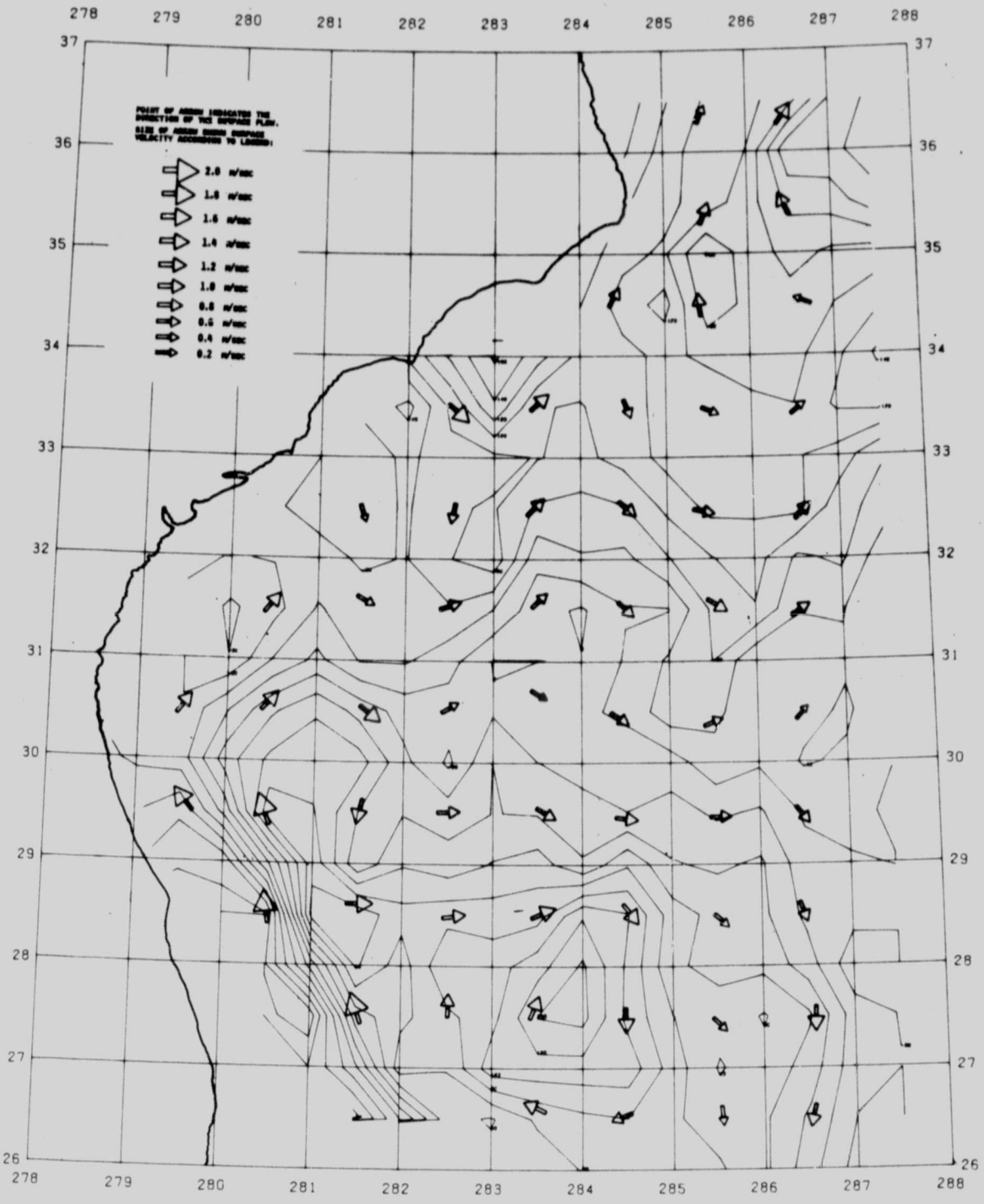

UTM PROJECTION OF MEAN SEA SURFACE FOR JANUARY 1978

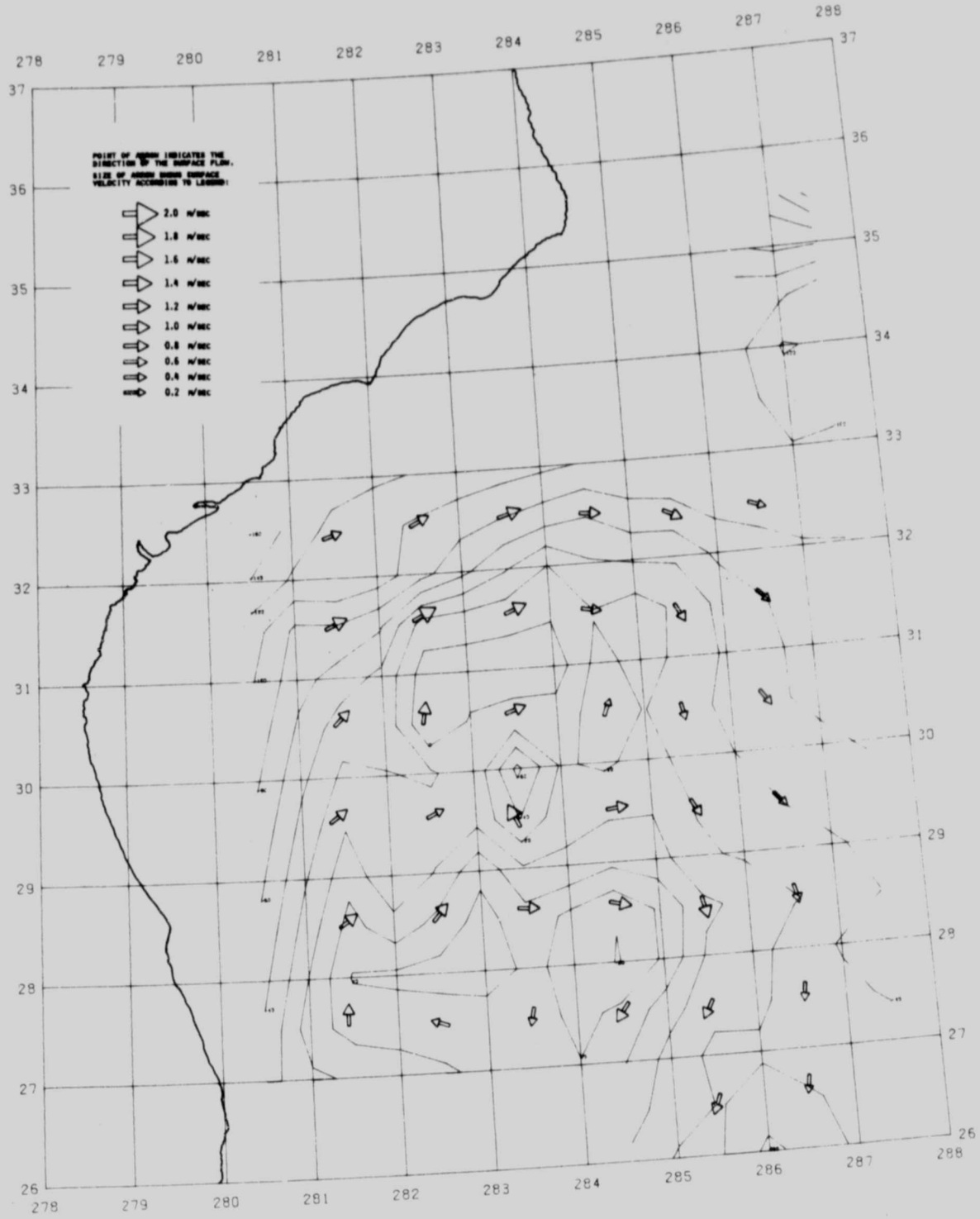

UTM PROJECTION OF MEAN SEA SURFACE FOR FEBRUARY 1978

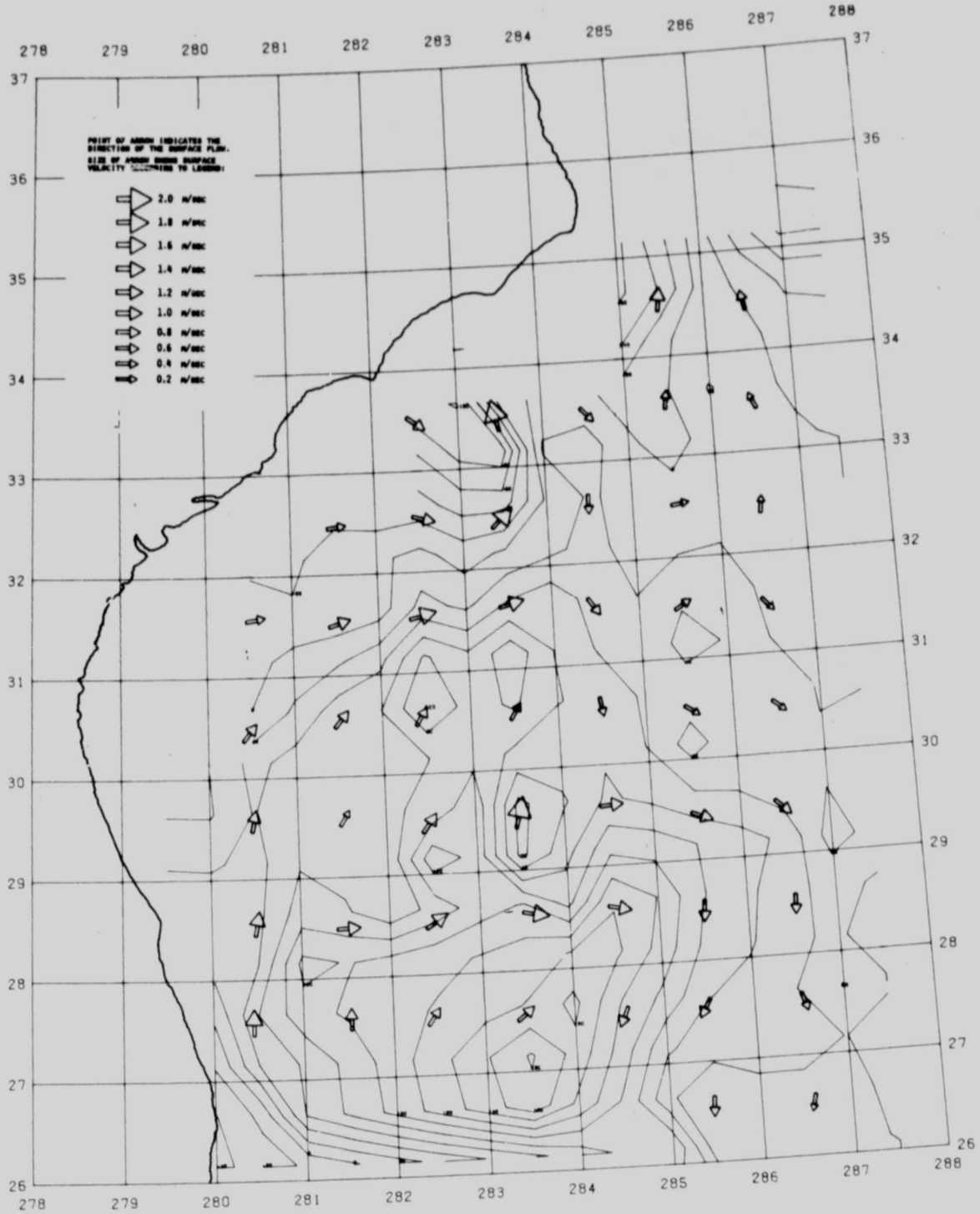

UTM PROJECTION OF MEAN SEA SURFACE FOR MARCH 1978

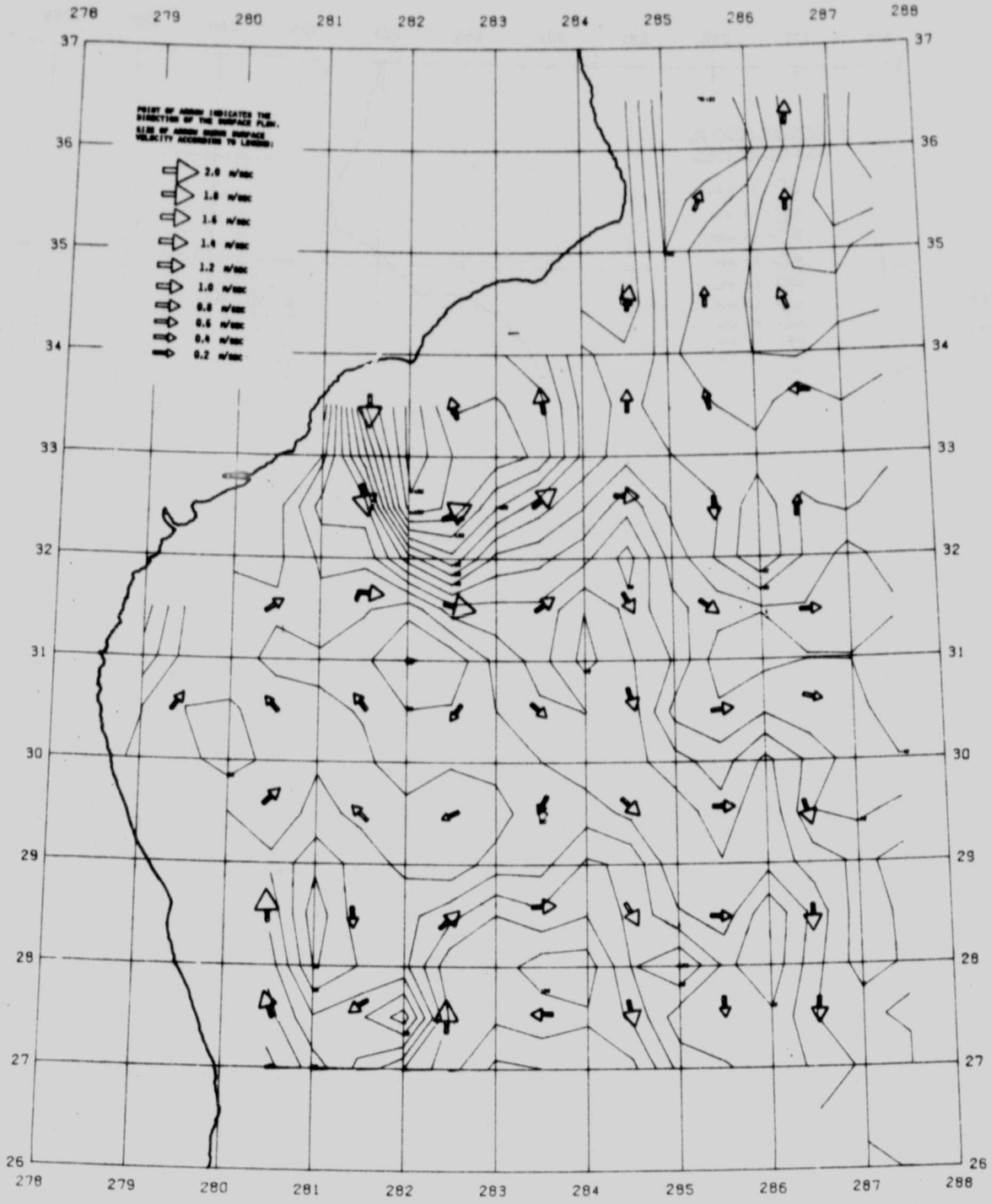

UTM PROJECTION OF MEAN SEA SURFACE FOR APRIL 1978

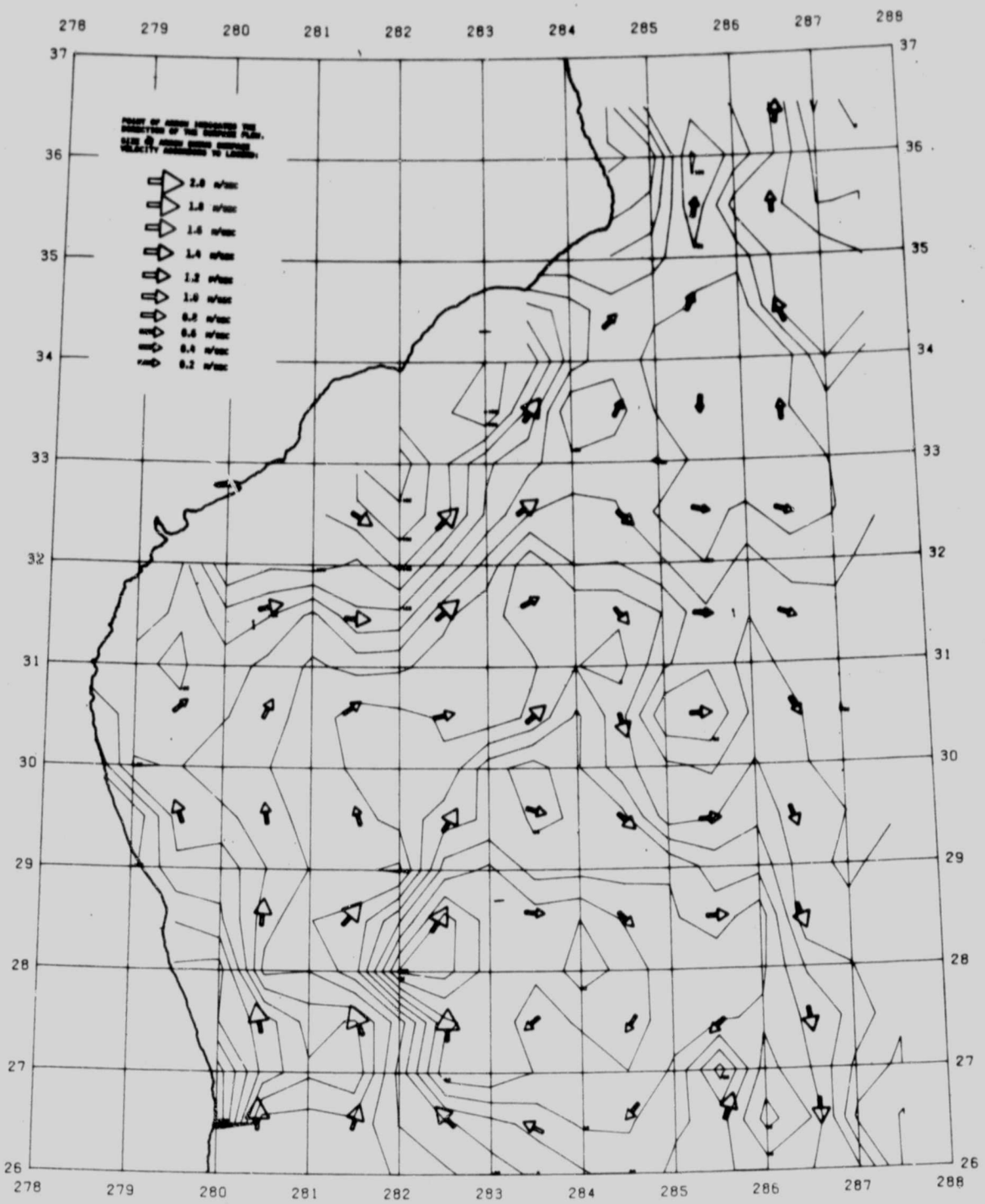

UTM PROJECTION OF MEAN SEA SURFACE FOR MAY 1978

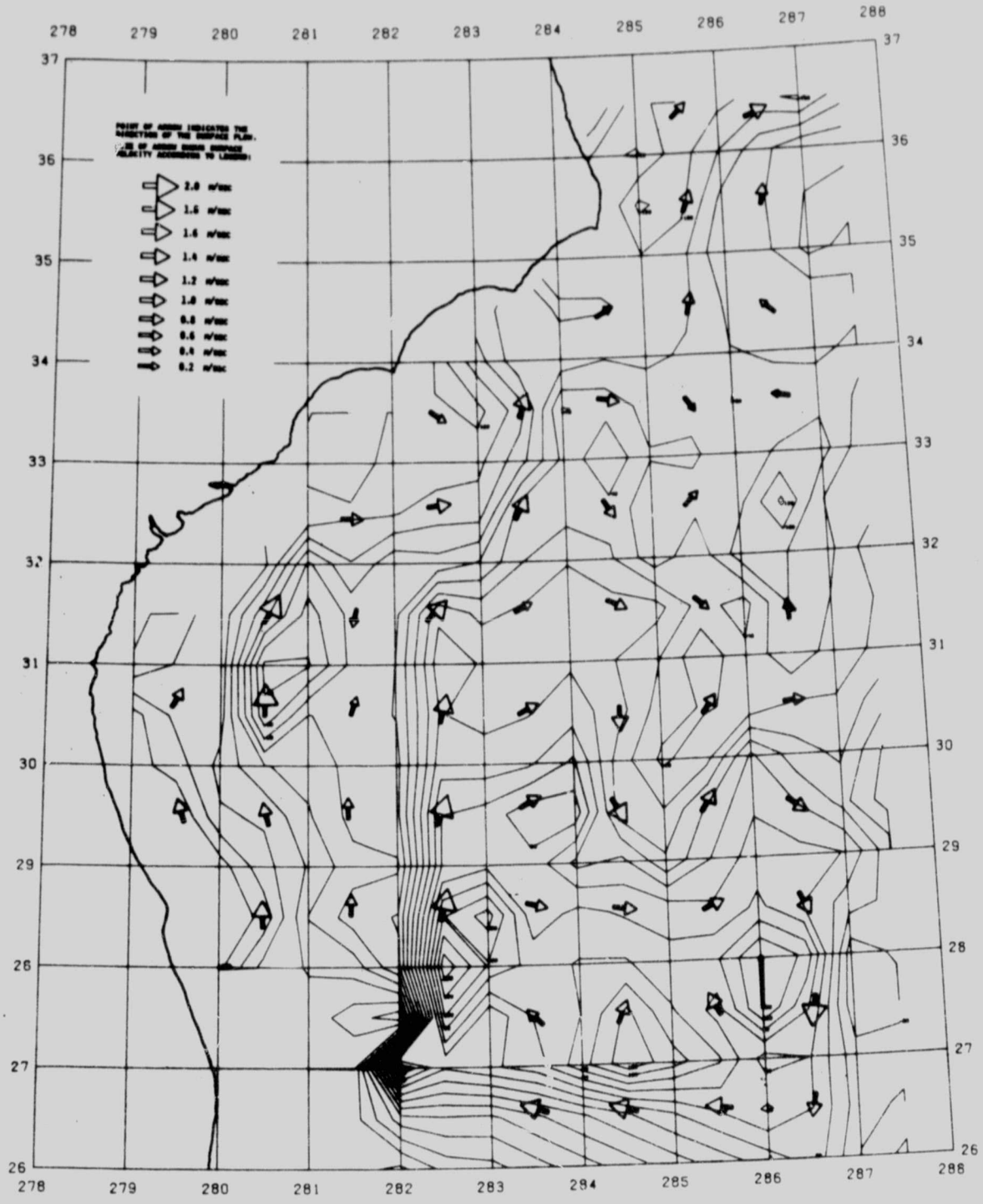

UTM PROJECTION OF MEAN SEA SURFACE FOR JUNE 1978

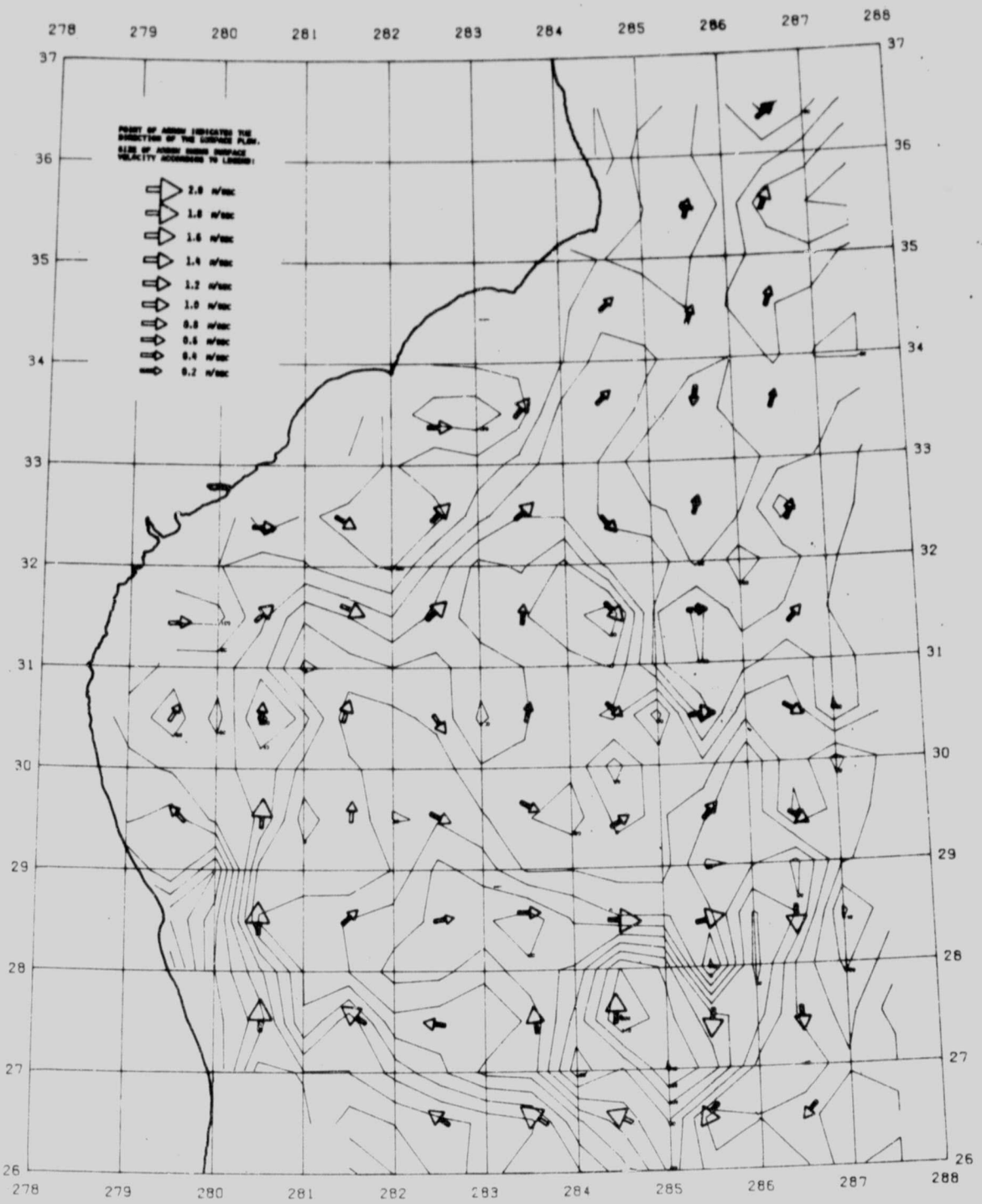

APPENDIX B

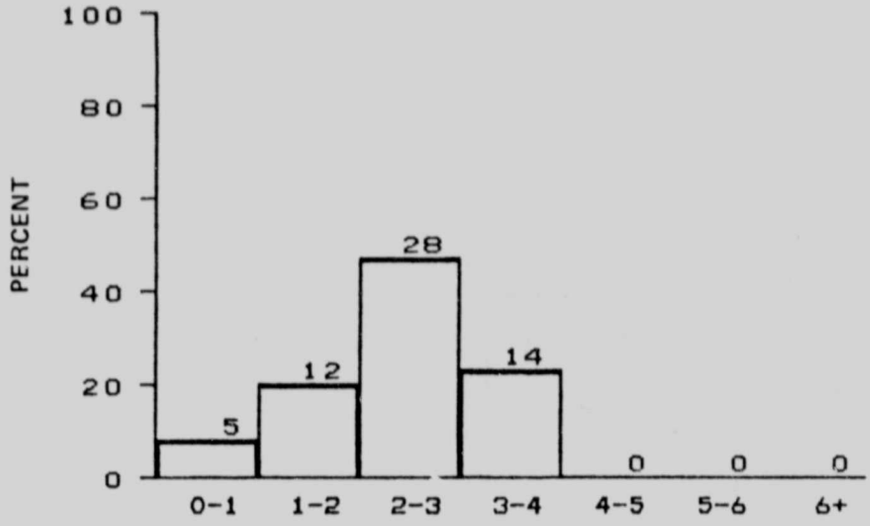

DISTRIBUTION OF SIGNIFICANT WAVE HEIGHT IN METERS
MONTH OF JANUARY
BLM AREA #1
N = 59, MEAN = 2.4, SIGMA = 0.87

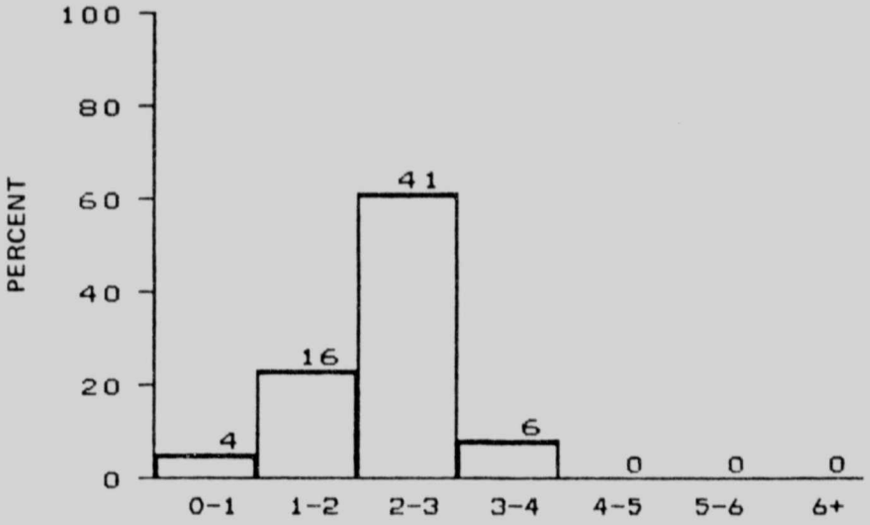

DISTRIBUTION OF SIGNIFICANT WAVE HEIGHT IN METERS
MONTH OF JANUARY
BLM AREA #2
N = 67, MEAN = 2.2, SIGMA = 0.70

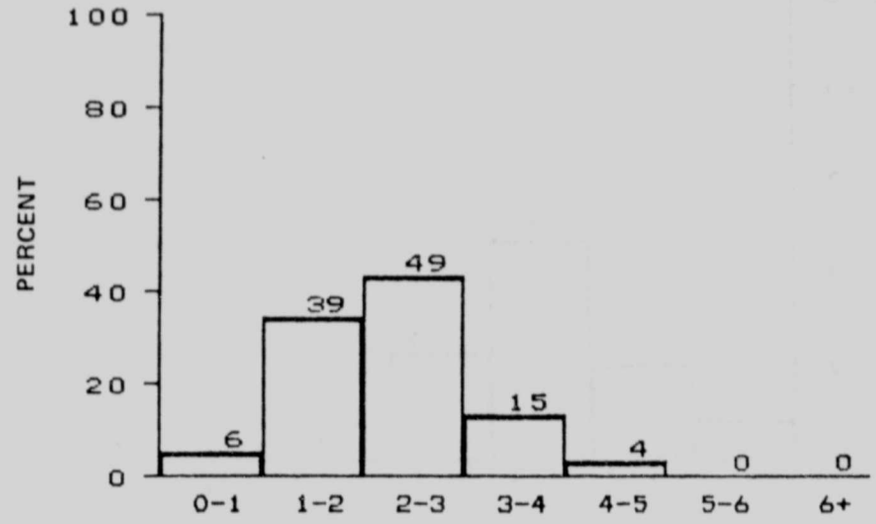

DISTRIBUTION OF SIGNIFICANT WAVE HEIGHT IN METERS
MONTH OF JANUARY
BLM AREA #3
N = 113, MEAN = 2.3, SIGMA = 0.88

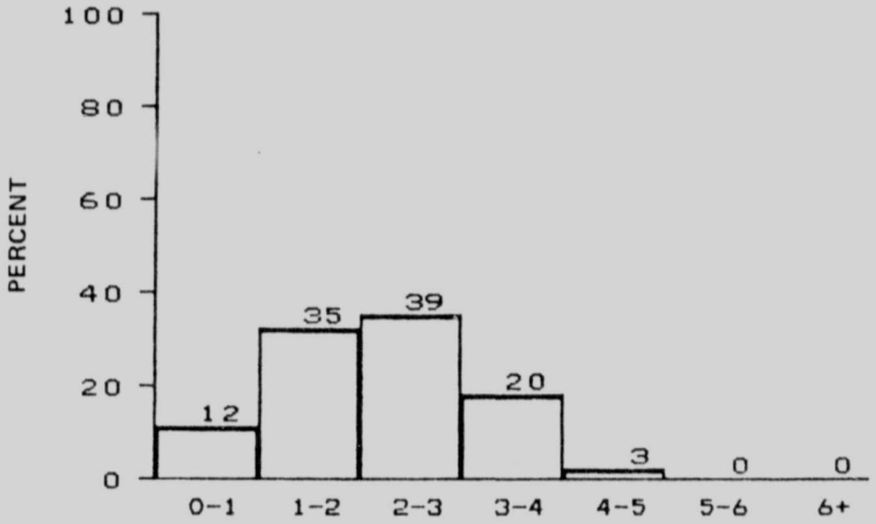

DISTRIBUTION OF SIGNIFICANT WAVE HEIGHT IN METERS
MONTH OF JANUARY
BLM AREA #4
N = 109, MEAN = 2.2, SIGMA = 0.98

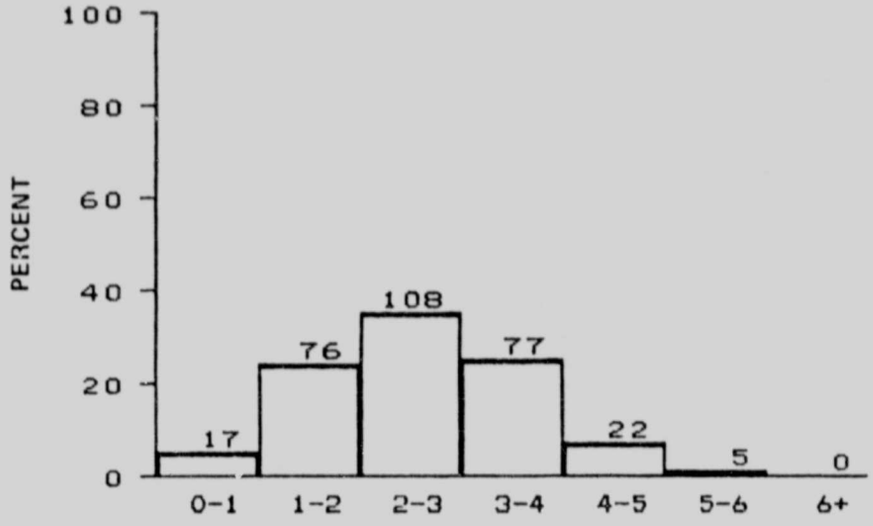

DISTRIBUTION OF SIGNIFICANT WAVE HEIGHT IN METERS
MONTH OF JANUARY
BLM AREA #5
N = 305, MEAN = 2.6, SIGMA = 1.1

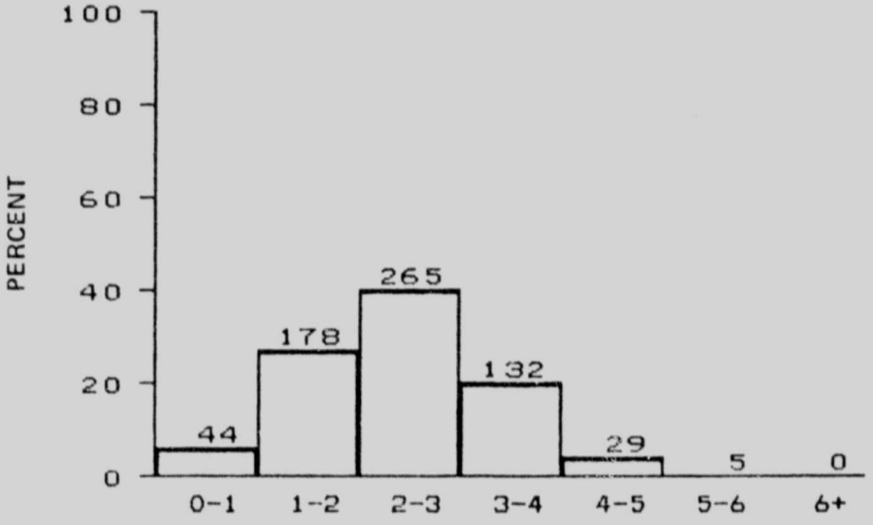

DISTRIBUTION OF SIGNIFICANT WAVE HEIGHT IN METERS
MONTH OF JANUARY
ALL BLM AREAS
N = 653, MEAN = 2.4, SIGMA = 0.99

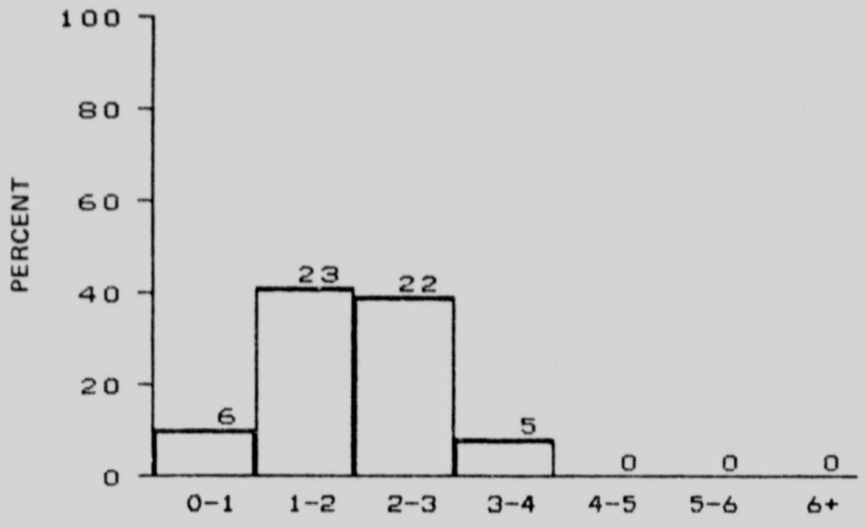

DISTRIBUTION OF SIGNIFICANT WAVE HEIGHT IN METERS
MONTH OF FEBRUARY
BLM AREA #1
N = 56, MEAN = 2.0, SIGMA = 0.80

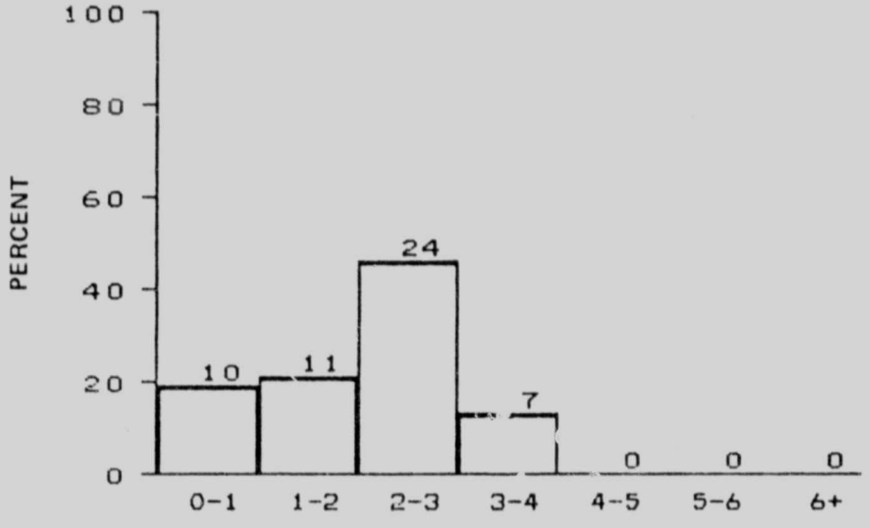

DISTRIBUTION OF SIGNIFICANT WAVE HEIGHT IN METERS
MONTH OF FEBRUARY
BLM AREA #2
N = 52, MEAN = 2.0, SIGMA = 0.95

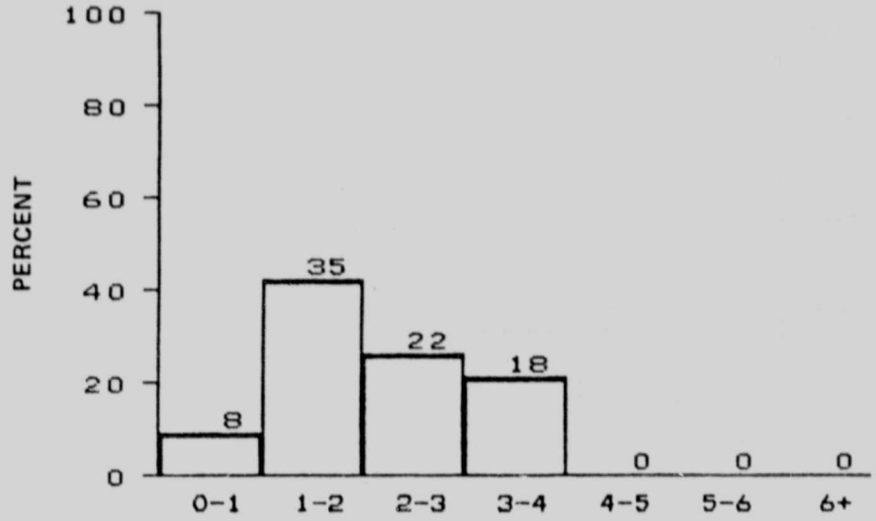

DISTRIBUTION OF SIGNIFICANT WAVE HEIGHT IN METERS
MONTH OF FEBRUARY
BLM AREA #3
N = 83, MEAN = 2.1, SIGMA = 0.93

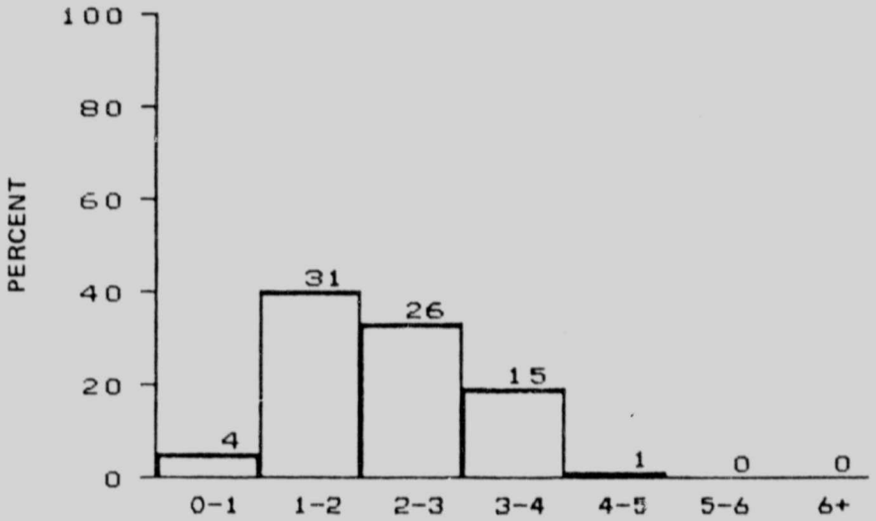

DISTRIBUTION OF SIGNIFICANT WAVE HEIGHT IN METERS
MONTH OF FEBRUARY
BLM AREA #4
N = 77, MEAN = 2.2, SIGMA = 0.88

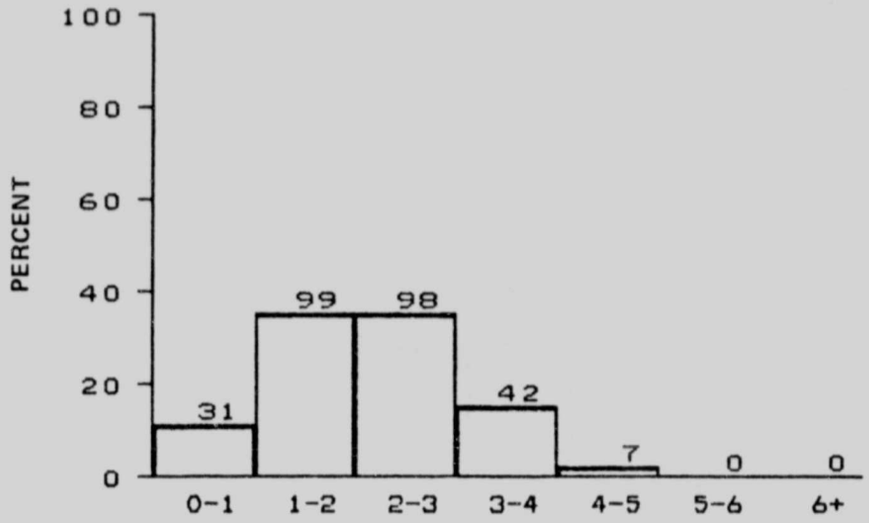

DISTRIBUTION OF SIGNIFICANT WAVE HEIGHT IN METERS
MONTH OF FEBRUARY
BLM AREA #5
N = 277, MEAN = 2.1, SIGMA = 0.96

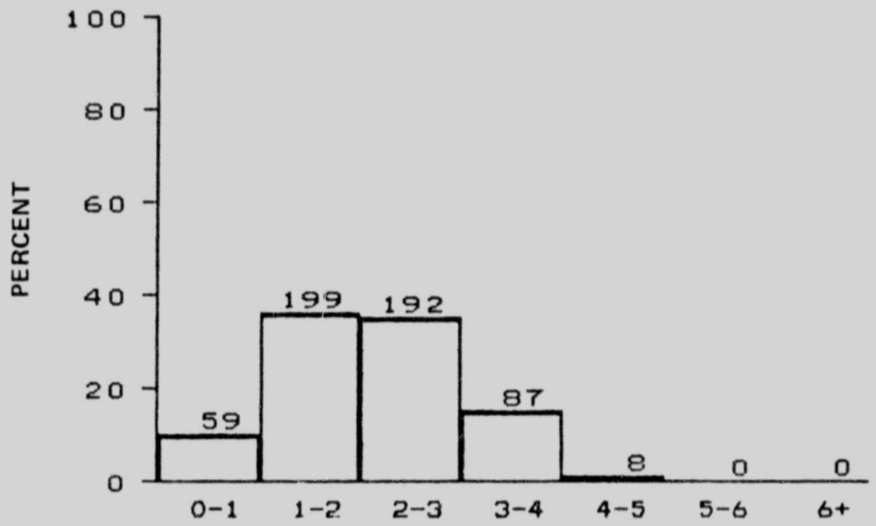

DISTRIBUTION OF SIGNIFICANT WAVE HEIGHT IN METERS
MONTH OF FEBRUARY
ALL BLM AREAS
N = 545, MEAN = 2.1, SIGMA = 0.93

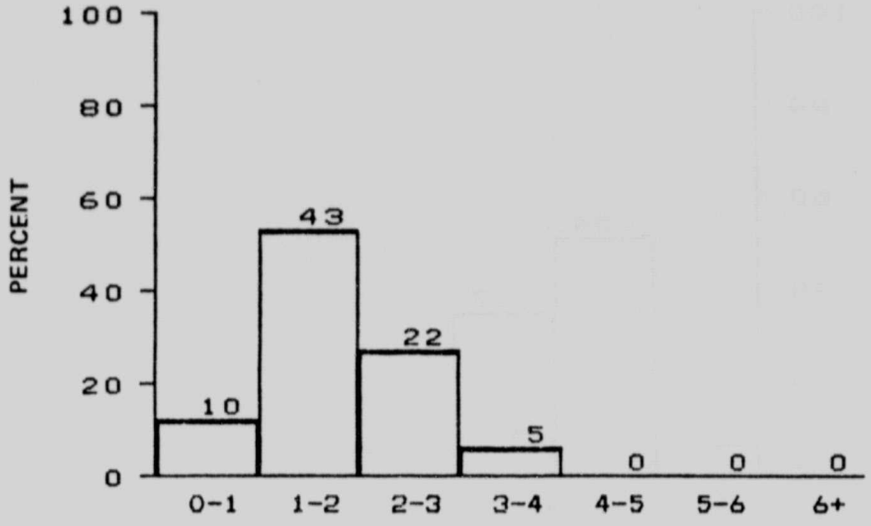

DISTRIBUTION OF SIGNIFICANT WAVE HEIGHT IN METERS
MONTH OF MARCH
BLM AREA #1
N = 80, MEAN = 1.8, SIGMA = 0.76

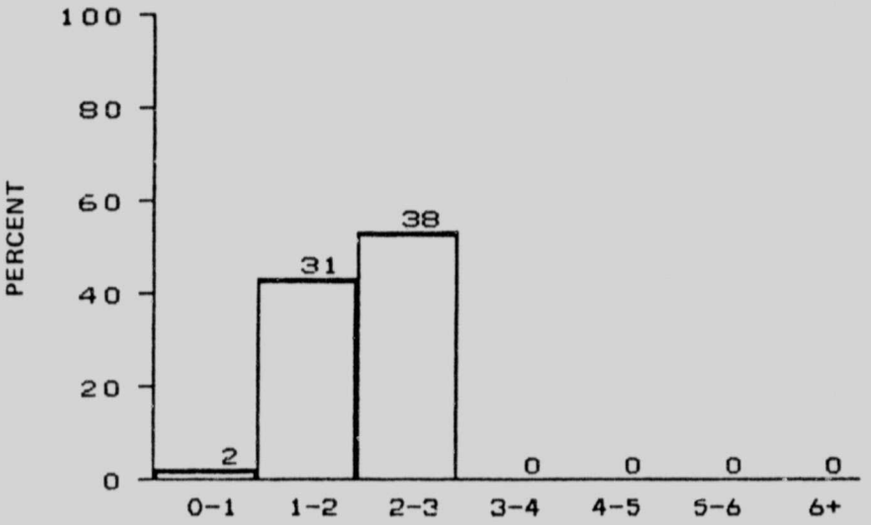

DISTRIBUTION OF SIGNIFICANT WAVE HEIGHT IN METERS
MONTH OF MARCH
BLM AREA #2
N = 71, MEAN = 2.0, SIGMA = 0.55

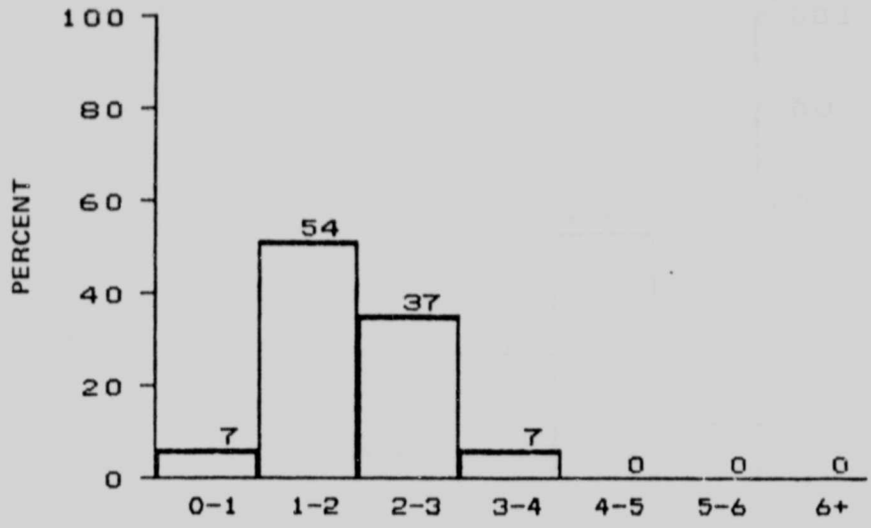

DISTRIBUTION OF SIGNIFICANT WAVE HEIGHT IN METERS
MONTH OF MARCH
BLM AREA #3
N = 105, MEAN = 1.9, SIGMA = 0.71

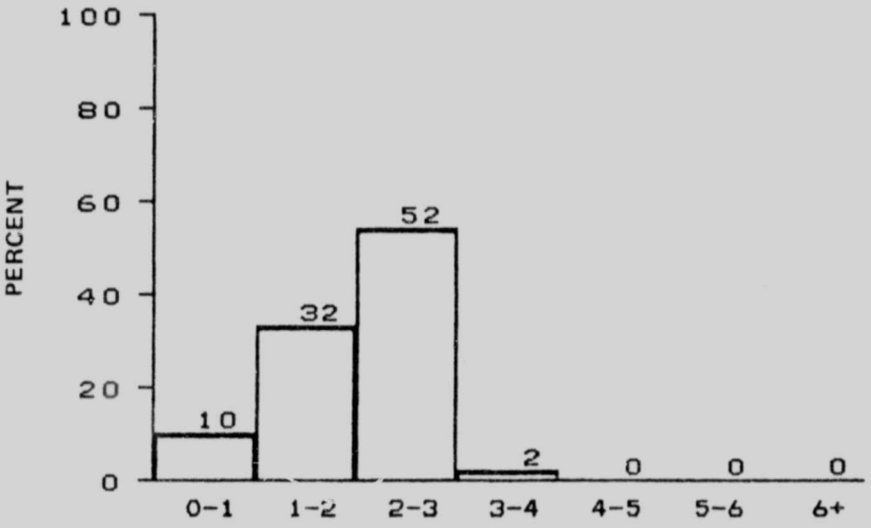

DISTRIBUTION OF SIGNIFICANT WAVE HEIGHT IN METERS
MONTH OF MARCH
BLM AREA #4
N = 96, MEAN = 2.0, SIGMA = 0.71

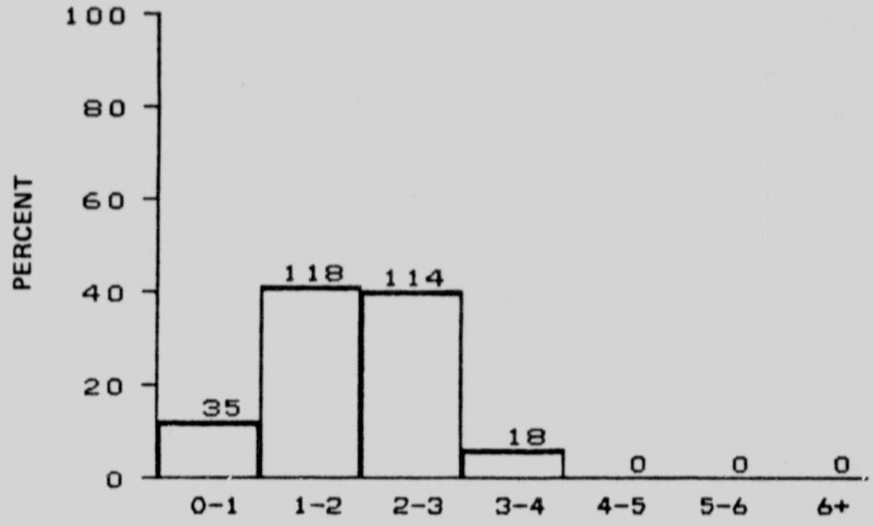

DISTRIBUTION OF SIGNIFICANT WAVE HEIGHT IN METERS
MONTH OF MARCH
BLM AREA #5
N = 285, MEAN = 1.9, SIGMA = 0.78

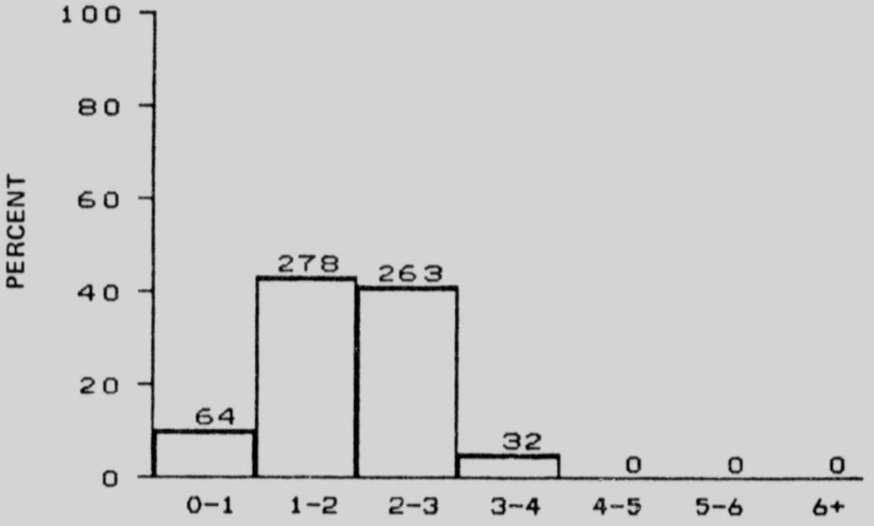

DISTRIBUTION OF SIGNIFICANT WAVE HEIGHT IN METERS
MONTH OF MARCH
ALL BLM AREAS
N = 637, MEAN = 1.9, SIGMA = 0.74

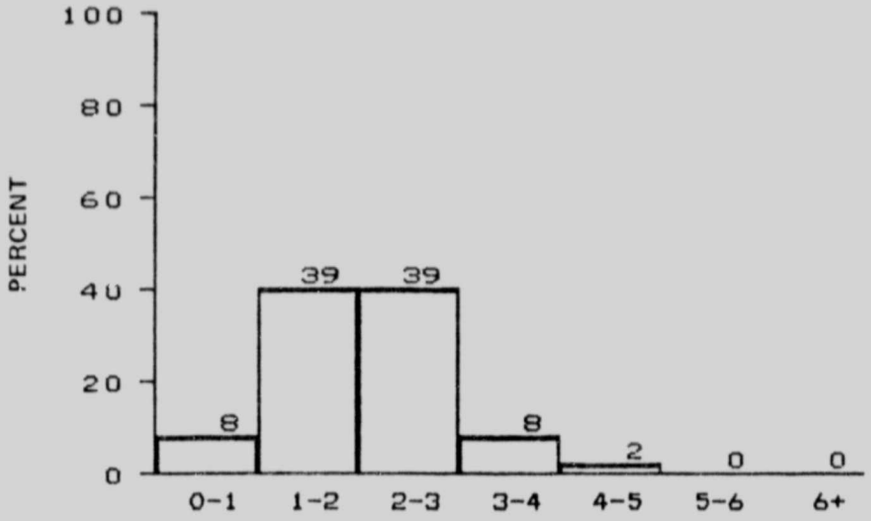

DISTRIBUTION OF SIGNIFICANT WAVE HEIGHT IN METERS
MONTH OF APRIL
BLM AREA #1
N = 96, MEAN = 2.1, SIGMA = 0.84

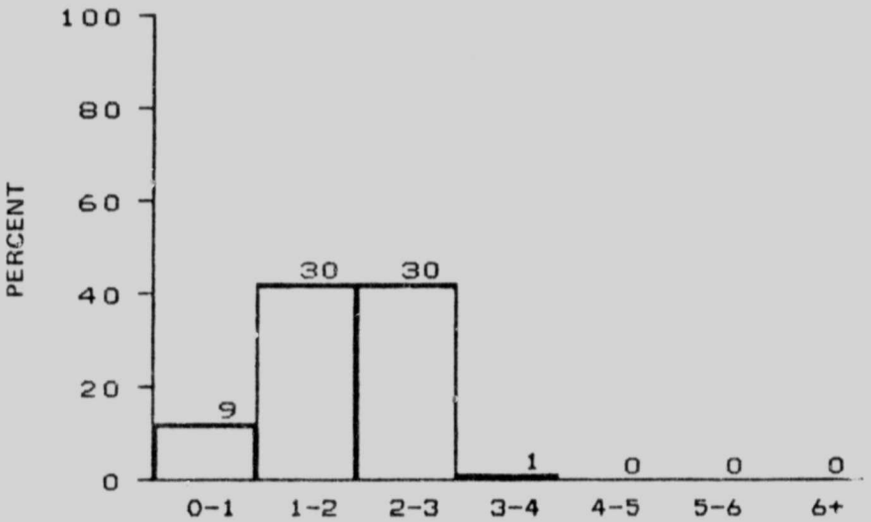

DISTRIBUTION OF SIGNIFICANT WAVE HEIGHT IN METERS
MONTH OF APRIL
BLM AREA #2
N = 70, MEAN = 1.8, SIGMA = 0.71

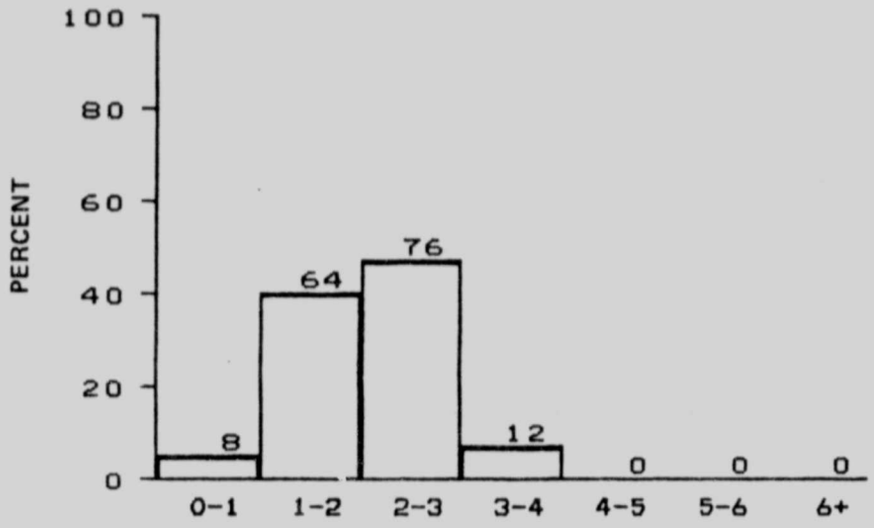

DISTRIBUTION OF SIGNIFICANT WAVE HEIGHT IN METERS
MONTH OF APRIL
BLM AREA #3
N = 160, MEAN = 2.1, SIGMA = 0.70

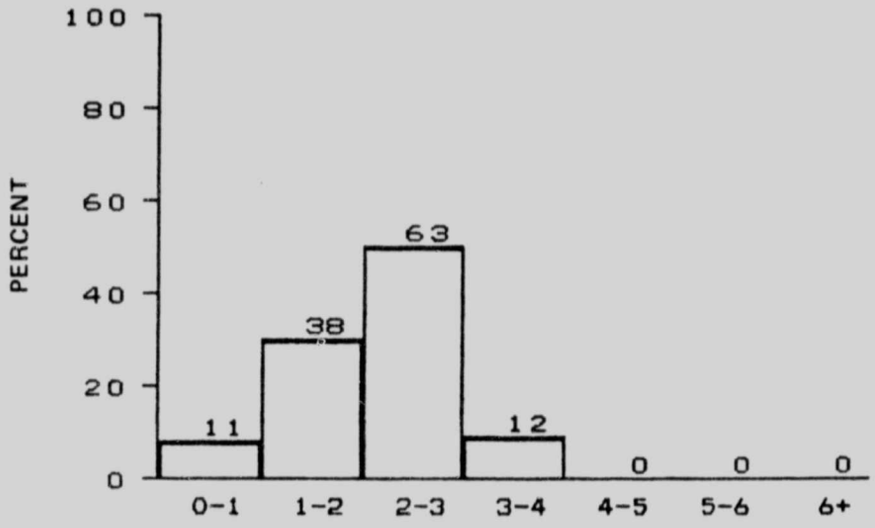

DISTRIBUTION OF SIGNIFICANT WAVE HEIGHT IN METERS
MONTH OF APRIL
BLM AREA #4
N = 124, MEAN = 2.1, SIGMA = 0.78

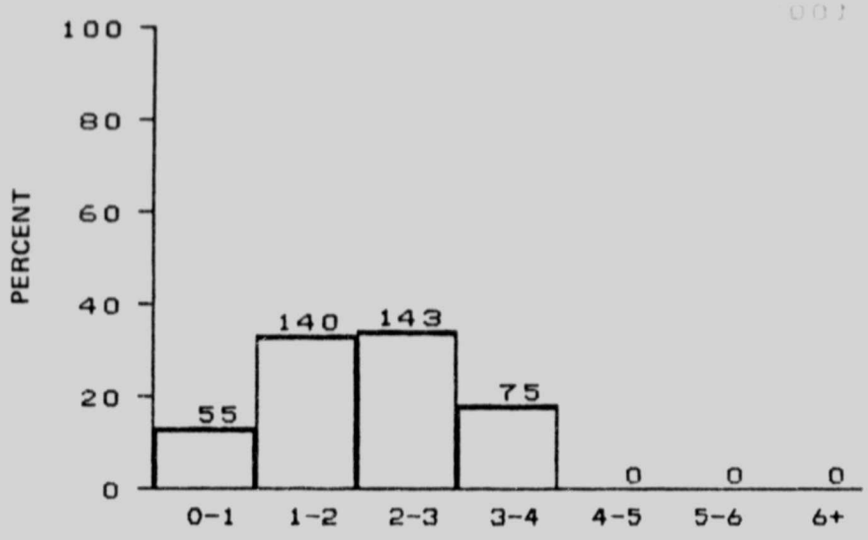

DISTRIBUTION OF SIGNIFICANT WAVE HEIGHT IN METERS
MONTH OF APRIL
BLM AREA #5
N = 413, MEAN = 2.1, SIGMA = 0.93

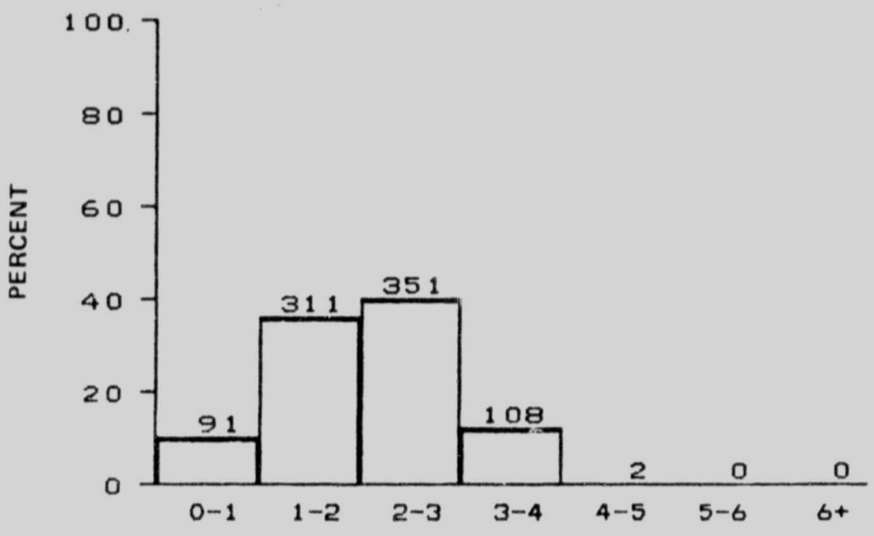

DISTRIBUTION OF SIGNIFICANT WAVE HEIGHT IN METERS
MONTH OF APRIL
ALL BLM AREAS
N = 863, MEAN = 2.1, SIGMA = 0.85

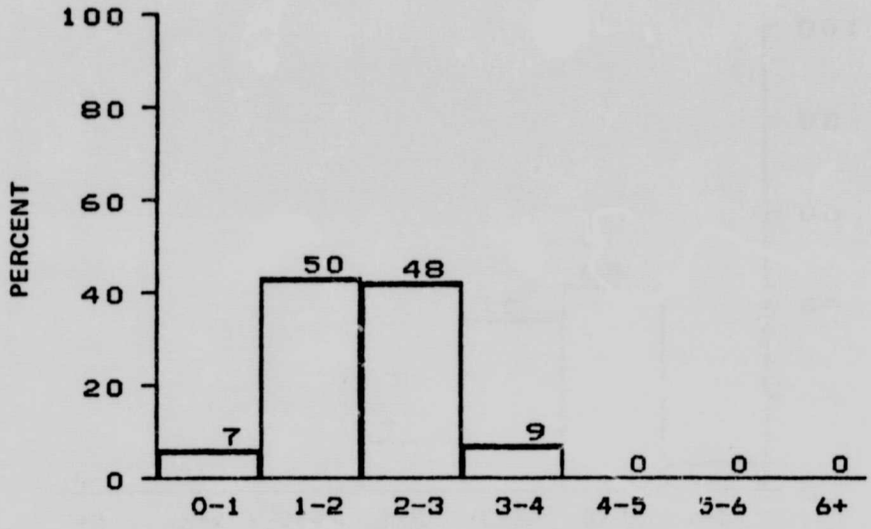

DISTRIBUTION OF SIGNIFICANT WAVE HEIGHT IN METERS
MONTH OF MAY
BLM AREA #1
N = 114, MEAN = 2.0, SIGMA = 0.73

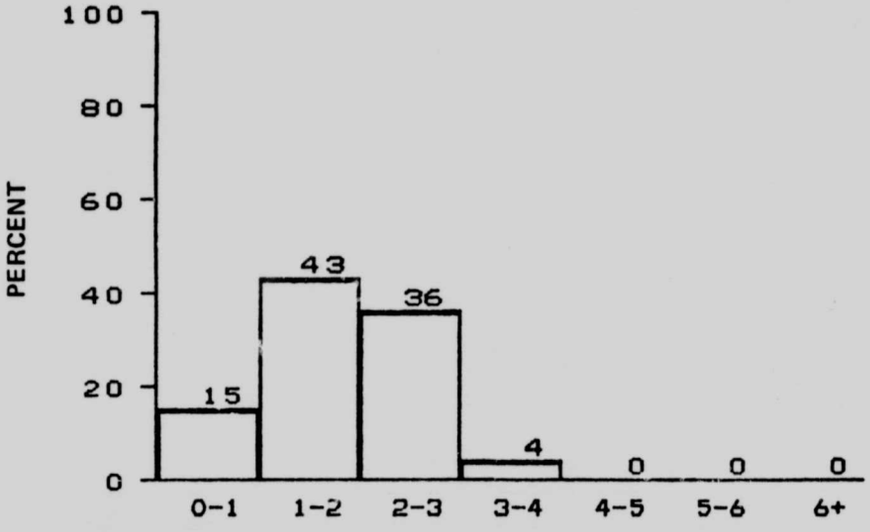

DISTRIBUTION OF SIGNIFICANT WAVE HEIGHT IN METERS
MONTH OF MAY
BLM AREA #2
N = 98, MEAN = 1.8, SIGMA = 0.77

C-2

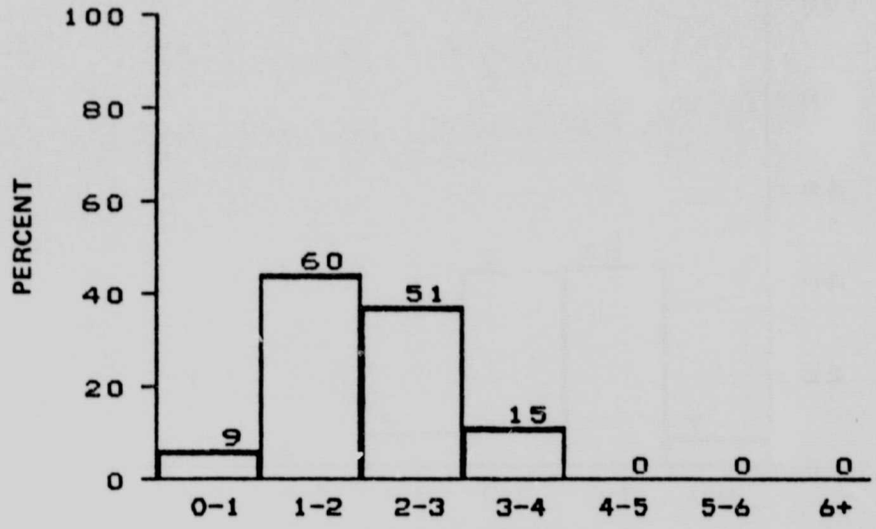

DISTRIBUTION OF SIGNIFICANT WAVE HEIGHT IN METERS
MONTH OF MAY
BLM AREA #3
N = 135, MEAN = 2.0, SIGMA = 0.78

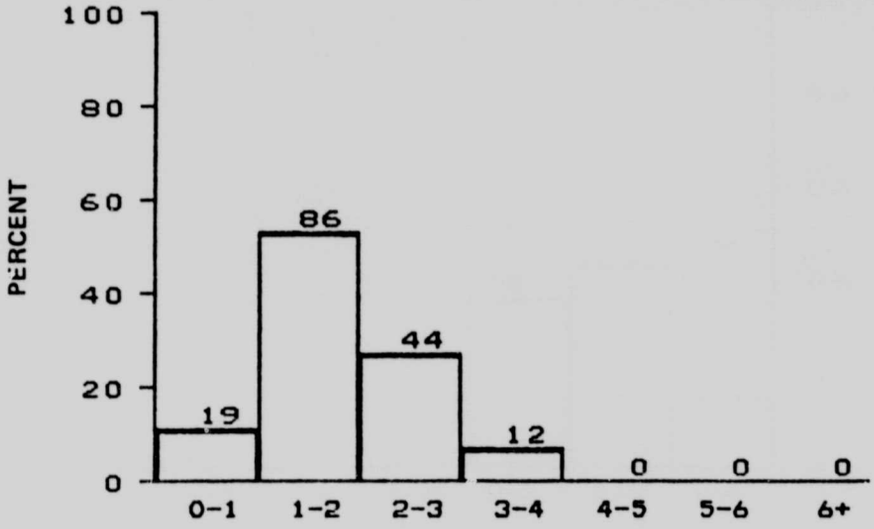

DISTRIBUTION OF SIGNIFICANT WAVE HEIGHT IN METERS
MONTH OF MAY
BLM AREA #4
N = 161, MEAN = 1.8, SIGMA = 0.77

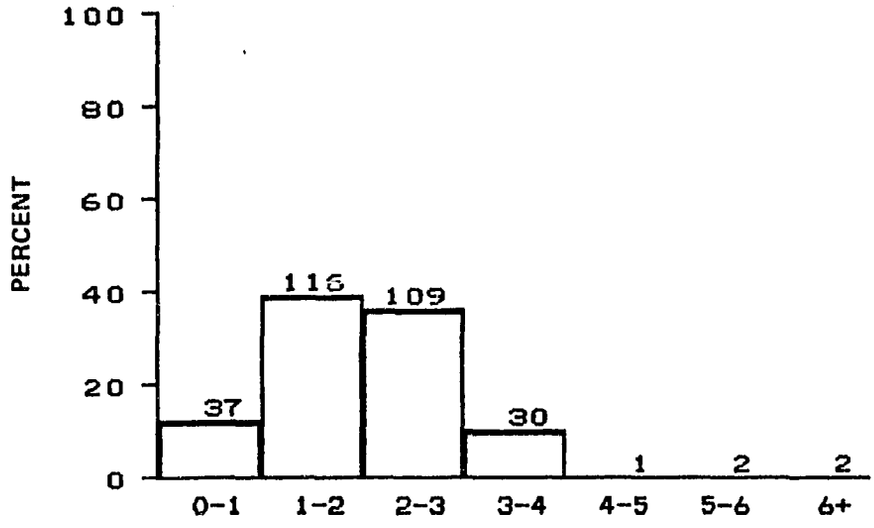

DISTRIBUTION OF SIGNIFICANT WAVE HEIGHT IN METERS
MONTH OF MAY
BLM AREA #5
N = 297, MEAN = 2.0, SIGMA = 0.97

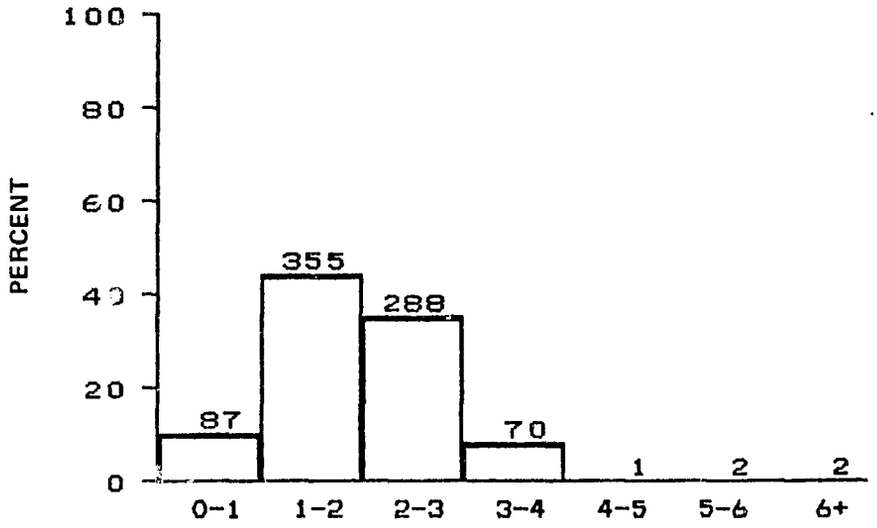

DISTRIBUTION OF SIGNIFICANT WAVE HEIGHT IN METERS
MONTH OF MAY
ALL BLM AREAS
N = 805, MEAN = 1.9, SIGMA = 0.85

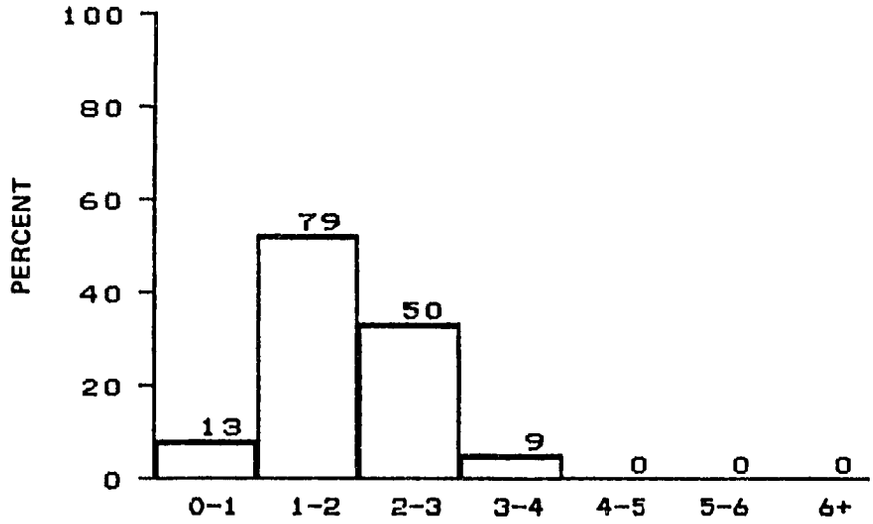

DISTRIBUTION OF SIGNIFICANT WAVE HEIGHT IN METERS
MONTH OF JUNE
BLM AREA #1
N = 151, MEAN = 1.9, SIGMA = 0.72

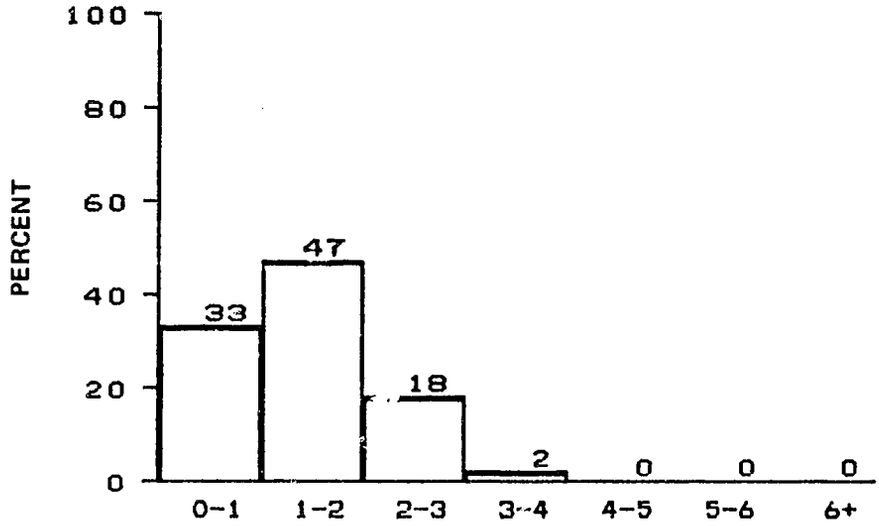

DISTRIBUTION OF SIGNIFICANT WAVE HEIGHT IN METERS
MONTH OF JUNE
BLM AREA #2
N = 100, MEAN = 1.4, SIGMA = 0.76

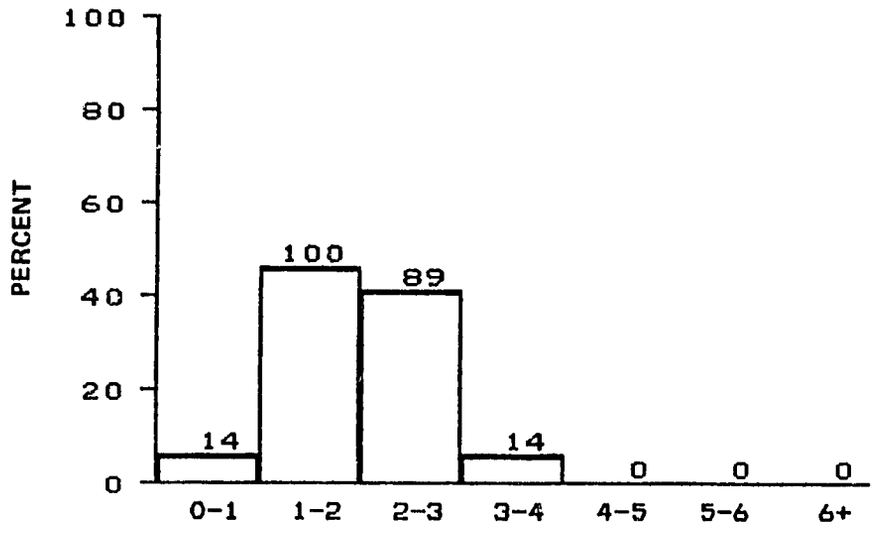

DISTRIBUTION OF SIGNIFICANT WAVE HEIGHT IN METERS
MONTH OF JUNE
BLM AREA #3
N = 217, MEAN = 2.0, SIGMA = 0.71

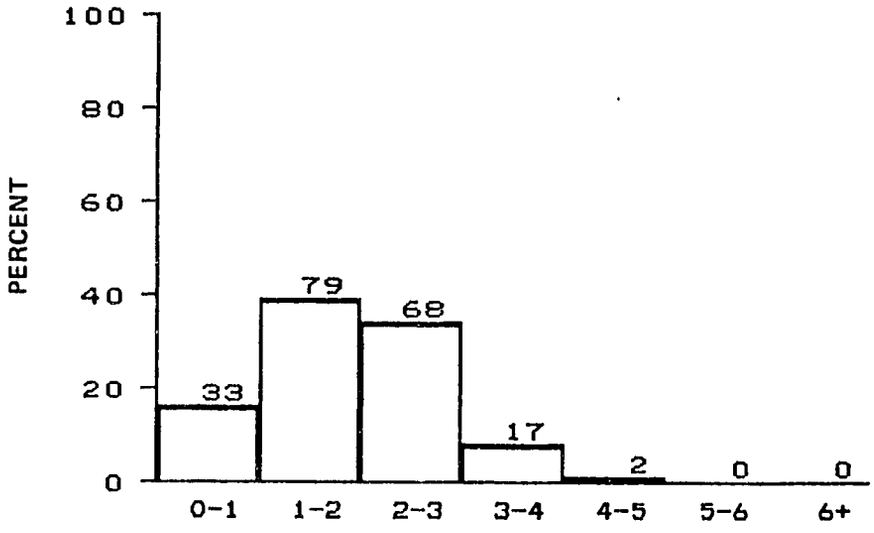

DISTRIBUTION OF SIGNIFICANT WAVE HEIGHT IN METERS
MONTH OF JUNE
BLM AREA #4
N = 199, MEAN = 1.9, SIGMA = 0.89

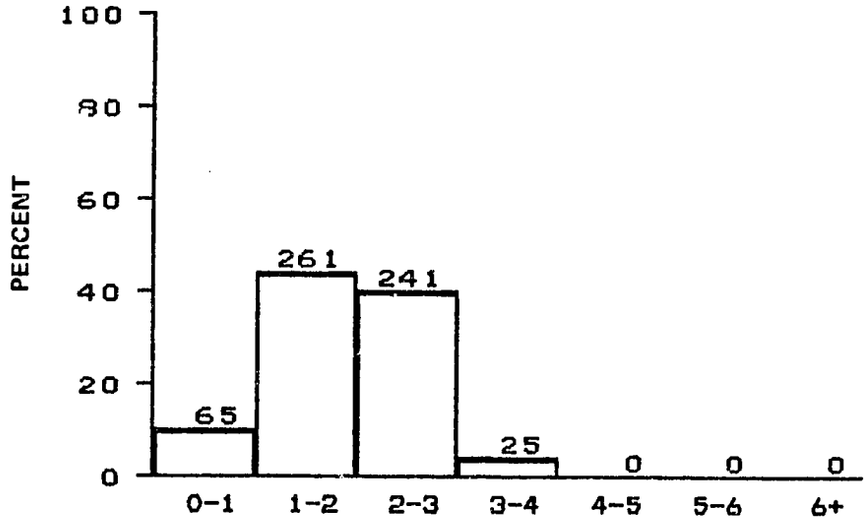

DISTRIBUTION OF SIGNIFICANT WAVE HEIGHT IN METERS

MONTH OF JUNE

BLM AREA #5

N = 592, MEAN = 1.9 SIGMA = 0.73

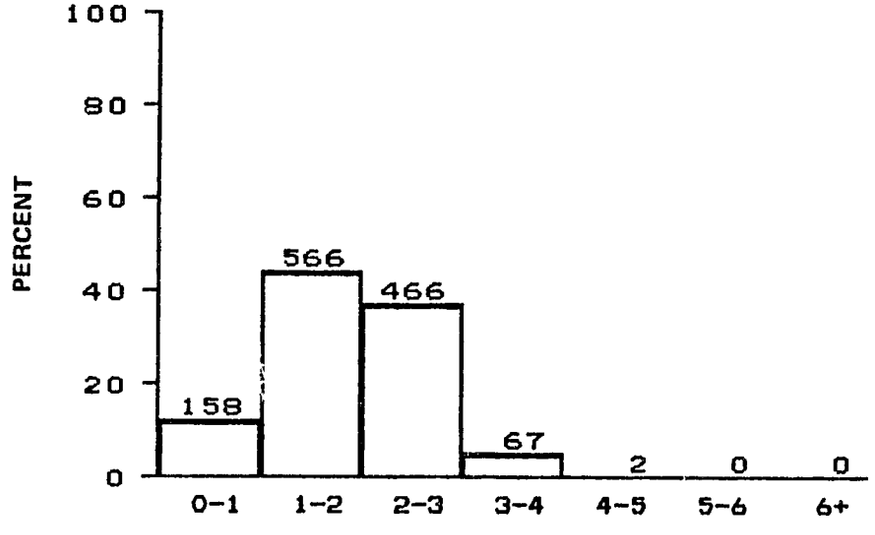

DISTRIBUTION OF SIGNIFICANT WAVE HEIGHT IN METERS

MONTH OF JUNE

ALL BLM AREAS

N = 1259, MEAN = 1.9, SIGMA = 0.77

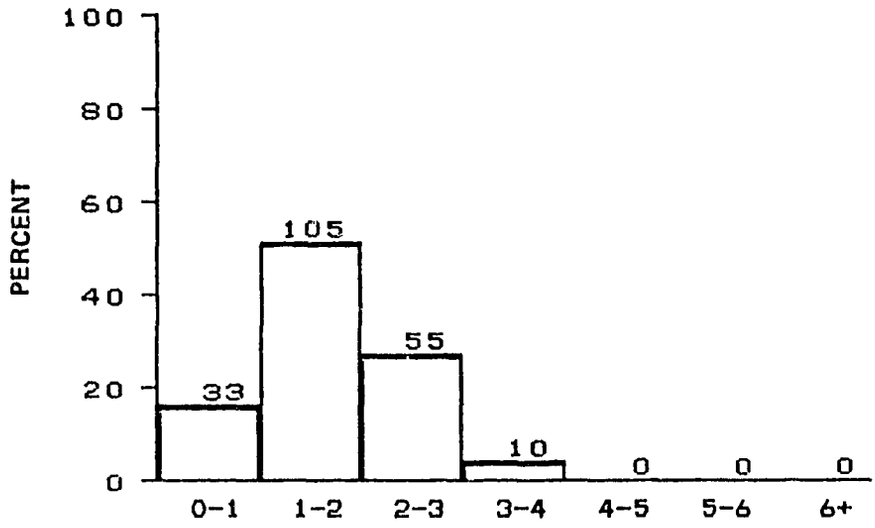

DISTRIBUTION OF SIGNIFICANT WAVE HEIGHT IN METERS
MONTH OF JULY
BLM AREA #1
N = 203, MEAN = 1.7, SIGMA = 0.77

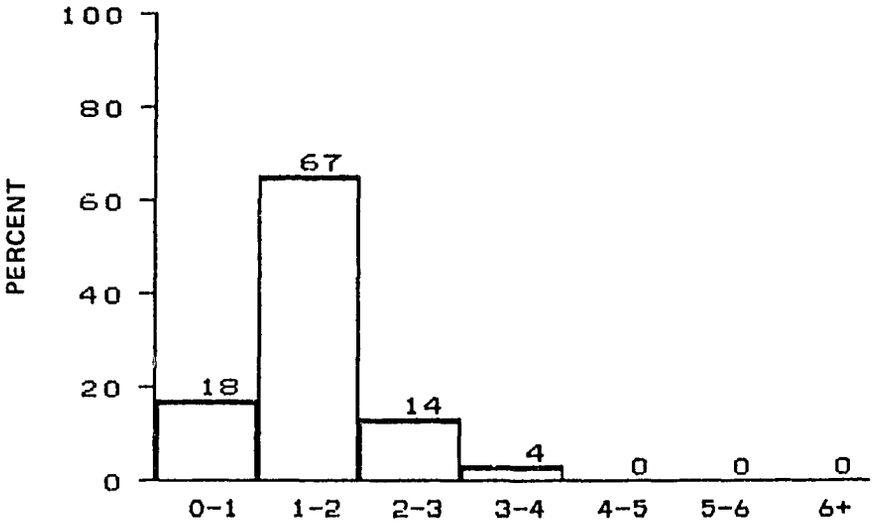

DISTRIBUTION OF SIGNIFICANT WAVE HEIGHT IN METERS
MONTH OF JULY
BLM AREA #2
N = 103, MEAN = 1.5, SIGMA = 0.68

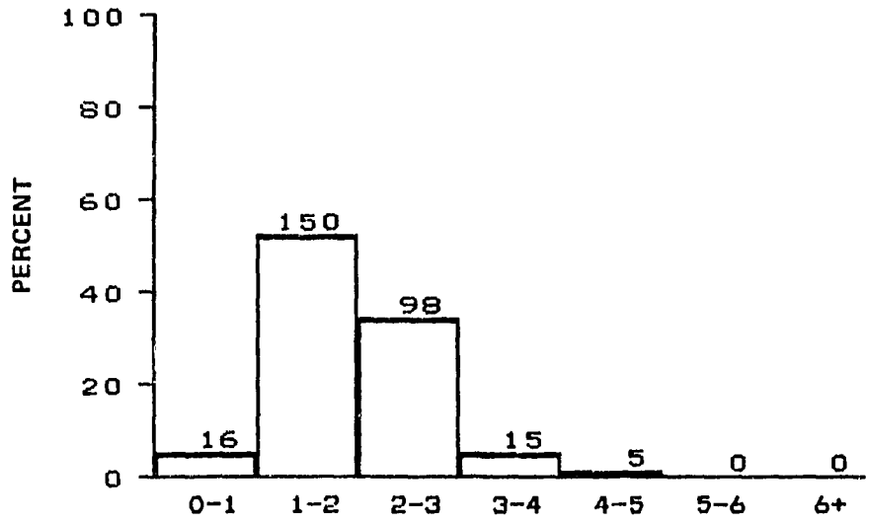

DISTRIBUTION OF SIGNIFICANT WAVE HEIGHT IN METERS
MONTH OF JULY
BLM AREA #3
N = 284, MEAN = 1.9, SIGMA = 0.76

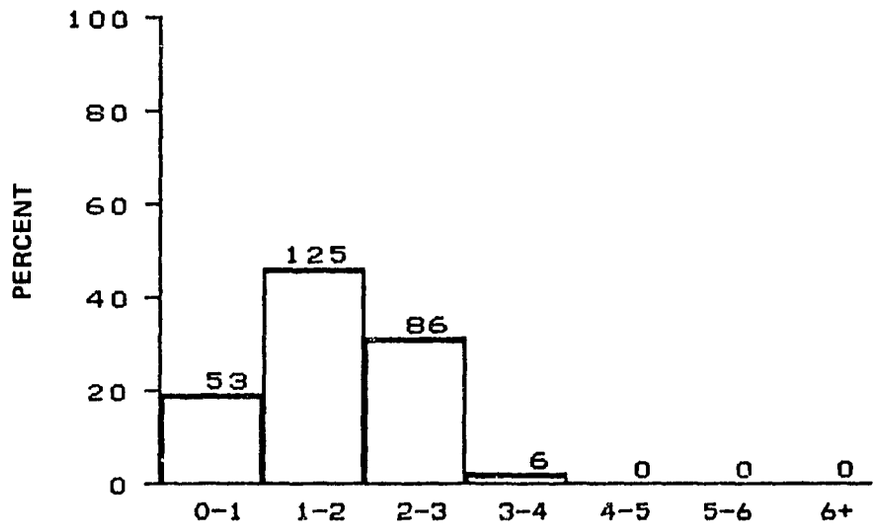

DISTRIBUTION OF SIGNIFICANT WAVE HEIGHT IN METERS
MONTH OF JULY
BLM AREA #4
N = 270, MEAN = 1.7, SIGMA = 0.76

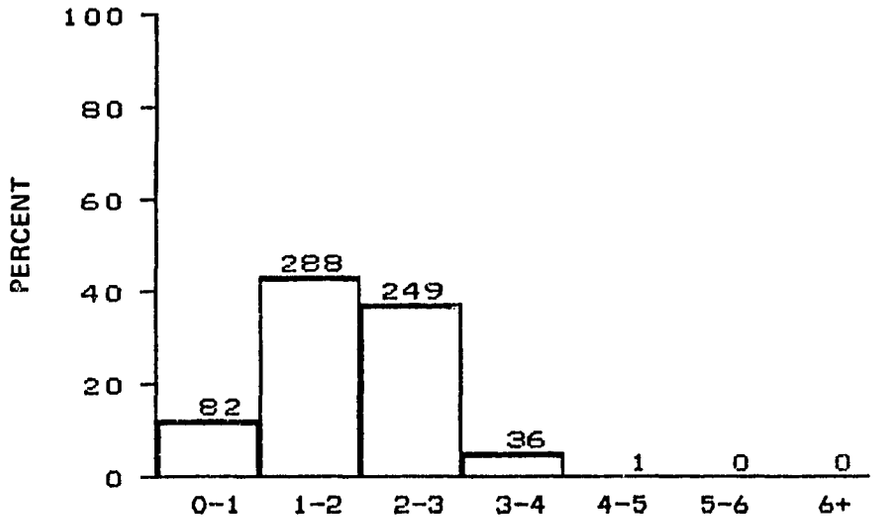

DISTRIBUTION OF SIGNIFICANT WAVE HEIGHT IN METERS
MONTH OF JULY
BLM AREA #5
N = 656, MEAN = 1.9, SIGMA = 0.78

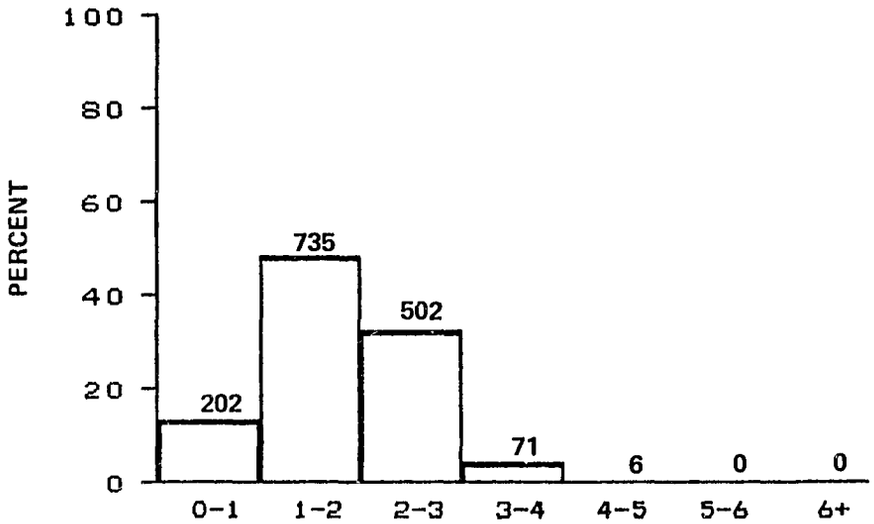

DISTRIBUTION OF SIGNIFICANT WAVE HEIGHT IN METERS
MONTH OF JULY
ALL BLM AREAS
N = 1516, MEAN = 1.8, SIGMA = 0.78

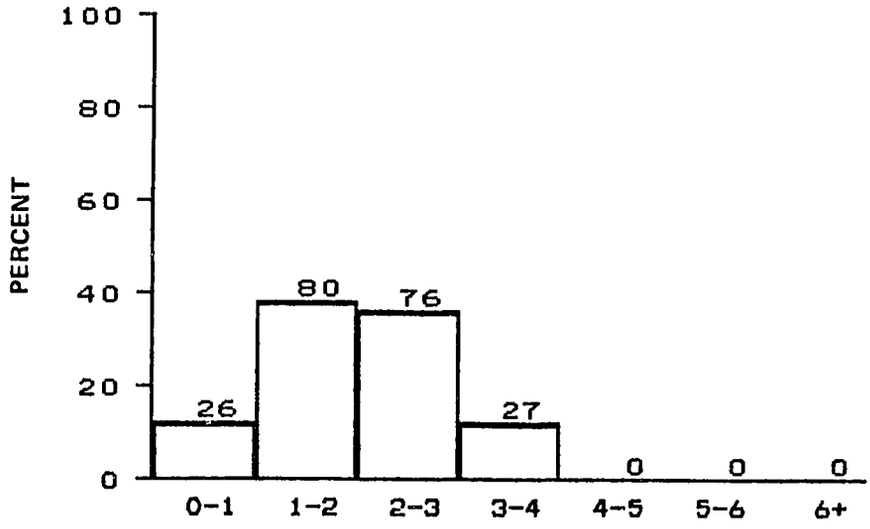

DISTRIBUTION OF SIGNIFICANT WAVE HEIGHT IN METERS
MONTH OF AUGUST
BLM AREA #1
N = 209, MEAN = 2.0, SIGMA = 0.87

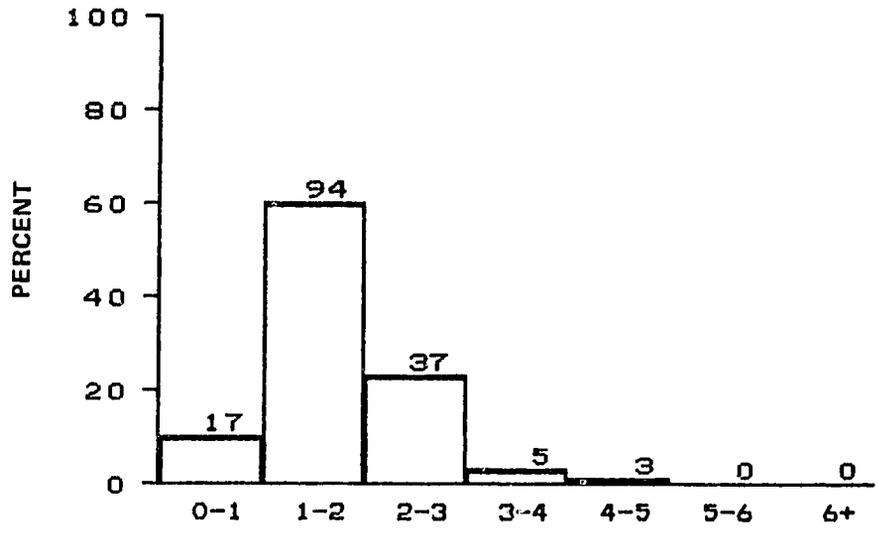

DISTRIBUTION OF SIGNIFICANT WAVE HEIGHT IN METERS
MONTH OF AUGUST
BLM AREA #2
N = 156, MEAN = 1.8, SIGMA = 0.76

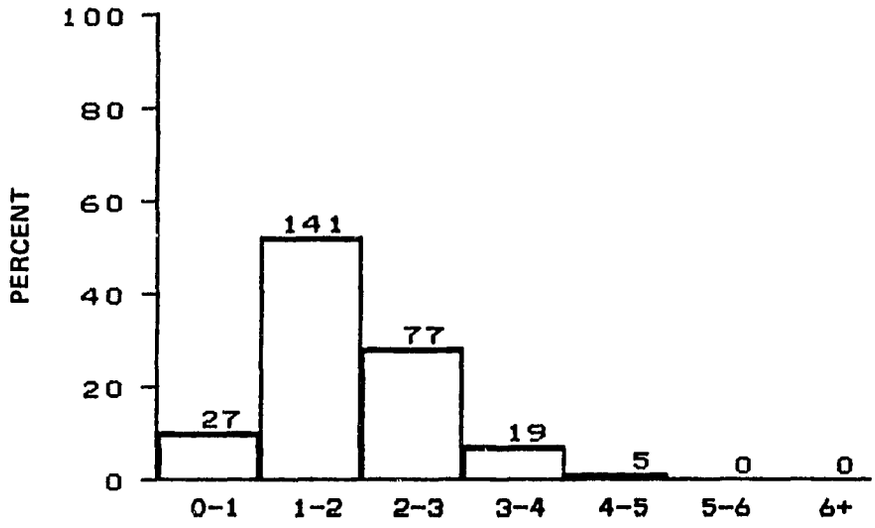

DISTRIBUTION OF SIGNIFICANT WAVE HEIGHT IN METERS
MONTH OF AUGUST
BLM AREA #3
N = 269, MEAN = 1.9, SIGMA = 0.83

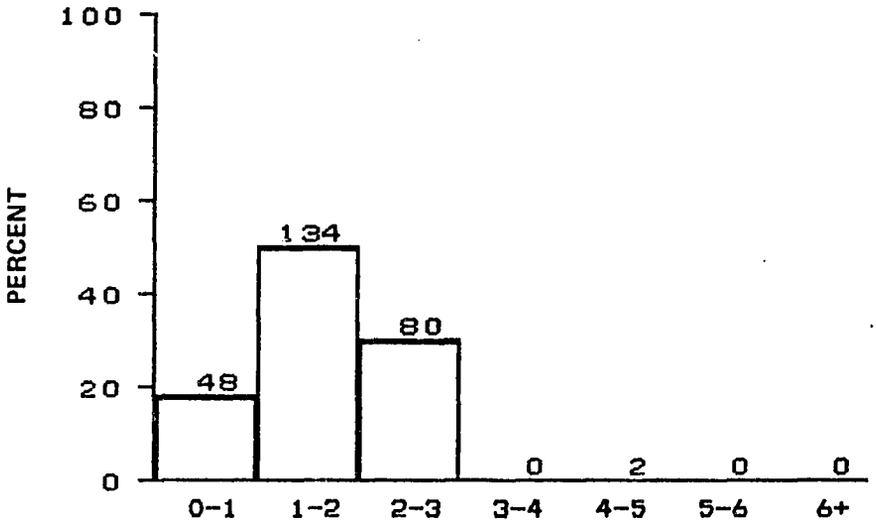

DISTRIBUTION OF SIGNIFICANT WAVE HEIGHT IN METERS
MONTH OF AUGUST
BLM AREA #4
N = 264, MEAN = 1.6, SIGMA = 0.73

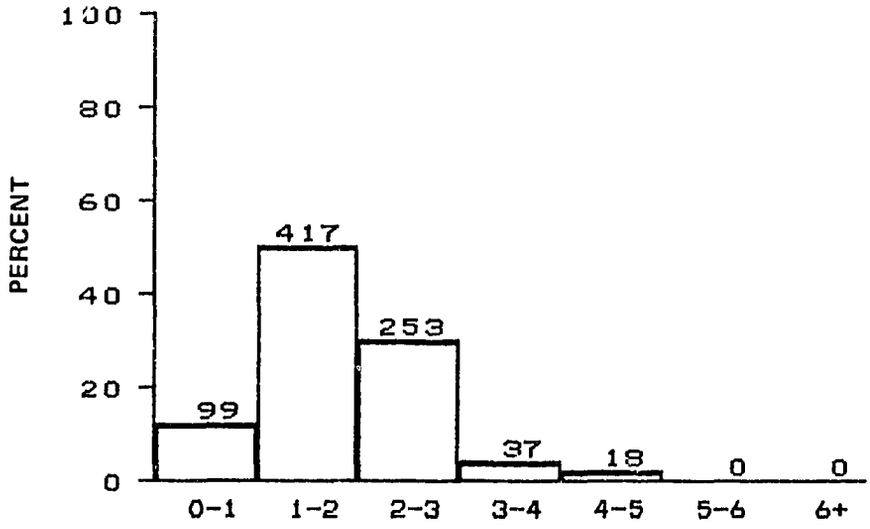

DISTRIBUTION OF SIGNIFICANT WAVE HEIGHT IN METERS
MONTH OF AUGUST
BLM AREA #5
N = 824, MEAN = 1.8, SIGMA = 0.83

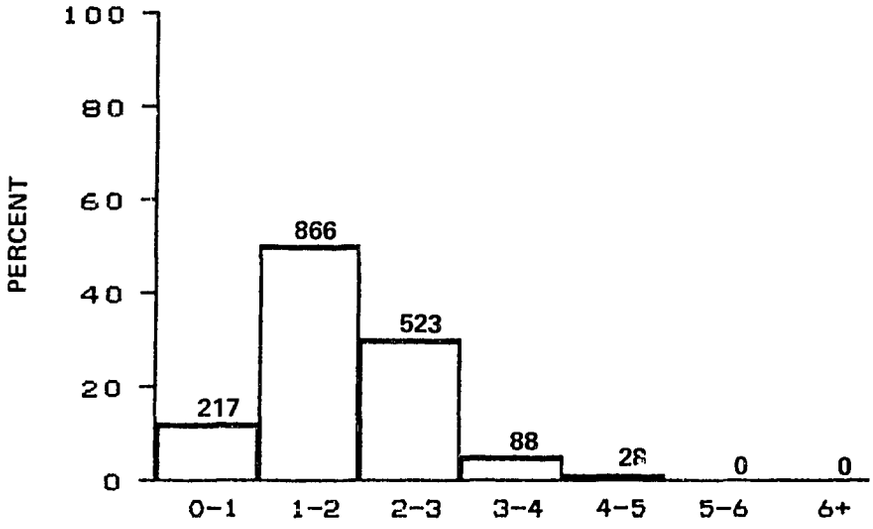

DISTRIBUTION OF SIGNIFICANT WAVE HEIGHT IN METERS
MONTH OF AUGUST
ALL BLM AREAS
N = 1722, MEAN = 1.8, SIGMA = 0.83

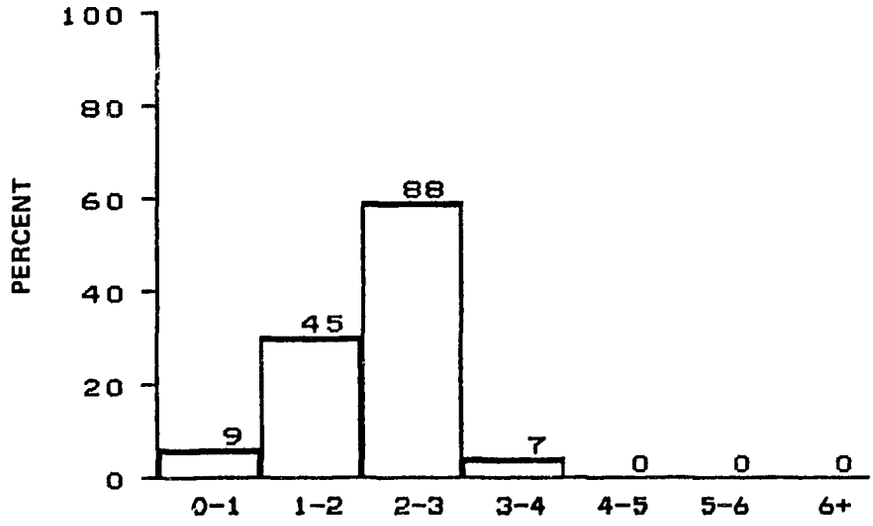

DISTRIBUTION OF SIGNIFICANT WAVE HEIGHT IN METERS
MONTH OF SEPTEMBER
BLM AREA #1
N = 149, MEAN = 2.1, SIGMA = 0.67

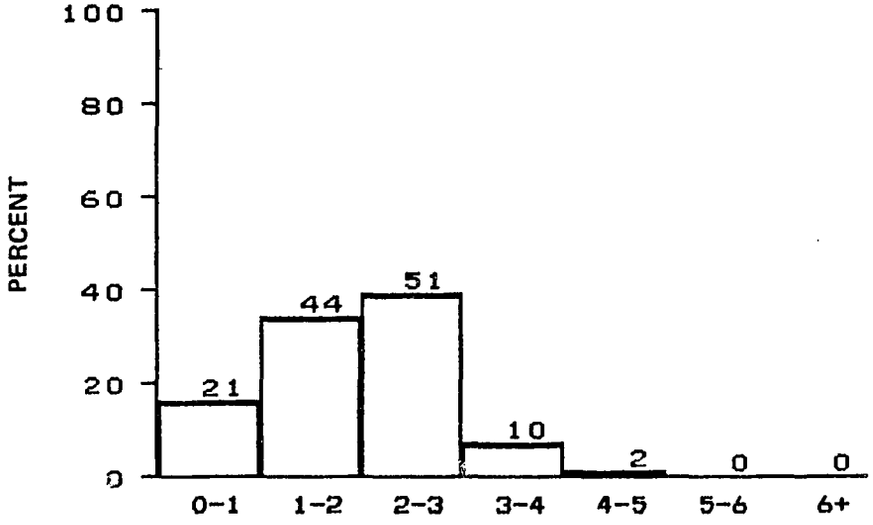

DISTRIBUTION OF SIGNIFICANT WAVE HEIGHT IN METERS
MONTH OF SEPTEMBER
BLM AREA #2
N = 128, MEAN = 1.9, SIGMA = 0.91

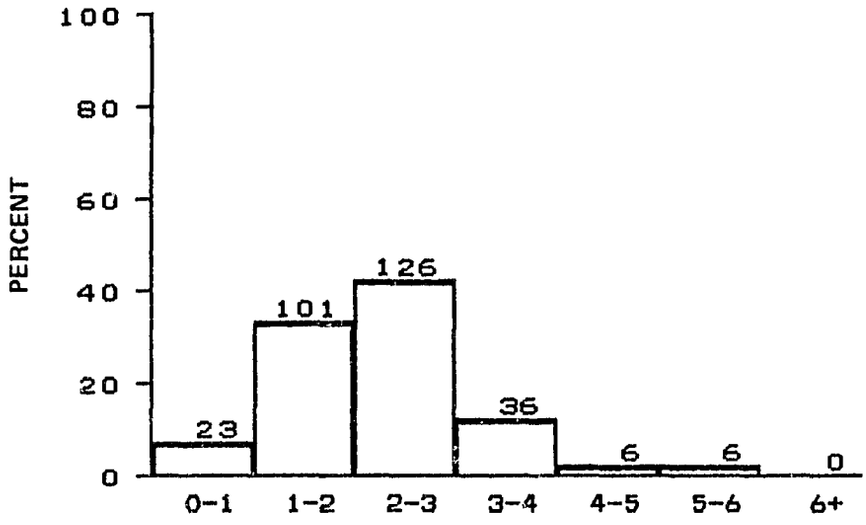

DISTRIBUTION OF SIGNIFICANT WAVE HEIGHT IN METERS
MONTH OF SEPTEMBER
BLM AREA #3
N = 298, MEAN = 2.2, SIGMA = 0.98

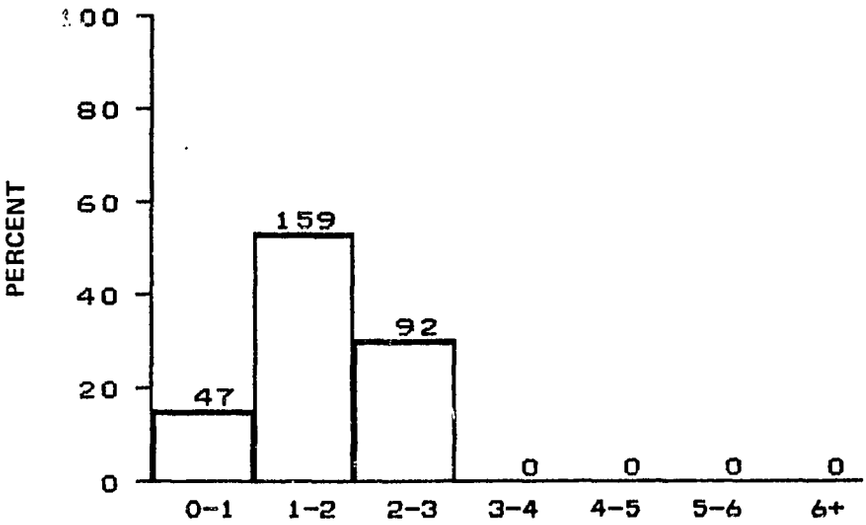

DISTRIBUTION OF SIGNIFICANT WAVE HEIGHT IN METERS
MONTH OF SEPTEMBER
BLM AREA #4
N = 298, MEAN = 1.7, SIGMA = 0.67

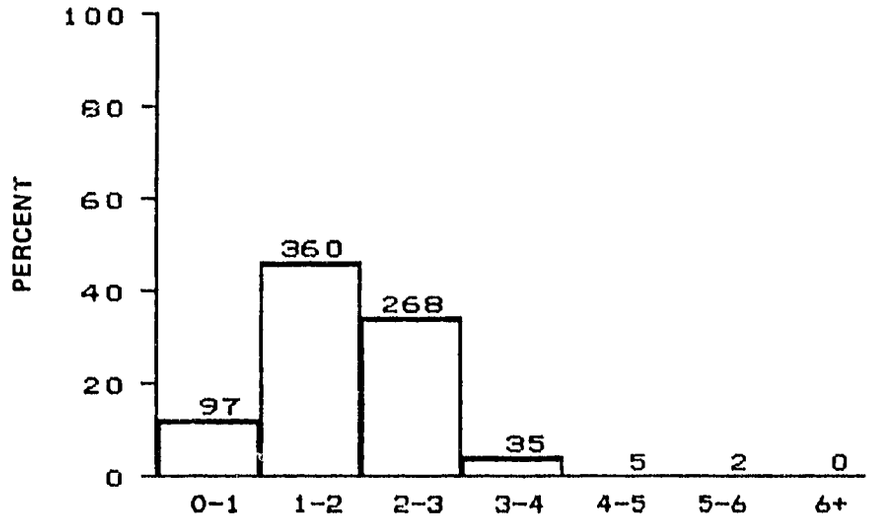

DISTRIBUTION OF SIGNIFICANT WAVE HEIGHT IN METERS
MONTH OF SEPTEMBER
BLM AREA #5
N = 767, MEAN = 1.8, SIGMA = 0.80

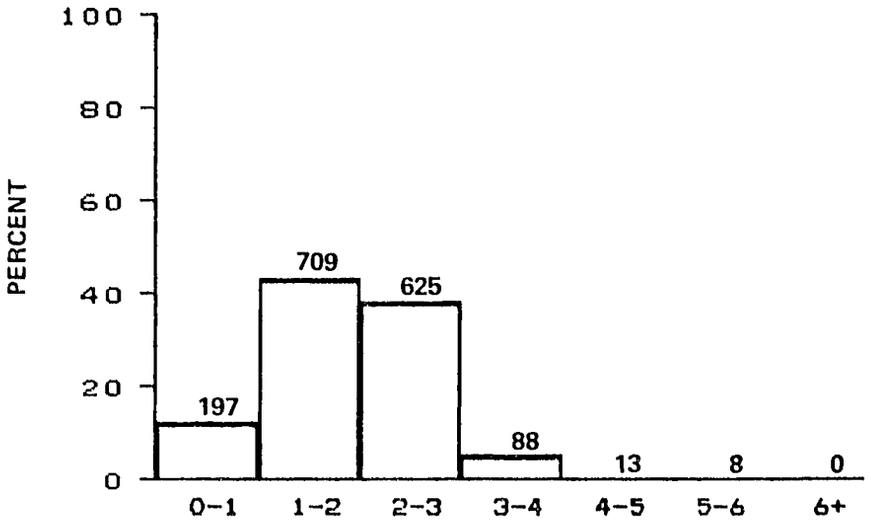

DISTRIBUTION OF SIGNIFICANT WAVE HEIGHT IN METERS
MONTH OF SEPTEMBER
ALL BLM AREAS
N = 1640, MEAN = 1.9, SIGMA = 0.84

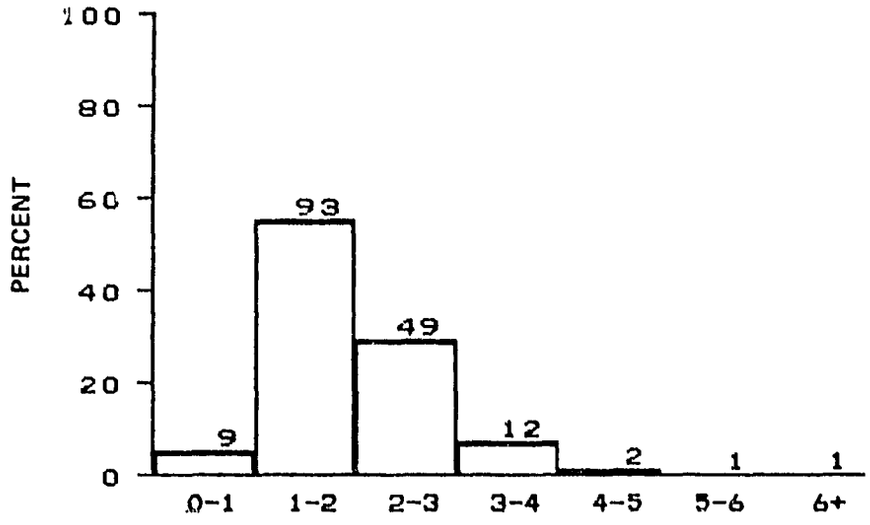

DISTRIBUTION OF SIGNIFICANT WAVE HEIGHT IN METERS
MONTH OF OCTOBER
BLM AREA #1
N = 167, MEAN = 2.0, SIGMA = 0.87

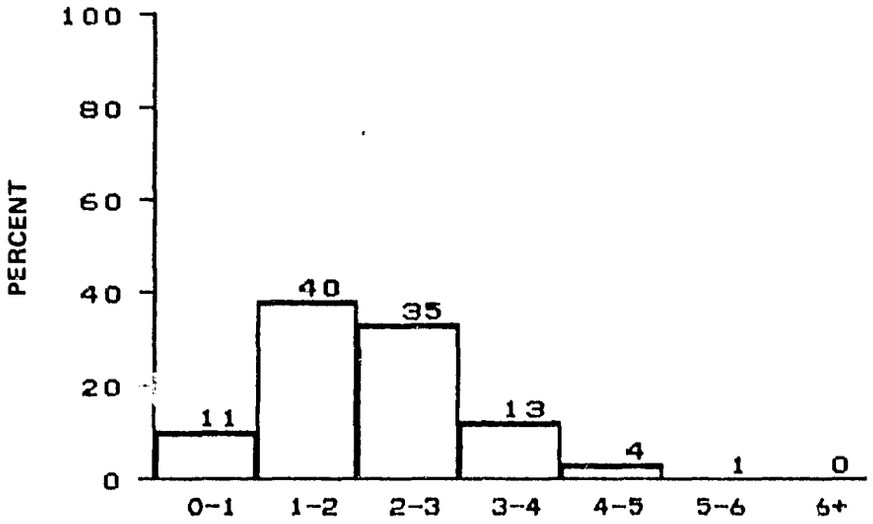

DISTRIBUTION OF SIGNIFICANT WAVE HEIGHT IN METERS
MONTH OF OCTOBER
BLM AREA #2
N = 104, MEAN = 2.1, SIGMA = 1.0

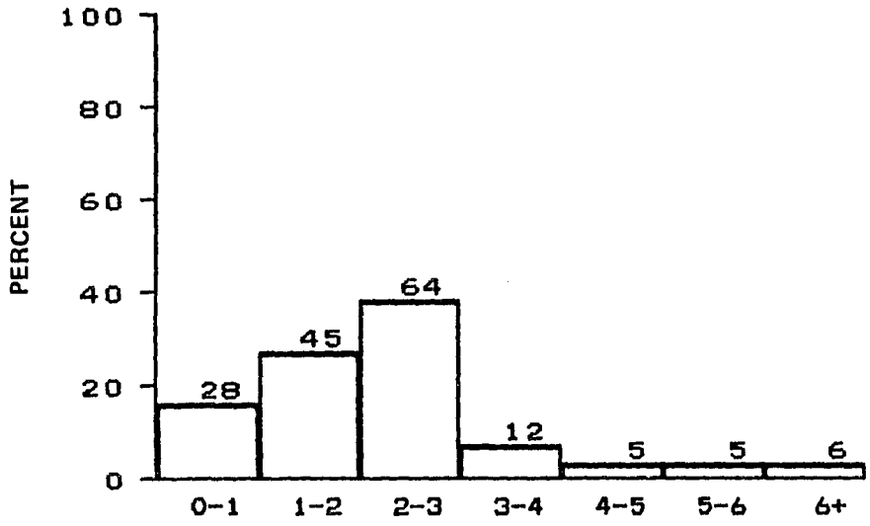

DISTRIBUTION OF SIGNIFICANT WAVE HEIGHT IN METERS
MONTH OF OCTOBER
BLM AREA #3
N = 165, MEAN = 2.3, SIGMA = 1.4

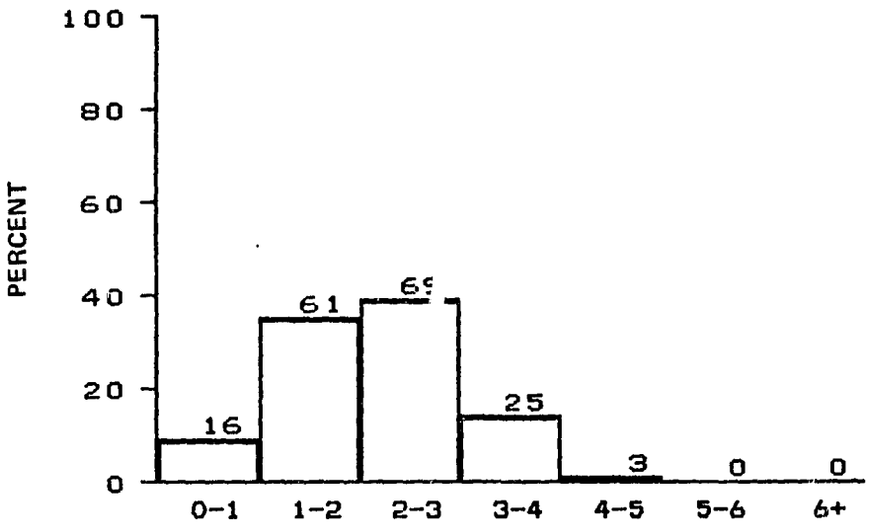

DISTRIBUTION OF SIGNIFICANT WAVE HEIGHT IN METERS
MONTH OF OCTOBER
BLM AREA #4
N = 174, MEAN = 2.1, SIGMA = 0.90

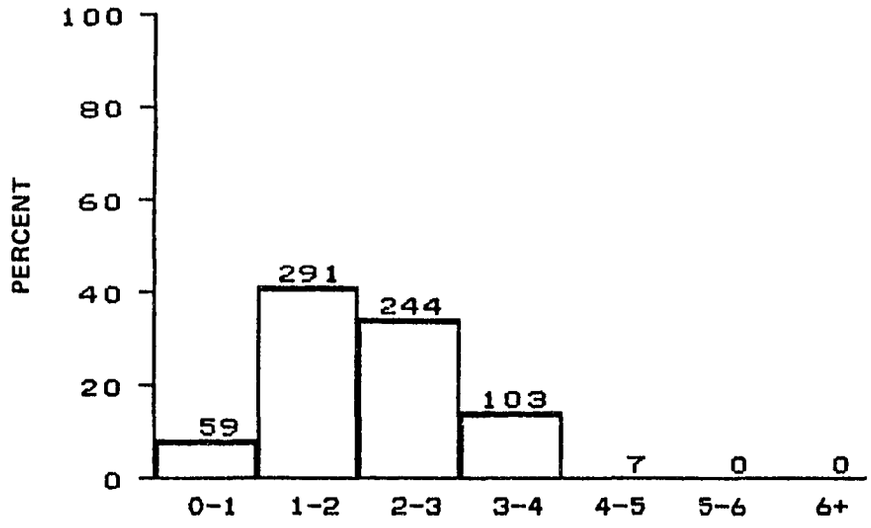

DISTRIBUTION OF SIGNIFICANT WAVE HEIGHT IN METERS
MONTH OF OCTOBER
BLM AREA #5
N = 704, MEAN = 2.1, SIGMA = 0.87

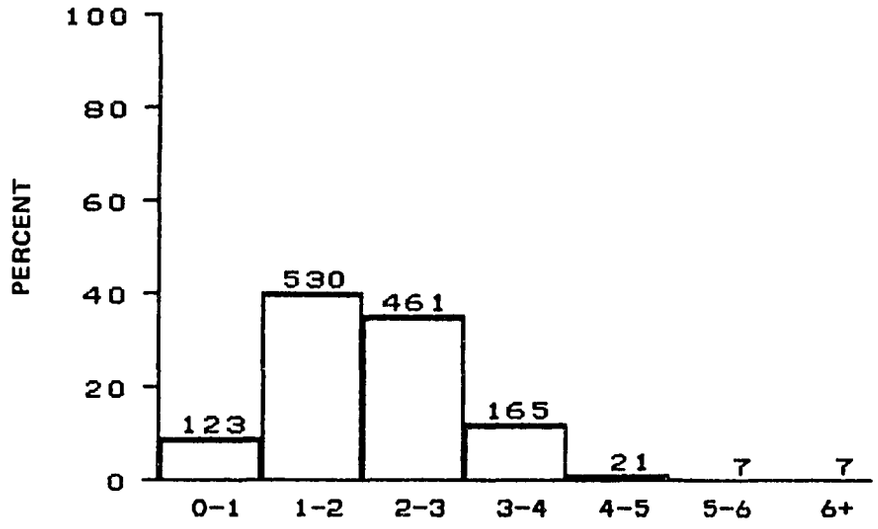

DISTRIBUTION OF SIGNIFICANT WAVE HEIGHT IN METERS
MONTH OF OCTOBER
ALL BLM AREAS
N = 1314, MEAN = 2.1, SIGMA = 0.97

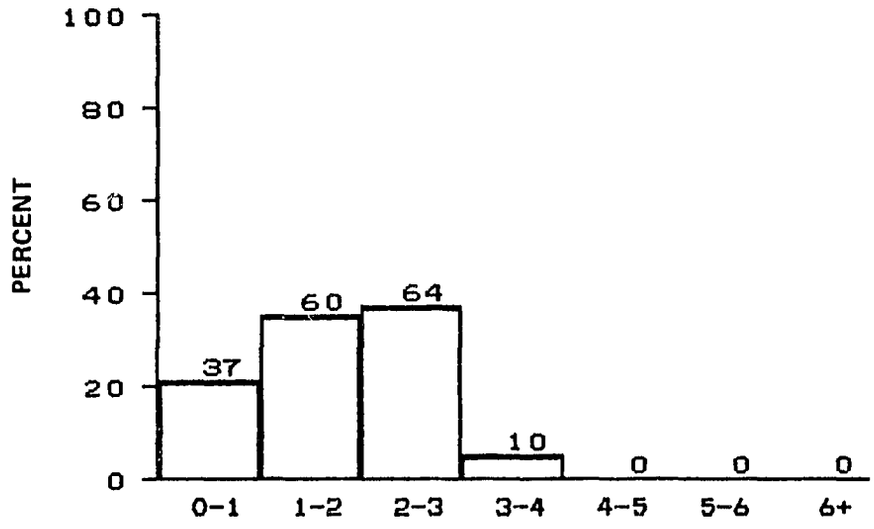

DISTRIBUTION OF SIGNIFICANT WAVE HEIGHT IN METERS
MONTH OF NOVEMBER
BLM AREA #1
N = 171, MEAN = 1.8, SIGMA = 0.87

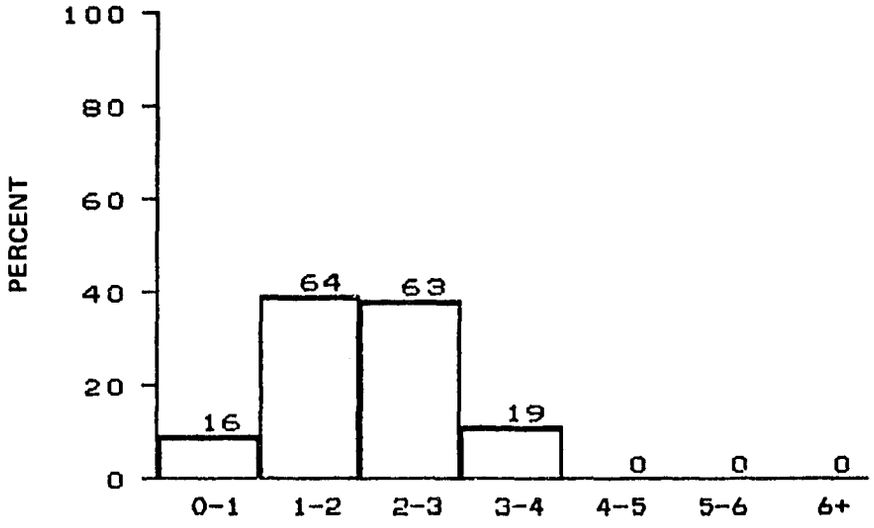

DISTRIBUTION OF SIGNIFICANT WAVE HEIGHT IN METERS
MONTH OF NOVEMBER
BLM AREA #2
N = 162, MEAN = 2.0, SIGMA = 0.83

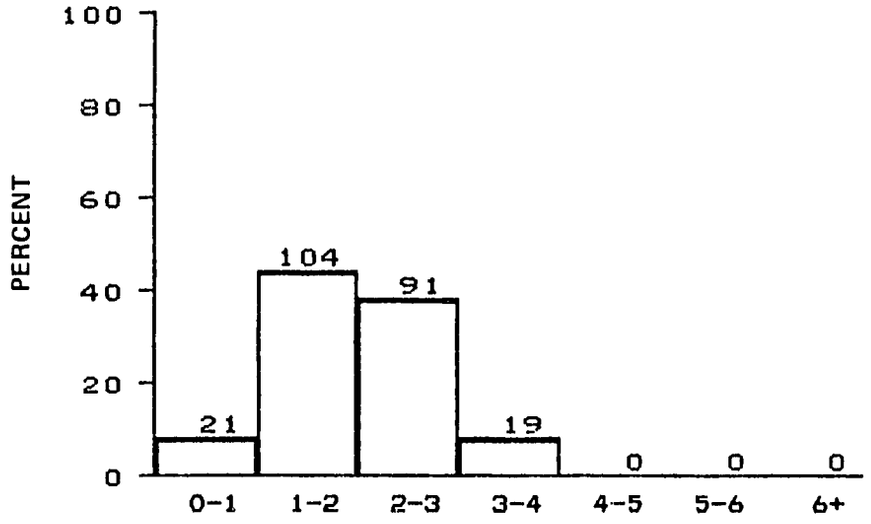

DISTRIBUTION OF SIGNIFICANT WAVE HEIGHT IN METERS
MONTH OF NOVEMBER
BLM AREA #3
N = 235, MEAN = 2.0, SIGMA = 0.77

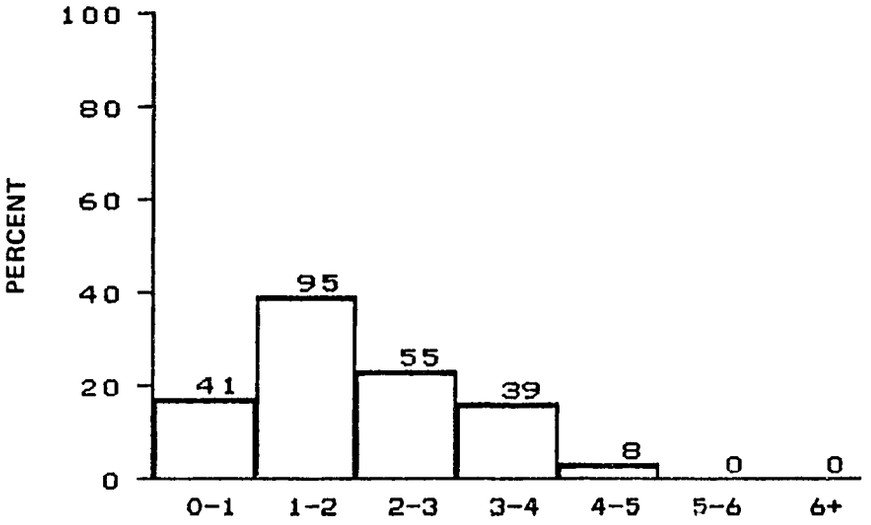

DISTRIBUTION OF SIGNIFICANT WAVE HEIGHT IN METERS
MONTH OF NOVEMBER
BLM AREA #4
N = 238, MEAN = 2.0, SIGMA = 1.1

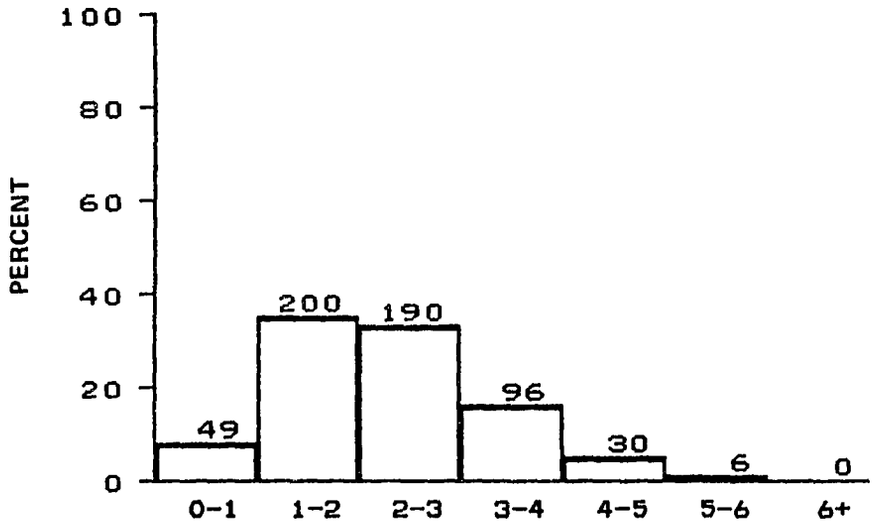

DISTRIBUTION OF SIGNIFICANT WAVE HEIGHT IN METERS
MONTH OF NOVEMBER
BLM AREA #5
N = 571, MEAN = 2.3, SIGMA = 1.1

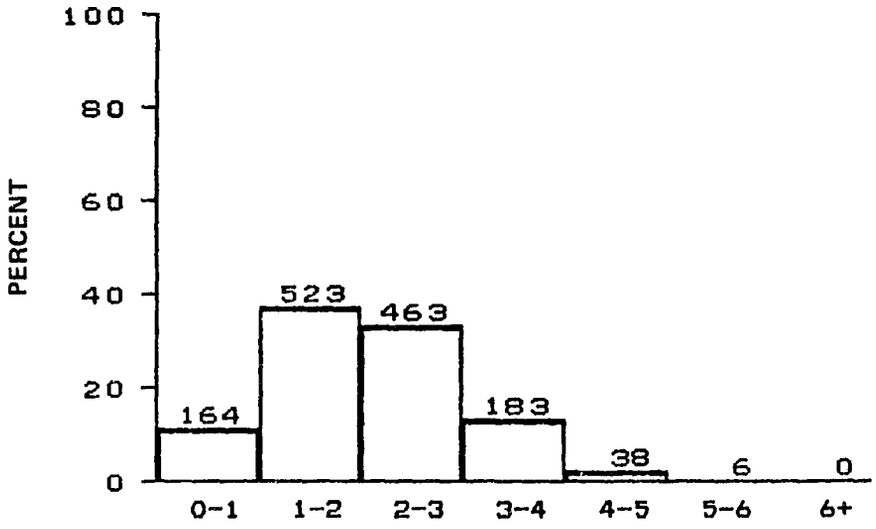

DISTRIBUTION OF SIGNIFICANT WAVE HEIGHT IN METERS
MONTH OF NOVEMBER
ALL BLM AREAS
N = 1377, MEAN = 2.1, SIGMA = 0.98

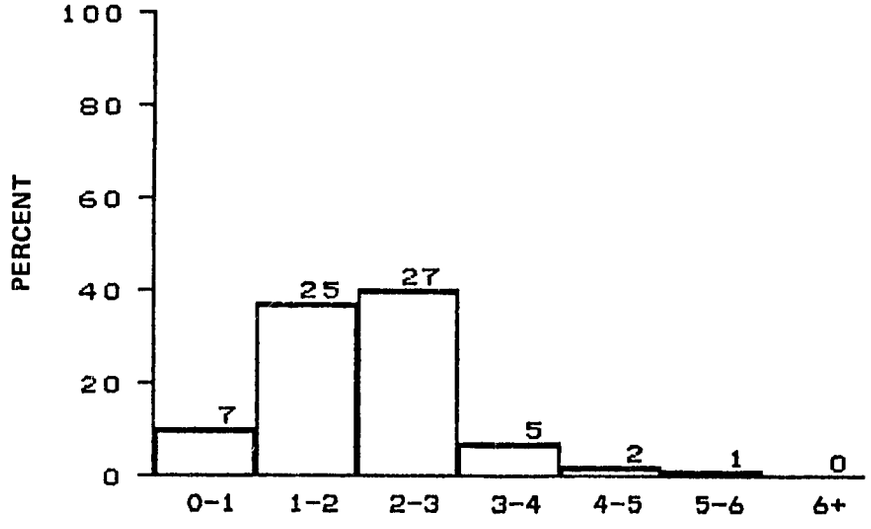

DISTRIBUTION OF SIGNIFICANT WAVE HEIGHT IN METERS
MONTH OF DECEMBER
BLM AREA #1
N = 67, MEAN = 2.1, SIGMA = 0.98

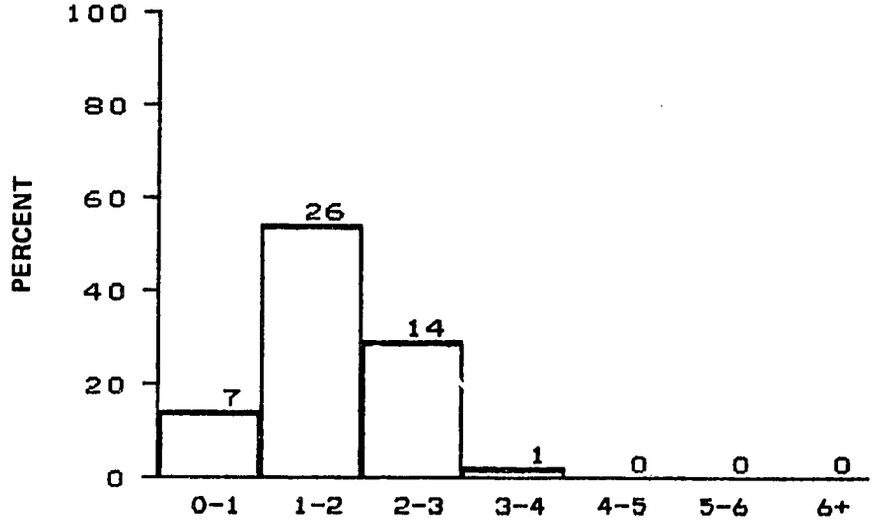

DISTRIBUTION OF SIGNIFICANT WAVE HEIGHT IN METERS
MONTH OF DECEMBER
BLM AREA #2
N = 48, MEAN = 1.7, SIGMA = 0.70

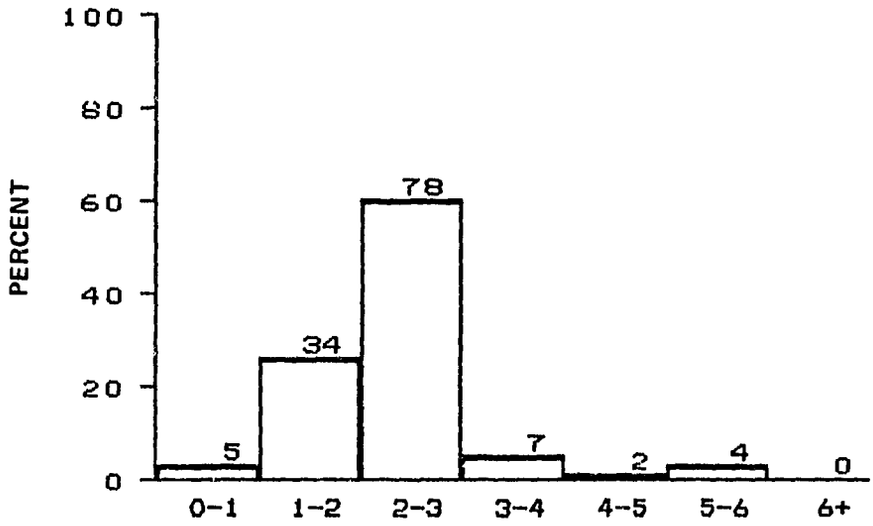

DISTRIBUTION OF SIGNIFICANT WAVE HEIGHT IN METERS
MONTH OF DECEMBER
BLM AREA #3
N = 130, MEAN = 2.3, SIGMA = 0.88

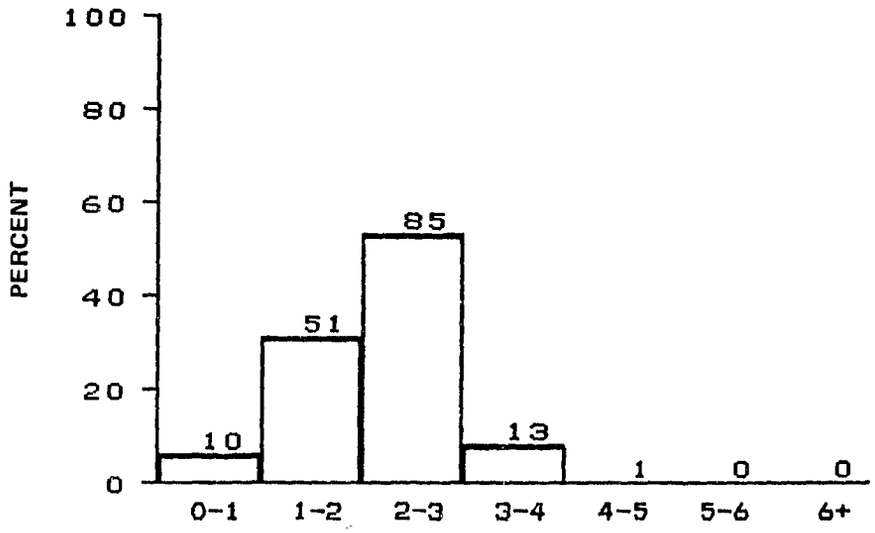

DISTRIBUTION OF SIGNIFICANT WAVE HEIGHT IN METERS
MONTH OF DECEMBER
BLM AREA #4
N = 160, MEAN = 2.2, SIGMA = 0.74

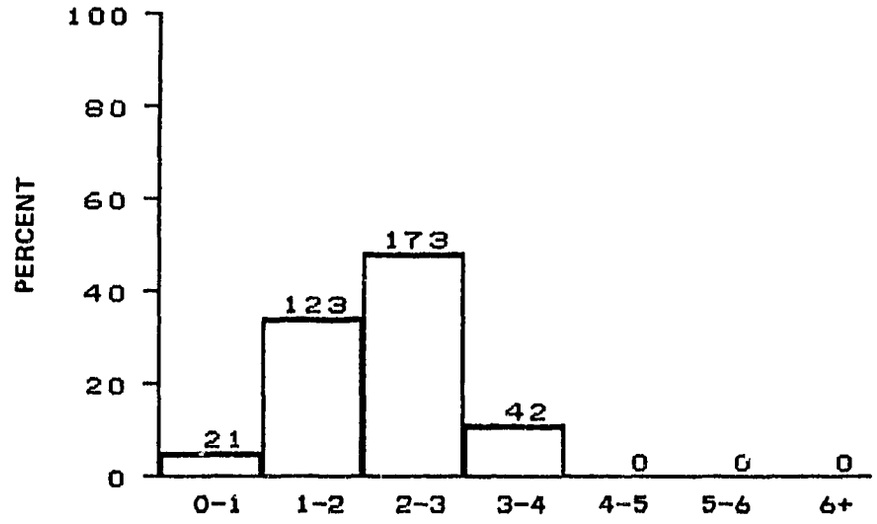

DISTRIBUTION OF SIGNIFICANT WAVE HEIGHT IN METERS
MONTH OF DECEMBER
BLM AREA #5
N = 359, MEAN = 2.2, SIGMA = 0.76

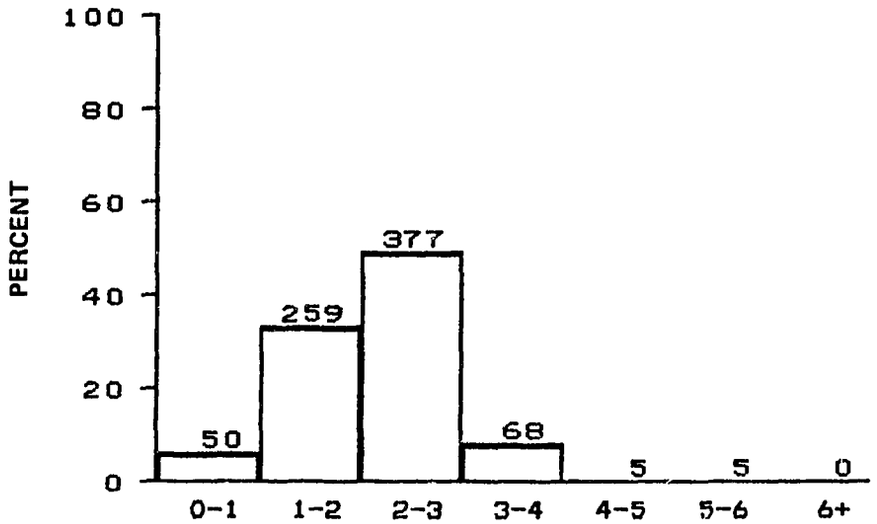

DISTRIBUTION OF SIGNIFICANT WAVE HEIGHT IN METERS
MONTH OF DECEMBER
ALL BLM AREAS
N = 764, MEAN = 2.2, SIGMA = 0.81

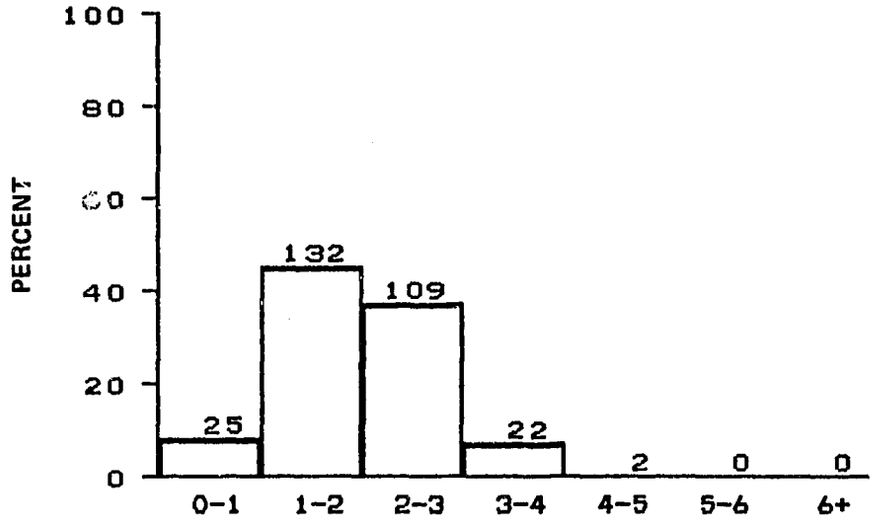

DISTRIBUTION OF SIGNIFICANT WAVE HEIGHT IN METERS
SPRING SEASON
BLM AREA #1
N = 290, MEAN = 2.0, SIGMA = 0.78

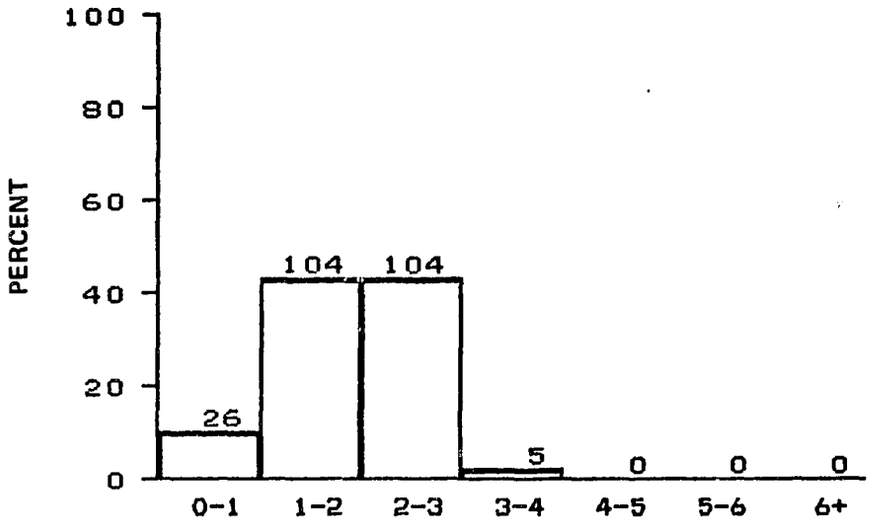

DISTRIBUTION OF SIGNIFICANT WAVE HEIGHT IN METERS
SPRING SEASON
BLM AREA #2
N = 239, MEAN = 1.9, SIGMA = 0.70

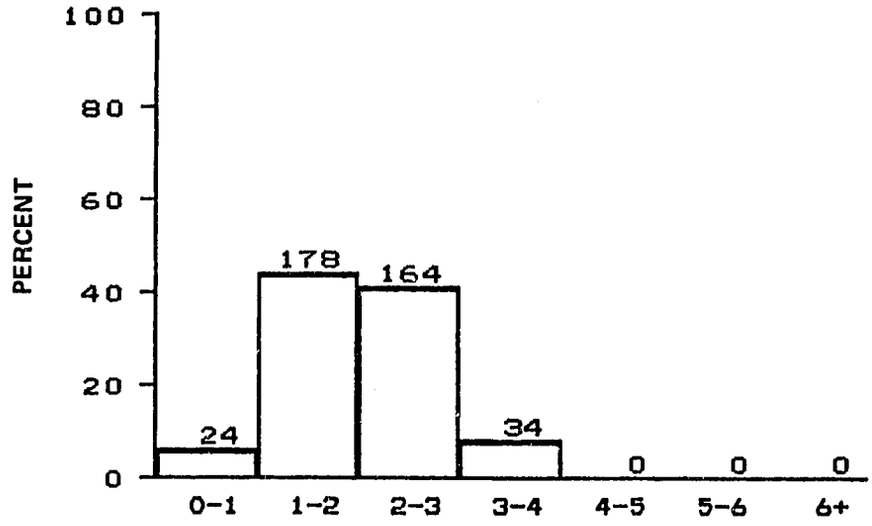

DISTRIBUTION OF SIGNIFICANT WAVE HEIGHT IN METERS
SPRING SEASON
BLM AREA #3
N = 400, MEAN = 2.0, SIGMA = 0.73

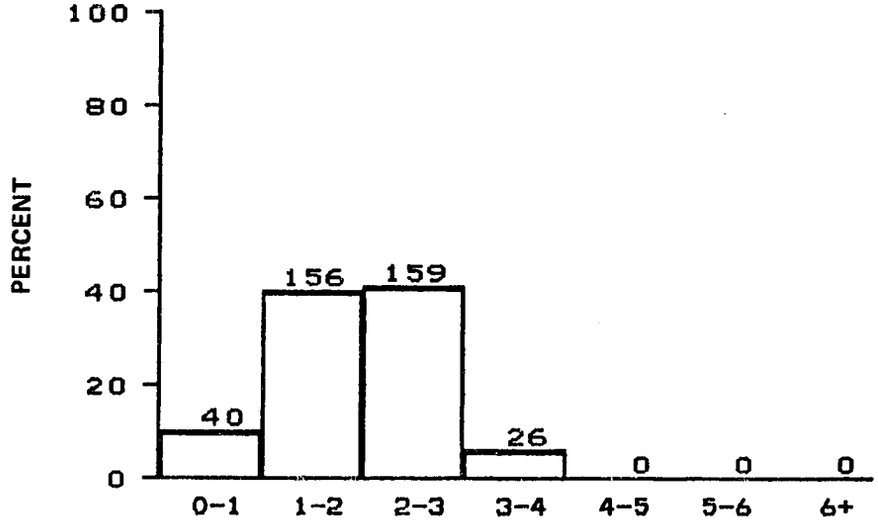

DISTRIBUTION OF SIGNIFICANT WAVE HEIGHT IN METERS
SPRING SEASON
BLM AREA #4
N = 381, MEAN = 1.9, SIGMA = 0.77

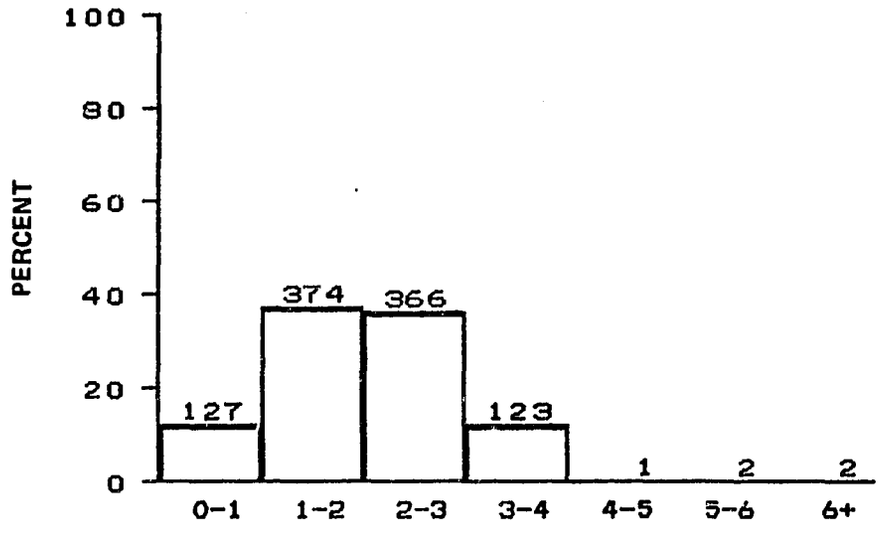

DISTRIBUTION OF SIGNIFICANT WAVE HEIGHT IN METERS
SPRING SEASON
BLM AREA #5
N = 995, MEAN = 2.0, SIGMA = 0.91

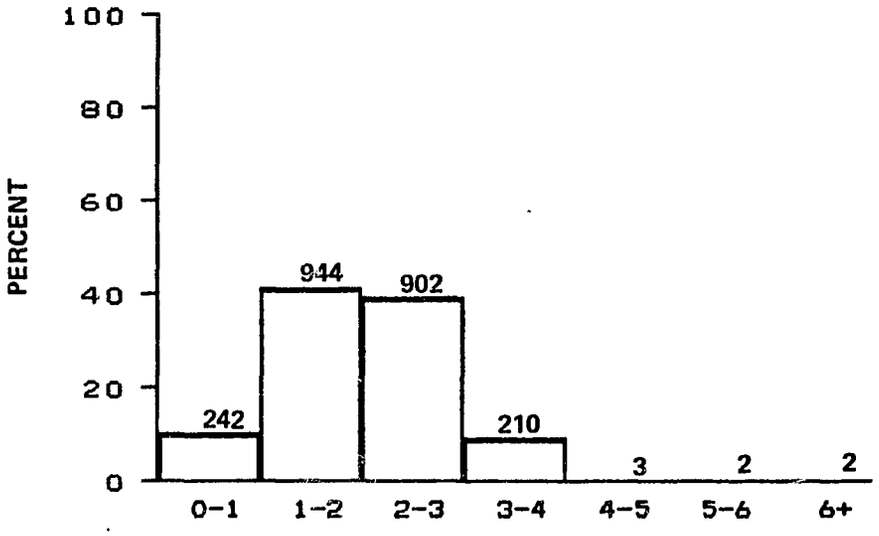

DISTRIBUTION OF SIGNIFICANT WAVE HEIGHT IN METERS
SPRING SEASON
ALL BLM AREAS
N = 2305, MEAN = 2.0, SIGMA = 0.80

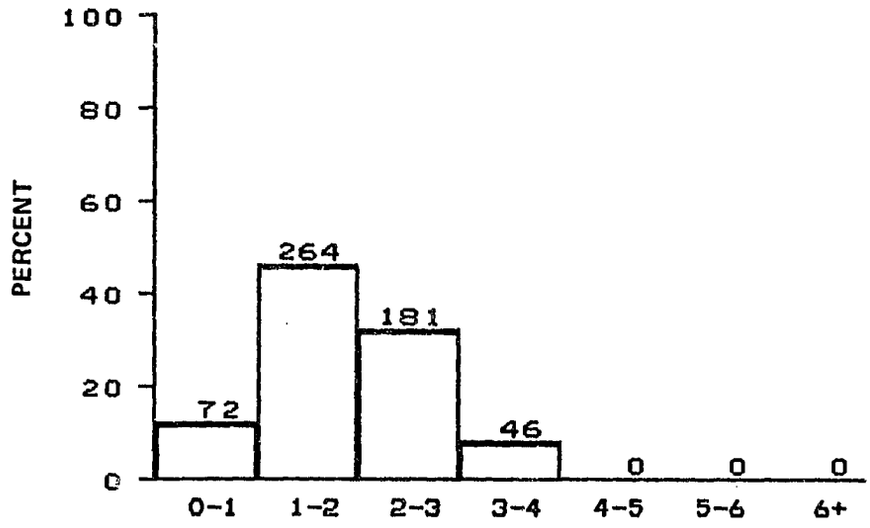

DISTRIBUTION OF SIGNIFICANT WAVE HEIGHT IN METERS

SUMMER SEASON

BLM AREA #1

N = 563, MEAN = 1.9, SIGMA = 0.81

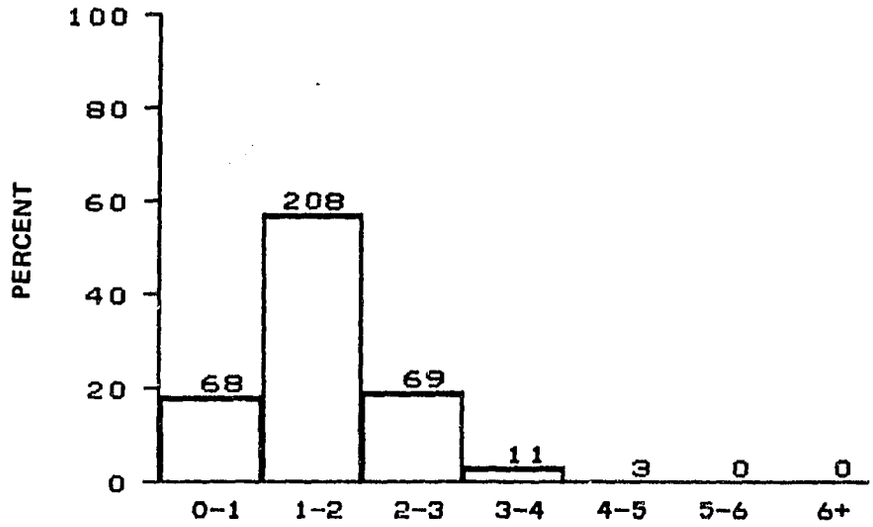

DISTRIBUTION OF SIGNIFICANT WAVE HEIGHT IN METERS

SUMMER SEASON

BLM AREA #2

N = 359, MEAN = 1.6, SIGMA = 0.76

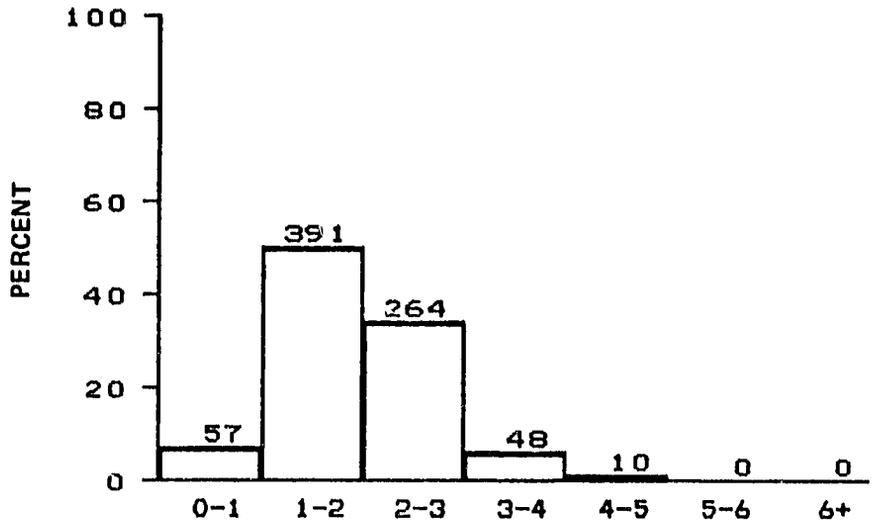

DISTRIBUTION OF SIGNIFICANT WAVE HEIGHT IN METERS
SUMMER SEASON
BLM AREA #3
N = 770, MEAN = 1.9, SIGMA = 0.77

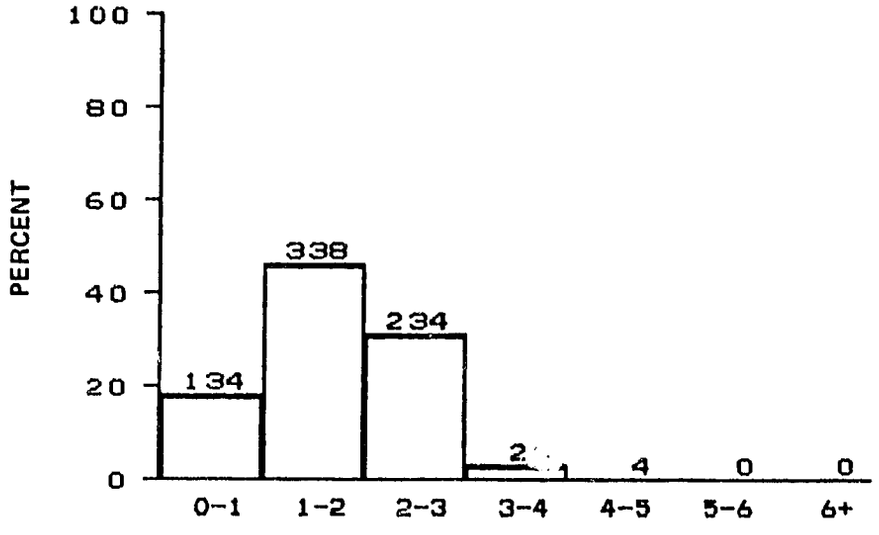

DISTRIBUTION OF SIGNIFICANT WAVE HEIGHT IN METERS
SUMMER SEASON
BLM AREA #4
N = 733, MEAN = 1.7, SIGMA = 0.79

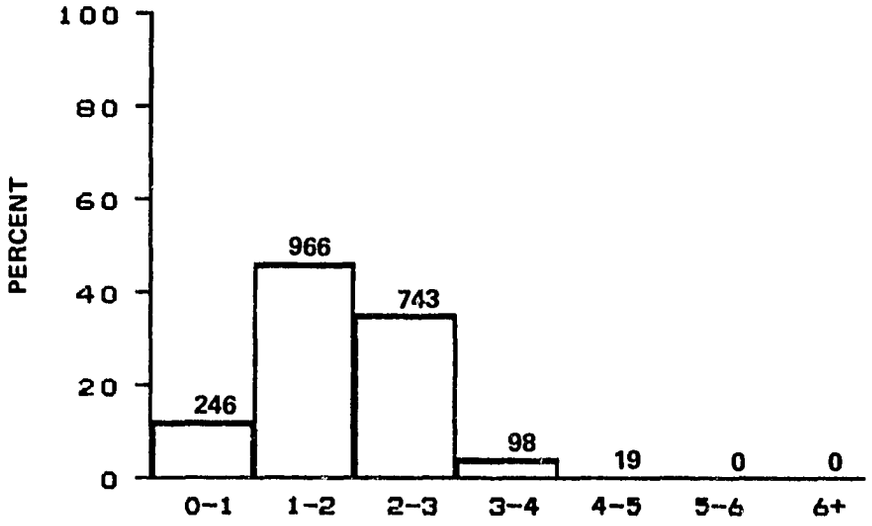

DISTRIBUTION OF SIGNIFICANT WAVE HEIGHT IN METERS
SUMMER SEASON
BLM AREA #5
N = 2072, MEAN = 1.9, SIGMA = 0.79

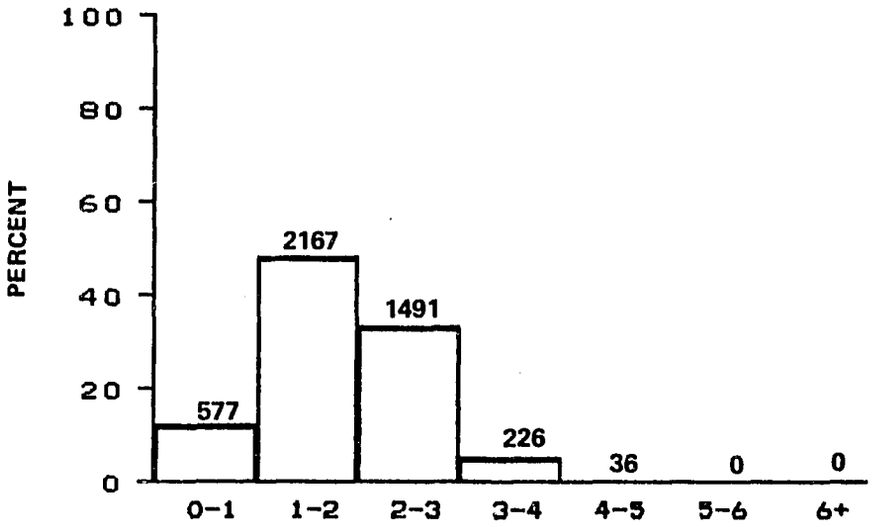

DISTRIBUTION OF SIGNIFICANT WAVE HEIGHT IN METERS
SUMMER SEASON
ALL BLM AREAS
N = 4497, MEAN = 1.8, SIGMA = 0.80

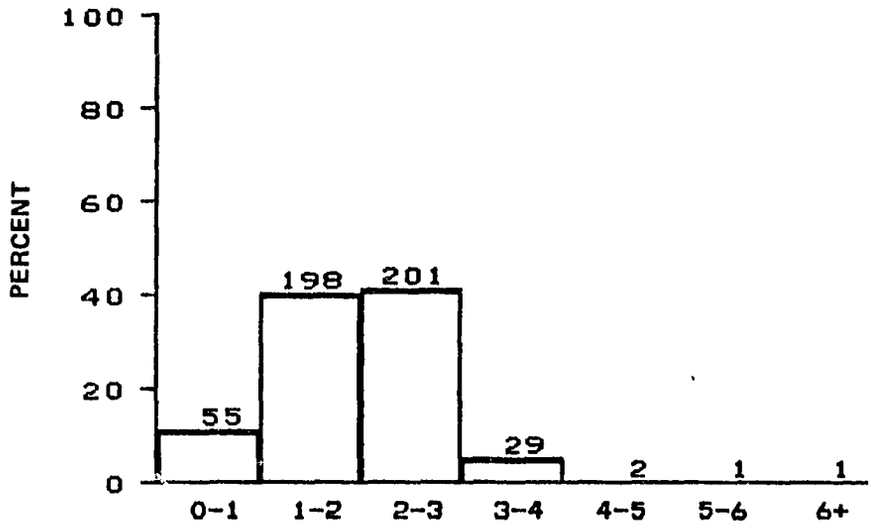

DISTRIBUTION OF SIGNIFICANT WAVE HEIGHT IN METERS
FALL SEASON
BLM AREA #1
N = 487, MEAN = 1.9, SIGMA = 0.83

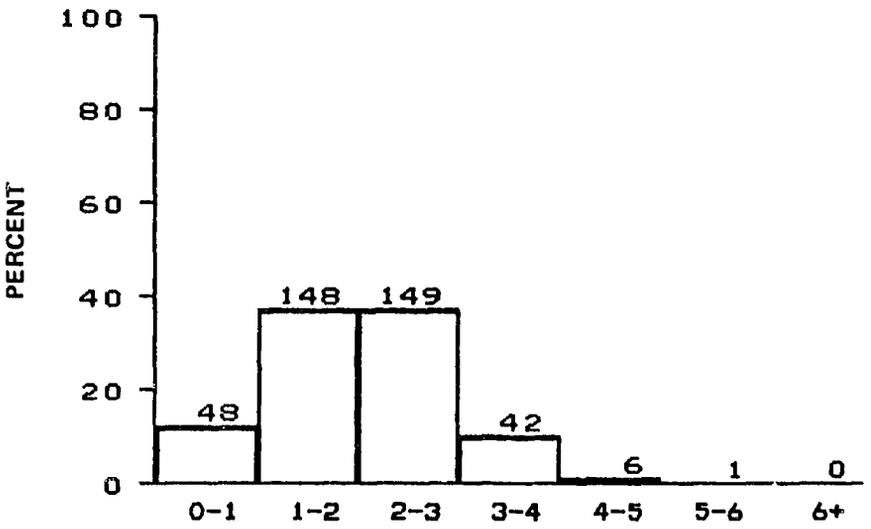

DISTRIBUTION OF SIGNIFICANT WAVE HEIGHT IN METERS
FALL SEASON
BLM AREA #2
N = 394, MEAN = 2.0, SIGMA = 0.91

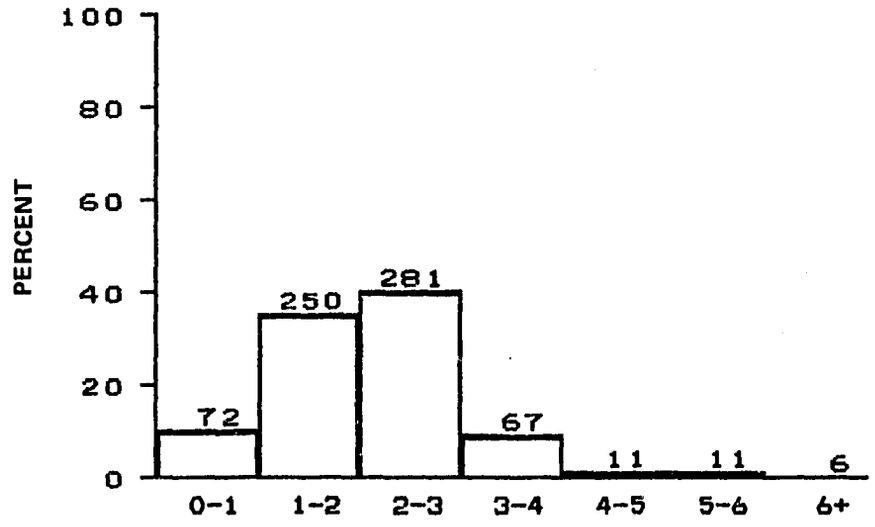

DISTRIBUTION OF SIGNIFICANT WAVE HEIGHT IN METERS

FALL SEASON

BLM AREA #3

N = 698, MEAN = 2.1, SIGMA = 1.0

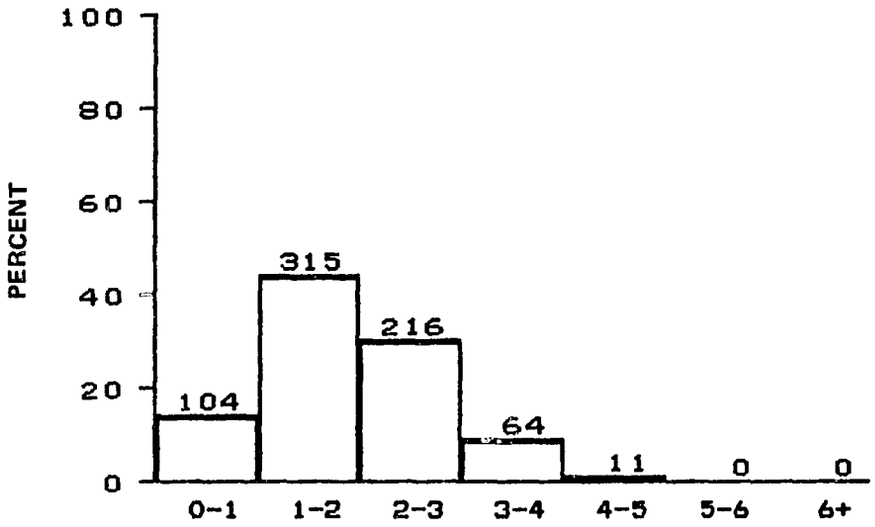

DISTRIBUTION OF SIGNIFICANT WAVE HEIGHT IN METERS

FALL SEASON

BLM AREA #4

N = 710, MEAN = 1.9, SIGMA = 0.90

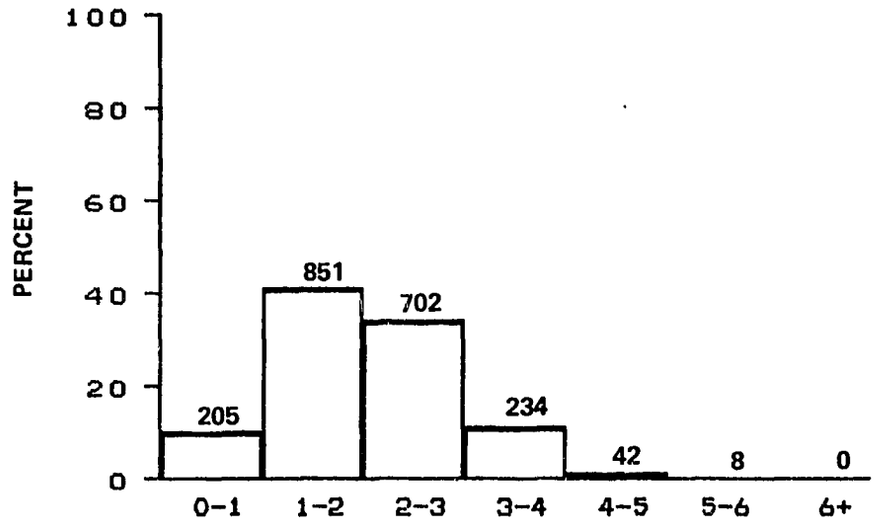

DISTRIBUTION OF SIGNIFICANT WAVE HEIGHT IN METERS
FALL SEASON
BLM AREA #5
N = 2042, MEAN = 2.0, SIGMA = 0.93

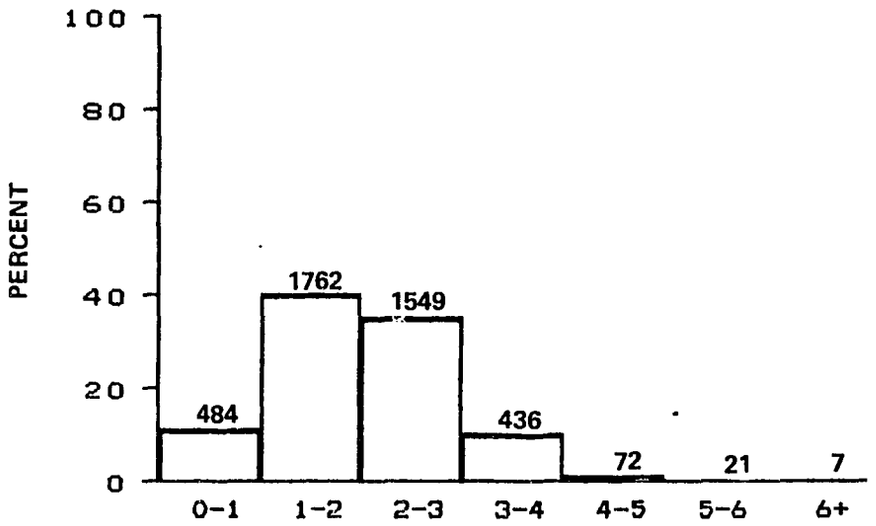

DISTRIBUTION OF SIGNIFICANT WAVE HEIGHT IN METERS
FALL SEASON
ALL BLM AREAS
N = 4331, MEAN = 2.0, SIGMA = 0.93

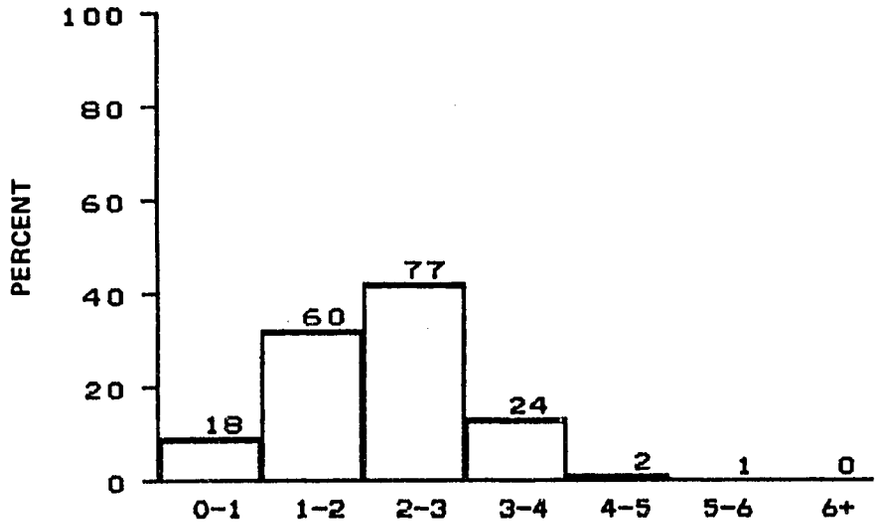

DISTRIBUTION OF SIGNIFICANT WAVE HEIGHT IN METERS
WINTER SEASON
BLM AREA #1
N = 182, MEAN = 2.1, SIGMA = 0.91

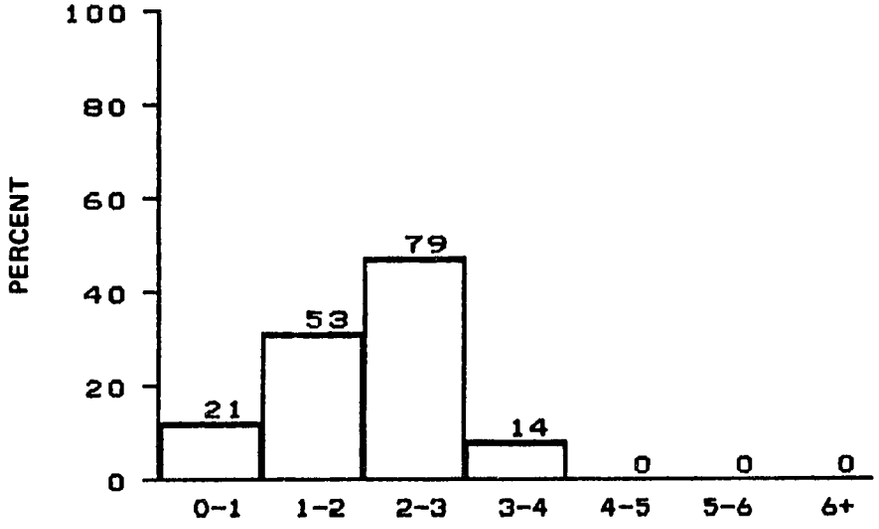

DISTRIBUTION OF SIGNIFICANT WAVE HEIGHT IN METERS
WINTER SEASON
BLM AREA #2
N = 167, MEAN = 2.0, SIGMA = 0.82

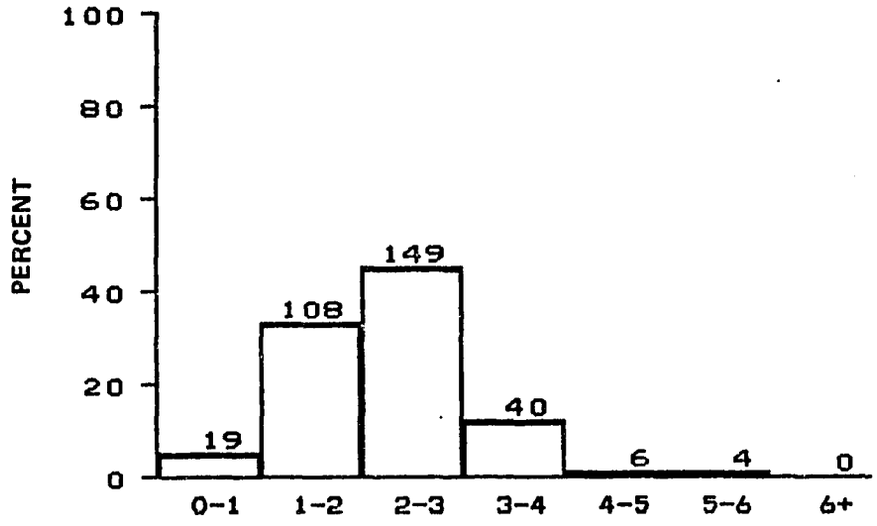

DISTRIBUTION OF SIGNIFICANT WAVE HEIGHT IN METERS
WINTER SEASON
BLM AREA #3
N = 326, MEAN = 2.2, SIGMA = 0.90

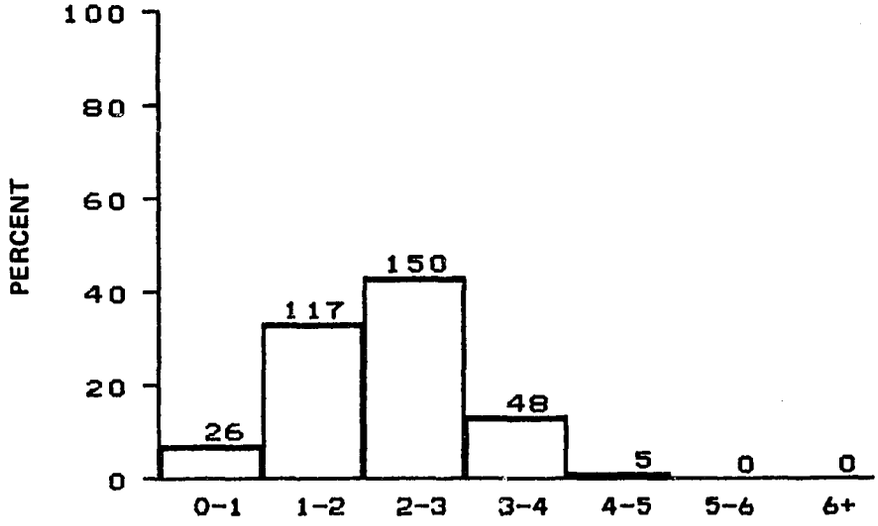

DISTRIBUTION OF SIGNIFICANT WAVE HEIGHT IN METERS
WINTER SEASON
BLM AREA #4
N = 346, MEAN = 2.2, SIGMA = 0.86

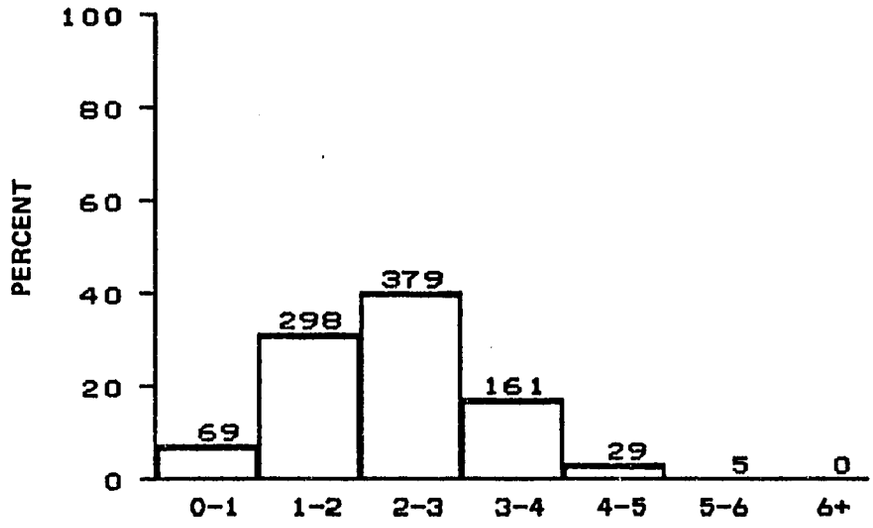

DISTRIBUTION OF SIGNIFICANT WAVE HEIGHT IN METERS
WINTER SEASON
BLM AREA #5
N = 941, MEAN = 2.3, SIGMA = 0.95

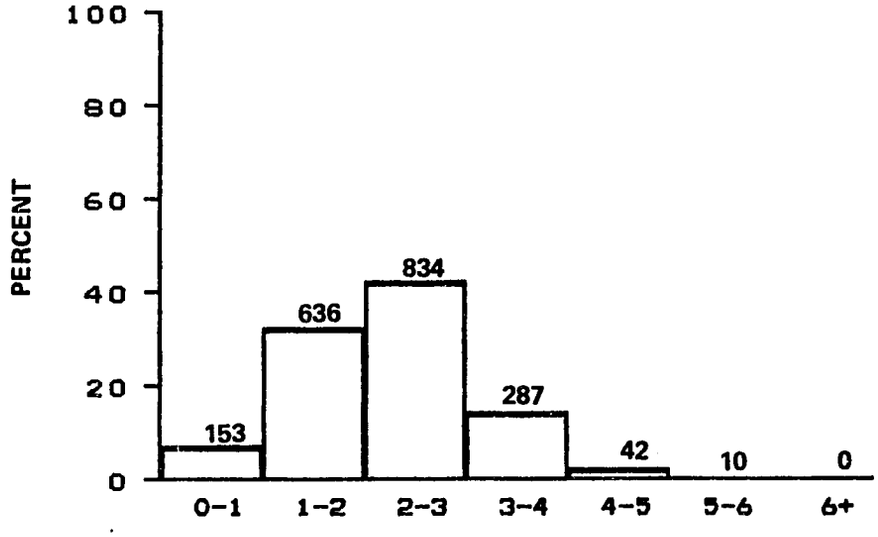

DISTRIBUTION OF SIGNIFICANT WAVE HEIGHT IN METERS
WINTER SEASON
ALL BLM AREAS
N = 1962, MEAN = 2.2, SIGMA = 0.91

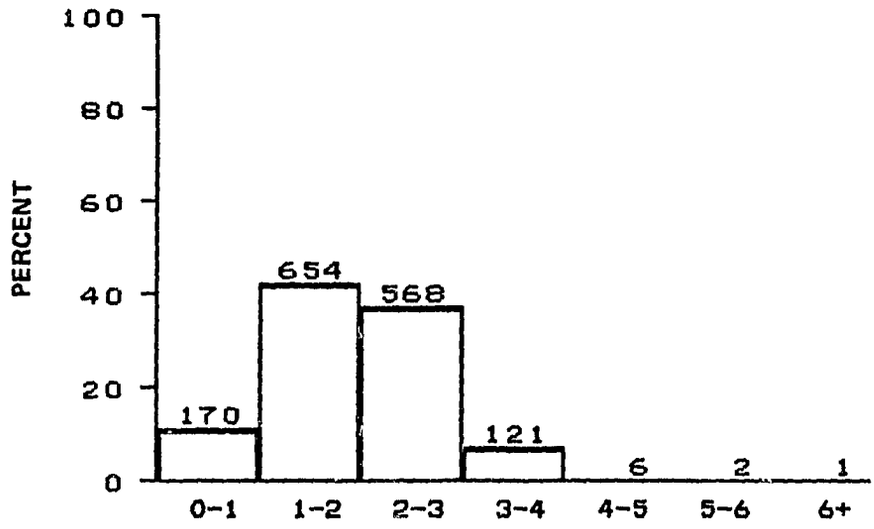

DISTRIBUTION OF SIGNIFICANT WAVE HEIGHT IN METERS
ENTIRE MISSION
BLM AREA #1
N = 1522, MEAN = 1.9, SIGMA = 0.83

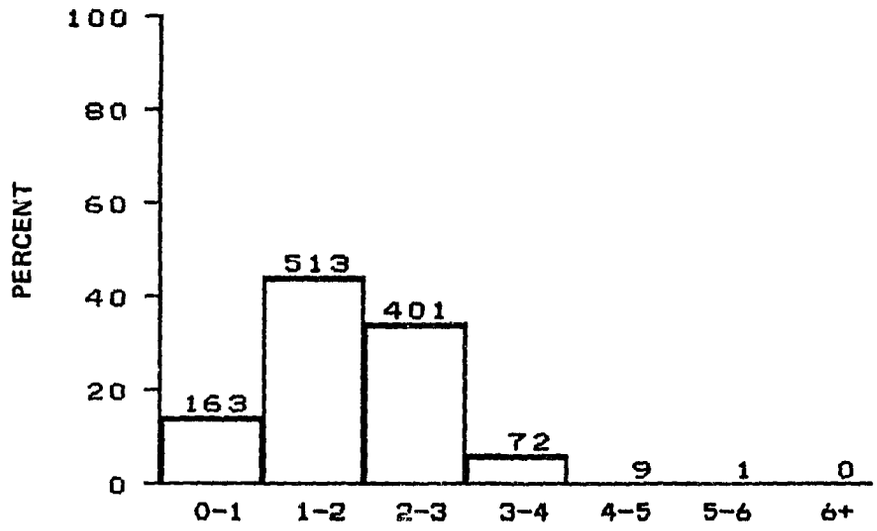

DISTRIBUTION OF SIGNIFICANT WAVE HEIGHT IN METERS
ENTIRE MISSION
BLM AREA #2
N = 1159, MEAN = 1.9, SIGMA = 0.83

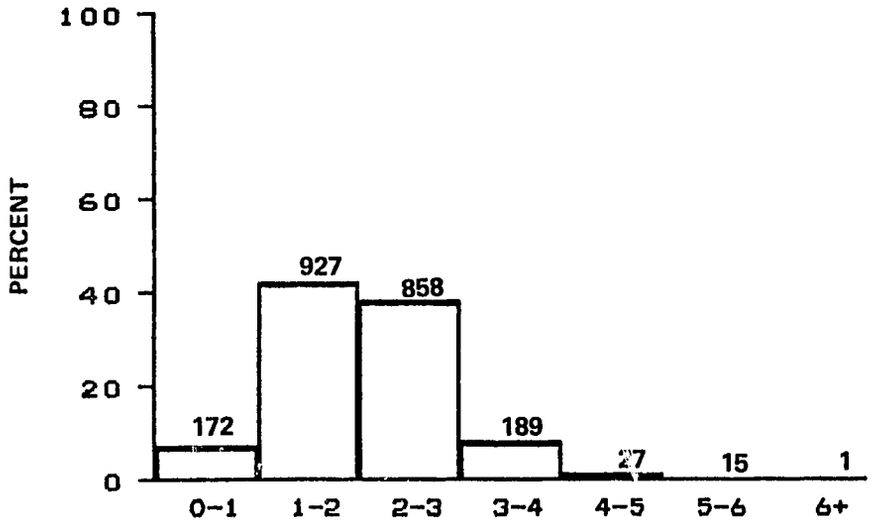

DISTRIBUTION OF SIGNIFICANT WAVE HEIGHT IN METERS
ENTIRE MISSION
BLM AREA #3
N = 2194, MEAN = 2.1, SIGMA = 0.92

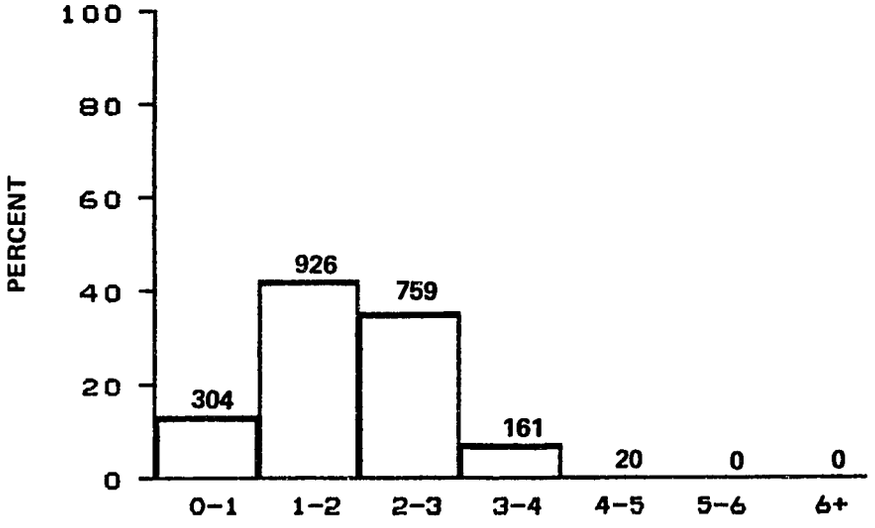

DISTRIBUTION OF SIGNIFICANT WAVE HEIGHT IN METERS
ENTIRE MISSION
BLM AREA #4
N = 2170, MEAN = 1.9, SIGMA = 0.85

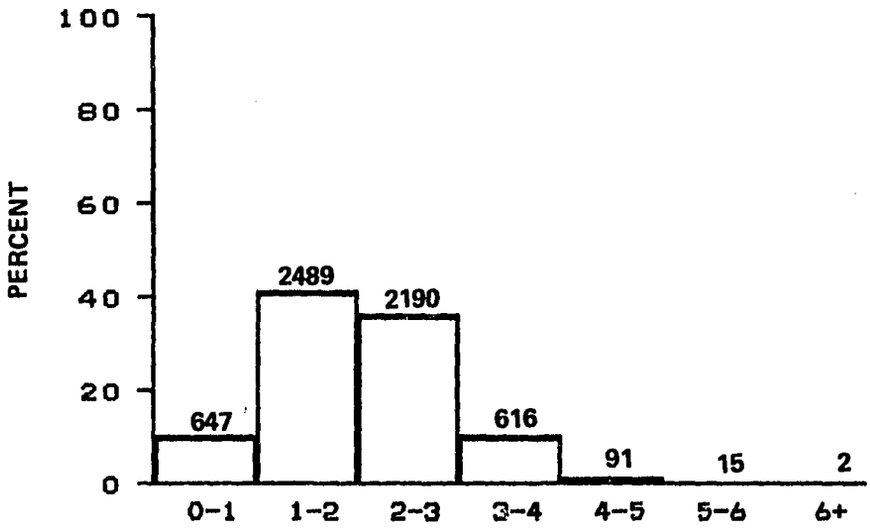

DISTRIBUTION OF SIGNIFICANT WAVE HEIGHT IN METERS

ENTIRE MISSION

BLM AREA #5

N = 6050, MEAN = 2.0, SIGMA = 0.89

APPENDIX C

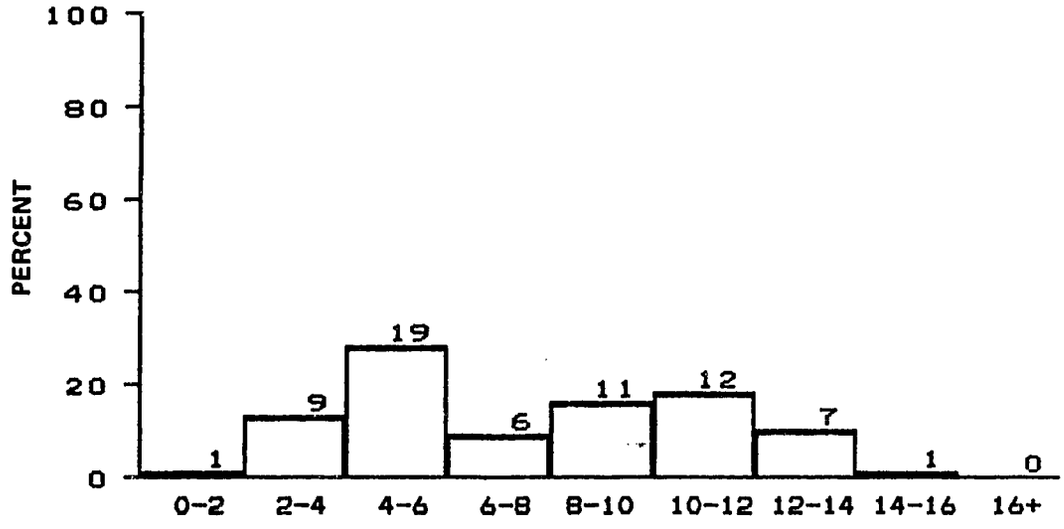

DISTRIBUTION OF WIND SPEED IN METERS PER SECOND
MONTH OF JANUARY
BLM AREA #1
N = 66, MEAN = 7.6, SIGMA = 3.4

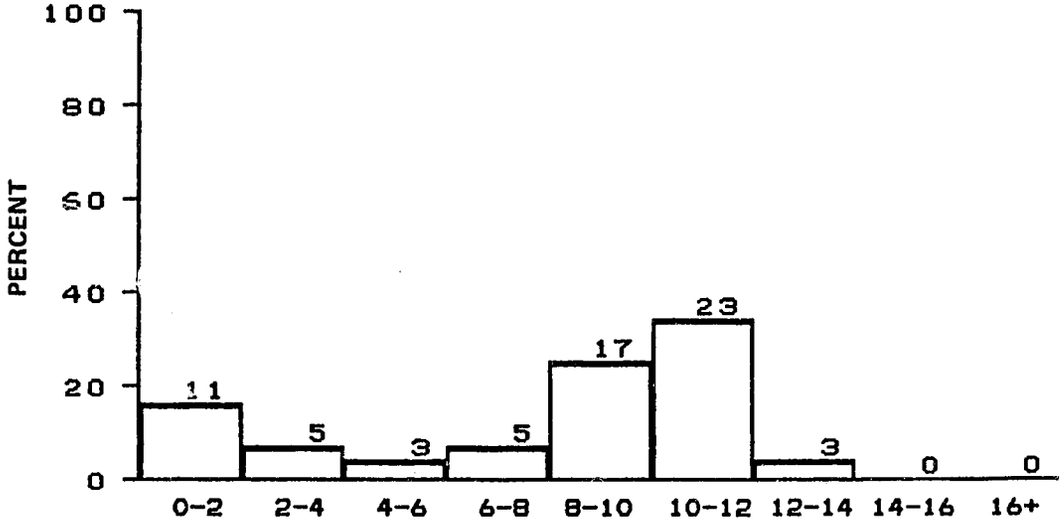

DISTRIBUTION OF WIND SPEED IN METERS PER SECOND
MONTH OF JANUARY
BLM AREA #2
N = 67, MEAN = 7.8, SIGMA = 3.8

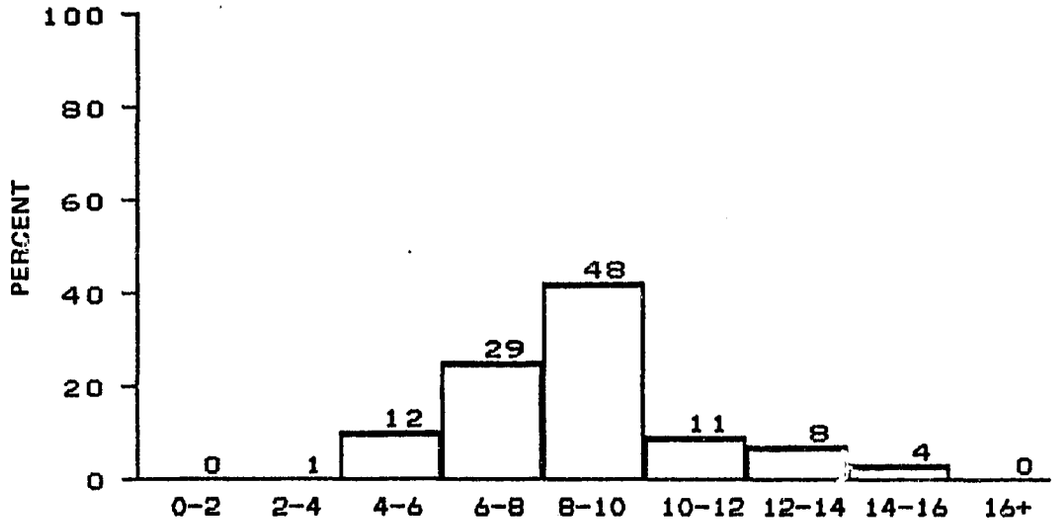

DISTRIBUTION OF WIND SPEED IN METERS PER SECOND
MONTH OF JANUARY
BLM AREA #3
N = 113, MEAN = 8.7, SIGMA = 2.4

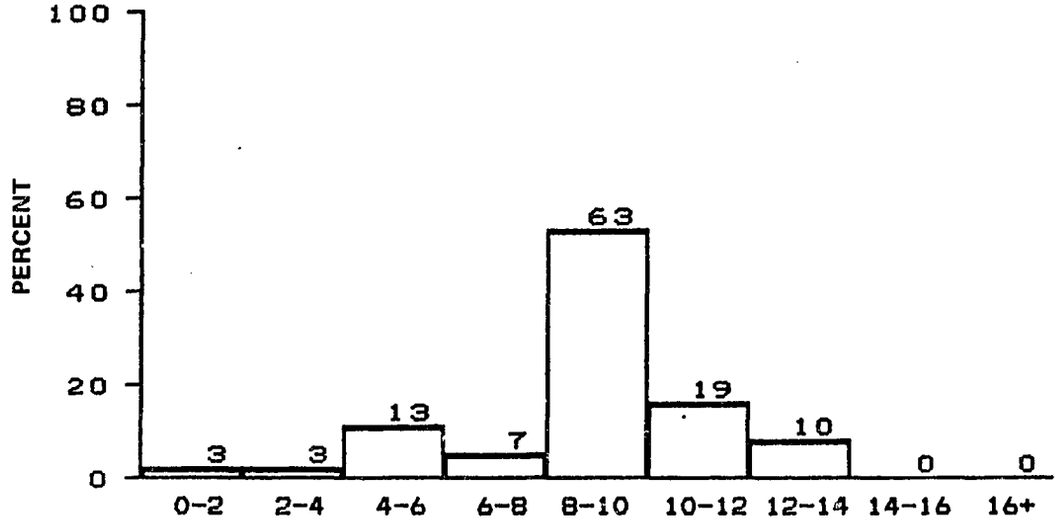

DISTRIBUTION OF WIND SPEED IN METERS PER SECOND
MONTH OF JANUARY
BLM AREA #4
N = 118, MEAN = 8.7, SIGMA = 2.5

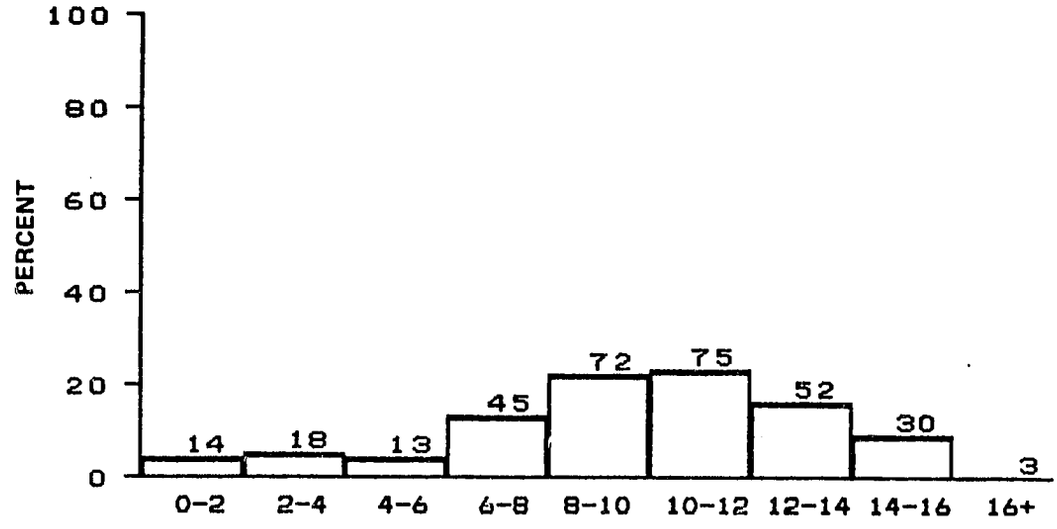

DISTRIBUTION OF WIND SPEED IN METERS PER SECOND
MONTH OF JANUARY
BLM AREA #5
N = 322, MEAN = 9.6, SIGMA = 3.6

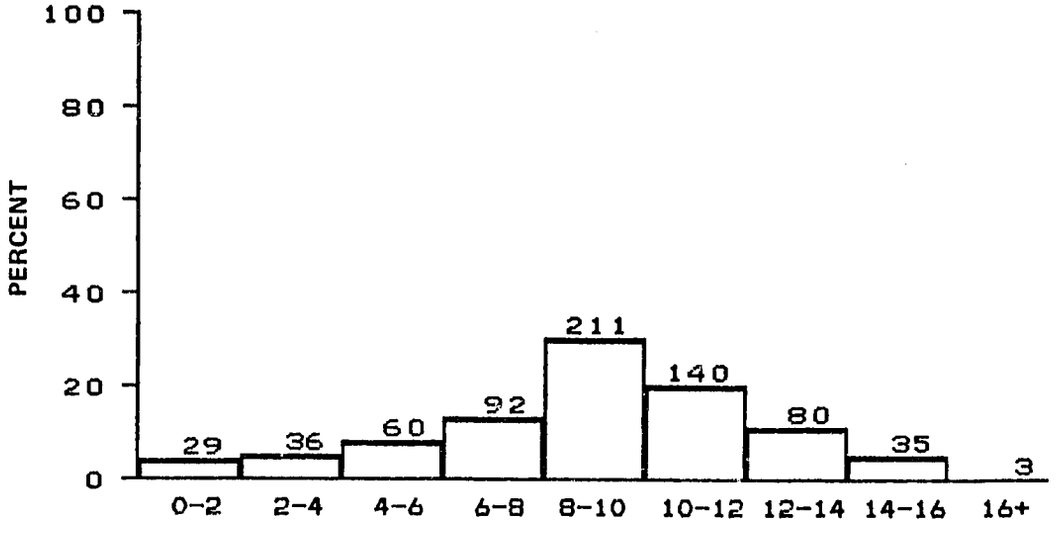

DISTRIBUTION OF WIND SPEED IN METERS PER SECOND
MONTH OF JANUARY
ALL BLM AREAS
N = 686, MEAN = 8.9, SIGMA = 3.4

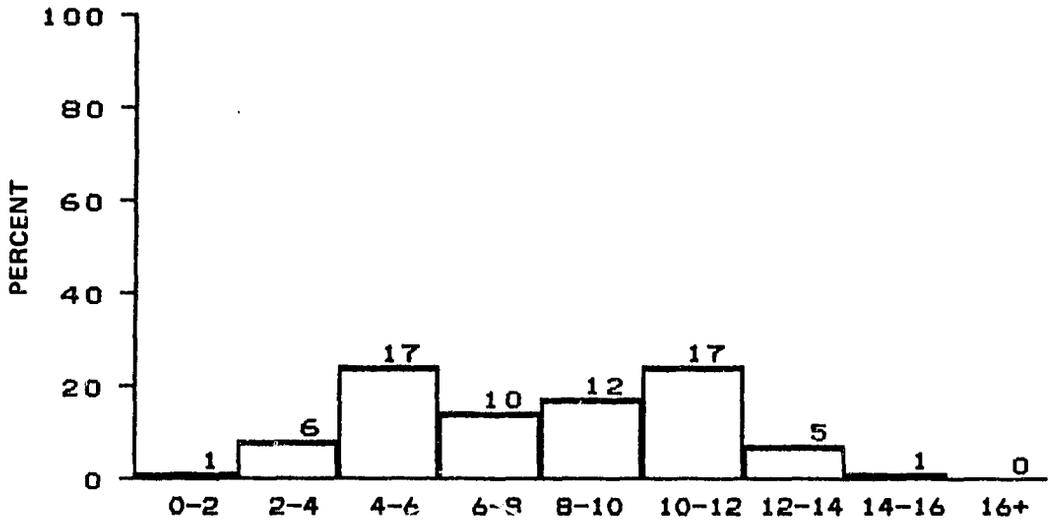

DISTRIBUTION OF WIND SPEED IN METERS PER SECOND
MONTH OF FEBRUARY
BLM AREA #1
N = 69, MEAN = 8.0, SIGMA = 3.2

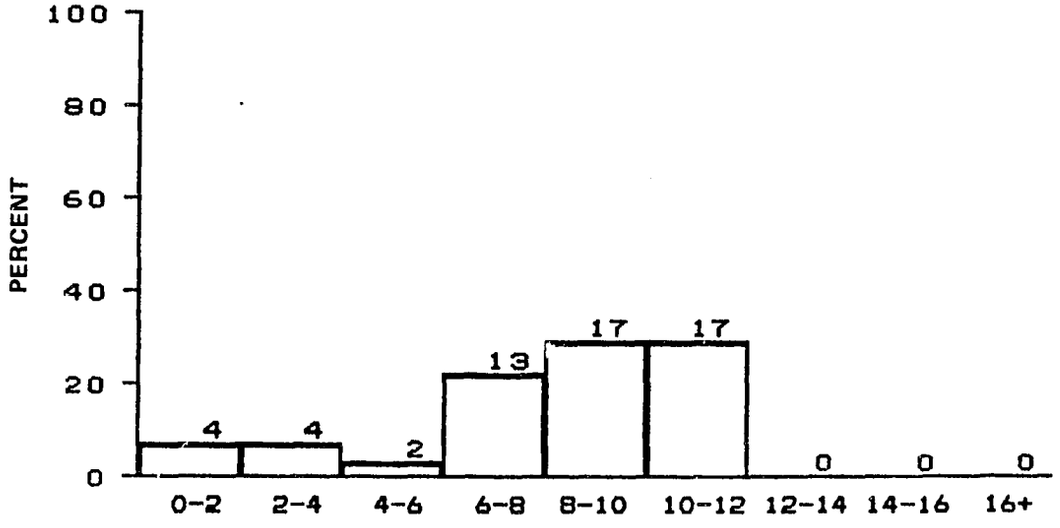

DISTRIBUTION OF WIND SPEED IN METERS PER SECOND
MONTH OF FEBRUARY
BLM AREA #2
N = 57, MEAN = 8.0, SIGMA = 3.0

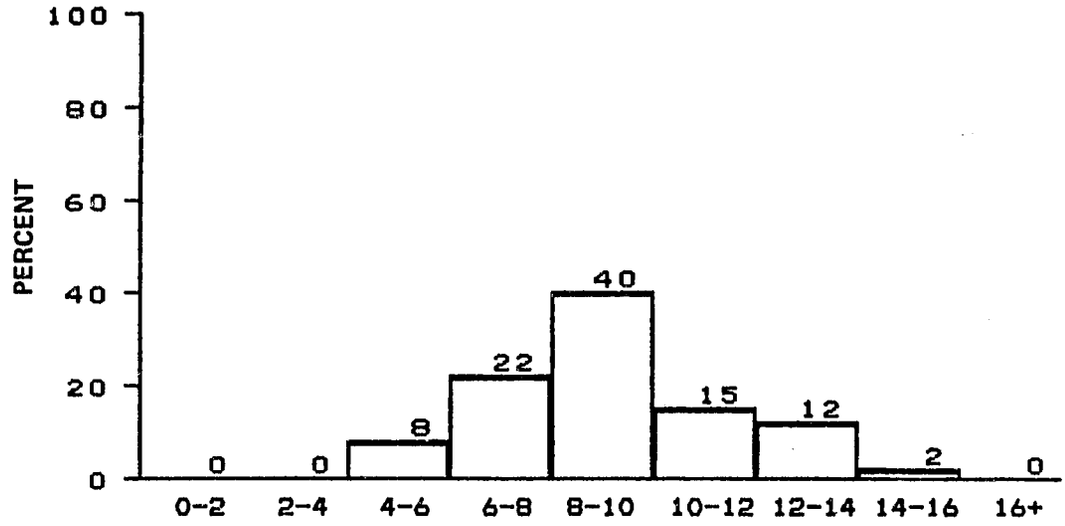

DISTRIBUTION OF WIND SPEED IN METERS PER SECOND
MONTH OF FEBRUARY
BLM AREA #3
N = 99, MEAN = 9.1, SIGMA = 2.3

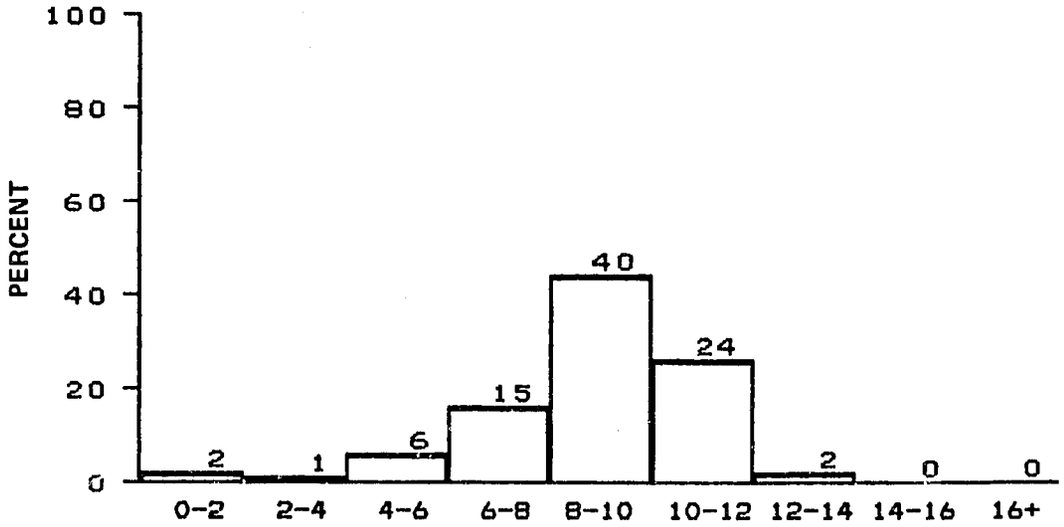

DISTRIBUTION OF WIND SPEED IN METERS PER SECOND
MONTH OF FEBRUARY
BLM AREA #4
N = 90, MEAN = 8.8, SIGMA = 2.2

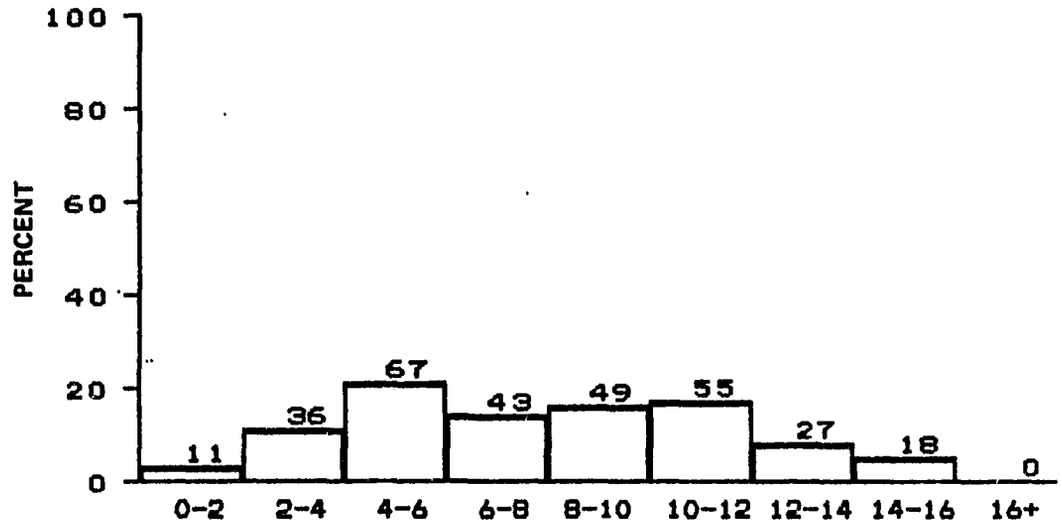

DISTRIBUTION OF WIND SPEED IN METERS PER SECOND
MONTH OF FEBRUARY
BLM AREA #5
N = 306, MEAN = 7.9, SIGMA = 3.7

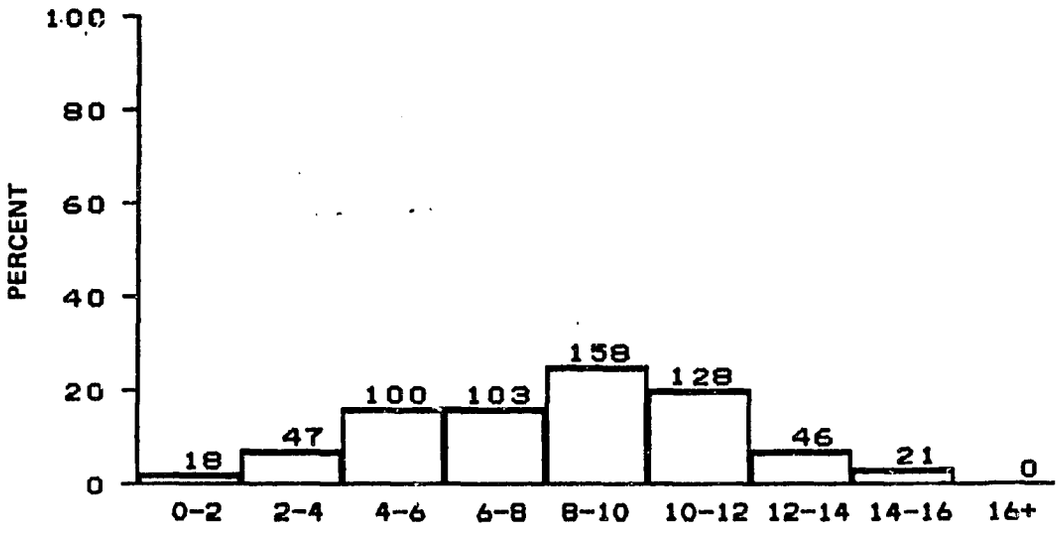

DISTRIBUTION OF WIND SPEED IN METERS PER SECOND
MONTH OF FEBRUARY
ALL BLM AREAS
N = 621, MEAN = 8.2, SIGMA = 3.2

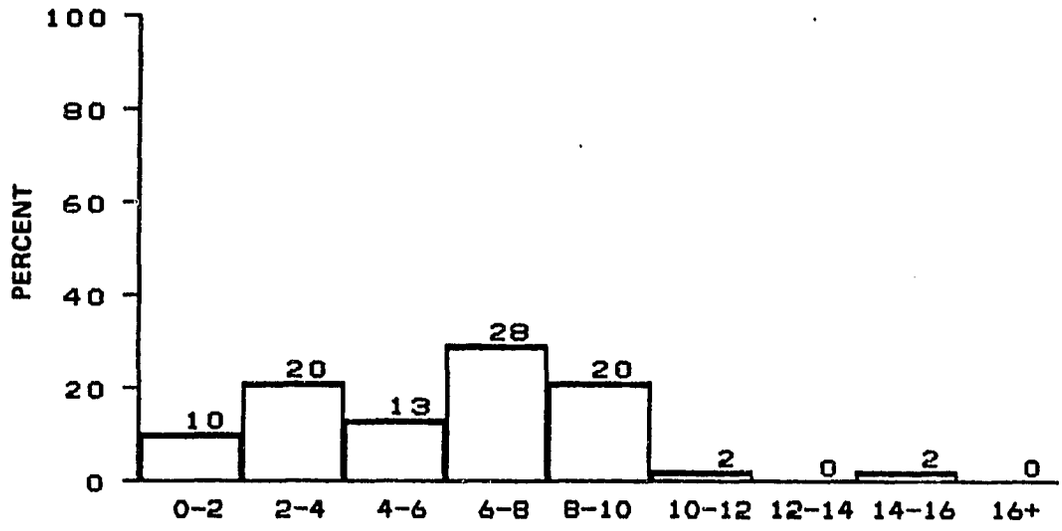

DISTRIBUTION OF WIND SPEED IN METERS PER SECOND
MONTH OF MARCH
BLM AREA #1
N = 95, MEAN = 5.9, SIGMA = 3.0

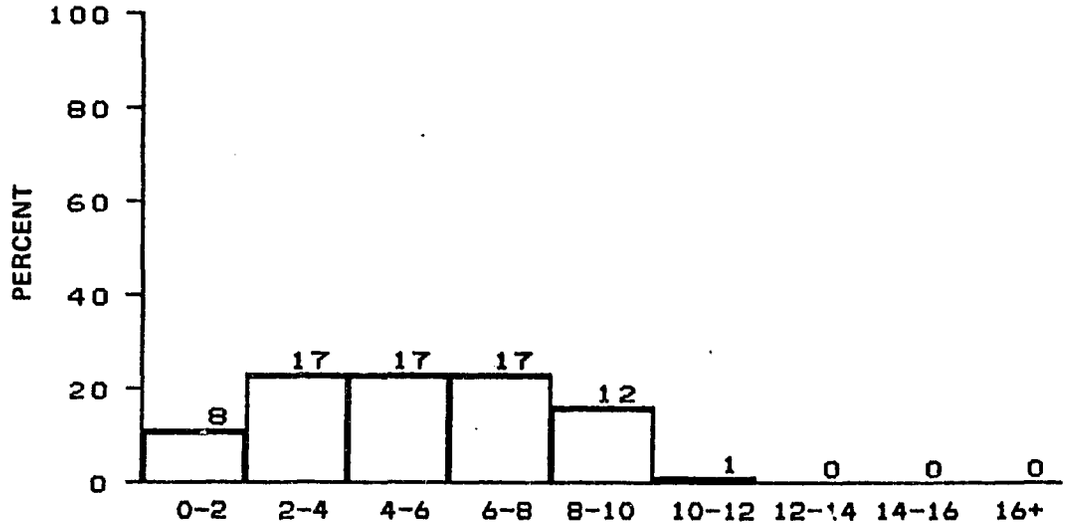

DISTRIBUTION OF WIND SPEED IN METERS PER SECOND
MONTH OF MARCH
BLM AREA #2
N = 72, MEAN = 5.3, SIGMA = 2.6

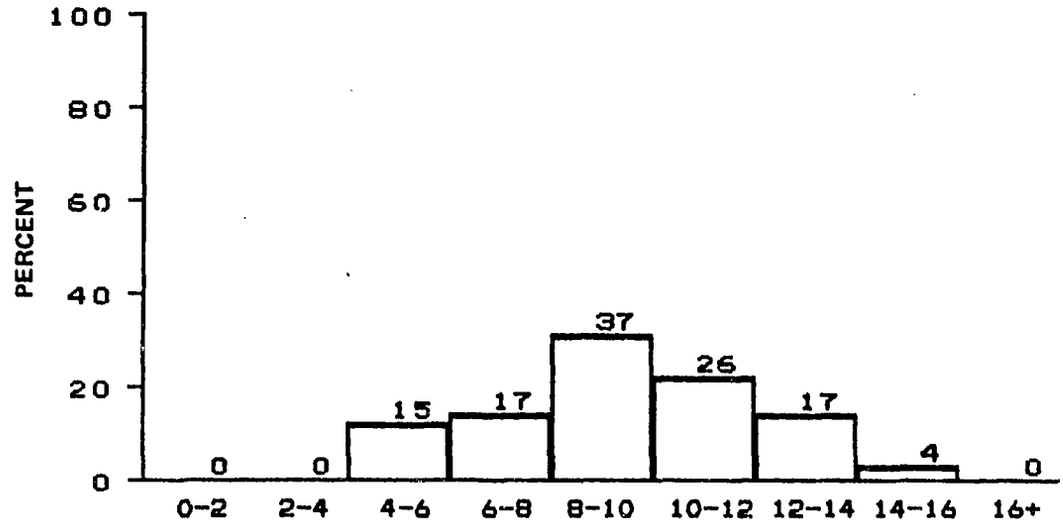

DISTRIBUTION OF WIND SPEED IN METERS PER SECOND
MONTH OF MARCH
BLM AREA #3
N = 116, MEAN = 9.4, SIGMA = 2.6

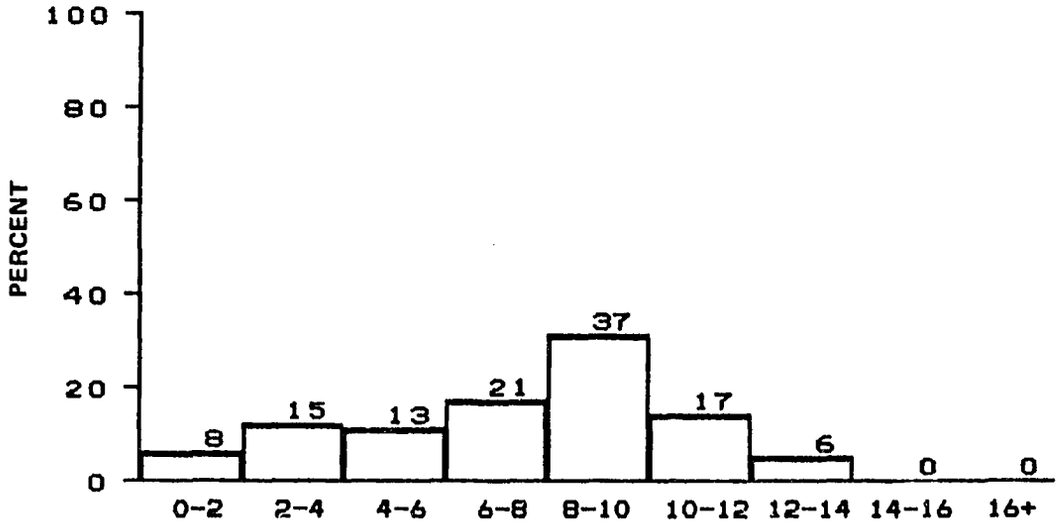

DISTRIBUTION OF WIND SPEED IN METERS PER SECOND
MONTH OF MARCH
BLM AREA #4
N = 117, MEAN = 7.4, SIGMA = 3.2

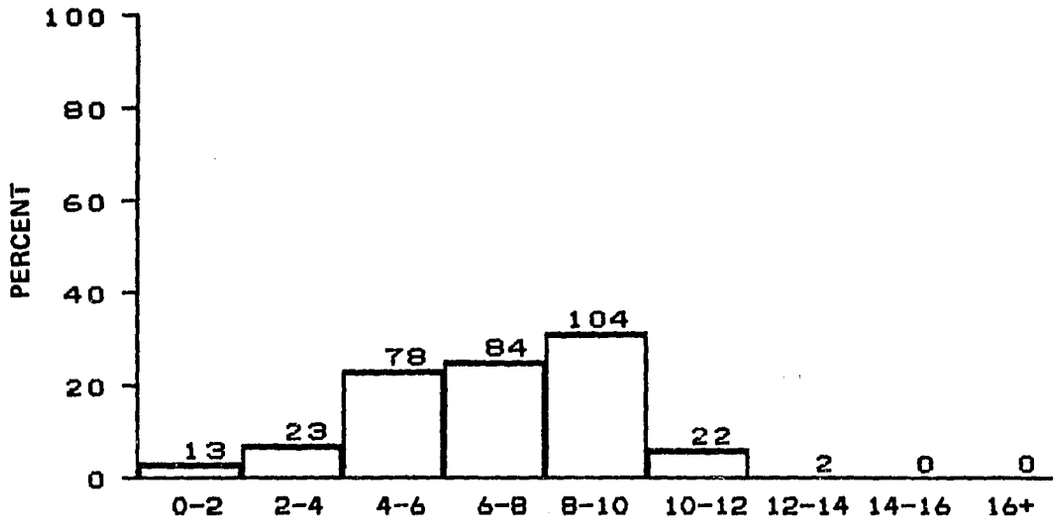

DISTRIBUTION OF WIND SPEED IN METERS PER SECOND
MONTH OF MARCH
BLM AREA #5
N = 326, MEAN = 6.9, SIGMA = 2.5

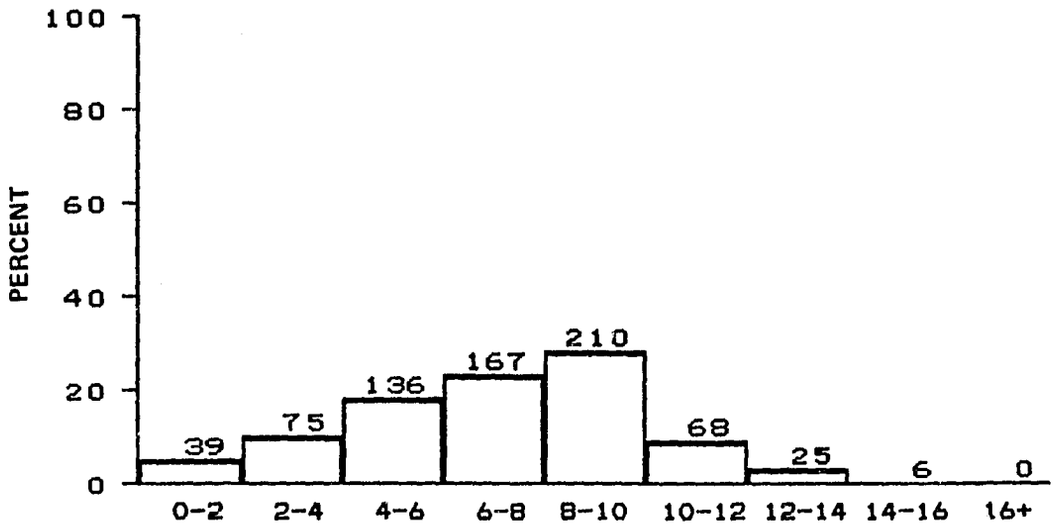

DISTRIBUTION OF WIND SPEED IN METERS PER SECOND
MONTH OF MARCH
ALL BLM AREAS
N = 726, MEAN = 7.1, SIGMA = 3.0

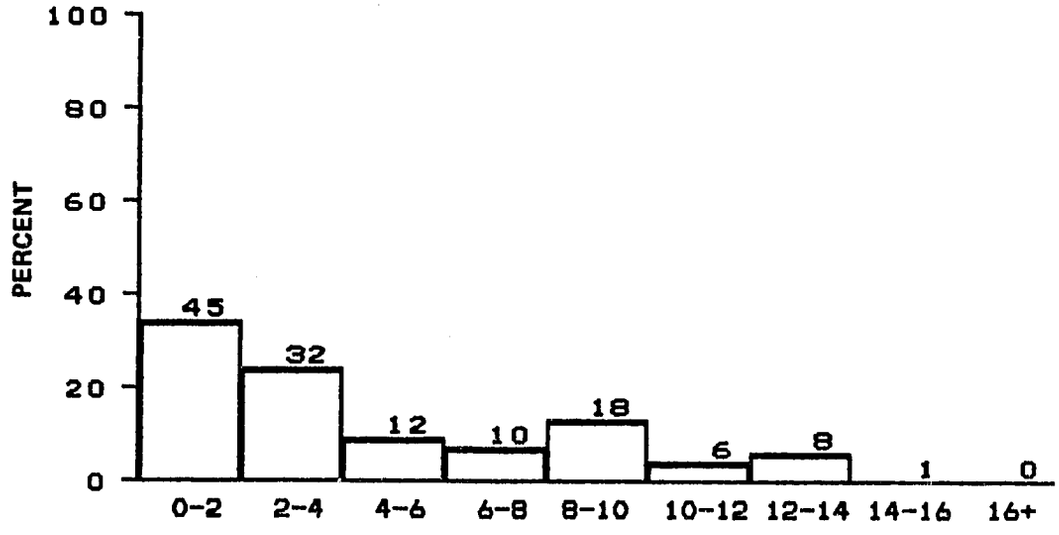

DISTRIBUTION OF WIND SPEED IN METERS PER SECOND
MONTH OF APRIL
BLM AREA #1
N = 132, MEAN = 4.7, SIGMA = 3.9

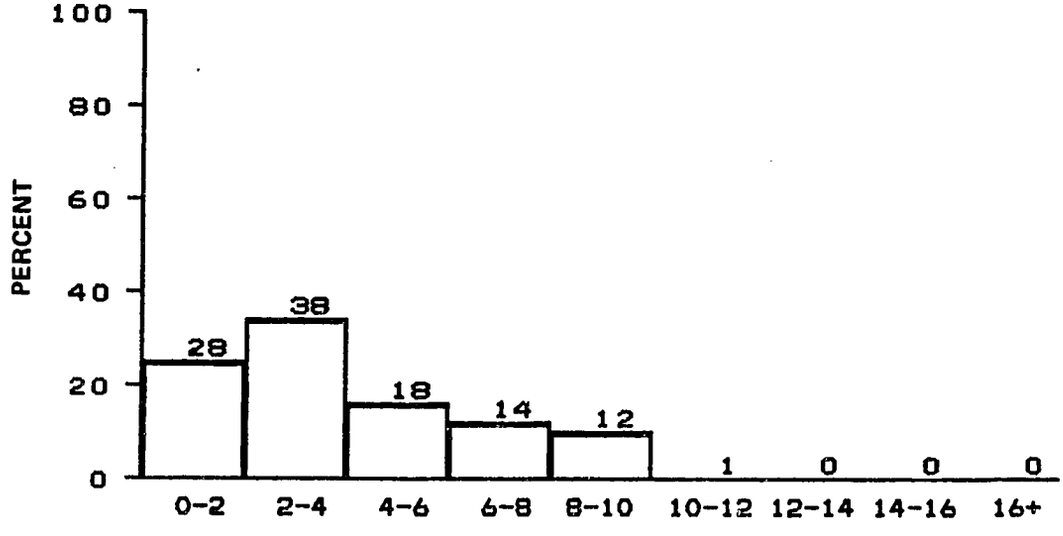

DISTRIBUTION OF WIND SPEED IN METERS PER SECOND
MONTH OF APRIL
BLM AREA #2
N = 111, MEAN = 4.0, SIGMA = 2.7

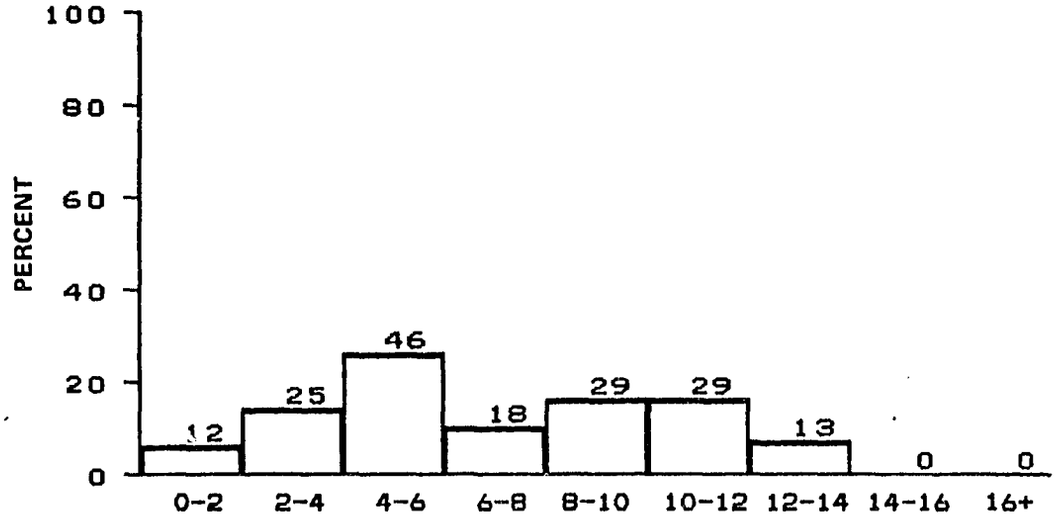

DISTRIBUTION OF WIND SPEED IN METERS PER SECOND
MONTH OF APRIL
BLM AREA #3
N = 172, MEAN = 6.9, SIGMA = 3.5

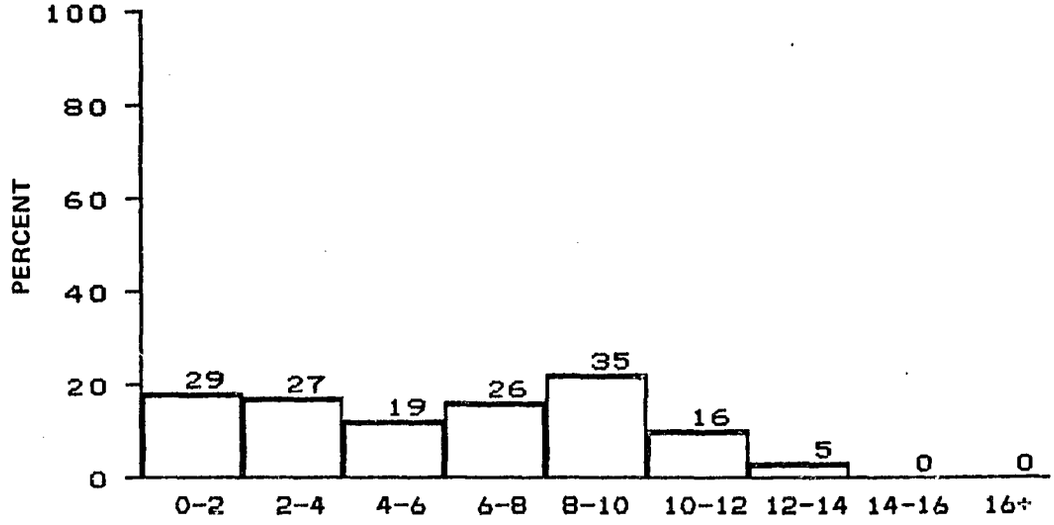

DISTRIBUTION OF WIND SPEED IN METERS PER SECOND
MONTH OF APRIL
BLM AREA #4
N = 157, MEAN = 6.0, SIGMA = 3.5

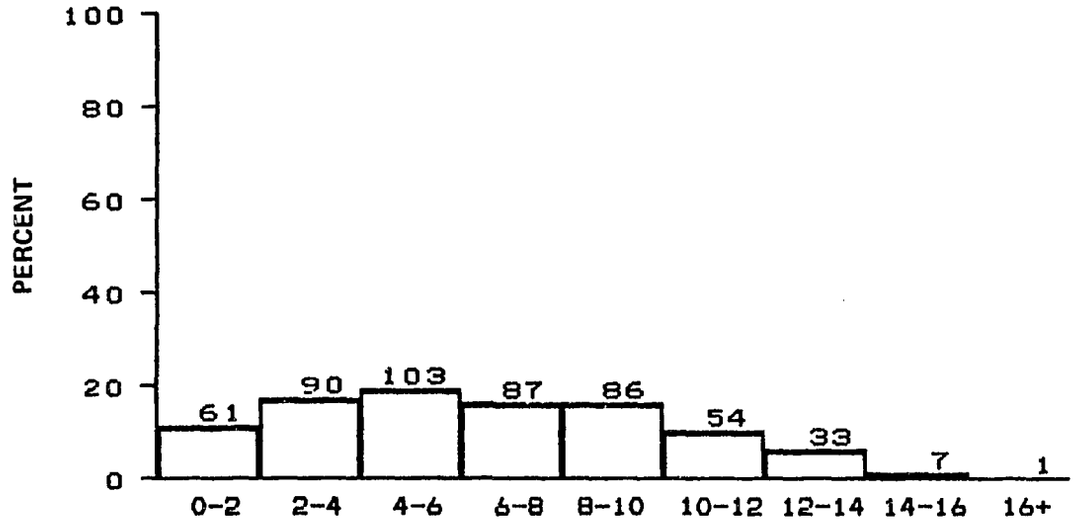

DISTRIBUTION OF WIND SPEED IN METERS PER SECOND
MONTH OF APRIL
BLM AREA #5
N = 522, MEAN = 6.5, SIGMA = 3.6

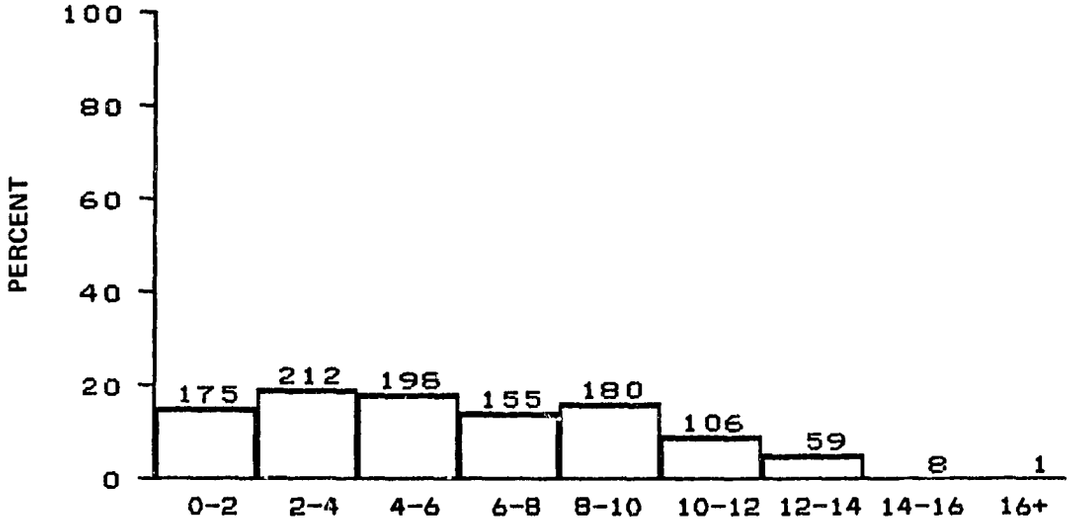

DISTRIBUTION OF WIND SPEED IN METERS PER SECOND
MONTH OF APRIL
ALL BLM AREAS
N = 1094, MEAN = 6.0, SIGMA = 3.6

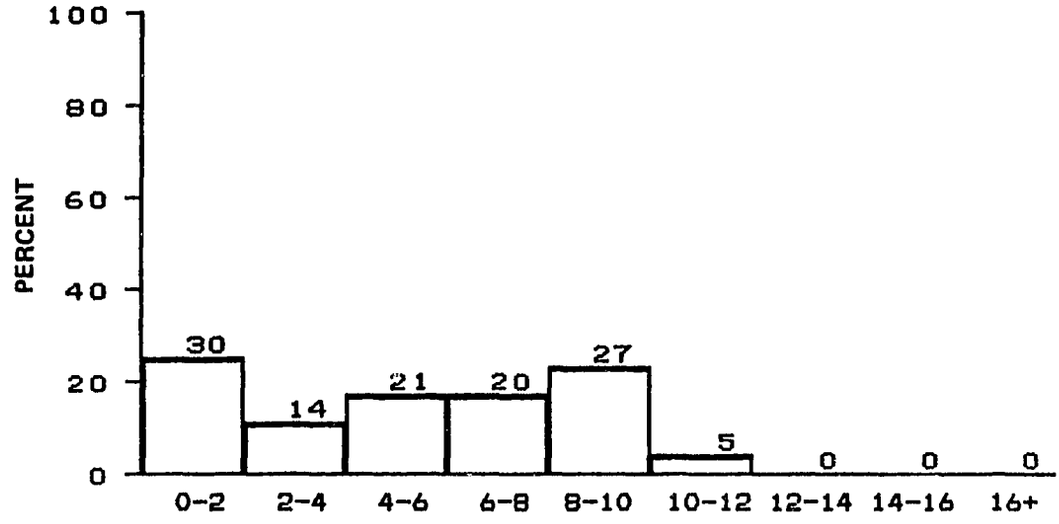

DISTRIBUTION OF WIND SPEED IN METERS PER SECOND
MONTH OF MAY
BLM AREA #1
N = 117, MEAN = 5.3, SIGMA = 3.2

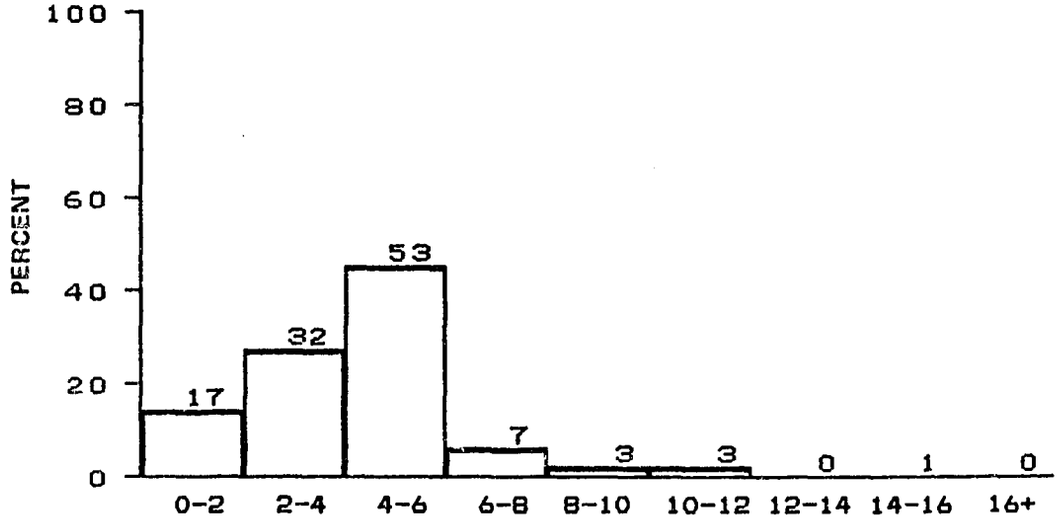

DISTRIBUTION OF WIND SPEED IN METERS PER SECOND
MONTH OF MAY
BLM AREA #2
N = 116, MEAN = 4.3, SIGMA = 2.3

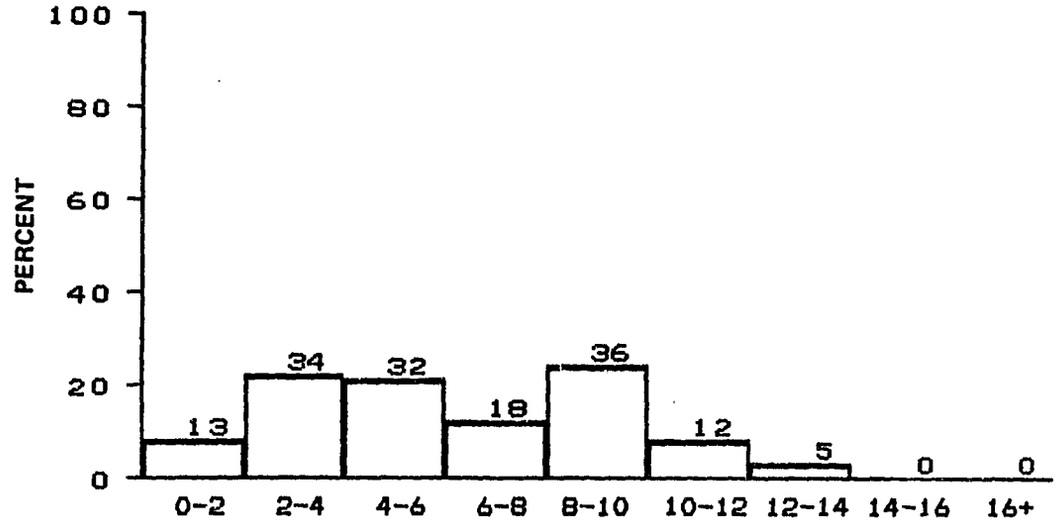

DISTRIBUTION OF WIND SPEED IN METERS PER SECOND
MONTH OF MAY
BLM AREA #3
N = 150, MEAN = 6.1, SIGMA = 3.2

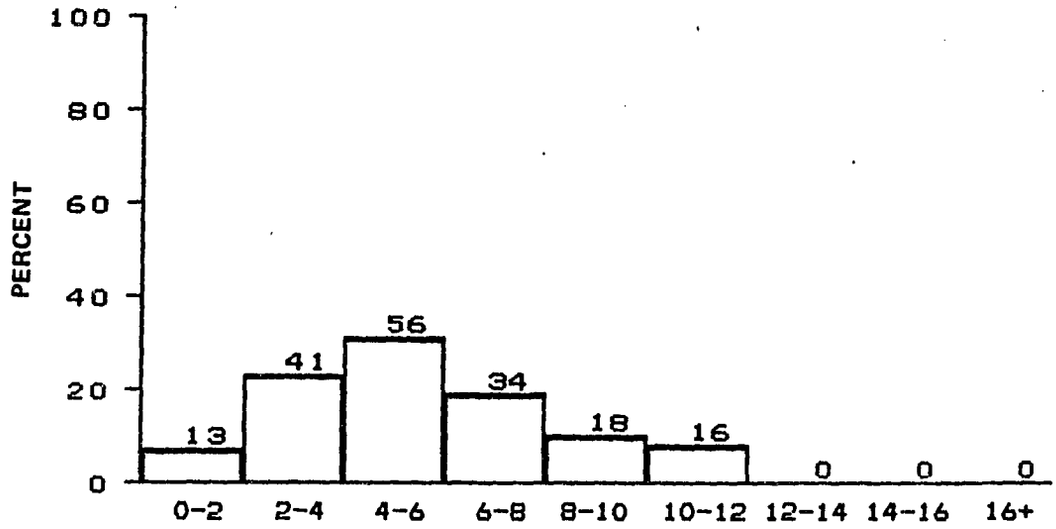

DISTRIBUTION OF WIND SPEED IN METERS PER SECOND
MONTH OF MAY
BLM AREA #4
N = 178, MEAN = 5.6, SIGMA = 2.7

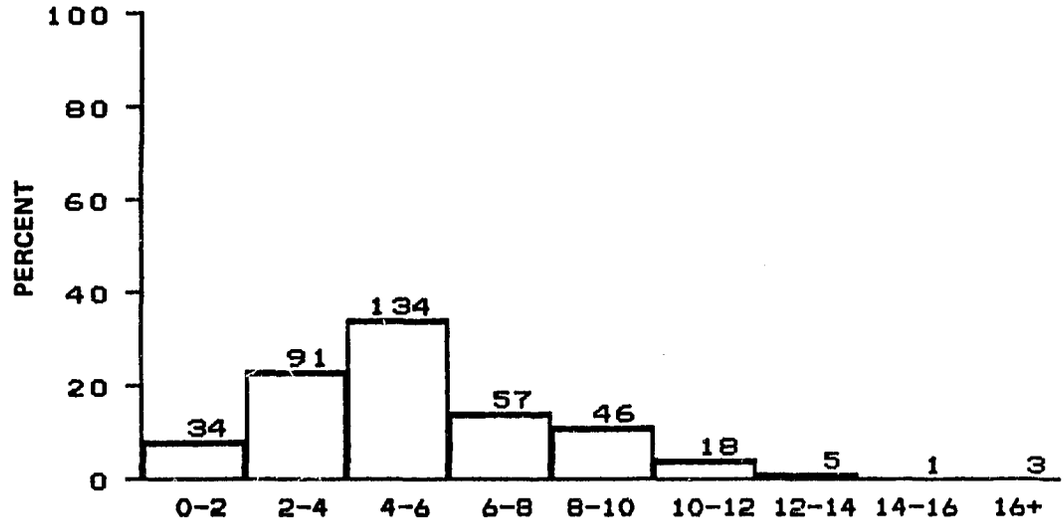

DISTRIBUTION OF WIND SPEED IN METERS PER SECOND
MONTH OF MAY
BLM AREA #5
N = 389, MEAN = 5.4, SIGMA = 2.9

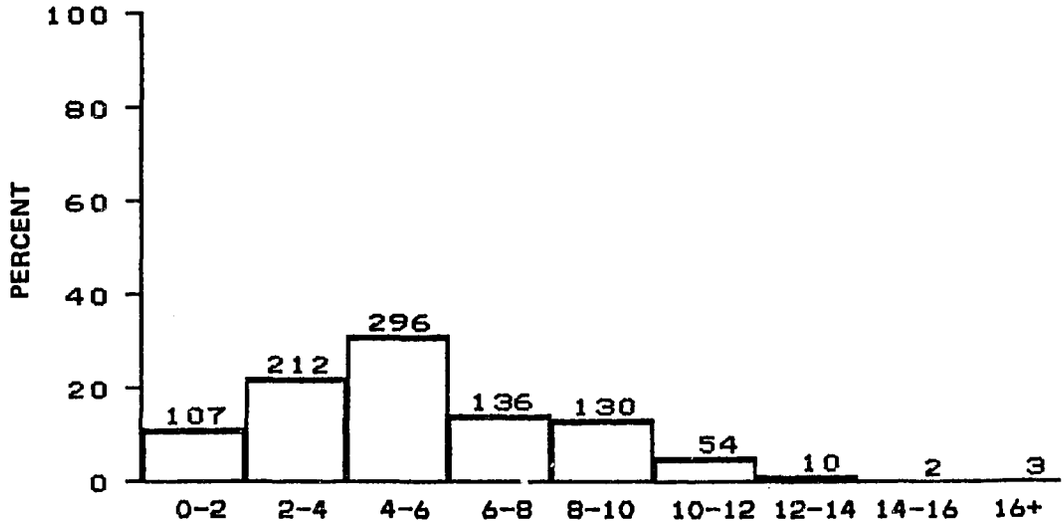

DISTRIBUTION OF WIND SPEED IN METERS PER SECOND
MONTH OF MAY
ALL BLM AREAS
N = 950, MEAN = 5.4, SIGMA = 2.9

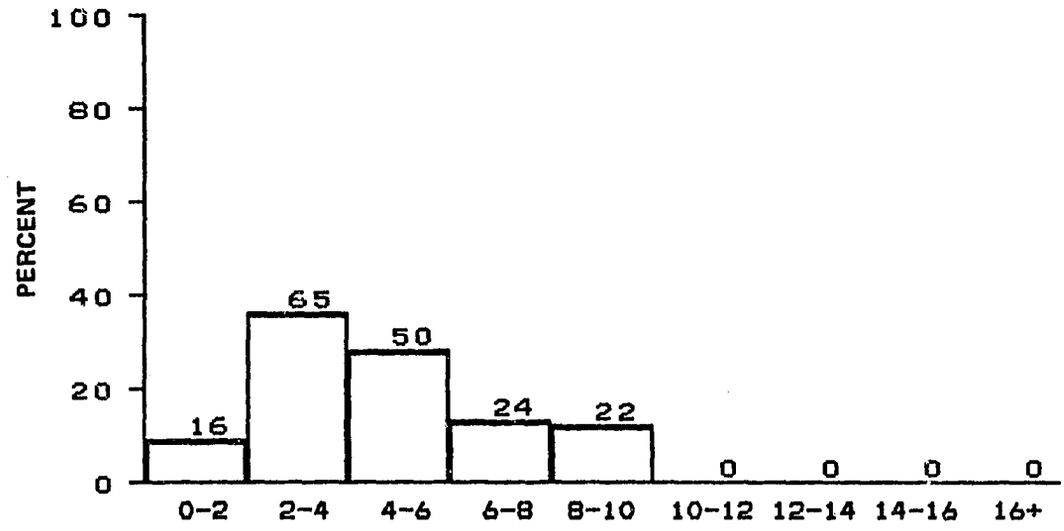

DISTRIBUTION OF WIND SPEED IN METERS PER SECOND
MONTH OF JUNE
BLM AREA #1
N = 177, MEAN = 4.7, SIGMA = 2.3

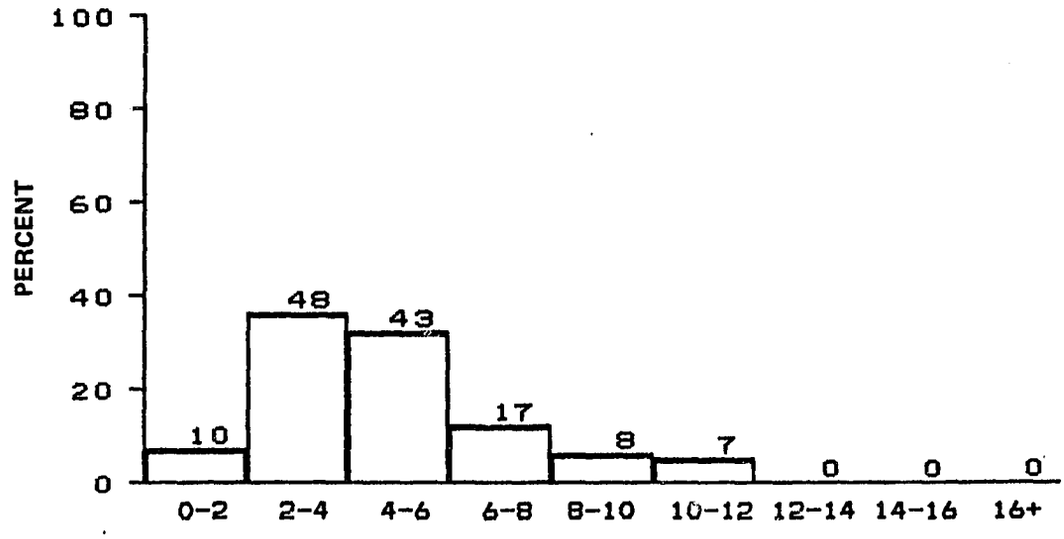

DISTRIBUTION OF WIND SPEED IN METERS PER SECOND
MONTH OF JUNE
BLM AREA #2
N = 133, MEAN = 4.8, SIGMA = 2.4

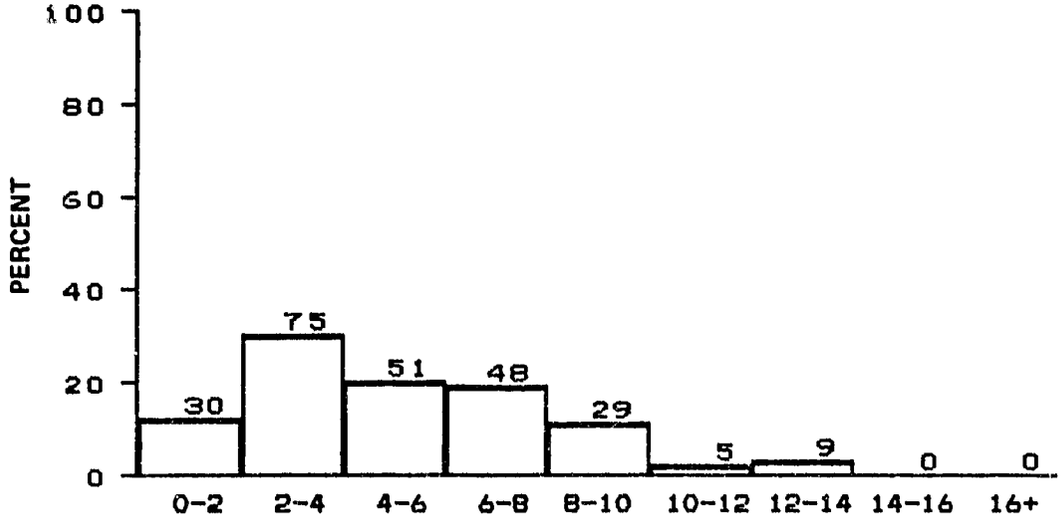

DISTRIBUTION OF WIND SPEED IN METERS PER SECOND
MONTH OF JUNE
BLM AREA #3
N = 247, MEAN = 5.2, SIGMA = 3.0

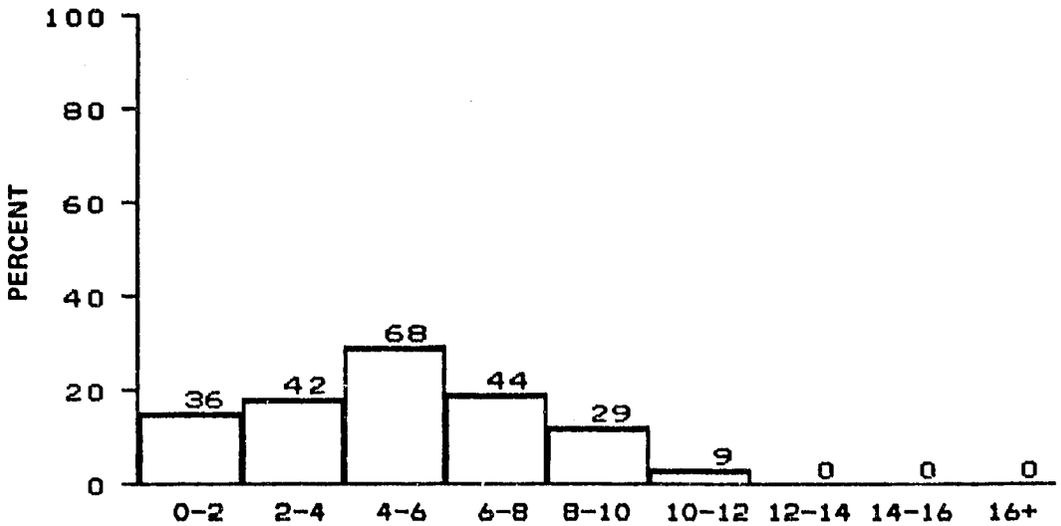

DISTRIBUTION OF WIND SPEED IN METERS PER SECOND
MONTH OF JUNE
BLM AREA #4
N = 228, MEAN = 5.1, SIGMA = 2.7

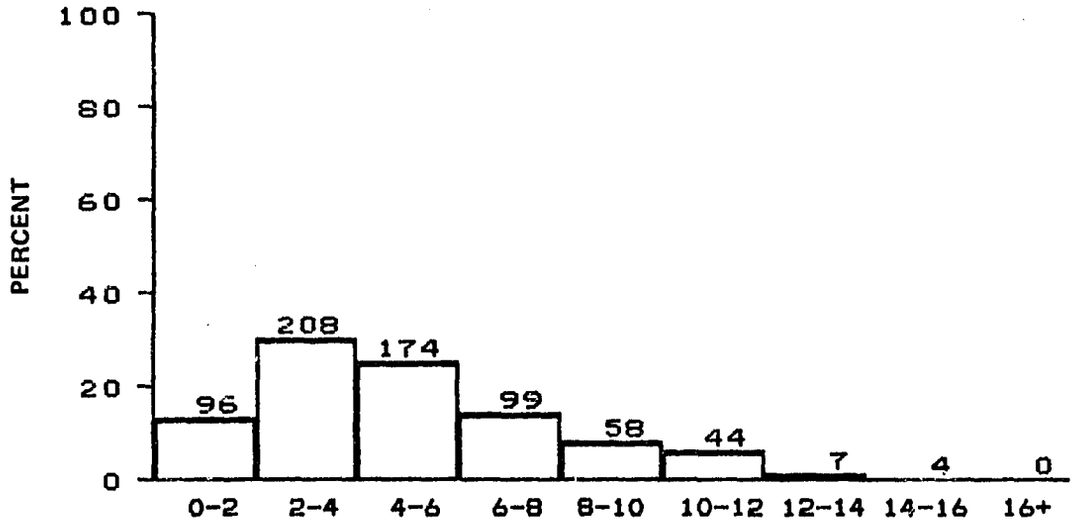

DISTRIBUTION OF WIND SPEED IN METERS PER SECOND
MONTH OF JUNE
BLM AREA #5
N = 690, MEAN = 5.0, SIGMA = 3.0

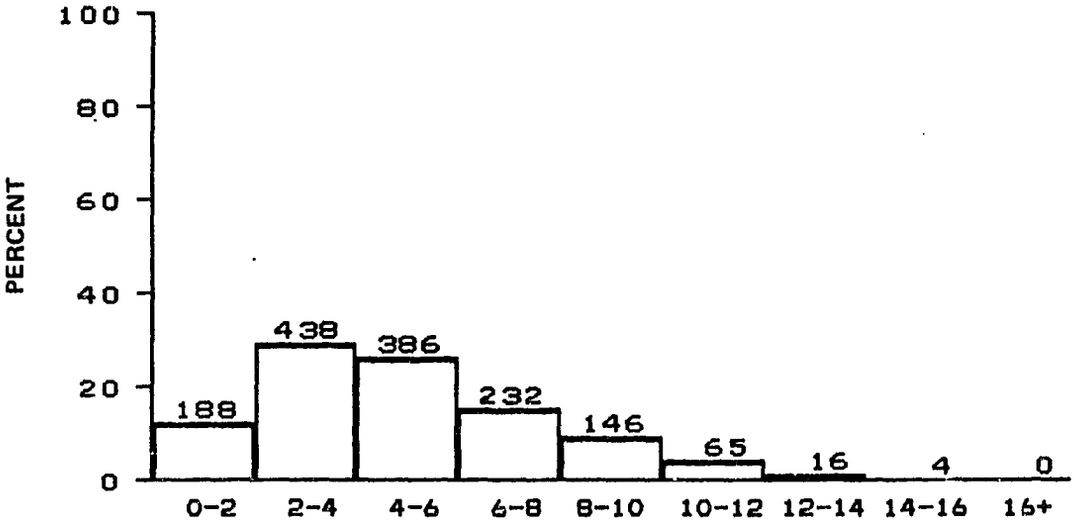

DISTRIBUTION OF WIND SPEED IN METERS PER SECOND
MONTH OF JUNE
ALL BLM AREAS
N = 1475, MEAN = 5.0, SIGMA = 2.8

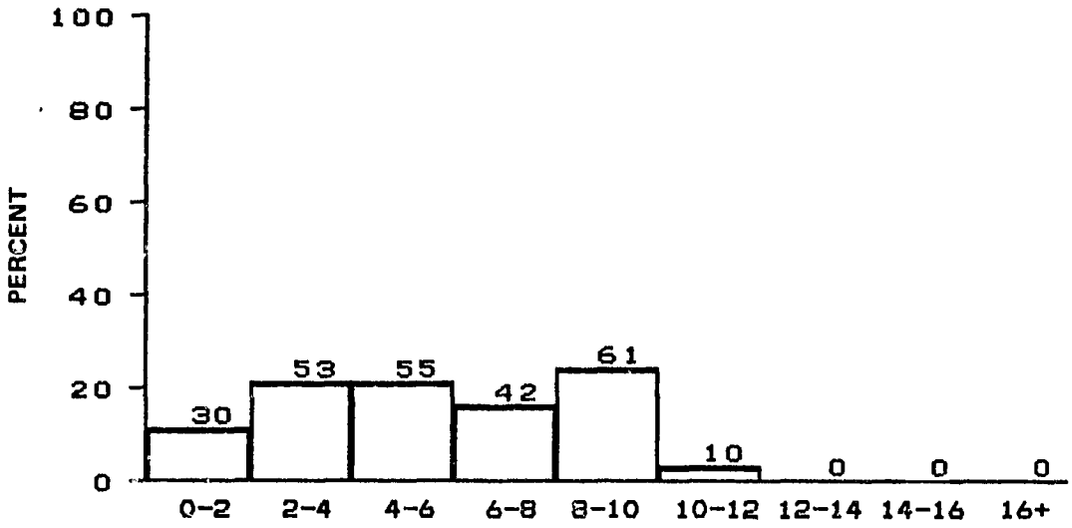

DISTRIBUTION OF WIND SPEED IN METERS PER SECOND
MONTH OF JULY
BLM AREA #1
N = 251, MEAN = 5.6, SIGMA = 2.9

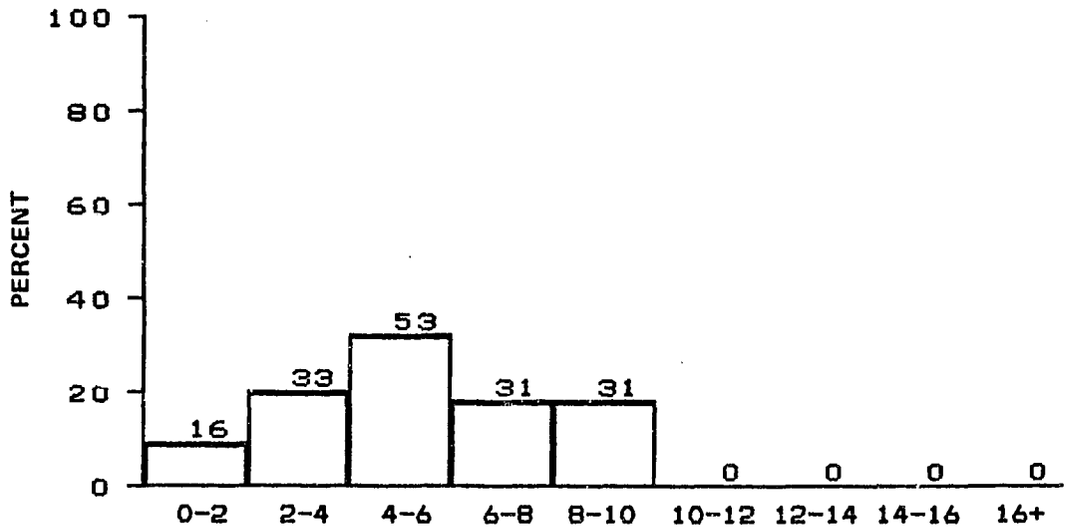

DISTRIBUTION OF WIND SPEED IN METERS PER SECOND
MONTH OF JULY
BLM AREA #2
N = 164, MEAN = 5.3, SIGMA = 2.5

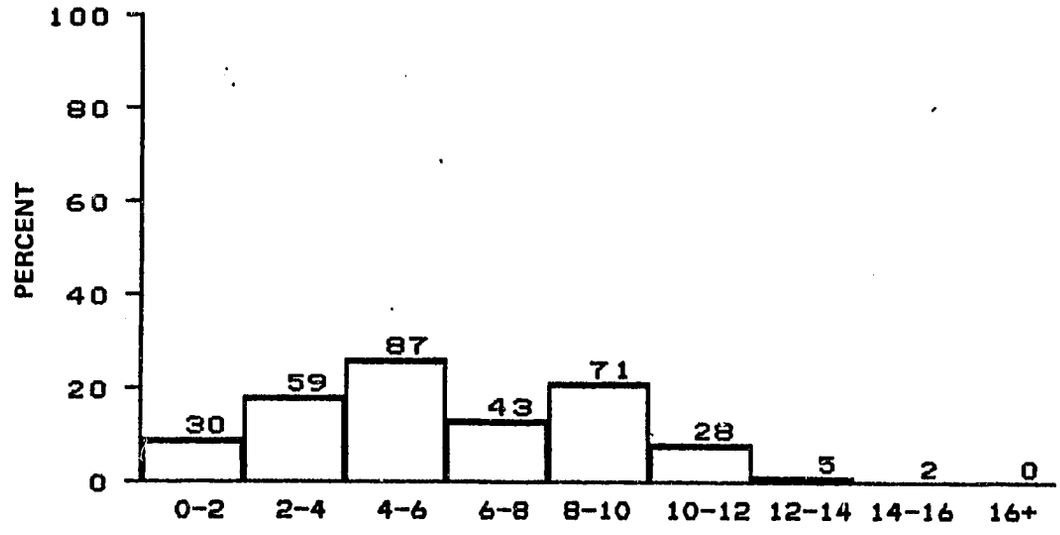

DISTRIBUTION OF WIND SPEED IN METERS PER SECOND
MONTH OF JULY
BLM AREA #3
N = 325, MEAN = 6.1, SIGMA = 3.1

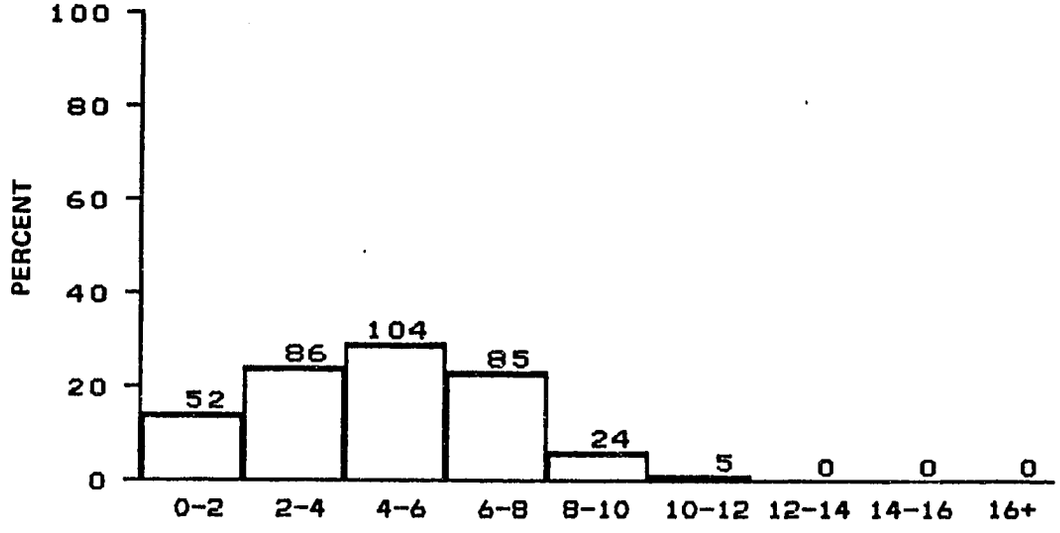

DISTRIBUTION OF WIND SPEED IN METERS PER SECOND
MONTH OF JULY
BLM AREA #4
N = 356, MEAN = 4.8, SIGMA = 2.4

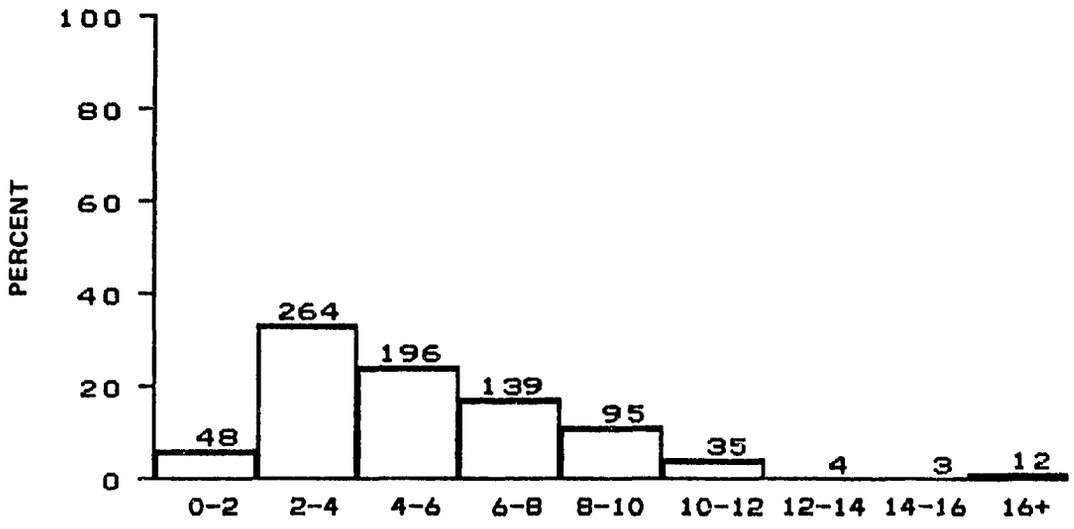

DISTRIBUTION OF WIND SPEED IN METERS PER SECOND
MONTH OF JULY
BLM AREA #5
N = 796, MEAN = 5.4, SIGMA = 3.0

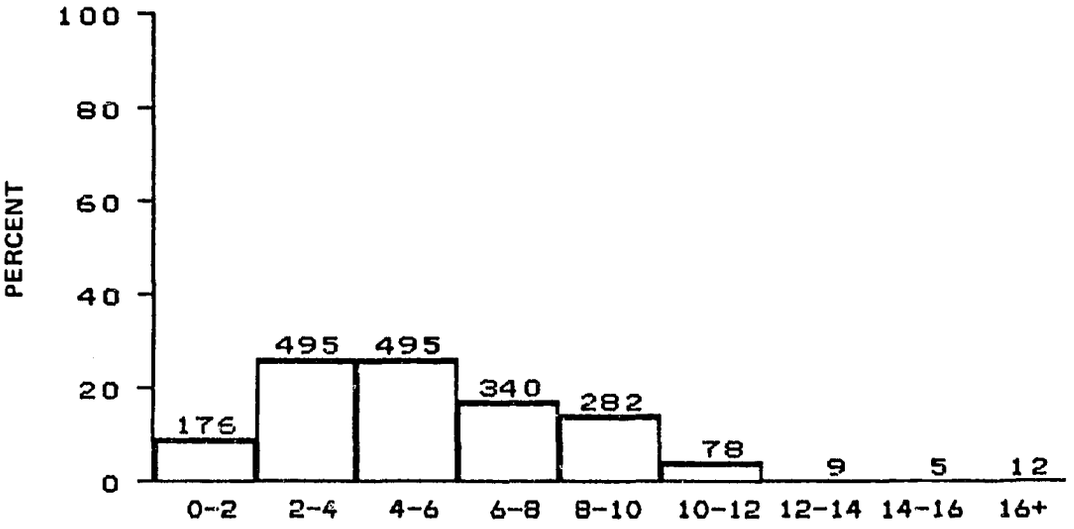

DISTRIBUTION OF WIND SPEED IN METERS PER SECOND
MONTH OF JULY
ALL BLM AREAS
N = 1892, MEAN = 5.4, SIGMA = 2.9

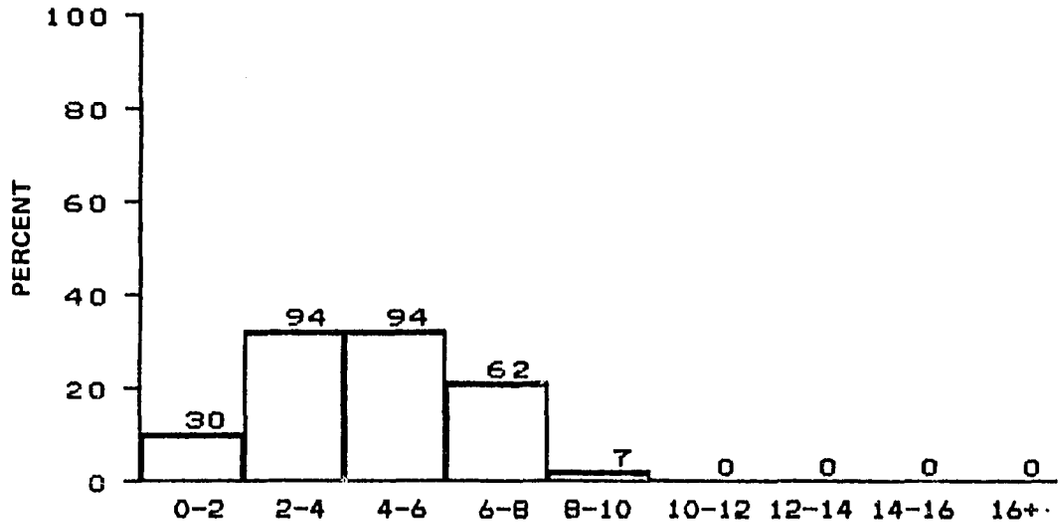

DISTRIBUTION OF WIND SPEED IN METERS PER SECOND
MONTH OF AUGUST
BLM AREA #1
N = 287, MEAN = 4.5, SIGMA = 2.0

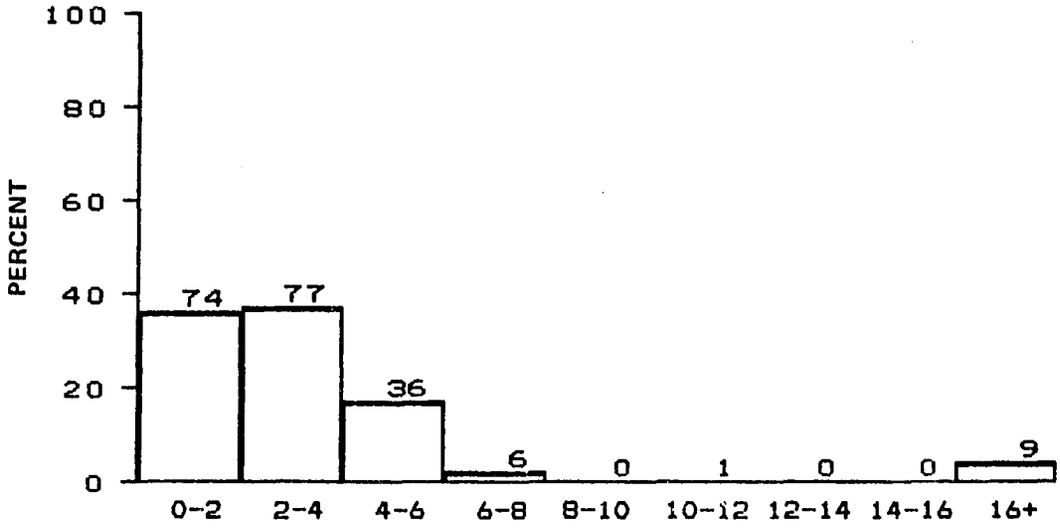

DISTRIBUTION OF WIND SPEED IN METERS PER SECOND
MONTH OF AUGUST
BLM AREA #2
N = 203, MEAN = 3.4, SIGMA = 3.4

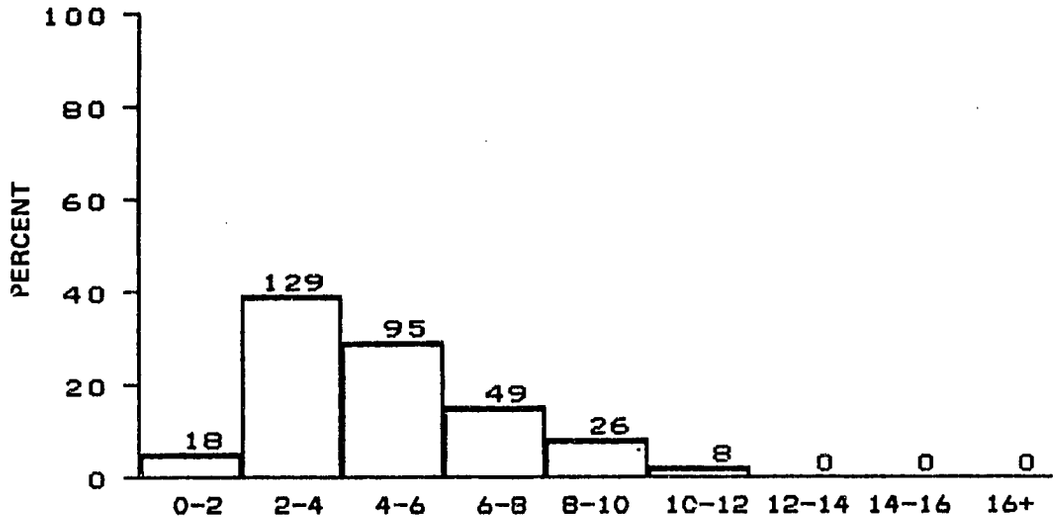

DISTRIBUTION OF WIND SPEED IN METERS PER SECOND
MONTH OF AUGUST
BLM AREA #3
N = 325, MEAN = 4.8, SIGMA = 2.3

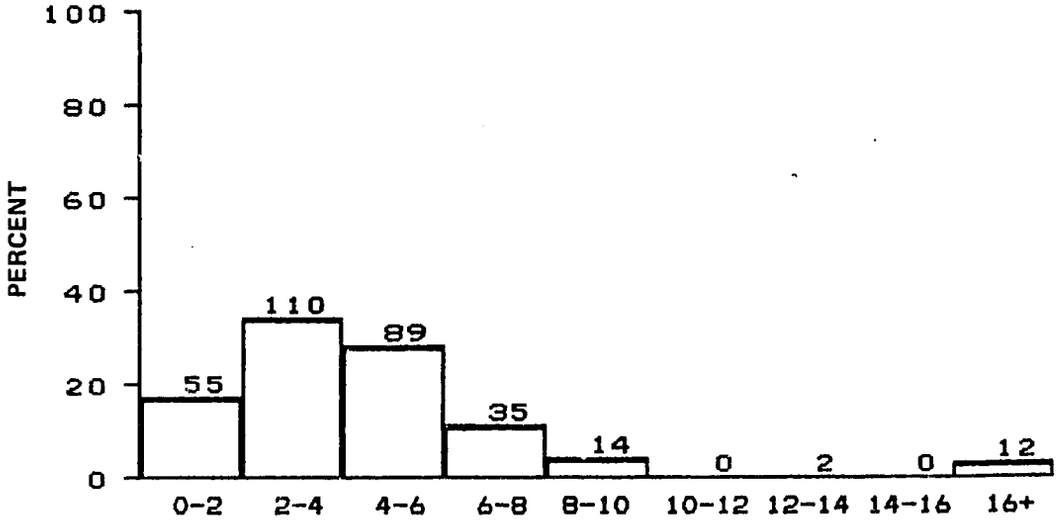

DISTRIBUTION OF WIND SPEED IN METERS PER SECOND
MONTH OF AUGUST
BLM AREA #4
N = 317, MEAN = 4.5, SIGMA = 3.3

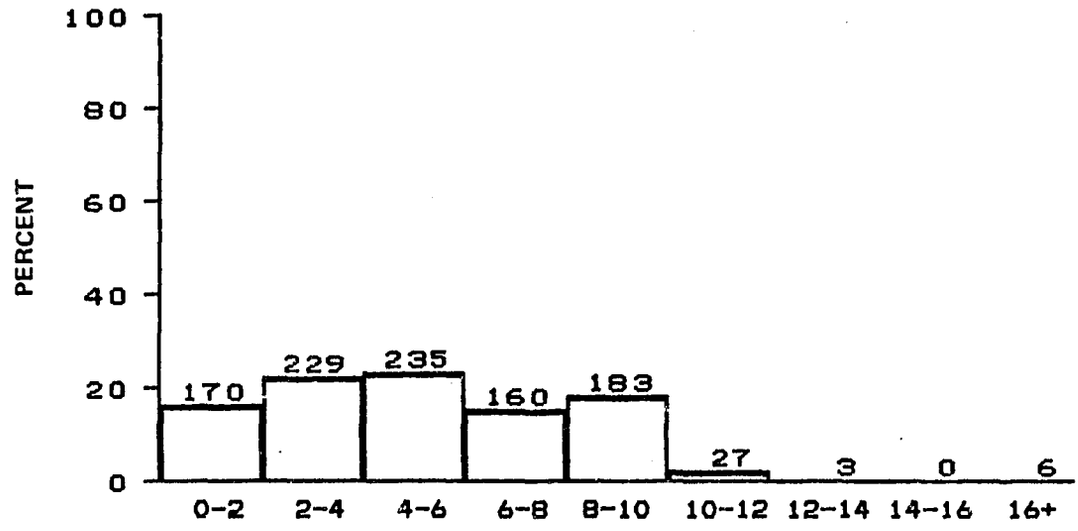

DISTRIBUTION OF WIND SPEED IN METERS PER SECOND
MONTH OF AUGUST
BLM AREA #5
N = 1013, MEAN = 5.2, SIGMA = 3.0

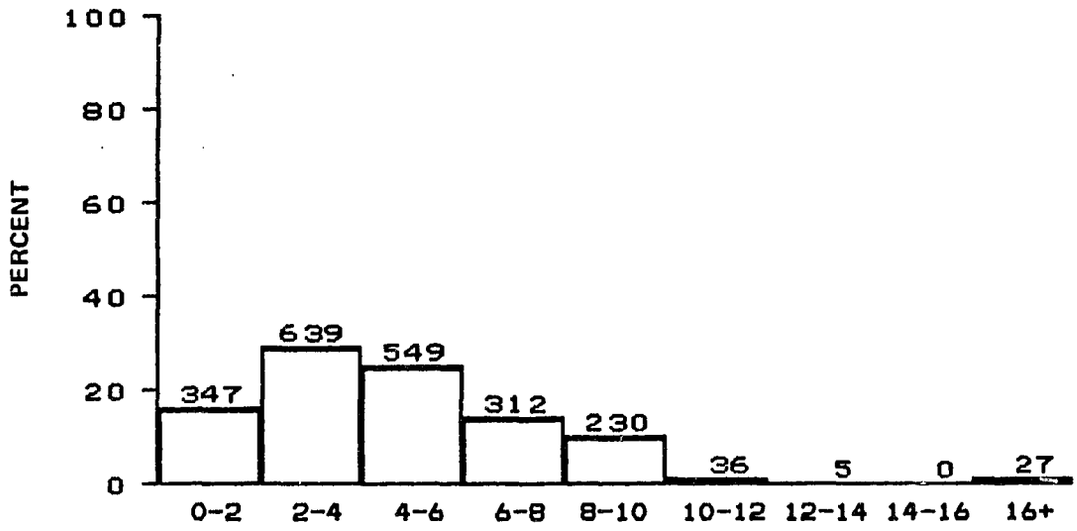

DISTRIBUTION OF WIND SPEED IN METERS PER SECOND
MONTH OF AUGUST
ALL BLM AREAS
N = 2145, MEAN = 4.7, SIGMA = 2.9

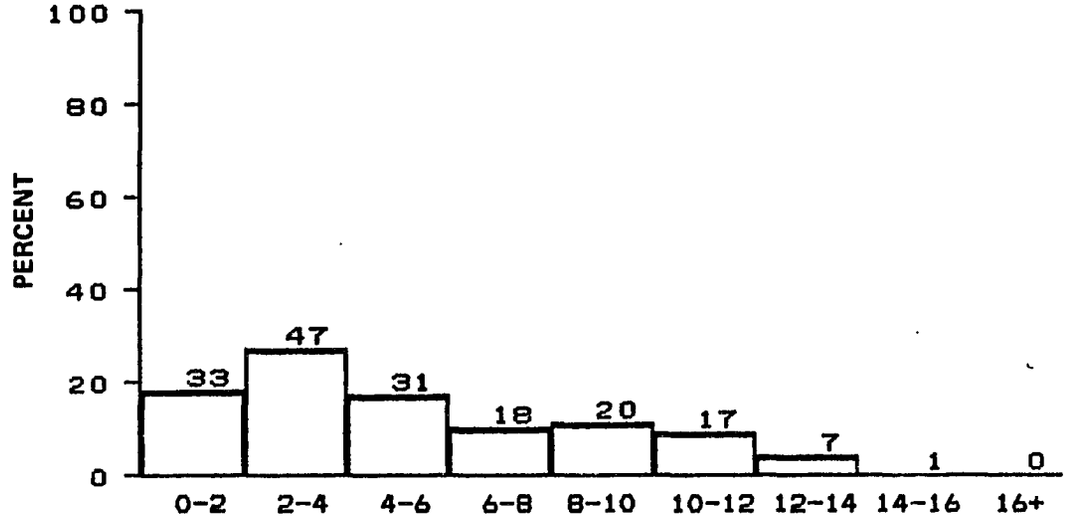

DISTRIBUTION OF WIND SPEED IN METERS PER SECOND
MONTH OF SEPTEMBER
BLM AREA #1
N = 174, MEAN = 5.3, SIGMA = 3.6

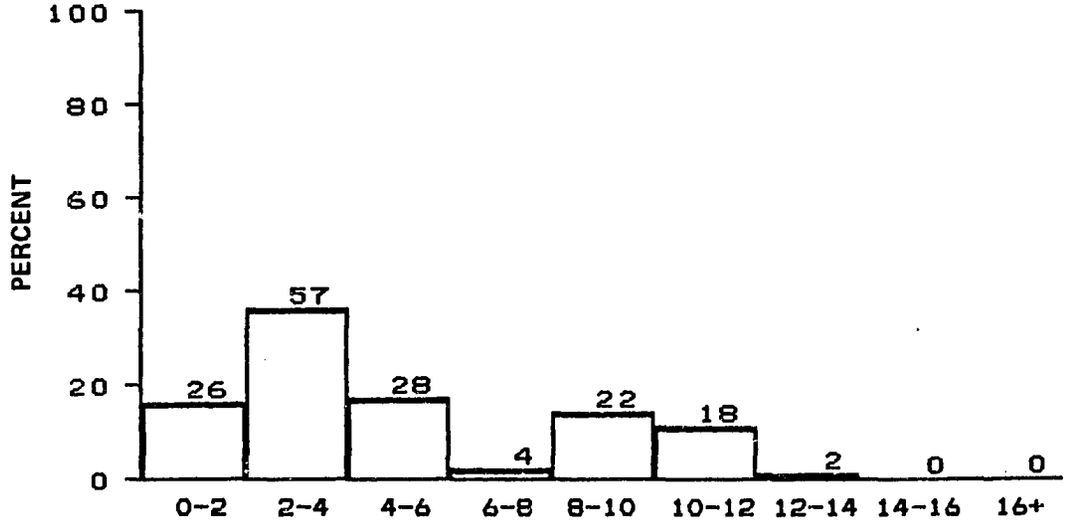

DISTRIBUTION OF WIND SPEED IN METERS PER SECOND
MONTH OF SEPTEMBER
BLM AREA #2
N = 157, MEAN = 5.0, SIGMA = 3.4

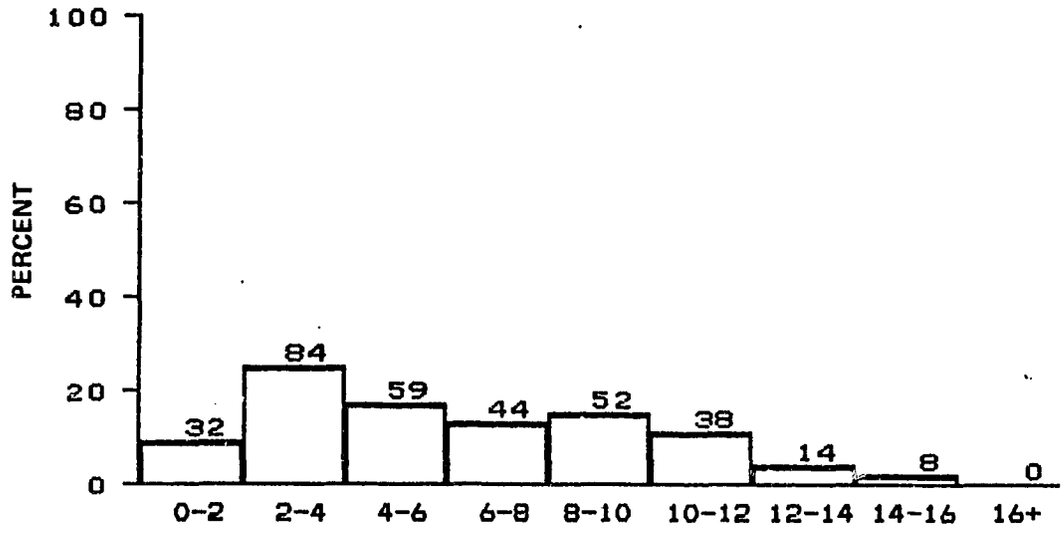

DISTRIBUTION OF WIND SPEED IN METERS PER SECOND
MONTH OF SEPTEMBER
BLM AREA #3
N = 331, MEAN = 6.3, SIGMA = 3.6

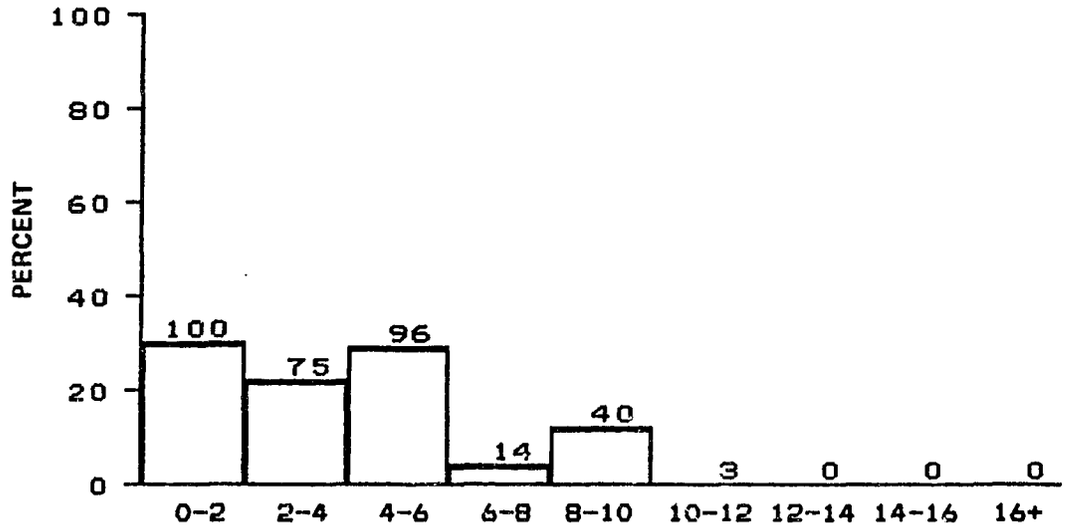

DISTRIBUTION OF WIND SPEED IN METERS PER SECOND
MONTH OF SEPTEMBER
BLM AREA #4
N = 328, MEAN = 4.0, SIGMA = 2.7

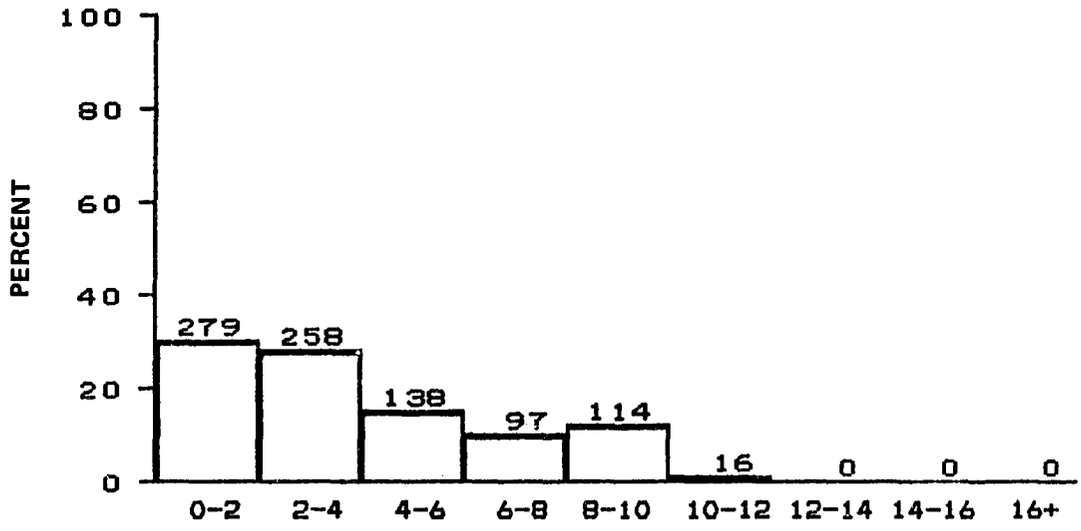

DISTRIBUTION OF WIND SPEED IN METERS PER SECOND
MONTH OF SEPTEMBER
BLM AREA #5
N = 902, MEAN = 4.0, SIGMA = 2.9

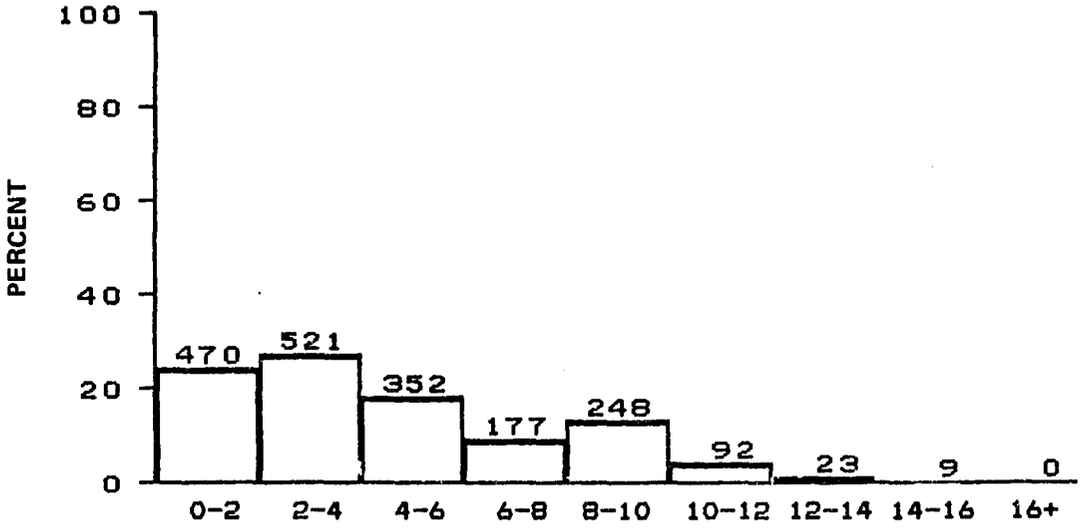

DISTRIBUTION OF WIND SPEED IN METERS PER SECOND
MONTH OF SEPTEMBER
ALL BLM AREAS
N = 1892, MEAN = 4.6, SIGMA = 3.2

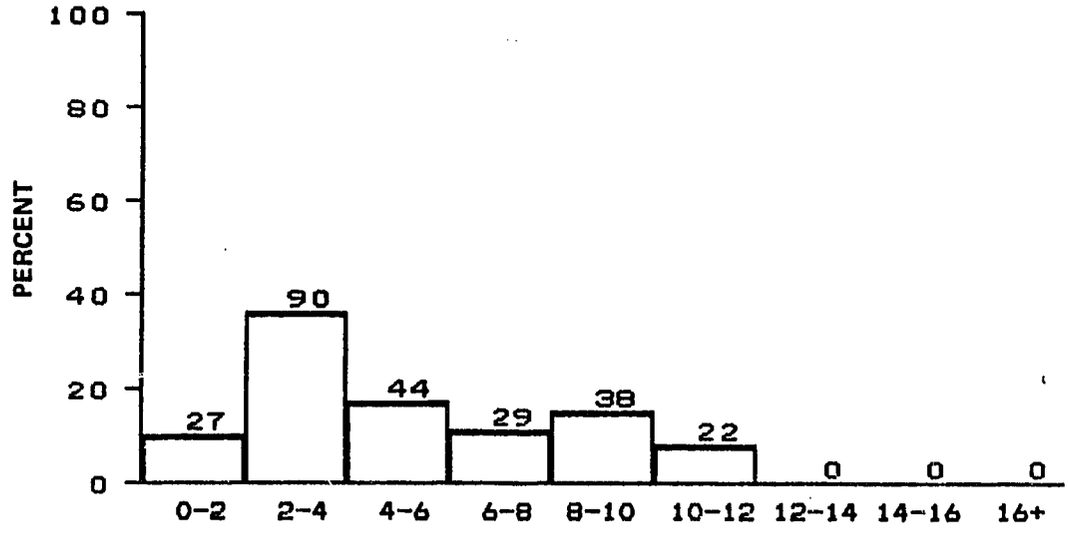

DISTRIBUTION OF WIND SPEED IN METERS PER SECOND
MONTH OF OCTOBER
BLM AREA #1
N = 250, MEAN = 5.2, SIGMA = 3.0

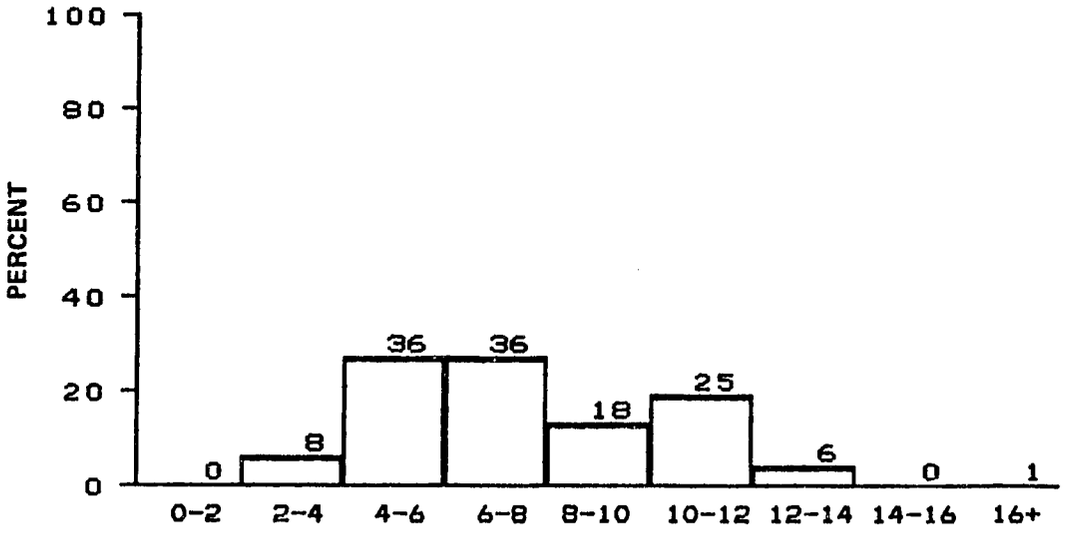

DISTRIBUTION OF WIND SPEED IN METERS PER SECOND
MONTH OF OCTOBER
BLM AREA #2
N = 130, MEAN = 7.6, SIGMA = 2.8

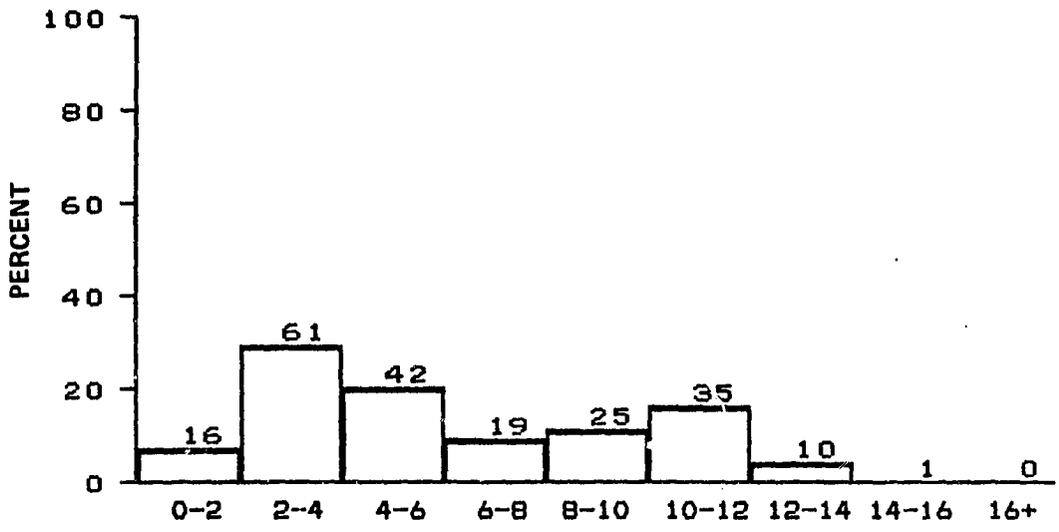

DISTRIBUTION OF WIND SPEED IN METERS PER SECOND
MONTH OF OCTOBER
BLM AREA #3
N = 209, MEAN = 6.2, SIGMA = 3.6

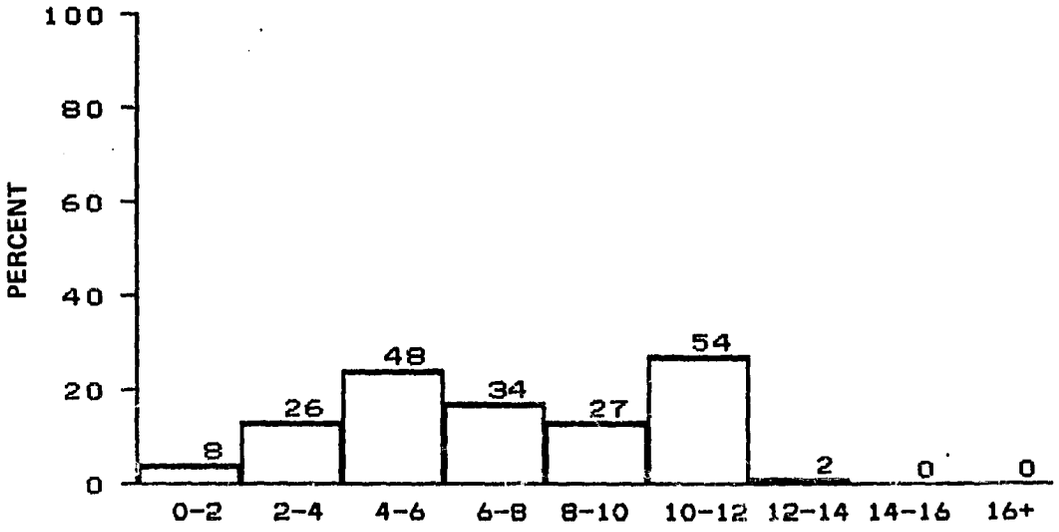

DISTRIBUTION OF WIND SPEED IN METERS PER SECOND
MONTH OF OCTOBER
BLM AREA #4
N = 199, MEAN = 7.2, SIGMA = 3.1

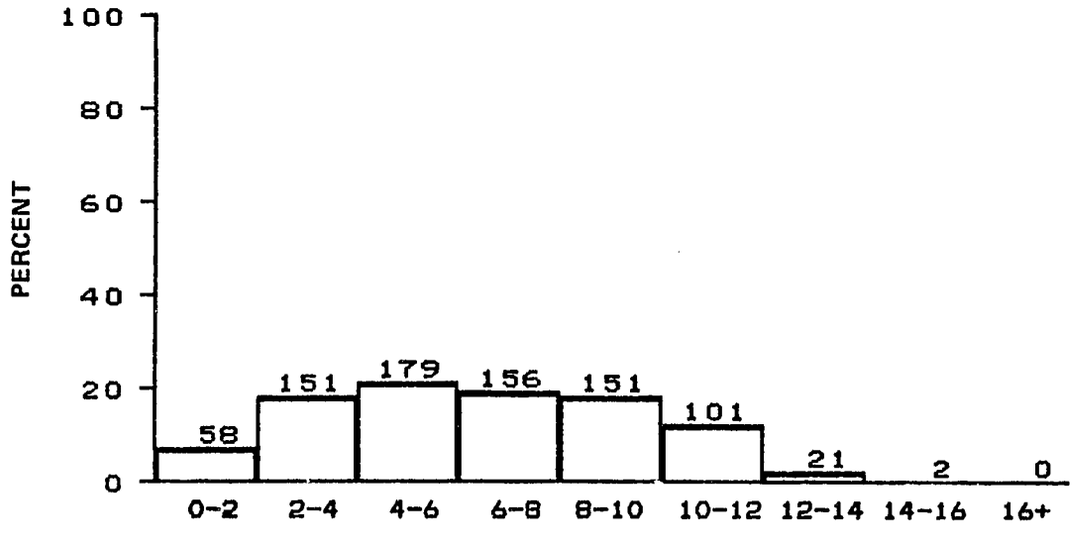

DISTRIBUTION OF WIND SPEED IN METERS PER SECOND
MONTH OF OCTOBER
BLM AREA #5
N = 819, MEAN = 6.4, SIGMA = 3.1

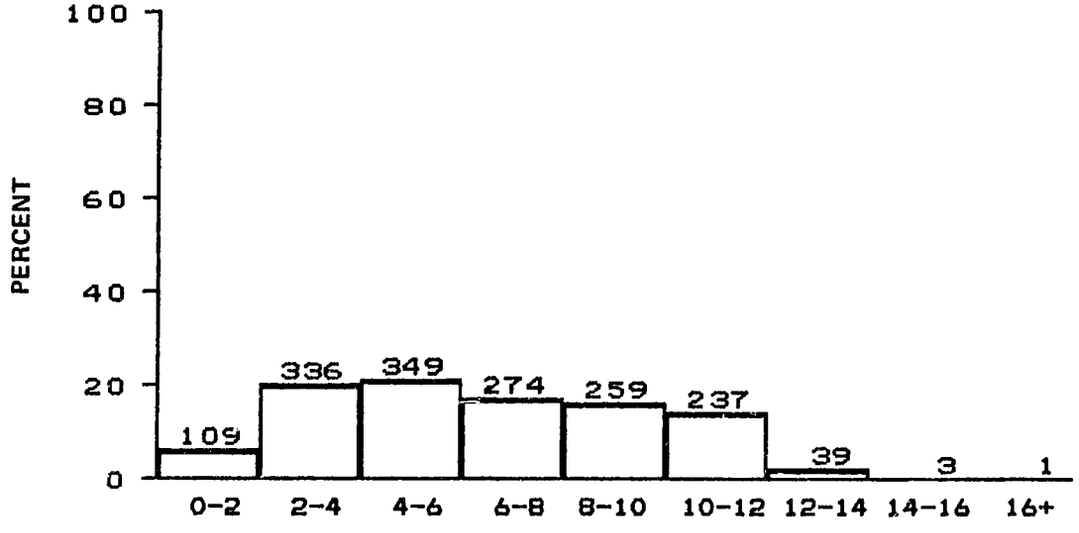

DISTRIBUTION OF WIND SPEED IN METERS PER SECOND
MONTH OF OCTOBER
ALL BLM AREAS
N = 1607, MEAN = 6.4, SIGMA = 3.2

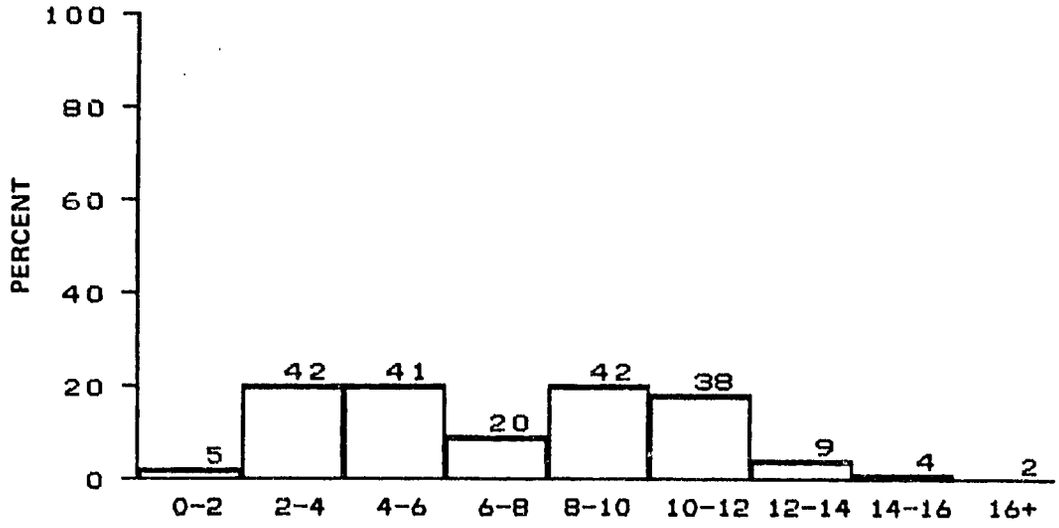

DISTRIBUTION OF WIND SPEED IN METERS PER SECOND
MONTH OF NOVEMBER
BLM AREA #1
N = 203, MEAN = 7.3, SIGMA = 3.5

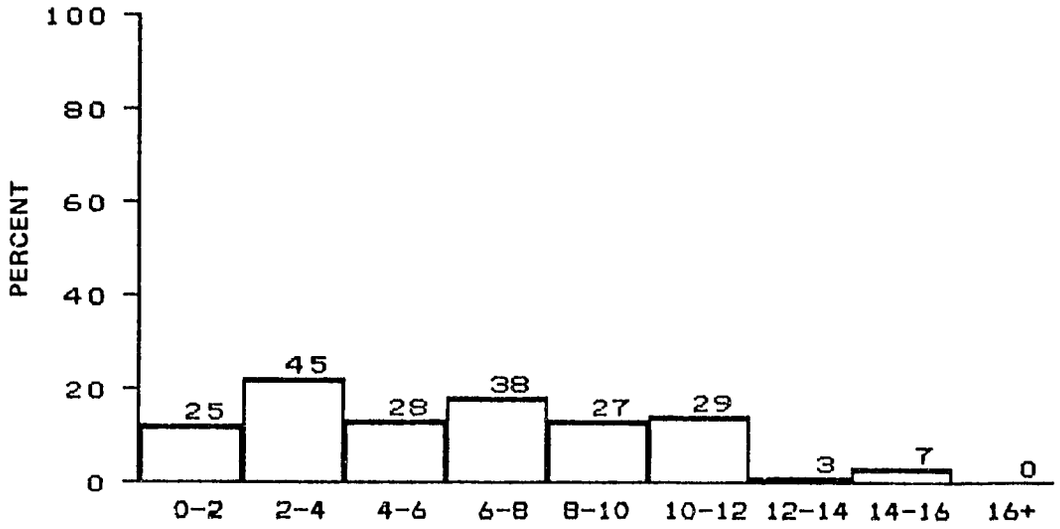

DISTRIBUTION OF WIND SPEED IN METERS PER SECOND
MONTH OF NOVEMBER
BLM AREA #2
N = 202, MEAN = 6.3, SIGMA = 3.7

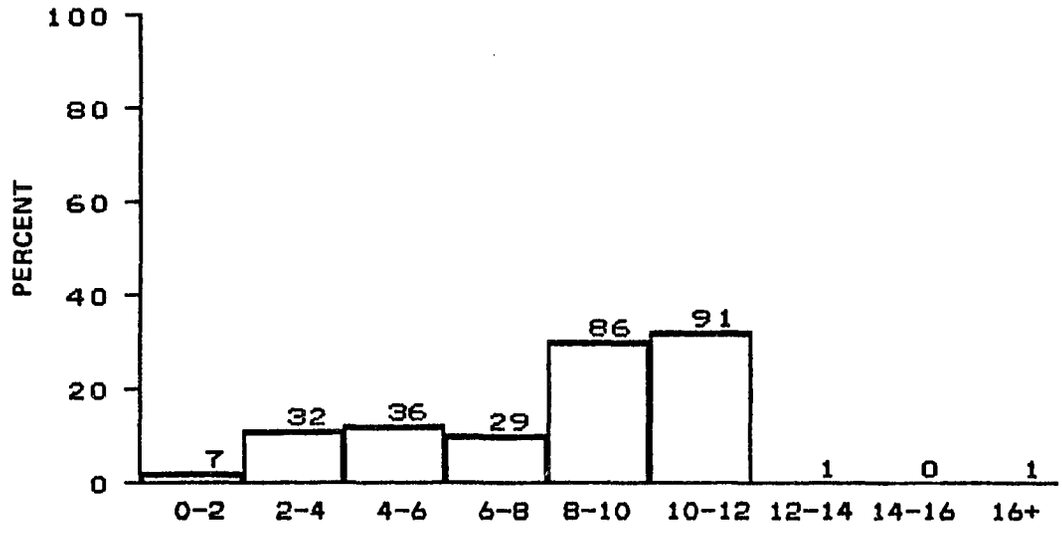

DISTRIBUTION OF WIND SPEED IN METERS PER SECOND
MONTH OF NOVEMBER
BLM AREA #3
N = 283, MEAN = 8.1, SIGMA = 3.0

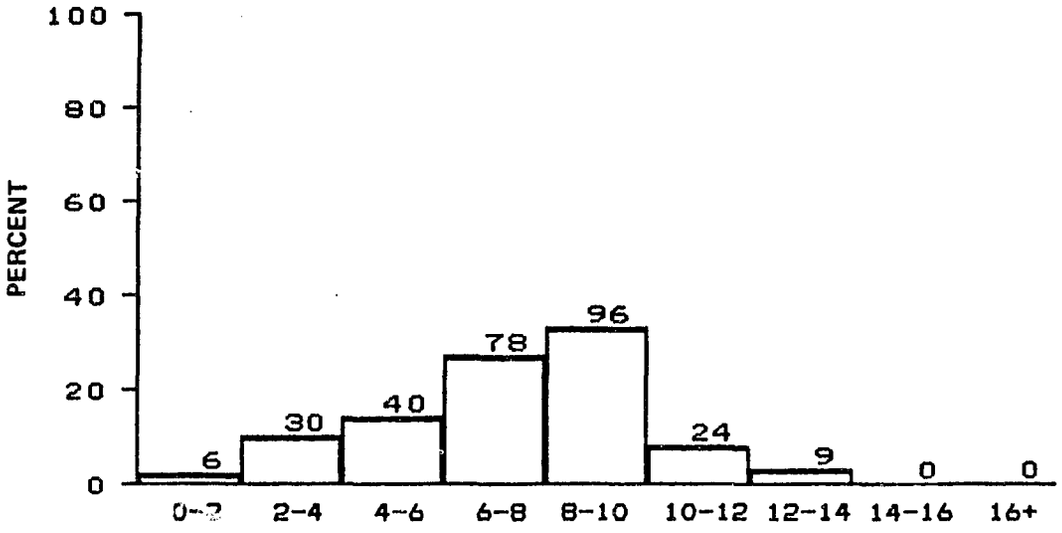

DISTRIBUTION OF WIND SPEED IN METERS PER SECOND
MONTH OF NOVEMBER
BLM AREA #4
N = 283, MEAN = 7.4, SIGMA = 2.6

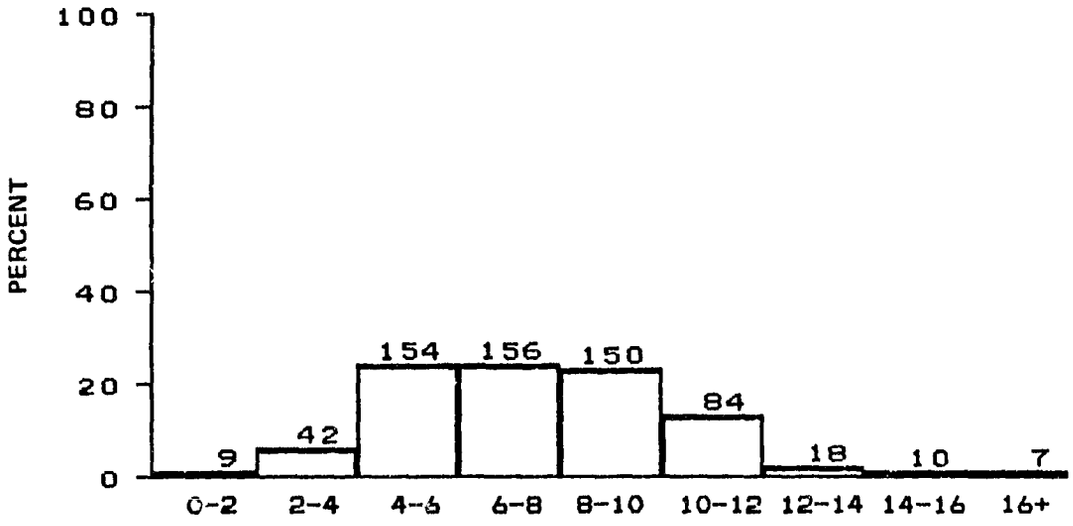

DISTRIBUTION OF WIND SPEED IN METERS PER SECOND
MONTH OF NOVEMBER
BLM AREA #5
N = 630, MEAN = 7.6, SIGMA = 2.9

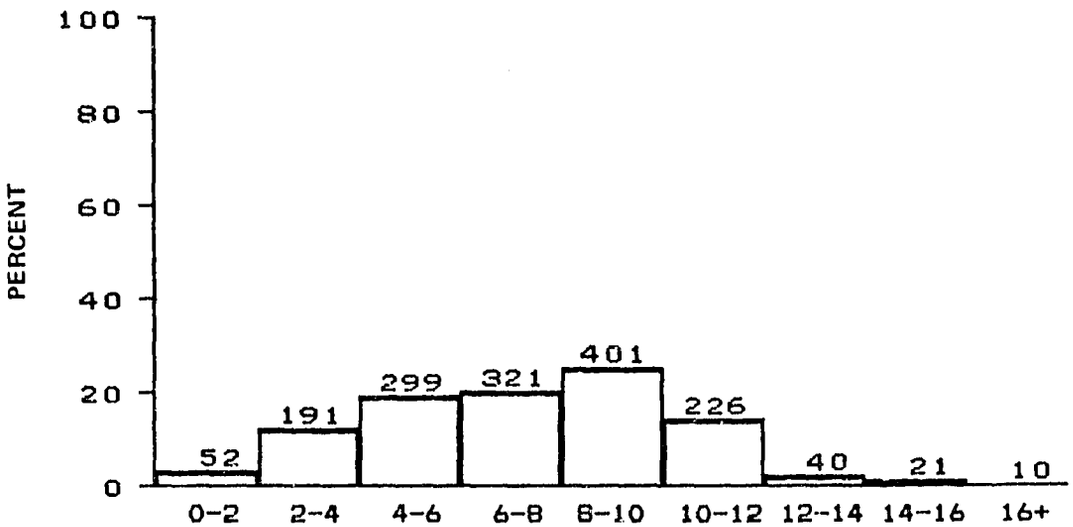

DISTRIBUTION OF WIND SPEED IN METERS PER SECOND
MONTH OF NOVEMBER
ALL BLM AREAS
N = 1561, MEAN = 7.3, SIGMA = 3.1

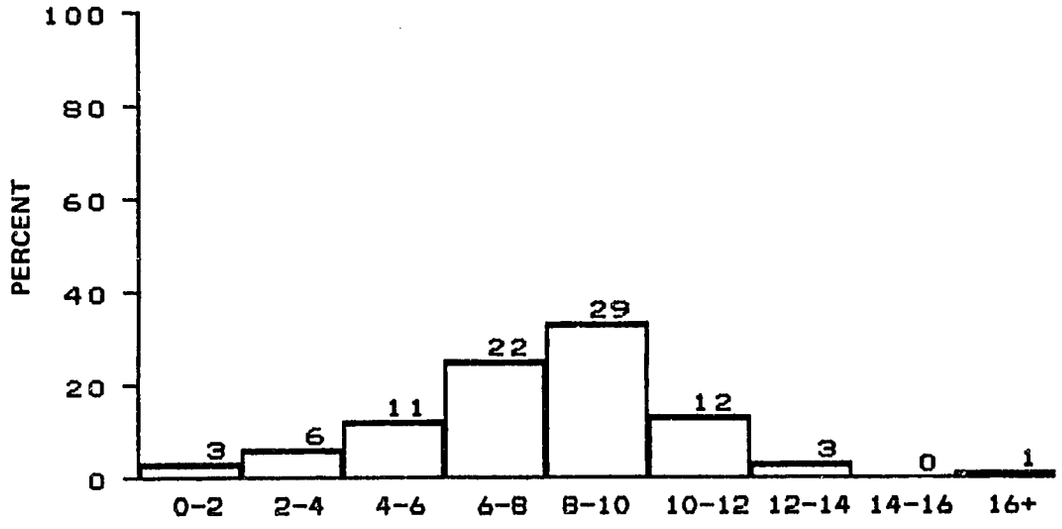

DISTRIBUTION OF WIND SPEED IN METERS PER SECOND
MONTH OF DECEMBER
BLM AREA #1
N = 87, MEAN = 7.8, SIGMA = 2.9

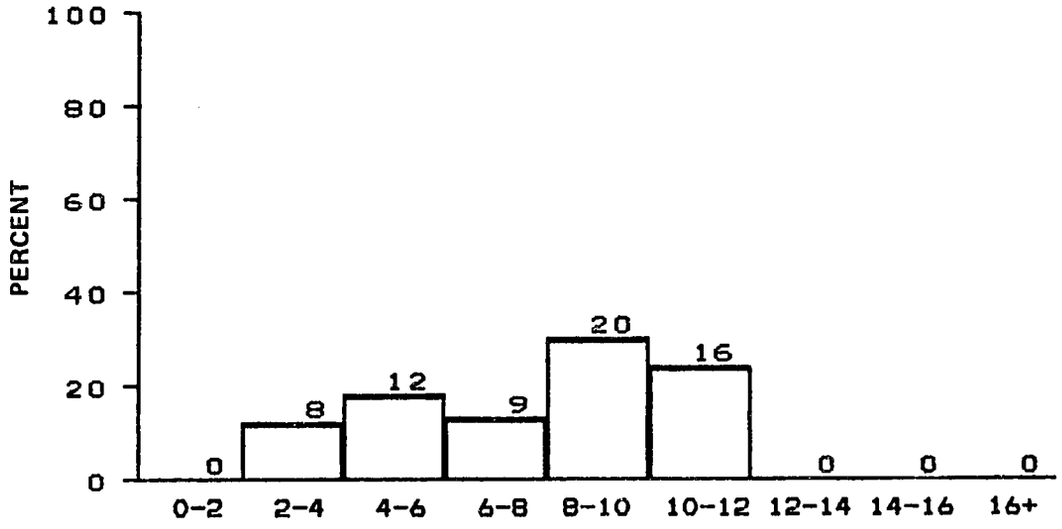

DISTRIBUTION OF WIND SPEED IN METERS PER SECOND
MONTH OF DECEMBER
BLM AREA #2
N = 65, MEAN = 7.7, SIGMA = 2.7

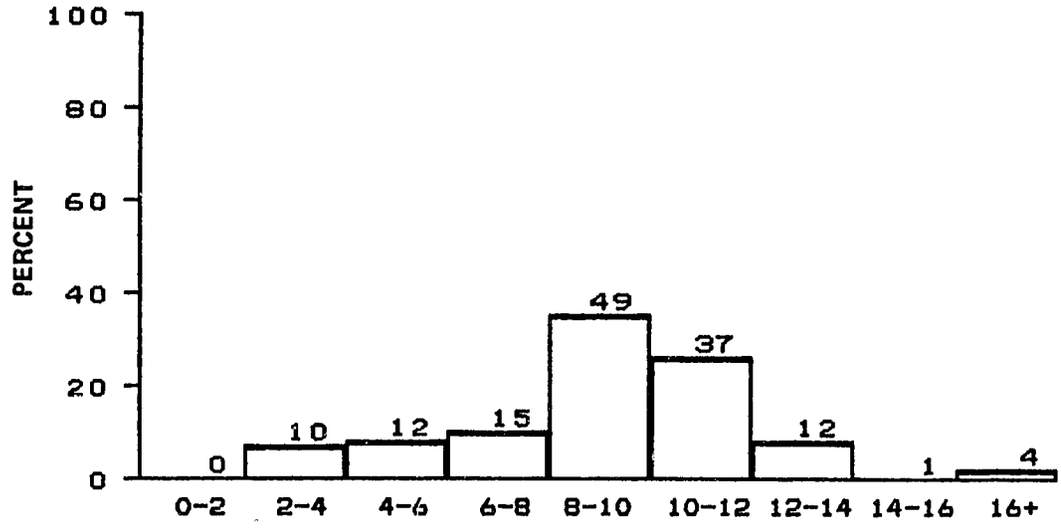

DISTRIBUTION OF WIND SPEED IN METERS PER SECOND
MONTH OF DECEMBER
BLM AREA #3
N = 140, MEAN = 9.2, SIGMA = 3.0

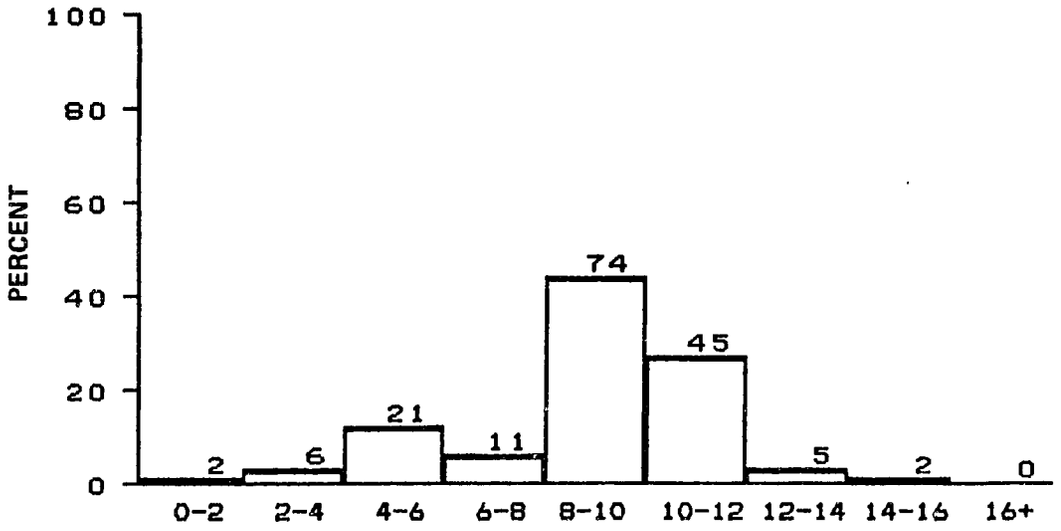

DISTRIBUTION OF WIND SPEED IN METERS PER SECOND
MONTH OF DECEMBER
BLM AREA #4
N = 166, MEAN = 8.8, SIGMA = 2.5

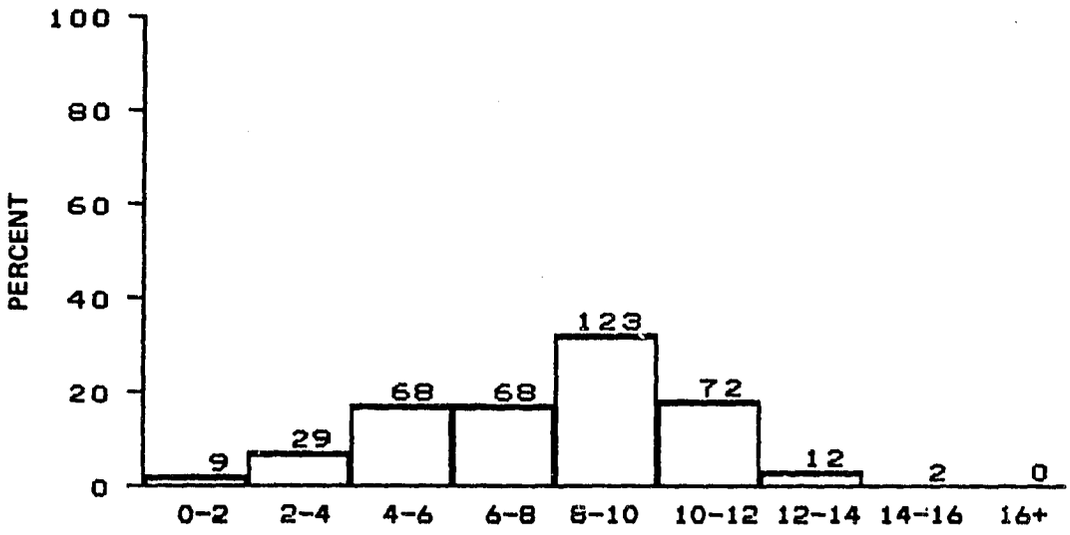

DISTRIBUTION OF WIND SPEED IN METERS PER SECOND
MONTH OF DECEMBER
BLM AREA #5
N = 383, MEAN = 7.8, SIGMA = 2.8

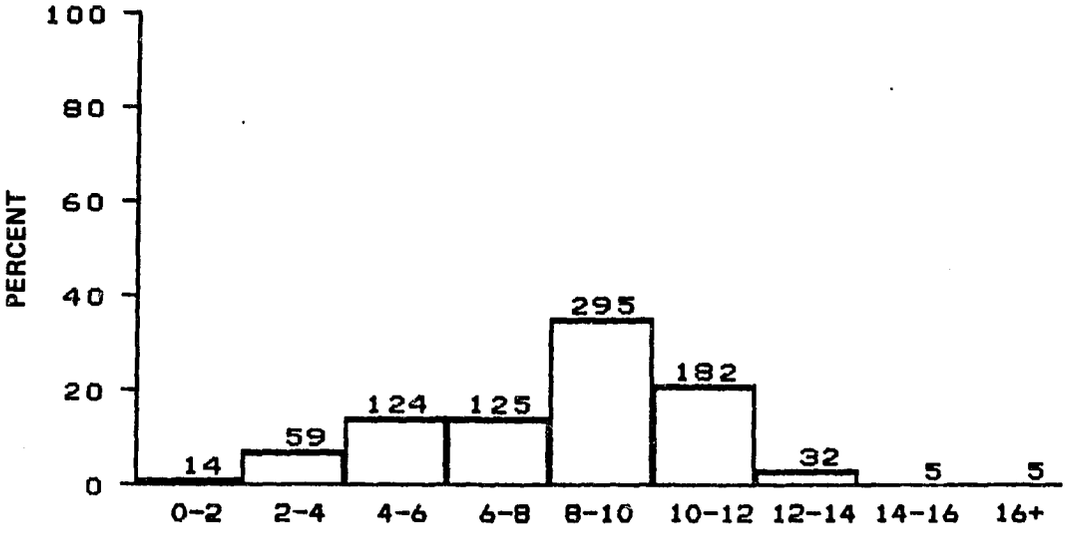

DISTRIBUTION OF WIND SPEED IN METERS PER SECOND
MONTH OF DECEMBER
ALL BLM AREAS
N = 841, MEAN = 8.2, SIGMA = 2.8

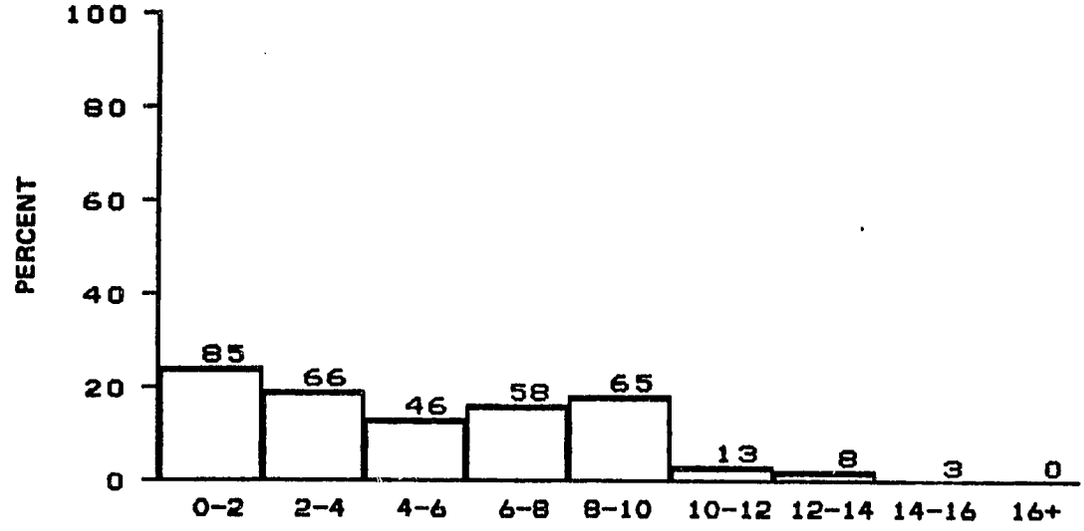

DISTRIBUTION OF WIND SPEED IN METERS PER SECOND
SPRING SEASON
BLM AREA #1
N = 344, MEAN = 5.2, SIGMA = 3.5

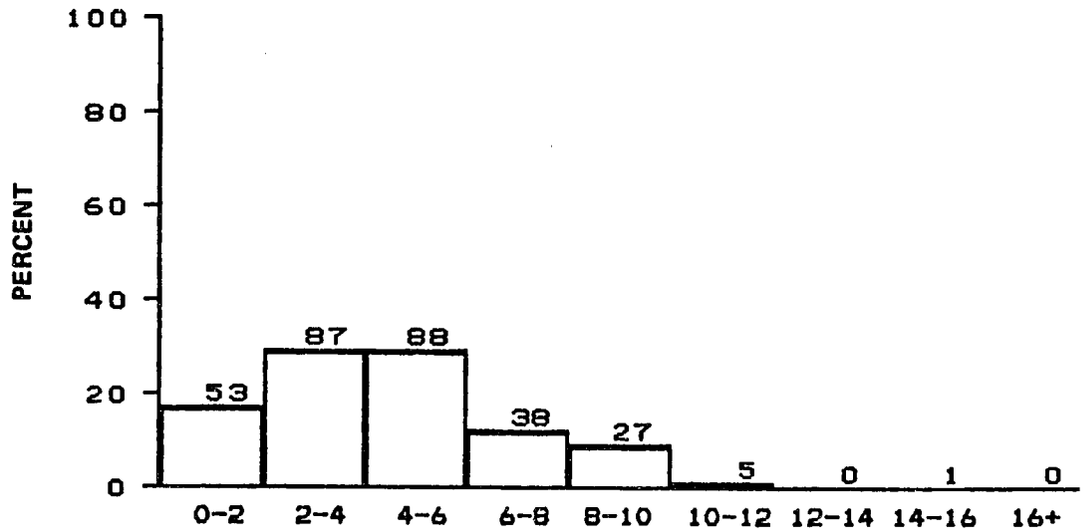

DISTRIBUTION OF WIND SPEED IN METERS PER SECOND
SPRING SEASON
BLM AREA #2
N = 299, MEAN = 4.5, SIGMA = 2.6

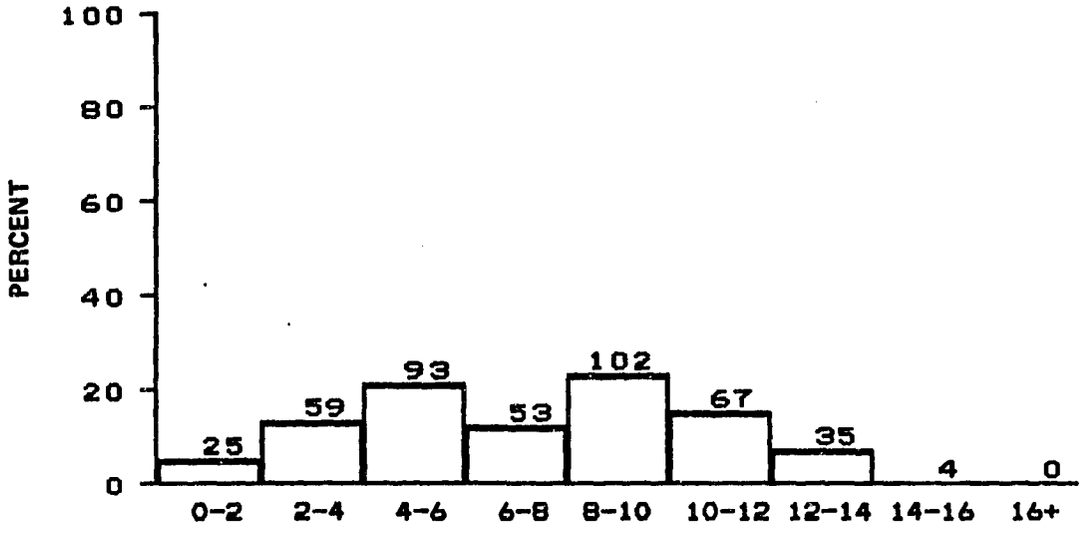

DISTRIBUTION OF WIND SPEED IN METERS PER SECOND
SPRING SEASON
BLM AREA #3
N = 438, MEAN = 7.3, SIGMA = 3.4

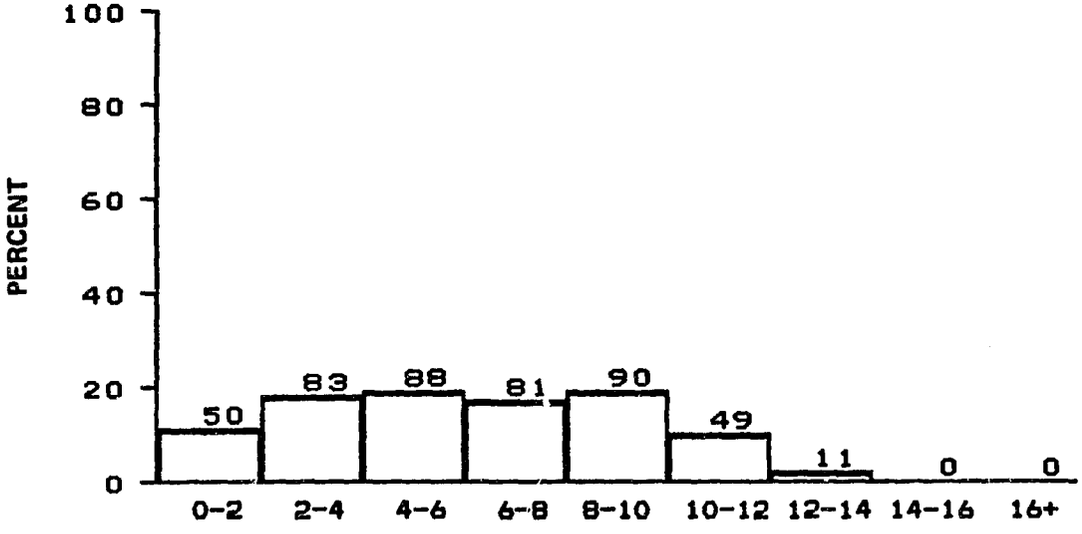

DISTRIBUTION OF WIND SPEED IN METERS PER SECOND
SPRING SEASON
BLM AREA #4
N = 452, MEAN = 6.2, SIGMA = 3.2

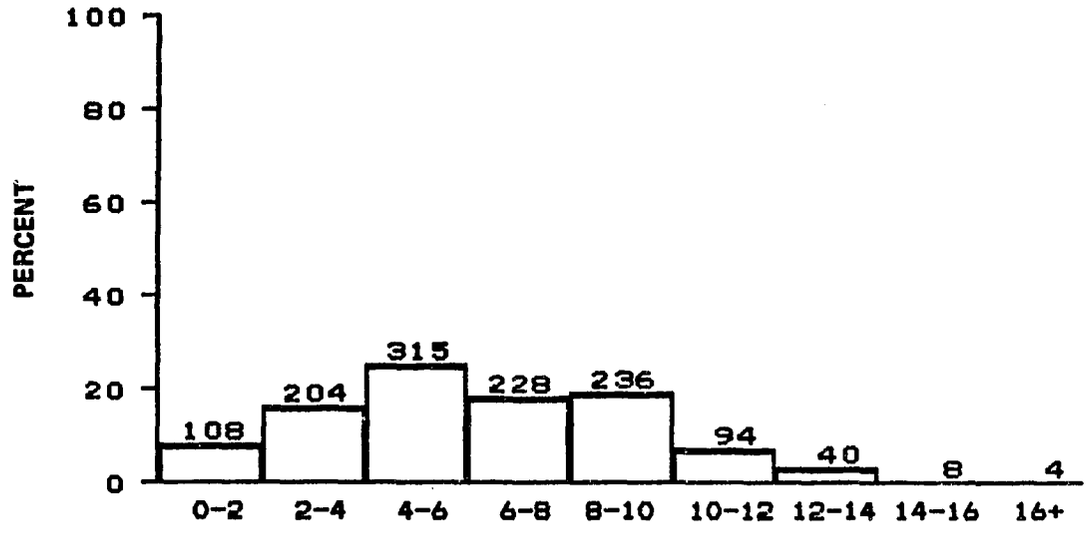

DISTRIBUTION OF WIND SPEED IN METERS PER SECOND
SPRING SEASON
BLM AREA #5
N = 1237, MEAN = 6.3, SIGMA = 3.2

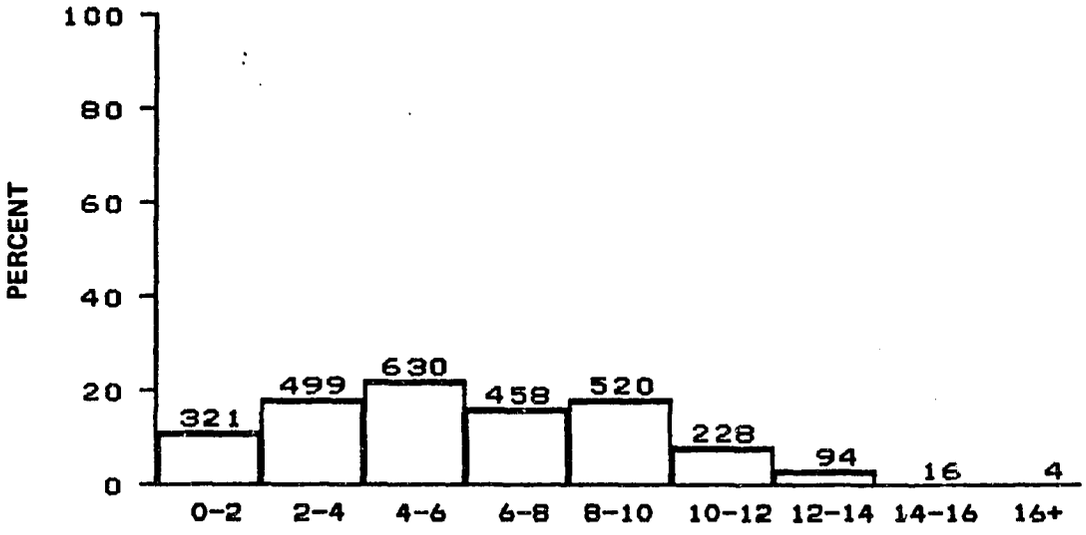

DISTRIBUTION OF WIND SPEED IN METERS PER SECOND
SPRING SEASON
ALL BLM AREAS
N = 2770, MEAN = 6.1, SIGMA = 3.3

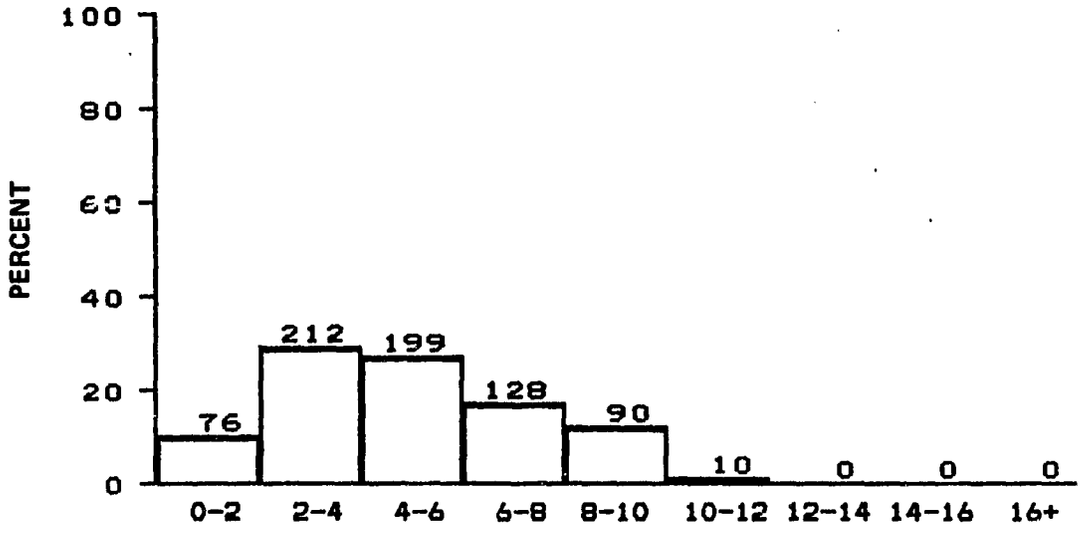

DISTRIBUTION OF WIND SPEED IN METERS PER SECOND
SUMMER SEASON
BLM AREA #1
N = 715, MEAN = 4.9, SIGMA = 2.5

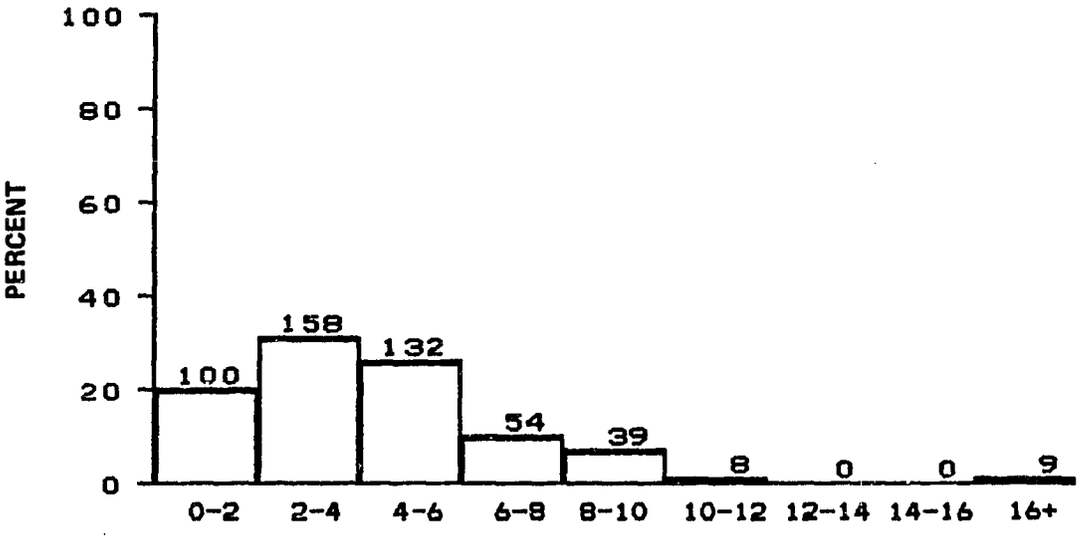

DISTRIBUTION OF WIND SPEED IN METERS PER SECOND
SUMMER SEASON
BLM AREA #2
N = 500, MEAN = 4.4, SIGMA = 3.0

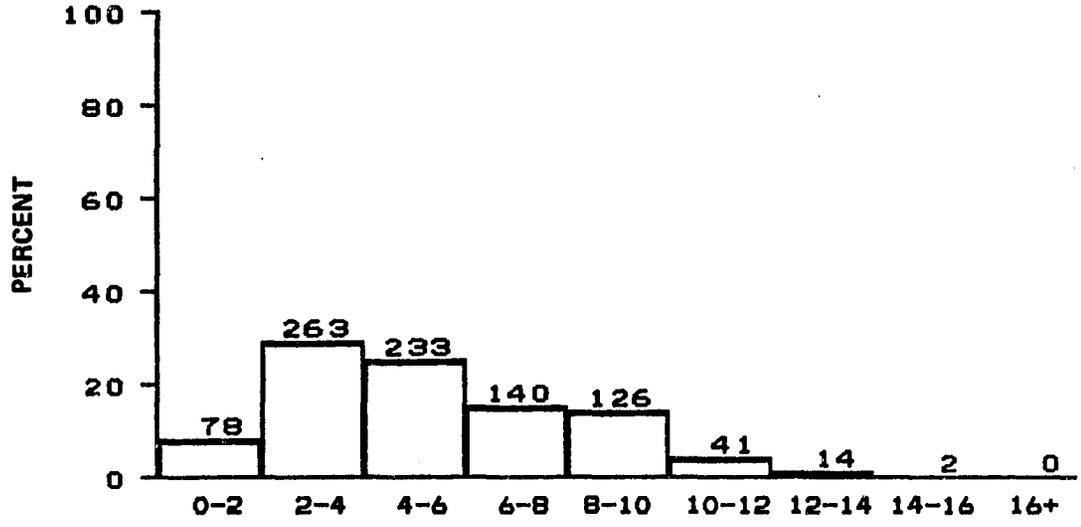

DISTRIBUTION OF WIND SPEED IN METERS PER SECOND
SUMMER SEASON
BLM AREA #3
N = 897, MEAN = 5.4, SIGMA = 2.9

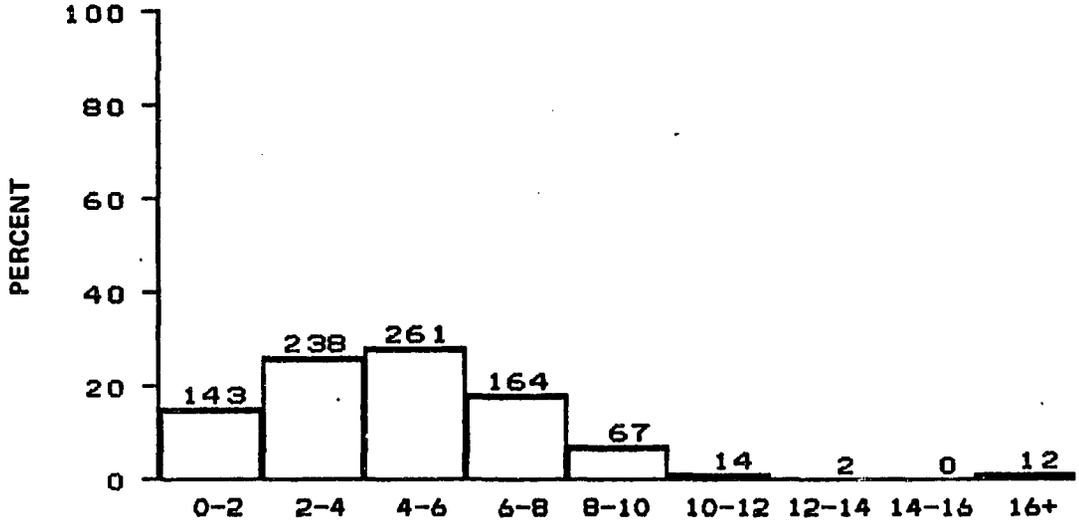

DISTRIBUTION OF WIND SPEED IN METERS PER SECOND
SUMMER SEASON
BLM AREA #4
N = 901, MEAN = 4.8, SIGMA = 2.8

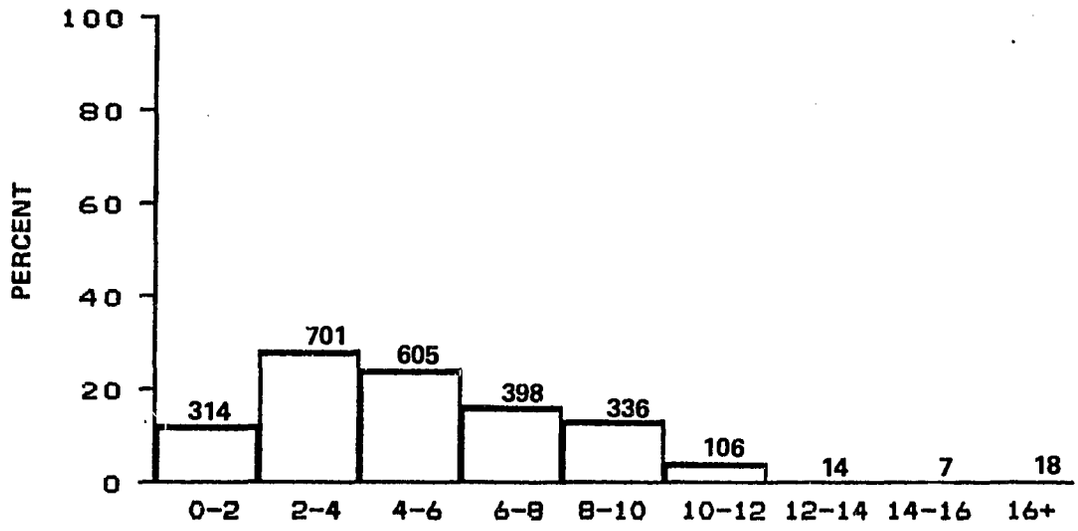

DISTRIBUTION OF WIND SPEED IN METERS PER SECOND
SUMMER SEASON
BLM AREA #5
N = 2499, MEAN = 5.2, SIGMA = 3.0

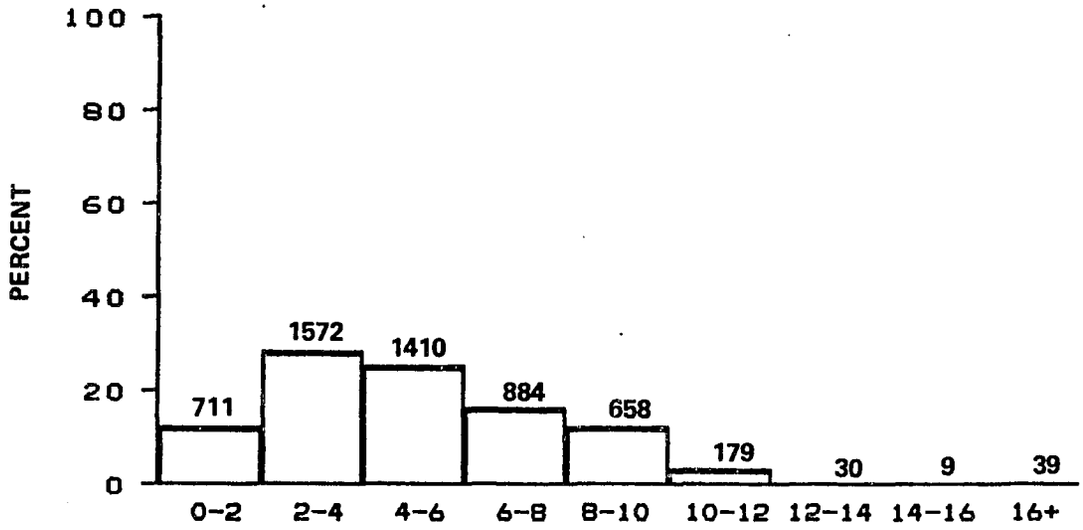

DISTRIBUTION OF WIND SPEED IN METERS PER SECOND
SUMMER SEASON
ALL BLM AREAS
N = 5492, MEAN = 5.1, SIGMA = 2.9

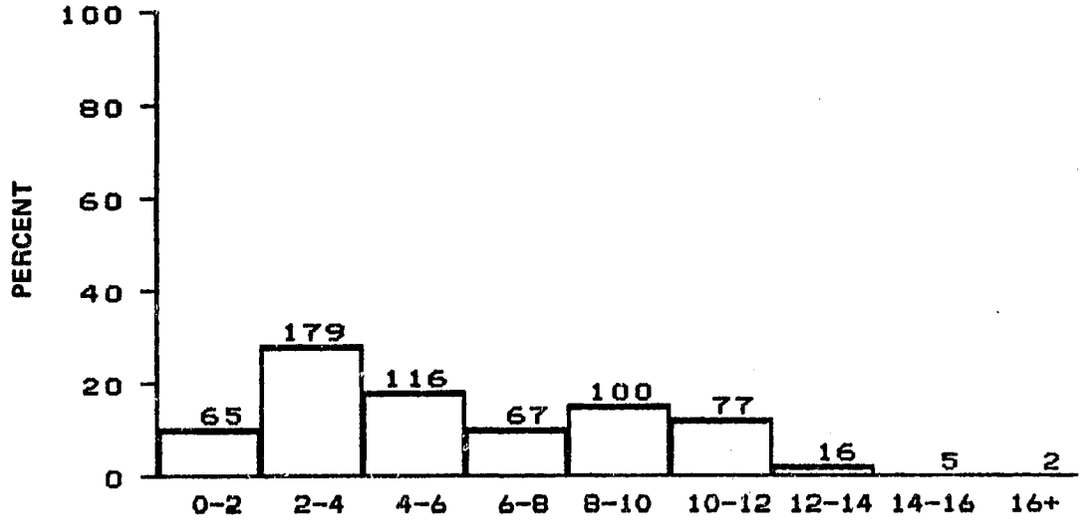

DISTRIBUTION OF WIND SPEED IN METERS PER SECOND

FALL SEASON

BLM AREA #1

N = 627, MEAN = 5.9, SIGMA = 3.5

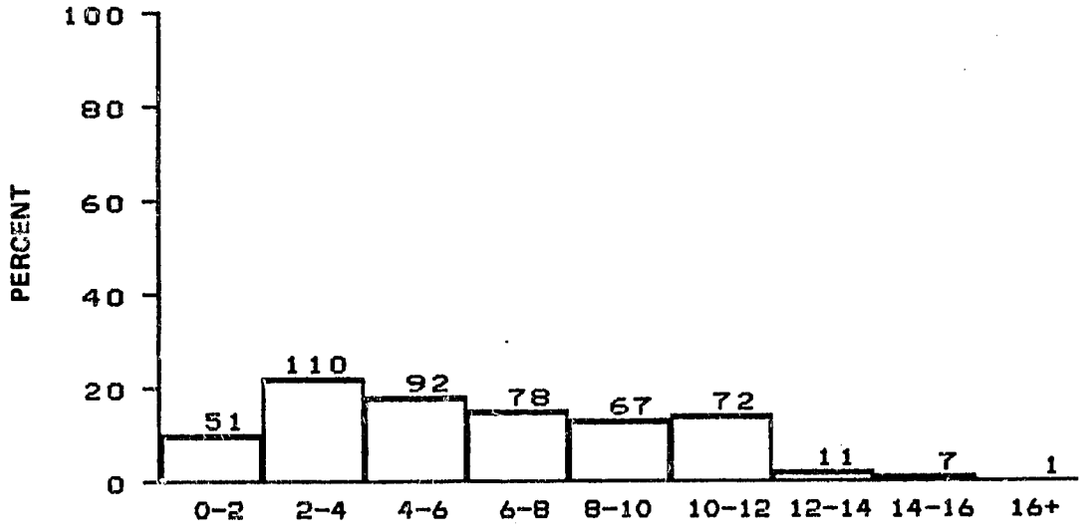

DISTRIBUTION OF WIND SPEED IN METERS PER SECOND

FALL SEASON

BLM AREA #2

N = 489, MEAN = 6.2, SIGMA = 3.5

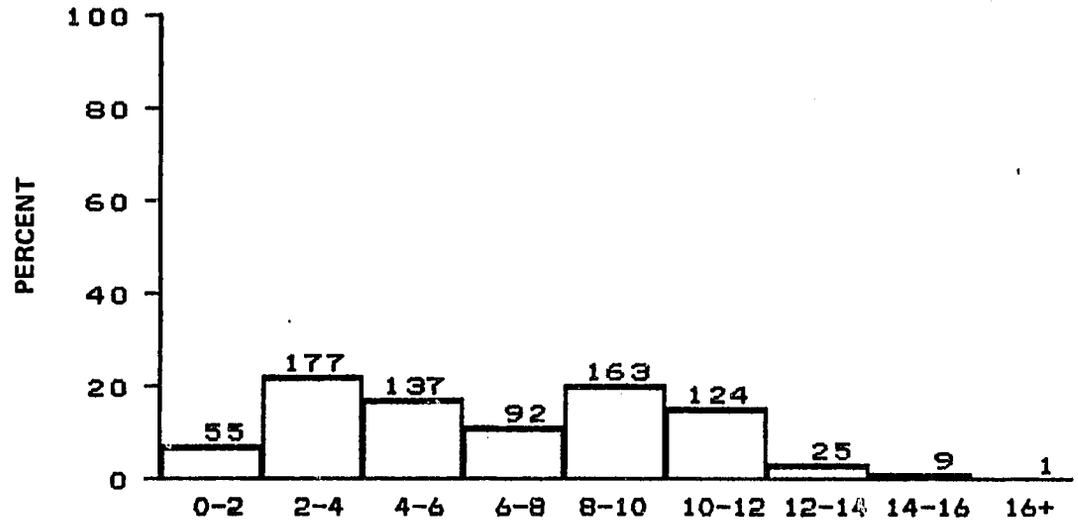

DISTRIBUTION OF WIND SPEED IN METERS PER SECOND
FALL SEASON
BLM AREA #3
N = 783, MEAN = 6.7, SIGMA = 3.5

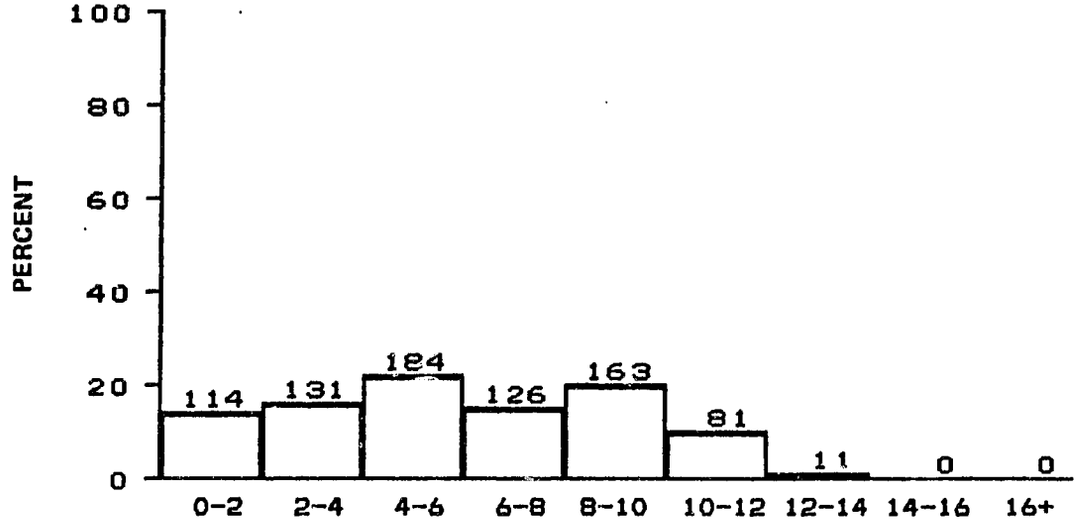

DISTRIBUTION OF WIND SPEED IN METERS PER SECOND
FALL SEASON
BLM AREA #4
N = 810, MEAN = 5.9, SIGMA = 3.2

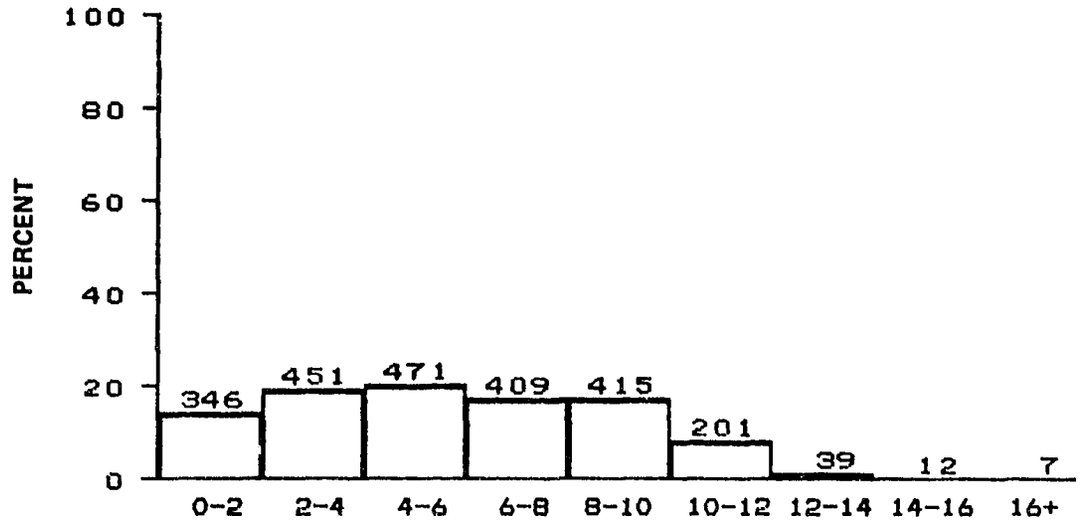

DISTRIBUTION OF WIND SPEED IN METERS PER SECOND

FALL SEASON

BLM AREA #5

N = 2351, MEAN = 5.8, SIGMA = 3.3

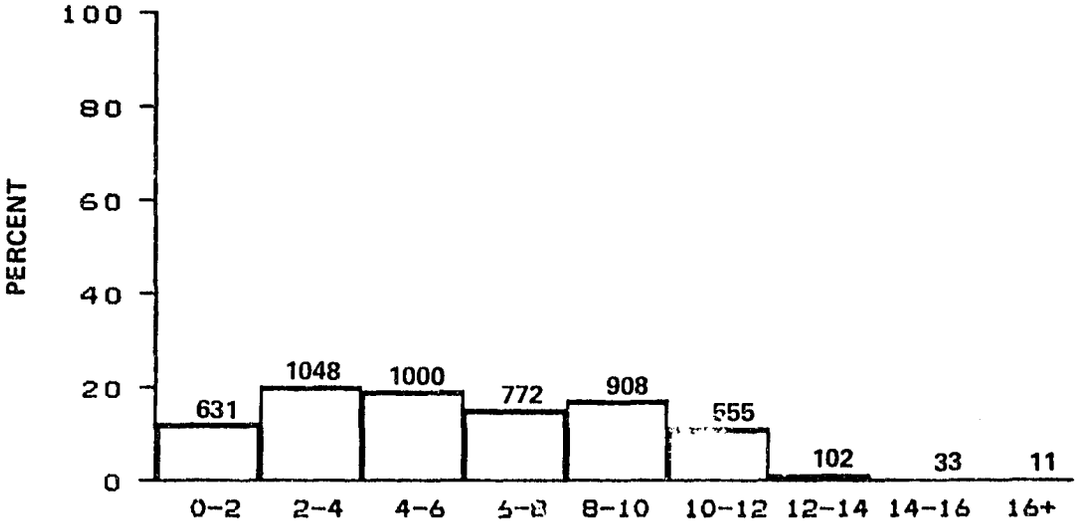

DISTRIBUTION OF WIND SPEED IN METERS PER SECOND

FALL SEASON

ALL BLM AREAS

N = 5060, MEAN = 6.0, SIGMA = 3.4

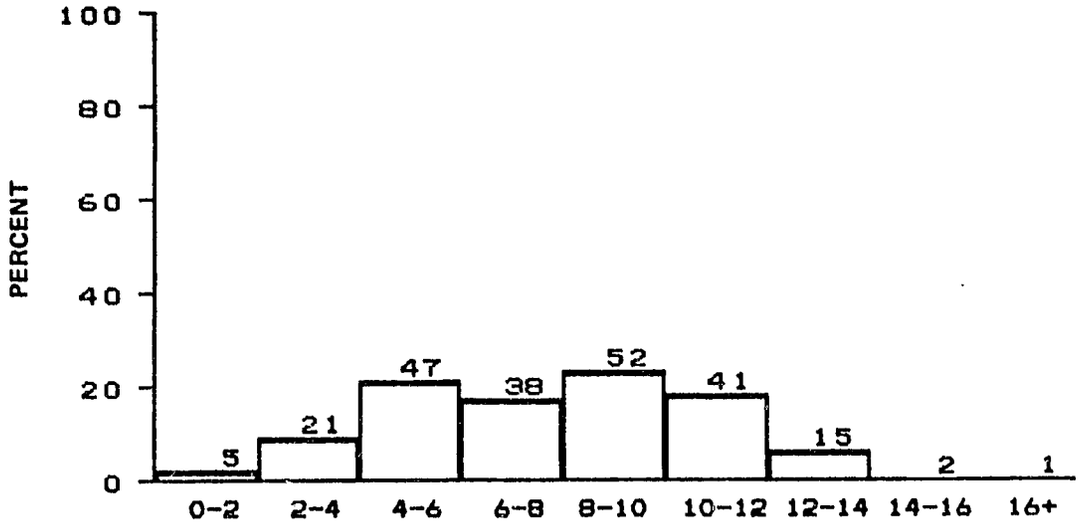

DISTRIBUTION OF WIND SPEED IN METERS PER SECOND
WINTER SEASON
BLM AREA #1
N = 222, MEAN = 7.8, SIGMA = 3.1

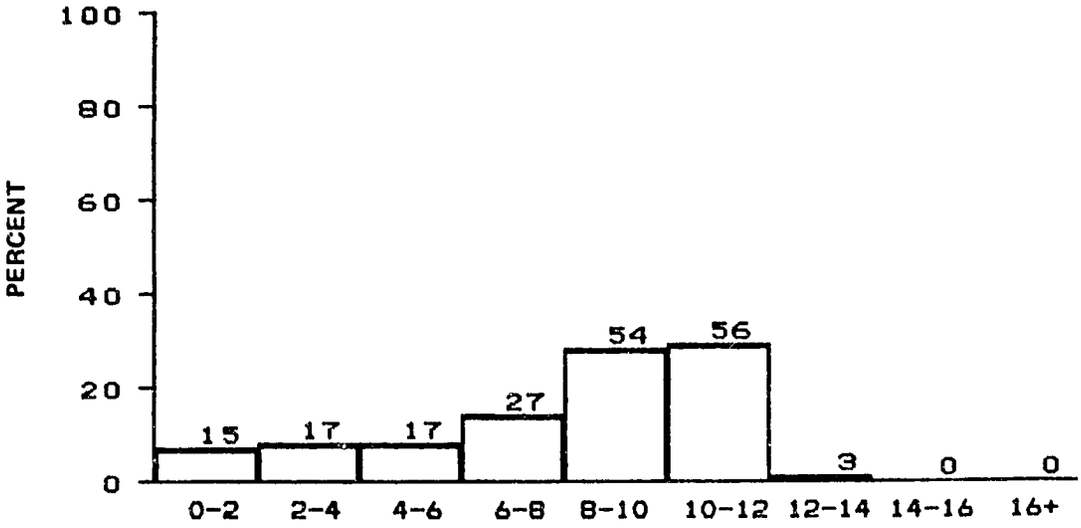

DISTRIBUTION OF WIND SPEED IN METERS PER SECOND
WINTER SEASON
BLM AREA #2
N = 189, MEAN = 7.8, SIGMA = 3.2

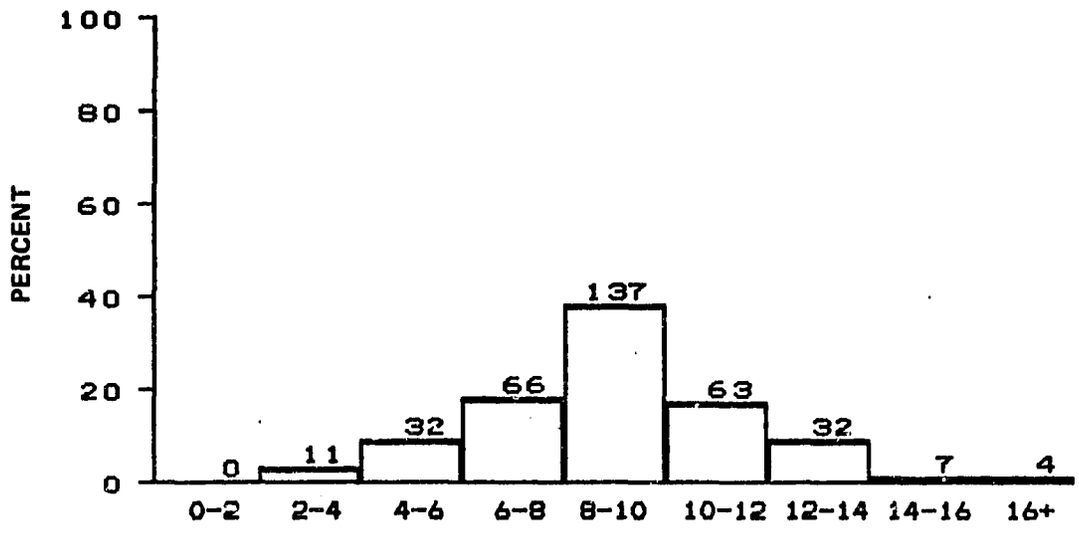

DISTRIBUTION OF WIND SPEED IN METERS PER SECOND
WINTER SEASON
BLM AREA #3
N = 352, MEAN = 9.0, SIGMA = 2.6

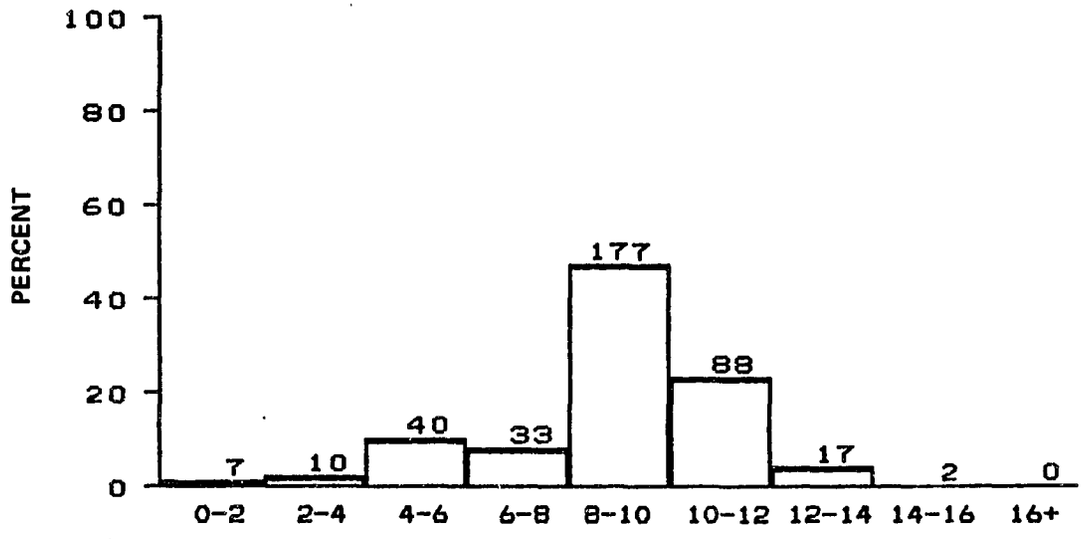

DISTRIBUTION OF WIND SPEED IN METERS PER SECOND
WINTER SEASON
BLM AREA #4
N = 374, MEAN = 8.8, SIGMA = 2.5

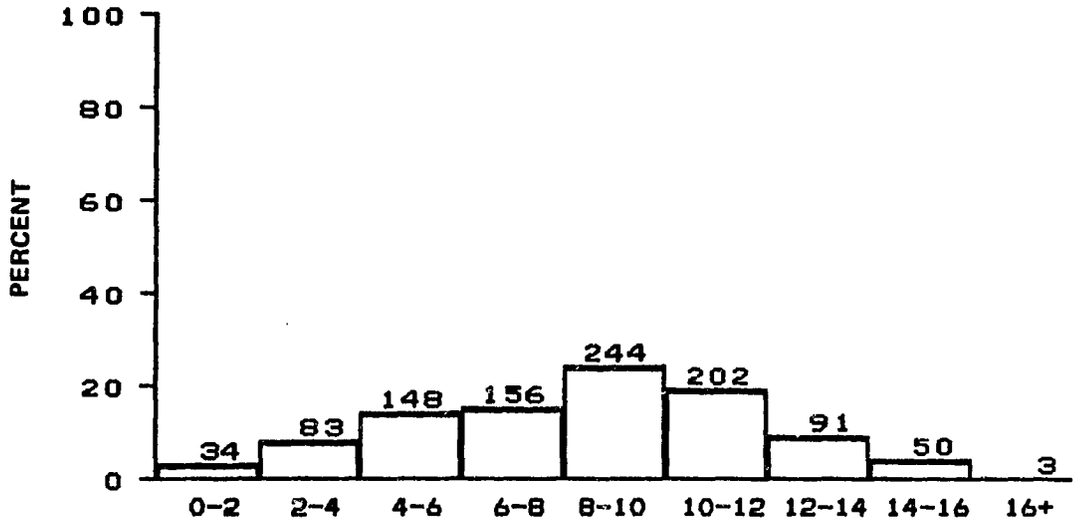

DISTRIBUTION OF WIND SPEED IN METERS PER SECOND
WINTER SEASON
BLM AREA #5
N = 1011, MEAN = 8.4, SIGMA = 3.5

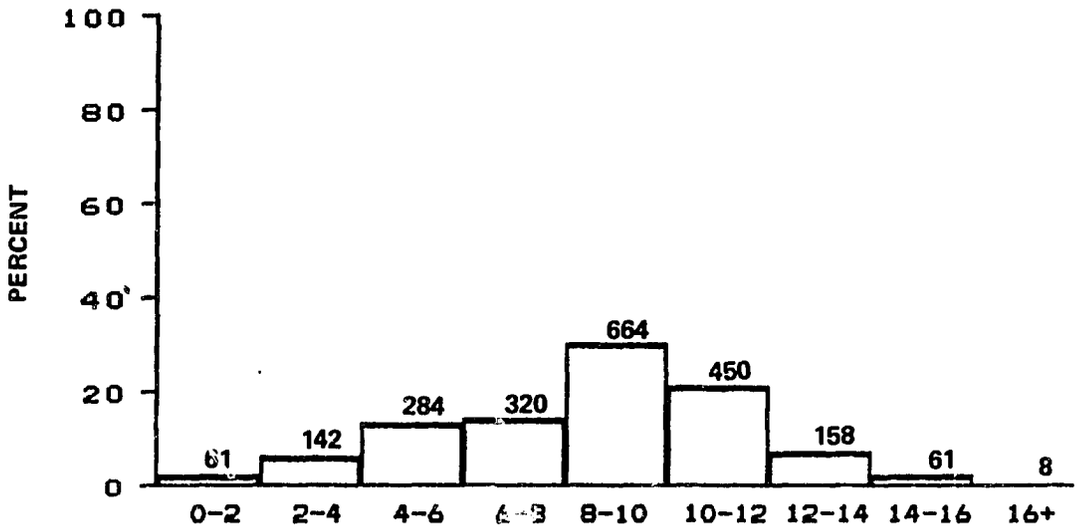

DISTRIBUTION OF WIND SPEED IN METERS PER SECOND
WINTER SEASON
ALL BLM AREAS
N = 2148, MEAN = 8.5, SIGMA = 3.2

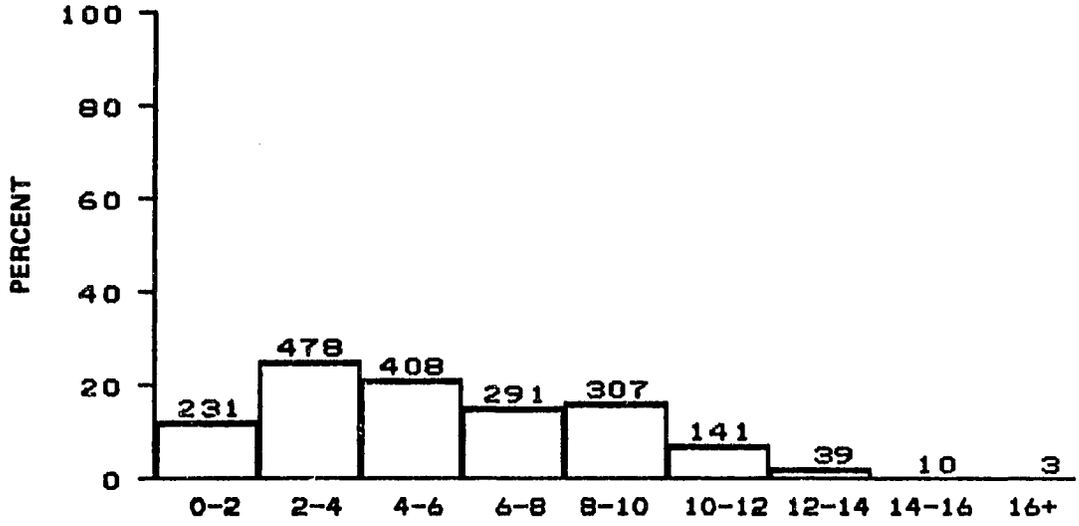

DISTRIBUTION OF WIND SPEED IN METERS PER SECOND
ENTIRE MISSION
BLM AREA #1
N = 1908, MEAN = 5.6, SIGMA = 3.2

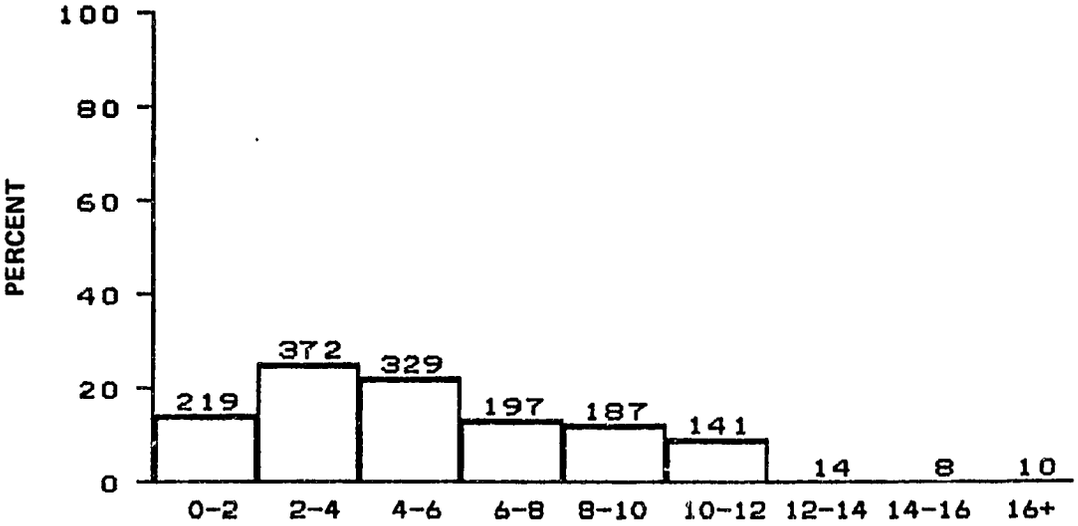

DISTRIBUTION OF WIND SPEED IN METERS PER SECOND
ENTIRE MISSION
BLM AREA #2
N = 1477, MEAN = 5.5, SIGMA = 3.4

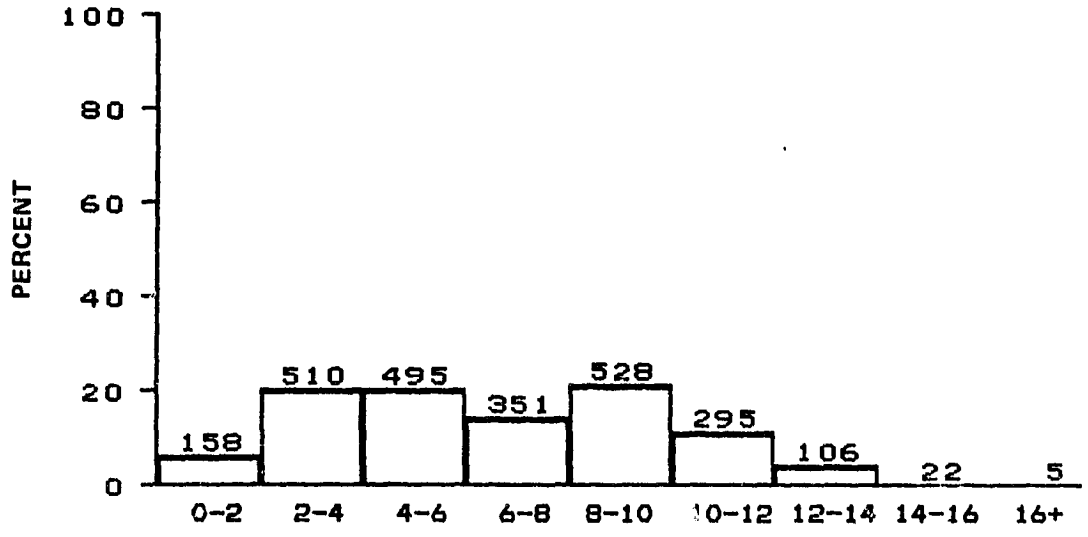

DISTRIBUTION OF WIND SPEED IN METERS PER SECOND
ENTIRE MISSION
BLM AREA #3
N = 2470, MEAN = 6.6, SIGMA = 3.4

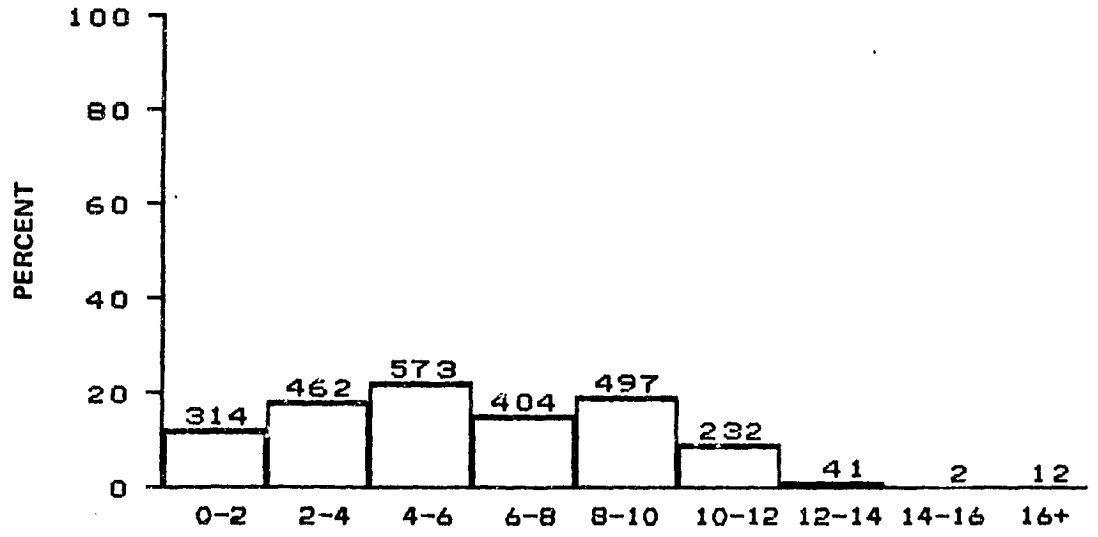

DISTRIBUTION OF WIND SPEED IN METERS PER SECOND
ENTIRE MISSION
BLM AREA #4
N = 2537, MEAN = 6.0, SIGMA = 3.3

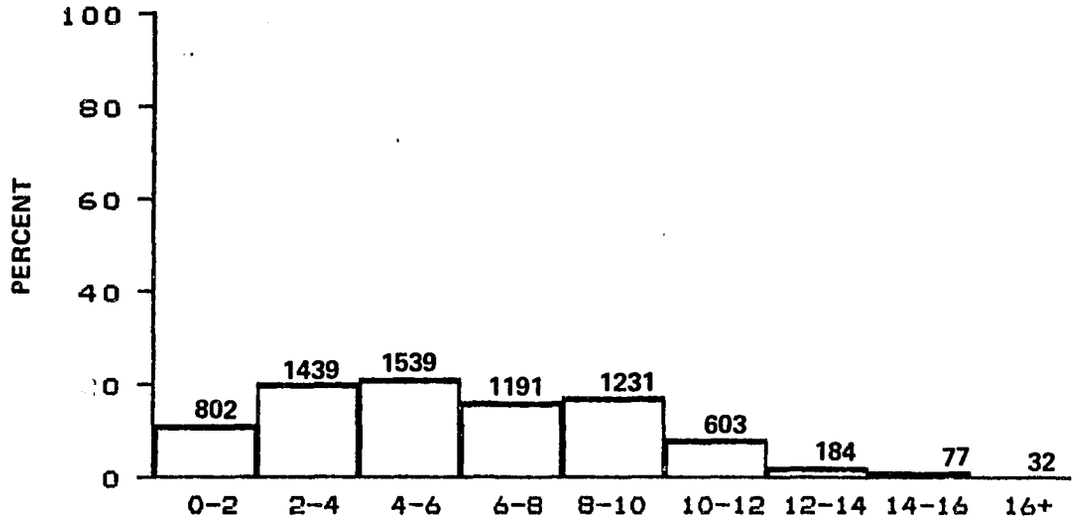

DISTRIBUTION OF WIND SPEED IN METERS PER SECOND

ENTIRE MISSION

BLM AREA #5

N = 7090, MEAN = 6.0, SIGMA = 3.4